SELF-HEALING OF HIGH STRENGTH CONCRETE BY SUPER ABSORBENT POLYMERS FOR AUTOGENOUS SHRINKAGE CONTROL

KARYNE FERREIRA DOS SANTOS

TESE DE DOUTORADO EM ESTRUTURAS E CONSTRUÇÃO CIVIL
DEPARTAMENTO DE ENGENHARIA CIVIL E AMBIENTAL

FACULDADE DE TECNOLOGIA

UNIVERSIDADE DE BRASÍLIA

FACULDADE DE TECNOLOGIA
DEPARTAMENTO DE ENGENHARIA CIVIL E AMBIENTAL

SELF-HEALING OF HIGH STRENGTH CONCRETE BY SUPER ABSORBENT POLYMERS FOR AUTOGENOUS SHRINKAGE CONTROL

KARYNE FERREIRA DOS SANTOS

ORIENTADORA: EUGÊNIA FONSECA DA SILVA.
COORIENTADOR: ANTÓNIO CARLOS BETTENCOURT SIMÕES RIBEIRO.

TESE DE DOUTORADO EM ESTRUTURAS E CONSTRUÇÃO CIVIL

PUBLICAÇÃO: E.TD-04A/21
BRASÍLIA/DF: MARÇO – 2021

UNIVERSIDADE DE BRASÍLIA

FACULDADE DE TECNOLOGIA
DEPARTAMENTO DE ENGENHARIA CIVIL E AMBIENTAL

SELF-HEALING OF HIGH STRENGTH CONCRETE BY SUPER ABSORBENT POLYMERS FOR AUTOGENOUS SHRINKAGE CONTROL

KARYNE FERREIRA DOS SANTOS

TESE DE DOUTORADO SUBMETIDA AO DEPARTAMENTO DE ENGENHARIA CIVIL E AMBIENTAL DA FACULDADE DE TECNOLOGIA DA UNIVERSIDADE DE BRASÍLIA COMO PARTE DOS REQUISITOS NECESSÁRIOS PARA A OBTENÇÃO DO GRAU DE DOUTORA EM ESTRUTURAS E CONSTRUÇÃO CIVIL.

APROVADA POR:

_____
Profa. Eugênia Fonseca da Silva, D.Sc. (UnB)
(Orientadora)

_____
Eng. António Carlos Bettencourt Simões Ribeiro, D.Sc. (LNEC)
(Coorientador)

_____
Prof. Rodrigo de Melo Lameiras, PhD. (UnB)
(Examinador Interno)

_____
Dra. Aline de Souza Oliveira, D.Sc. (COPPE/UFRJ)
(Examinador Externo)

_____
Prof. Romildo Dias Toledo Filho, D.Sc. (COPPE/UFRJ)
(Examinador Externo)

BRASÍLIA/DF, 01 DE MARÇO DE 2021

FICHA CATALOGRÁFICA

SANTOS, KARYNE FERREIRA DOS
Self-Healing of High Strength Concrete by Super Absorbent Polymers for Autogenous Shrinkage Control [Distrito Federal] 2021.
xvii, 215 p., 297 mm (ENC/FT/UnB, Doutor, Estruturas e Construção Civil, 2021).
Tese de Doutorado - Universidade de Brasília. Faculdade de Tecnologia.
Departamento de Engenharia Civil e Ambiental.
1. Superabsorbent polymers 2. Self-healing
3. High Strength Concrete 4. Cracking Method
5. Autogenous shrinkage
I. ENC/FT/UnB II. Título (série)

REFERÊNCIA BIBLIOGRÁFICA

SANTOS, K. F (2021). Self-Healing of High Strength Concrete by Super Absorbent Polymers for Autogenous Shrinkage Control. Tese de Doutorado em Estruturas e Construção Civil, Publicação E.TD-04A/21, Departamento de Engenharia Civil e Ambiental, Universidade de Brasília, Brasília, DF, 215 p.

CESSÃO DE DIREITOS

AUTORA: Karyne Ferreira dos Santos
TÍTULO: Self-Healing of High Strength Concrete by Super Absorbent Polymers for Autogenous Shrinkage Control.
GRAU: Doutor ANO:2021

Karyne Ferreira dos Santos
SMPW Quadra 10 conj.01 lote 4, casa D, Park Way.
CEP:7174-1011 – Brasília – DF – Brasil.
karyne.ferreira@gmail.com

AGRADECIMENTOS

Primeiramente agradeço a Deus por tudo, por sempre iluminar o meu caminho e me guiar.

Aos meus pais, Jairo e Enoi, por serem pessoas maravilhosas, pelo amor incondicional, pelo carinho e paciência. Por entenderem a jornada difícil de um doutorado, por me apoiar e incentivar em todos os momentos.

A minha orientadora e professora Eugênia Fonseca da Silva, pelo carinho, paciência, dedicação, pelo apoio, por ser uma pessoa tão humana e por fim, pela oportunidade de trabalhar com um tema tão apaixonante.

Ao meu coorientador e professor António Carlos Bettencourt Simões Ribeiro, pela generosidade, pelas valiosas orientações e paciência, pela oportunidade de trabalhar neste local acolhedor e de elevadíssimo nível que é o LNEC, pelo incentivo e parceria, pela sempre disposição em ajudar e pelas várias sugestões e enriquecimento ao trabalho.

Ao professor Romildo Dias Toledo Filho, pela parceria, pelo conhecimento de altíssimo nível e pela doação das fibras de aço, agradeço por fazer parte da família do NUMATS mesmo estando longe.

A professora Leila Aparecida de Castro Motta, pelo carinho, pela amizade, por toda a ajuda, sou eternamente grata por ter começado a carreira acadêmica sob a sua orientação e por voltar a trabalhar com você nesta fase da minha vida.

Aos amigos que contribuíram diretamente neste trabalho: a Aline Oliveira pelo companheirismo, pela troca de ensinamentos e pelas diversas horas no WhatsApp sobre self-healing e a vida, por ser uma amiga que me encorajou durante todos os momentos desse doutorado. A Tamara Moreira, pela troca de conhecimento e pela ajuda com a doação das fibras de aço. Agradeço ainda a todos os amigos do NUMATS e COPPE, por me receberem e me ajudarem nessa fase do doutorado, em especial a Alfredo Quiroga e Oscar Mendoza.

Aos amigos do LNEC, sem os quais a pesquisa não seria possível e que tornaram os dias mais curtos e felizes, Etelvina Leitão, Fernanda Simões, Nuno Silvestre, Victor Fialho,

em especial ao Pedro Amaral para quem não tenho palavras para agradecer toda ajuda disposição e paciência, foi essencial em todos os momentos, se tornou um verdadeiro amigo nessa jornada do doutorado. A equipa de engenheiros do LNEC que contribuíram diretamente e indiretamente na pesquisa Paula Miguel, Isabel Martins, Manuel Vieira, Arlindo Gonçalves, Sofia Ribeiro, João Custódio e André Monteiro.

Aos amigos e colegas da Universidade Federal de Uberlândia, em especial a técnica Cristine Pires, pela ajuda e disposição e ao Goubyan Borges, pela amizade e companheirismo desde os tempos de faculdade.

Aos amigos e colegas do PECC, ao grupo de pesquisa da professora Eugênia: Paulo Francinete, Lívia Agostinho, Thyala Cunha, Paulo Reis e Juliana Borges. Ao grupo de pesquisa do professor Evangelista, NEXUM. Aos amigos de sala: Jéssica Souza, Jéssica Borges, Iago, Nelson e Carlos. Agradecimento em especial a Jéssyca Mendes por ser uma verdadeira amiga em todas as horas, inclusive longe.

Ao professor Ole Mejlhede pela doação do polímero.

Ao Erich da Empresa Grace, pela doação dos aditivos ADVA e CONCERA.

A CAPES, pelo suporte durante todo o doutorado e pela bolsa de doutorado sanduíche em Portugal.

RESUMO

AUTO CICATRIZAÇÃO DE CONCRETO DE ALTA RESISTÊNCIA COM POLÍMEROS SUPER ABSORVENTES USADOS PARA O CONTROLE DA RETRAÇÃO AUTÓGENA

Autora: Karyne Ferreira dos Santos
Orientadora: Eugênia Fonseca da Silva
Programa de Pós-graduação em Estruturas e Construção Civil
Brasília, março de 2021.

O material autocicatrizante é uma tecnologia recente para aumentar a durabilidade das estruturas e reduzir os custos de manutenção. Atualmente, encontra-se sob investigação o uso de polímeros superabsorventes como agente cicatrizante autógeno. Além disso, o uso de polímeros superabsorventes já está consolidado para controlar a retração autógena. No entanto, para concretos de alta resistência, onde SAP é usado principalmente para mitigar a retração autógena, há uma lacuna no potencial de auto cicatrização desses polímeros. Este estudo teve como objetivo investigar o grau de cicatrização que um polímero superabsorvente com a função de controlar a retração autógena pode atingir em concretos de alta resistência. A pesquisa foi dividida em duas etapas, uma desenvolvida no Brasil para investigar um concreto de alta resistência com reforço de fibra de aço para controlar a abertura da fissura, e outra em Portugal investigando um concreto sem adição de fibras. Na primeira etapa, o conteúdo SAP máximo foi avaliado com base nos testes de resistência à compressão e trabalhabilidade. Testes de tração direta com correlação digital de imagens foram conduzidos para investigar os mecanismos de fissuração das fibras de aço com SAP. Na segunda etapa, foram avaliadas a retração autógena e as propriedades mecânicas do concreto sem fibras e, em seguida, desenvolvida uma nova metodologia de fissuração. Com base nesta metodologia, foram investigadas quatro formas de avaliar a auto cicatrização: recuperação mecânica, fechamento de fissuras por imagens microscópicas, testes de permeabilidade ao ar e à água. Com base nesta metodologia, foram avaliados dois teores de SAPs (0,3% e 0,6%) para uma fissura de 200 µm e ciclos diários de molhagem e secagem por quatro meses, com duas idades de fissuração (7 e 28 dias). A metodologia foi validada e pode-se concluir que é simples e fácil de ser implementada em outros laboratórios, de baixo custo e com alta repetibilidade, pode isolar o efeito do agente de cicatrização sem a interferência do reforço da fibra. A metodologia de fissuração produziu uma única fissura no tamanho desejado em um padrão linear e uniforme, apresentando mínima influência com o material e mantendo a largura da fissura durante o processo de cicatrização. Os resultados mostraram um baixo nível de cicatrização para uma fissura com 200 µm durante os quatro meses de ciclos de molhagem e secagem diários. A adição de SAP para controle da retração autógena apontou para um pequeno aumento nas propriedades de auto cicatrização.

Palavras-chave: polímero superabsorvente, auto cicatrização, concreto de alta resistência, método de fissuração, retração autógena.

ABSTRACT

EXPERIMENTAL STUDY OF HIGH STRENGTH CEMENTITIOUS MATERIALS MODIFIED WITH SUPERABSORBENT POLYMERS (SAP) AS INTERNAL CURING AGENTS

Author: Karyne Ferreira dos Santos
Supervisor: Eugênia Fonseca da Silva
Post-Graduate Program on Structures and Civil Construction
Brasília, March 2021.

Self-healing material is a recent technology to increase the durability of structures and reduce maintenance costs. Currently, the use of superabsorbent polymers as an autogenous healing agent is being under investigation. Additionally, the use of a superabsorbent polymer is already consolidated to control autogenous shrinkage. However, for high-strength concretes, where SAP is used primarily to mitigate autogenous shrinkage, there is a gap in these polymers' self-healing potential. This study aimed to investigate the degree of healing that a superabsorbent polymer with the function to control autogenous shrinkage can achieve in high-strength concrete. The research was divided into two stages, one developed in Brazil to investigate a high strength concrete with steel fiber reinforcement to control crack width, and the other in Portugal investigating a concrete without fiber addition. In the first stage, maximum SAP content was evaluated based on the compressive strength and workability tests. Direct tensile test digital image correlation was conducted to investigate the effect of SAP on the steel fibers' crack-bridging mechanisms. In the second stage, the autogenous shrinkage and mechanical properties were evaluated, and then a new cracking methodology was developed. Assed on this methodology, four ways to assess self-healing were investigated: mechanical recovery, crack closure by microscopic images, air and water permeability tests. Based on this methodology, two SAPs contents were evaluated (0,3% and 0,6%) for a crack of 200 μm and daily wetting and drying cycles for four months, with two cracking ages (7 and 28 days). The methodology was validated, and it can be concluded that it is simple and easy to be implemented in other laboratories, low cost, and can be highly repeatable. It can isolate the effect of the healing agent without the interference of fiber reinforcement. The cracking methodology produced a single crack at the desired size in a linear and uniform pattern, showing minimum influence with the material and maintaining the crack width during the healing process. The results showed a low level of healing for a crack with 200 μm under the four months of daily wetting and drying cycles. The SAP addition for autogenous shrinkage control pointed to a minor increase in the self-healing properties.

Key words: superabsorbent polymers, self-healing, high strength concrete, cracking method, autogenous shrinkage.

INDEX

LIST OF TABLES

LIST OF FIGURES

LIST OF SYMBOLS, NOMENCLATURE AND ABBREVIATIONS

G_F	Total fracture energy
E	Young's modulus
E_m	Matrix Young's modulus
σ_{cc}	Stress rupture of the material
δ_m	Matrix crack opening
δ	Crack opening
σ_{fc}	First crack opening
σ_0	Crack-bridging stress
σ_{ss}	Stable crack growth stress
δ_{ss}	Plane crack opening
J_{tip}	Crack tip tenacity
σ_0	Maximum bonding stress
σ_{yy}	Normal stress
τ_{yx}	Shear stress
τ_{yz}	Antiplane shear stress
σ-w	Stress vs crack opening graph
σ-ε	Stress vs strain graph
L_{ch}	Characteristic crack length
f_t	Tensile strength
W_0	Under curve area of the stress x crack opening graph
P_0	Maximum load at 3-point bending test
u_0	Maximum deflection at the 3-point bending test
A^*	Angular coefficient of line that describes the linear part of the graph obtained in the test
$v(\alpha_0)$	Dimensionless value of the geometry dependency and contour conditions.
$\sigma_{\substack{máx \\ 1ª\ crack}}$	Maximum stress of the first crack

$\sigma_{\text{unload, pre cracking}}$	Unload stress of the pre cracked sample
$\sigma_{\text{máx stress, after self healing}}$	Maximum stress after cracking and exposed to healing procedure
k_i	Permeability coefficient measured after pre-cracking
k_f	Permeability coefficient measured after the sample is exposed to self-healing conditions
W_i	Initial crack opening after pre cracking
W_r	Residual crack opening after the sample is exposed to self-healing conditions
w/b	Water/binder ratio
w/b_{Basic}	Basic water/binder ratio
w/b_{Total}	Total water/binder ratio

Abbreviations

ABNT	Brazilian Association of Technical Standards (Associação Brasileira de Normas Técnicas)
ACI	American Concrete Institute
AFt	Ettringite
ASTM	American Society for Testing and Materials
C_3A	Tricalcium Aluminate
HSC	High Strength Concrete
$CaSO_4$	Calcium Sulfate
CMOD	Crack Mouth Opening Displacement
COPPE	Alberto Luiz Coimbra Institute of Post graduate Studies and Research in Engineering (Instituto Alberto Luiz Coimbra de Pós-Graduação e Pesquisa em Engenharia)
COST	European Cooperation in Science and Technology
C-S-H.	Calcium Silicate Hydrate
DIC	Digital Image Correlation
DIN	German Institute for Standardization
RXD	X Ray Diffraction
DTU	Technical University of Denmark
AE	Acoustic Emission
ECC	Engineered Cementitious Composite
EDS	Energy-dispersive
EN	European Standards
FHWA	U.S Federal Highway Administration
FPZ	Fracture Process Zone
FRC	Fiber Reinforced Concrete
HPFRC	High Performance Fiber Reinforced Concrete
HPSFRC	High Performance Steel Fiber Reinforced Concrete
CCI	Crack closure index
SHEMR	Self-healing mechanical recovery index
DRI	Durability recovery index

JCI	Japan Concrete Institute
JSCE	Japan Society of Civil Engineers
LNEC	Portuguese National Laboratory for Civil Engineering (Laboratório Nacional de Engenharia Civil)
LVDT	Linear Variable Differential Transducer
SEM	Scanning electron microscope
PVA	Polyvinyl acetate
RILEM	International Union of Laboratories and Experts in Construction Materials, Systems and Structures
SAP	Superabsorbent Polymers
SARCOS	Self-healing As prevention Repair of COncrete Structures
TEMAC	Theory of the Meta Analytical Consolidated Approach
TG	Thermogravimetric Analysis
T_{int}	Intermediate SAP content
$T_{máx}$	Maximum SAP content
UFRJ	Federal University of Rio de Janeiro (Universidade Federal do Rio de Janeiro)
UFU	Federal University of Uberlandia (Universidade Federal de Uberlândia)
UnB	University of Brasília (Universidade de Brasília)

1 INTRODUCTION

During the second half of the twentieth century, there was a significant improvement in technology and new materials, which influenced the construction and building engineering. High-strength concrete (HSC) development was one of these innovations, which started to be used in the 1960s. However, the compressive strength of 50 MPa of the first HSRs seemed modest by current standards. It should be remembered that the commercial water reducers available at that time were based on lignosulfonate. In the late 1960s, superplasticizers were used for the first time in concretes almost simultaneously in Japan and Germany, exceeding the resistance of 60MPa (ACI 363R, 2005; ZIA, 1991).

Currently, the American Concrete Institute (ACI) defines HSC as concrete with a specified compressive strength of 55 MPa or higher. In Brazil, according to the ABNT NBR 8953: 2015 standard, the compressive strength should range from 55 up to 100 MPa. However, according to ABNT NBR 6118: 2014, the use of HSCs in structural projects is only allowed until 90 MPa.

In order to produce HSCs, the water/cement (w/c) ratio should be reduced, and the mixture must have proper workability. Thus, to achieve such conditions, it is usually needed to adjust the aggregate particle size, use mineral additions and superplasticizers. Thus, a dense internal concrete microstructure with a refined pore structure is created. However, the low w/c ratio, the inclusion of some supplementary cementitious materials (e.g., silica fume), associated with higher cement consumption, result in a significant increase of autogenous shrinkage in conventional concrete.

The autogenous shrinkage phenomenon occurs inside the cement paste due to the rapid development of porous and thin networks. The internal desiccation due to the hydration generates a high capillary tension, which may lead to cracking in concrete, compromise its structural integrity, and negatively affect the durability; in some cases, the damage may even completely restrict its use.

Remarkably, the advent of HSCs is only convenient if associates with durability-related aspects. Therefore, some alternatives to prevent the macro cracks should be studied and implemented in concrete, aiming to increase the durability.

Several alternatives have already been studied to prevent cracking due to autogenous shrinkage, including size and distribution control of cement particles, as well as the use of shrinkage reducing admixtures, expansive cements, soaked porous aggregates and superabsorbent polymers (SAPs). Among them, the use of SAPs to promote the inner curing of high strength concrete showed the most effective results and continues to be the target of investigation in the world.

According to Lee *et al.* (2016), for a successful application in civil engineering structures, new materials need to meet many criteria, including accessibility, availability, robustness, durability, performance in a variety of exposure environments, chemically inert, and low toxicology. SAP is a promising class of materials that potentially meets these criteria.

SAPs have an intrinsic property of absorbing moisture and fluids from the environment. These hydrogels can increase up to 500 times their size, retaining the liquid in their structure without dissolving. A state-of-the-art report on the applications of superabsorbent polymer in concrete was published by RILEM TC 225-SAP by Mechtcherine and Reinhardt (2012). This topic is still a target of RILEM's active committee, the 260-RSC: Recommendations for the use of superabsorbent polymers in concrete construction.

In Brazil, Manzano (2016), Silva Junior (2017), and Reis (2019) proved that the use of superabsorbent polymer mitigates or even eliminates autogenous shrinkage. Enough contents of SAPs may even prevent concrete from cracking by autogenous shrinkage. However, the use of these polymers can decrease the compressive strength of concrete. Therefore, their use must be restricted to a minimum amount that mitigates the autogenous shrinkage. For a w/c ratio of 0.3 at 28 days and an SAP content of 0.3% concerning cement mass, Manzano (2016) found a 97% decrease in autogenous shrinkage. For a 0.35 w/c ratio at 28 days, the reduction was 100% for the same SAP content.

The primary mechanism of the polymer is to promote the internal curing of concrete. Thus, a hypothesis was assumed that this polymer might perform internal curing and promote the self-healing of the concrete as soon as the cracks appear throughout its lifespan by hydrating anhydrous cement and forming new hydrates.

An intrinsic problem of concrete is its low tensile strength, which causes most structures to crack. A crack formation affects the durability of the material due to the entry of harmful agents through them and can affect the ability to resist the stresses of the structure.

The crack opening control is a crucial aspect of improving the performance of concrete. That could lead to reducing the need for maintenance and rehabilitation of structures, which are costly. Another negative point associated with cracking is that, although several techniques and methods have been developed to inspect cracks, they are often inaccessible or invisible, such as in underground and infrastructure structures, so as bridges and highways (MECHTCHERINE and REINHARDT, 2012).

According to Freyermuth (2001), repair and maintenance costs are approximately half of the annual construction budget. Likewise, Yunovich and Thompson (2003) claimed that the cost of bridge reconstruction in the United States is estimated between $ 20 billion to $ 200 billion, while the annual maintenance average of these bridges is in the order of 5,2 billion dollars.

Even though the Brazilian data is not available to access, and the portion of these costs associated with the cracking occurrence is not accounted for, the expenses may also take on an equally or even greater relevant proportion of Brazil's wealth. The tropical climate, mainly characterized by high humidity, helps propagate water and harmful agents' entry into the concrete.

In contrast, the improvement in the durability of concrete structures reduces the demand for new structures. This also decreases the use of raw materials and consequently reduces pollution, energy consumption, and CO^2 production.

In this scenario, the development of concrete that can self-regenerate, minimizing maintenance and repair operations can bring significant economic and ecological benefits

to the country. For this reason, self-healing concrete has attracted the attention of researchers, but it is still a very recent topic, which the potential and proof of efficiency are still under discussion (DE ROOIJ *et al*., 2013; FERRARA *et al*., 2018; DE BELIE *et al*., 2018).

Pioneering studies proposing SAP as a concrete healing agent have been showing promising. There are two mechanisms: blocking cracks by swelling SAP (sealing) and filling cracks with hydrates from the hydration of anhydrous cement (self-healing) by the interaction of SAP as an internal curing agent. These concepts are detailed in Chapter 2.

The first researchers were Tsuji *et al.* (1998) and Tsuji (1999), who proved the sealing of cracks. Soon after, the concept was better explained and developed by Lee *et al.* (2010) *et al.*, Snoeck *et al.* (2012), Snoeck *et al.* (2014), Lee *et al.* (2016), Araujo *et al.* (2016), and Gruyaert *et al.* (2016) that proved the material's self-healing.

These studies indicated that self-healing depends directly on the crack size of the concrete. Moreover, to control the crack size was used fiber reinforced concrete. The associate use of two different self-healing strategies, the conjunction of SAP with fiber reinforcement, was expected to obtain durable concrete with the ability to seal and heal cracks. To isolate effects, it was also desired to study self-healing without fiber reinforcement. However, there is not yet a methodology that produced a uniform and linear crack to investigate the self-healing properties of a non-fiber reinforced concrete.

Only one research group works on self-healing with superabsorbent polymers and publishing recent articles (2012-2020). The approach for this team at Ghent University in Belgium is to focus on concrete healing independent of the compressive strength. The results obtained by Snoeck *et al.* (2014) were promising concerning self-healing, despite the strength of the concrete decreased considerably with the addition of levels higher than 1% of the superabsorbent polymers. This may occur due to the voids caused by the use of SAP with large granulometry increasing the size of the voids.

In Brazil, at the University of Brasília (UnB), SAP has been researched since 2008. The research group has been developing studies on mitigating strategies for autogenous shrinkage in high-strength concretes, having already produced: a book chapter (TOLEDO FILHO *et al*., 2012); three doctoral theses (REIS, 2019; SILVA

JUNIOR, 2017; MANZANO, 2016) five master's dissertations (BORGES, 2019; AGOSTINHO, 2017; SANTOS, 2016; COUTO, 2015; SUAREZ, 2015; ORDÓÑEZ, 2013); articles published in international journals (REIS, EVANGELISTA JUNIOR and SILVA, 2020; CUNHA *et al.*, 2016; LOPES *et al.*, 2013; MECHTCHERINE *et al.*, 2013) and articles published in several national and international congresses (CUSTODIO *et al.*, 2019; FRANCINETE JÚNIOR *et al.*, 2019; SANTOS *et al.*, 2019; AZAMBUJA *et al.*, 2019; REIS *et al.*, 2018; SANTOS *et al.*, 2017; SANTOS *et al.*, 2016; MANZANO *et al.*, 2015; MANZANO *et al.*, 2014; SILVA *et al.*, 2014; GONZALEZ *et al.*, 2014; TRALDI *et al.*, 2014; SILVA *et al.*, 2013a; SILVA *et al.*, 2013b; ORDOÑEZ *et al.*, 2013; ORDOÑEZ *et al.*, 2012; SILVA *et al.*, 2012; LOPES *et al.*, 2012; SILVA *et al.*, 2011a; SILVA *et al.*, 2011b; SILVA *et al.*, 2011c; SILVA *et al.*, 2010; SILVA *et al.*, 2008).

The Brazilian research group has proven that the SAPs developed by the research group from Denmark led by Professor Ole Mejlhede Jensen are more suitable for construction applications. The smaller particle size, adequate swelling, and water release time provided by these SAPs ensured a better behavior, verified by Manzano (2016), Santos (2016), and Silva Junior (2017). As a result, this polymer has been studied and used extensively by this research group. It is believed that the use of this polymer can produce durable concrete with better mechanical properties than those shown by Snoeck *et al.* (2014).

There are few studies regarding self-healing in concrete in Brazil. Among them, the most relevant are: Oliveira (2019), whose research focused on the influence of crystalline admixtures on the self-healing of cracks in cementitious systems for oil wells, and Moreira (2017), who studied the self-healing of HSCs with steel and sisal fibers, both performed at COPPE - UFRJ. It is worth mentioning that Moreira (2016) studied the effect of the permeability-reducing admixture in concretes with different types of Portland cement and the contribution to the self-healing processes developed at the University of Brasília. Other studies in Brazil were carried out by Takagi (2014) and Cezario (2017).

In conclusion, it is worth emphasizing that the present thesis is the first work in Brazil of self-healing concrete using superabsorbent polymer, with partnership of the Portuguese National Laboratory for Civil Engineering, LNEC in Portugal. This study

aimed to verify the self-healing of high-strength concrete with the addition of superabsorbent polymers used to mitigate autogenous shrinkage. The work was structured into seven chapters. Each chapter is a self-contained document, following a typical paper structure. The Pilot Study shown in Chapter 4 is already published in Santos *et al*. (2020).

Chapter 2 presents the literature review, with an overall perspective that deals with SAPs in HSCs applications, concrete self-healing, techniques, methodologies for evaluating self-healing, self-healing in fiber-reinforced concrete (FRC). Moreover, presents a literature review based on the consolidated meta-analytical approach's theory focusing on the self-healing concrete with SAPs.

Guided by the literature review Chapter 3 presents the research proposal, the general and specific objectives of this work, brief of the methodology, and the characterization of all the experimental program's raw materials.

The methodology and results were divided into two phases. The first one focused on steel fiber reinforced concrete (SFRC) evaluated in Brazil (Chapter 4). The second one referred to HSC without the fibers performed in Portugal, where the autogenous shrinkage was investigated (Chapter 5). A new approach for the self-healing evaluation was proposed in Chapters 6 and 7.

Chapter 4 focuses on developing HPCs with steel fibers and SAPs. A mixture had to contain the highest possible SAPs content and classified as HSCs. Two self-healing techniques were combined to improve the effects of SAPs and steel fibers. It was desired to obtain a strain hardening behavior to control the crack width, so the hydration of the anhydrous cement by the water released from SAP is sufficient to produce enough hydrates to self-heal the crack.

Chapter 5 investigates and confirms the concrete mix design with Portuguese materials and the maximum SAP content with the concrete still being high strength. It also verifies the mitigation of the autogenous shrinkage of the new concrete mixture in the different SAP contents.

Chapter 6 presents the new cracking methodology developed for cementitious materials and evaluating strength recovery after the self-healing phenomenon.

Next, Chapter 7 exhibits the self-healing evaluation based on durability parameters. Adaptations of the water and air permeability tests were performed in fractured sections of the new cracking approach.

Chapter 8 gives the conclusions, presents an overview of the problems and future research perspectives.

Finally, Chapter 9 shows the bibliography.

2 LITERATURE REVIEW

Abstract

It is known that concrete has a self-healing capacity and that superabsorbent polymers can reduce autogenous shrinkage by mitigation self-desiccation and can also promote internal concrete curing. Both topics are still relatively recent, deserving increasing publications and new research.

This chapter presents a comprehensive review of the use of superabsorbent polymers in concrete to autogenous shrinkage control and a general understanding of self-healing in concrete toward interconnecting these subjects in the meta-analysis.

A systematic literature review using the consolidated meta-analytical approach theory (TEMAC) was performed, to find and correlate all the relevant information regarding the SAP and self-healing concrete. The main results of this analytical approach are presented in the following section. It was concluded that the self-healing results, due to the SAP particles, have significant dispersion, and that the techniques for accurately determining the crack closure are not yet sufficiently developed or are too expensive.

Therefore, there are several knowledge gaps still to be filled in, especially concerning the size of the cracks that can be healed by SAP. There are different polymers that can be used as superabsorbent materials, but only a few of them have been investigated for the self-healing phenomena. In addition, in most studies SAP was used in combination with fiber reinforcement, and the SAP's contribution is difficult to isolate. Nevertheless, it was possible to understand the mechanisms of SAP to seal cracks. Some studies show that, over time, SAP can provide conditions for completely heal and close cracks.

2.1 Superabsorbent polymer for autogenous shrinkage control

One intrinsic property of the high strength concrete is a dense microstructure with fine pores. Because of that, the HSC tends to exhibit significant autogenous shrinkage. A brief description of this phenomenon is presented in this section to explain the

mechanisms by which the superabsorbent polymers act to mitigate the autogenous shrinkage to acceptable levels.

Autogenous shrinkage can be understood as the volume reduction of the cementitious system after the solid-suspension transition, without water loss to the external environment, also disregarding thermal load and load deformations. This phenomenon occurs due to the decrease of free water in the pores, which is consumed in the hydration reactions, as well as is adsorbed on the surface of the newly formed C-S-H crystals. Therefore, this causes a decrease in the internal relative humidity (relative vapor pressure above a meniscus) in the capillary pores partially filled with water (here understood as pore solution), leading to tension in the liquid according to Kelvin and Young-Laplace equations. This phenomenon is known as self-desiccation (BENTZ and JESEN, 2004, SILVA, 2007). The tension in the liquid is balanced by compressive stresses in the solid body, causing shrinkage.

According to CEB / FIP (1991), in autogenous shrinkage, the smaller the pores, the greater the tension in the capillary liquid (in the Young-Laplace equation, tension is inversely proportional to the pore radius). And consequently, the volumetric reduction is more prominent. Hence, when the microstructure of the paste is more refined, the autogenous shrinkage is higher. For normal strength concrete, the internal desiccation is usually negligible due to the higher water/cement, but for HSC, internal desiccation can cause stresses of higher magnitude than that caused by desiccation due to external drying.

Several methods have been investigated to mitigate autogenous shrinkage. The general solution that stands out is the internal cure through materials such as light porous aggregates, wood derivatives, fine recycled materials, and superabsorbent polymers (SAPs). In high-strength concretes, the use of SAPs has become the most efficient and promising strategy to mitigate the autogenous shrinkage.

In the early 1980s, superabsorbent polymers were developed. The first use of these materials was in the production of disposable diapers. They belong to a group of polymeric materials that can absorb and retain a large amount of liquid without dissolving. These polymers can have a water absorption of up to 5000 times their weight in an aqueous environment. However, in solutions with diluted salts, the absorption

capacity is reduced to between 50 and 100 grams of solution for each gram of polymer (JENSEN and HANSEN, 2001; FRIEDRICH, 2012; ASSMANN, 2013).

There are several types of superabsorbent polymers, the most known commercially are polyacrylates interconnected by cross-covalent bonds and copolymerized polyacrylates/polyacrylamides (JENSEN and HANSEN, 2001). Buchholz and Graham apud Mönnig (2009) classify superabsorbent polymers according to their ionic or non-ionic nature. The ionic group can still be subdivided into anionic and cationic polymers (MÖNNIG, 2009).

SAPs exist in two distinct states, dry (also called collapsed) and swollen (JENSEN and HANSEN, 2001). According to Mönnig (2009), the swelling process is quite complex. The mechanisms for transporting water into the superabsorbent polymer particles involve osmotic pressure, electrostatic interaction, entropy, capillary action, and Coulomb interaction.

One of the most important parameters for the swelling of SAP is the salinity of the aqueous solution. The ions in solution change the inter and intramolecular interactions of the polyelectrolytes due to the protection of the polymeric chain charges. Besides, as the concentration of ions outside the polymer increases, the osmotic pressure inside the gel decreases and, consequently, leads to a reduction in the swelling of the polymer (JENSEN and HANSEN, 2001; LURA *et al.*, 2012). This parameter is required in the sealing mechanism of the self-healing concrete, as we will see later. In the cementitious mixture, the polymer swells less due to the ions present and then, with the supply of pure water, the polymer swell more and thus may block the crack.

The polymer grain size also influences its absorption capacity. According to Jensen and Hansen (2002), there is an optimum dimension for the particle size of the polymer. The authors suggest that the optimal dimension is approximately 100 μm in the swollen state. Particles much larger or much smaller than this optimum size are less effective in mitigating autogenous shrinkage.

In addition, if the polymer inclusions are large, they may not be able to fully supply all parts of the cement paste with water during hydration. The larger particles of the polymers may also show a reduction in the efficiency of water absorption due to

insufficient time for absorption during mixing. On the other hand, if the polymer inclusions are small, their effects in reducing shrinkage can be partially offset by filling with hydration products or have reduced absorption due to a less active surface area compared to the whole (JENSEN and HANSEN, 2002; LURA *et al.*, 2012).

Esteves (2010) presented results that confirm that the particle size of the superabsorbent polymer significantly influences both the amount of solution absorbed and the rate of absorption. Polymers with the ideal dimensions to mitigate the autogenous shrinkage have not yet been studied for the self-healing concrete, but it is believed that these dimensions also improve the material's internal cure.

The desorption kinetics of the superabsorbent polymer in a cement paste depends on the properties of the polymer, the kinetics of hydration reactions, the microstructure of the paste and the interface between the cement paste and the polymer, through which water transport occurs (LURA *et al.*, 2007b).

According to Lura *et al.*, (2007a), when the self-drying of the cement paste begins due to hydration reactions, a gradient of water activity within the concrete between the water inside the polymer and the pore solution is generated. Part of this gradient of water activity is established by the capillary pressure developed in the pore solution as a result of emptying the pores due to hydration or drying (LURA *et al.*, 2003; WEISS *et al.*, 2008).

An additional contribution comes from the osmotic pressure since the composition of the pore solution during the setting and hardening of the paste may be different from the solution initially absorbed by the polymer during mixing. The polymer desorption process can be described as a competition for water between the polymer and the cement paste (MÖNNING, 2009).

Manzano (2016) proposed a schematic model of the polymer's mechanism of action, associated with the three hydration stages of the calorimetric curve method (TAYLOR, 1997), which is shown in Figure 1.

Figure 1 a) shows the concrete constituents (cement, aggregates, and SAP), in dry conditions. To simplify the illustration, the shape of the cement particles was considered

spherical, also three SAP particles of different diameters (10µm, 20µm, and 40µm) were evenly distributed.

Figure 1 b) displays the initial hydration period, where there are dissolution and hydration of Tricalcium Aluminate (C_3A) and Calcium Sulfate ($CaSO_4$), forming ettringite (AFt). In this period, the SAP particle, right after the addition of the mixing water, swells by water absorption. For simplification and better examination of the SAP effect, only one polymer particle with a dry diameter equal to 10µm was represented.

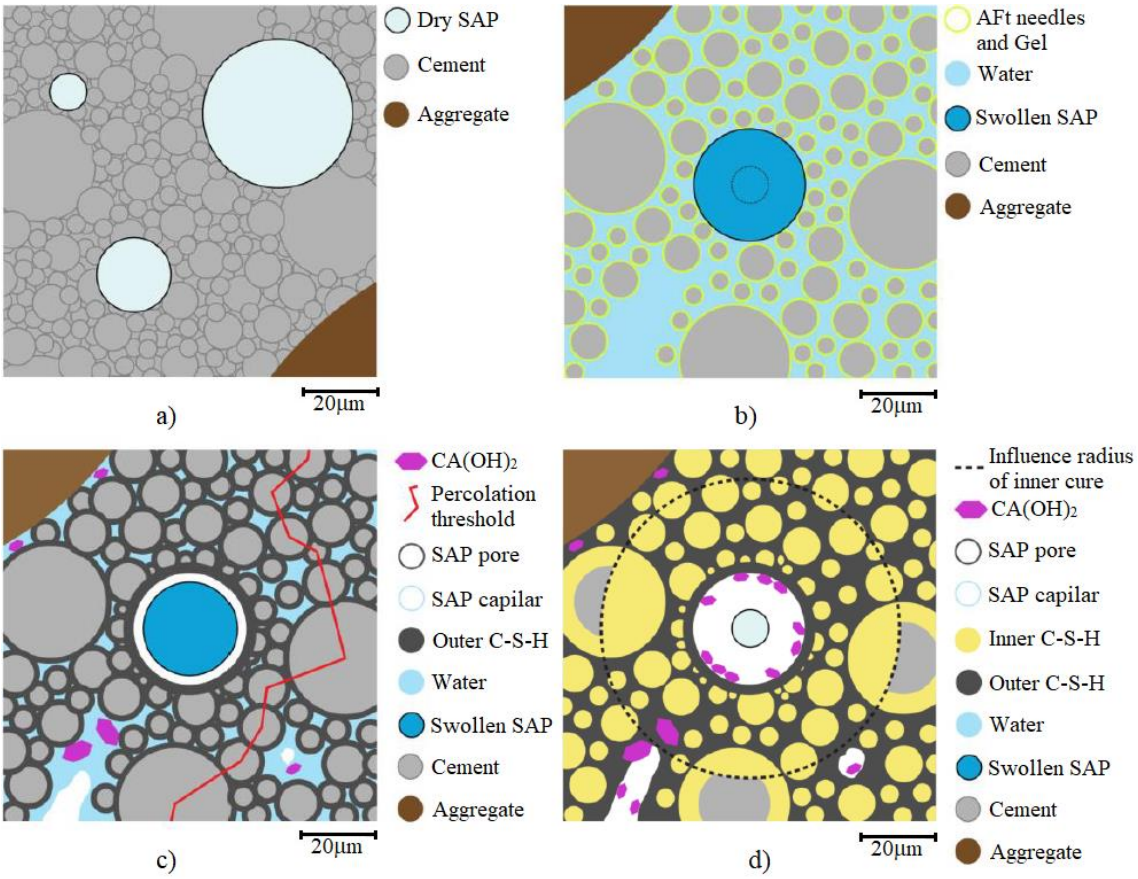

Figure 1 - Schematic model of the SAP action mechanism as internal curing agent in HSC: a) Mixing the dry concrete components; b) Adding water to the mixture; c) During setting, and first hours; d) final hydration period, days after concrete hydration. Source: Manzano (2016).

Figure 1 c) represents the evolution period of the hydration reactions, when the main constituents of cement react with water and forming mainly outer hydrated calcium silicate (C-S-H) and calcium hydroxide. The outer C-S-H sheets around the anhydrous grain particles bond and form the first solid path, starting the hardening phase of the

material, this moment may be considered as the beginning of suspension-solid transition or level of percolation (time zero).

From that moment on, when some solid-like behavior can be assumed, cavities may appear arising vapor pressure. In low water/cement mixtures the relative humidity decreases due to the continuous hydration process (while water is available) causing the development of autogenous shrinkage. However, the presence of SAP changes the scenario, as the relative humidity decrease in the cementitious matrix may be hindered due to desorption of internal water from the polymer particle. This release of water into the cementitious matrix around the SAP particles prevents the emptying of capillary pores and the liquid depression under a meniscus (capillary tension), preventing the self-drying and promoting further hydration.

Finally, Figure 1 d) illustrates the final hydration period, all the water is consumed in the reactions and the capillary porosity of the concrete is formed. The hydration products formed near the surfaces of the anhydrous cement grains prevent diffusion through the layers and then the internal C-S-H is formed. The polymer releases all the internal curing water, and it is predicted a radius of influence of the internal curing from the polymer particle, represented by dashed circumference, where the self-drying of the cement matrix was mitigated. A void is created at the location where the SAP particle was located.

It is believed that the internal cure promoted by SAP, is capable of self-healing the cracks in the concrete, due to formation of new CSH gel and calcium carbonate from the hydration of remaining anhydrous cement particles. As we will see next, the self-healing mechanism will involve the swelling process of the SAP and the subsequent hydration of anhydrous cement.

The main objective of using superabsorbent polymer in high-strength concrete is to mitigate or reduce self-desiccation and autogenous shrinkage to acceptable levels. The solution of a problem must not create new ones. Therefore, when the superabsorbent polymer is added to the concrete, it is very important to know how this component influences the other properties, especially the compressive strength. For instance, studies by Jensen and Hansen (2002), Mechtcherine *et al.* (2006) Piérard *et al*. (2006) showed

that the addition of SAP to the mixture reduces the compressive strength of pastes, mortars and concretes.

Attentive to the decrease in compressive strength, in some studies (KUMM, 2009; MECHTCHERINE *et al*., 2013; MANZANO, 2016) comparisons were made of mixtures containing superabsorbent polymer with a reference mixture (without polymer) with a water/cement ratio equal to the total water/cement ratio of the polymer mixture, as the loss of strength may be due to the increase of water/cement ratio caused by the addition of extra water for internal curing. The total water/cement ratio is the sum of the incorporated water/cement ratio and the basic water/cement ratio. Therefore, the authors consider that the comparison is more appropriate and does not penalize mixtures with the polymer. However, maintaining the same total water/cement ratio, with and without polymer, provides concretes with different workability, unless the dosage of superplasticizer is changed. In self-healing studies using SAP, this analysis has not yet been done. The mixtures are compared with the basic water/cement ratio, the method also used in this study. However, for future studies, it is suggested that additional reference mixtures should be produced with a water/cement ratio equal to the total water/cement ratio of the polymer mixture.

2.2 Concrete self-healing

Self-healing concrete is an innovative technology that has a direct relationship with the durability of concrete. This concrete was developed to avoid or minimize costs with maintenance and repair of structures.

For instance, Figure 2 (a) expresses a model of the relationship between time and the performance of a traditional structure. The durability of a building can be expressed through a correlation between durability performance and the required structural performance.

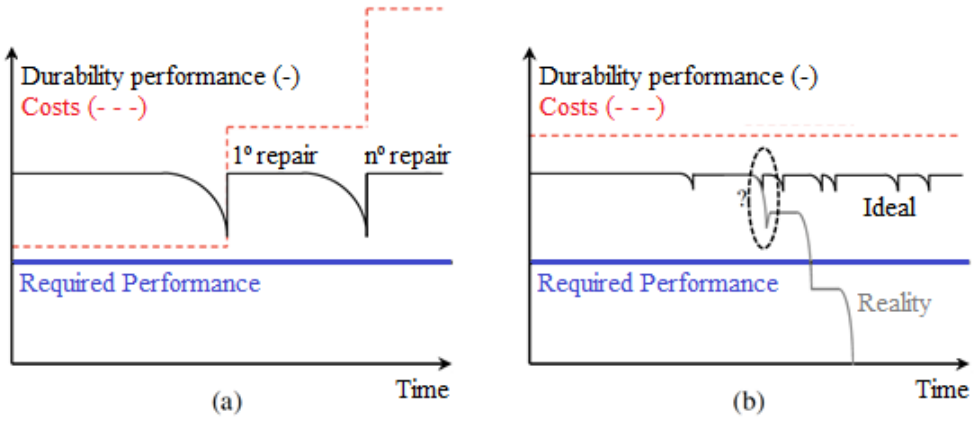

Figure 2 - (a) Durability and costs as a function of time with the necessary manual repair interventions in a traditional structure; (b) Durability and costs as a function of time for an ideal self-healing material, and in gray the current reality. Source: Van Breugel (2007).

When the durability performance is lower than requested, for example, associated with a large crack opening, there is an increase in the speed of degradation of the structure. If the failure is not noticed and repaired, the construction may cease to be suitable for its use, and, at the limit, may collapse.

To increase durability and rehabilitate the structure, preventive work is required. The dashed curve illustrates the magnitude of the relative costs. Eventually, costs gradually increase over time due to these interventions and the need for monitoring (Van Breugel, 2007). However, if an ideal self-healing material were used, durability could be guaranteed, without human intervention, shown in Figure 2 (b).

Currently, there are about a thousand scientific articles on self-healing of concrete, most of them published between the years 2015 to 2020. In the last three years, this research field almost doubled the number of publications, and the growing interest tends to increase, being the recent project called SMARTINCs, financed by the European Union, a good example of this development. Also, some independent committees to study the subject were formed, three of them stand out for their relevance: JCI Technical Committee in Japan TC-075B, RILEM TC 221-SHC Technical Committee, and the Organization “Self-healing As prevention Repair of COncrete Structures” (SARCOS) in Europe.

TC-075B worked from 2007 to 2009, and this committee produced the first state of the art published by researchers Igarashi, Kunieda, and Nishiwaki (2009). This

committee focused on autogenous self-healing in cementitious materials. The first definitions concerning autogenous healing were established by this committee, which was later updated by RILEM. In this thesis, the most recent definitions from RILEM and SARCOS committees were used, published by Ferrara *et al.* (2018) and De Belie *et al.* (2018).

The RILEM Technical Committee TC 221-SHC, published a second state of the art in the subject, entitled “Self-healing phenomena in cement-based materials” by Rooij *et al.* (2013). Different definitions for self-healing concrete, using the terms "autogenous" and "autonomous" were proposed. Additionally, a set of methods to evaluate self-healing in concrete was published. Nevertheless, it was concluded from this committee that there is no standardization, nor universal tests, for the evaluation of self-healing in concrete, requiring further studies in the area.

Currently, RILEM has another committee on the subject called TC SHE: Self-healing concrete - Its efficiency and evaluation. This will address, from two points of view the efficiency and evaluation of self-healing concrete, due to damage and due to protection functionality recovery. The work of this committee aims to create recommendations for test methods to evaluate these two matters.

The Self-healing As prevention Repair of COncrete Structures (SARCOS) organization was created to bring together European researchers to provide synergy and multiply the effect of individual efforts. To do so, the European Cooperation in Science and Technology (COST), financed this project with the affiliation of the University of Cambridge and RILEM. This association intended to effectively promote the concepts of self-healing and related technologies in the market.

There were three research fronts: WG1, which aimed to elaborate preventive repair solutions; WG2 investigated the characterization techniques and WG3 that performed numerical modeling.

SARCOS published three review papers, two of them, Ferrara *et al.* (2018), and De Belie *et al.* (2018), addresses the WG1 and WG2 fronts, describing experimental methods and techniques to characterize and quantify the self-sealing and self-healing

capacity of cement-based materials, also reporting the correlation between crack closure and recovery of mechanical properties.

Furthermore, Jefferson *et al.* (2018) discussed the WG3 front, presenting research progress on numerical models for self-healing cementitious materials, providing a summary of the mechanical models, transport processes in materials with embedded healing systems, fully coupled models and other modeling techniques used to simulate self-healing behavior. With these articles, it was concluded that only through an effective domain of technology knowledge, it is possible to transfer to the market the proper standards, test methods, and design guidelines.

SARCOS will end in 2021, and a new project was born in 2020, the SMARTINCS - Ph.D. Training Network on Self-healing Multifunctional Advanced Repair Technologies in Cementitious System, funded by the European Commission (H2020 program). The purpose is to train a new generation of creative and entrepreneurial early-stage researchers in the prevention of deterioration of (i) new concrete infrastructure by innovative, multifunctional self-healing strategies and (ii) existing concrete infrastructure by advanced repair technologies.

2.2.1 Autogenous concrete self-healing

According to Rooij *et al.* (2013), self-healing is any process by the material itself involving the recovery and hence improvement of a performance after an earlier action that had reduced the performance of the material.

This mechanism can be autogenic when the recovery process uses materials components that could otherwise also be present when not specifically designed for self-healing (own generic materials). And it is autonomic when the recovery process uses materials components that would otherwise not be found in the material (engineered additions), (ROOIJ *et al.*, 2013). According to De Belie *et al.* (2018), the autogenous ability to heal cracks can also be stimulated through additions that promote healing.

Inspired by the self-healing of plastics and polymers, the autonomic systems that received the most attention were those that incorporated a material foreign to concrete, dispersing chemicals in response to crack formation. Based on this method, they are

autonomous encapsulated self-healing, performed with microcapsules or macro capsules; self-healing mechanisms activated by heating devices; vascular self-healing systems; bioconcretes where microorganism excreted minerals and healing occurs (ROOIJ *et al.*, 2013); (DE BELIE *et al.*, 2018). They are not the scope of this work and will not be covered in this review.

The French Academy of Sciences in 1836 verified the first record that concrete has a natural ability to heal cracks. Cracks in tubes and water retention structures were noted over time to be healed (HEARN *et al.*, 1998). In the last century, there was extensive research focusing on autogenous self-healing described by Mihashi and Nishiwaki (2012), Rooij *et al.* (2013), Van Tittelboom and De Belie (2013) and Snoeck (2015), including both theoretical and experimental approaches. It was concluded that the phenomenon of autogenous healing is mainly related to complex physical, mechanical and chemical interferences within the matrix.

There are five main mechanisms and their combinations that govern autogenous healing, illustrated in Figure 3. These were investigated by Edvardsen (1999), Hearn (1998), Neville (2002), Ter Heide (2005), Granger *et al.* (2007), Van Breugel (2007), Yang (2008), Homma *et al.* (2009) and Jia *et al.*, (2010).

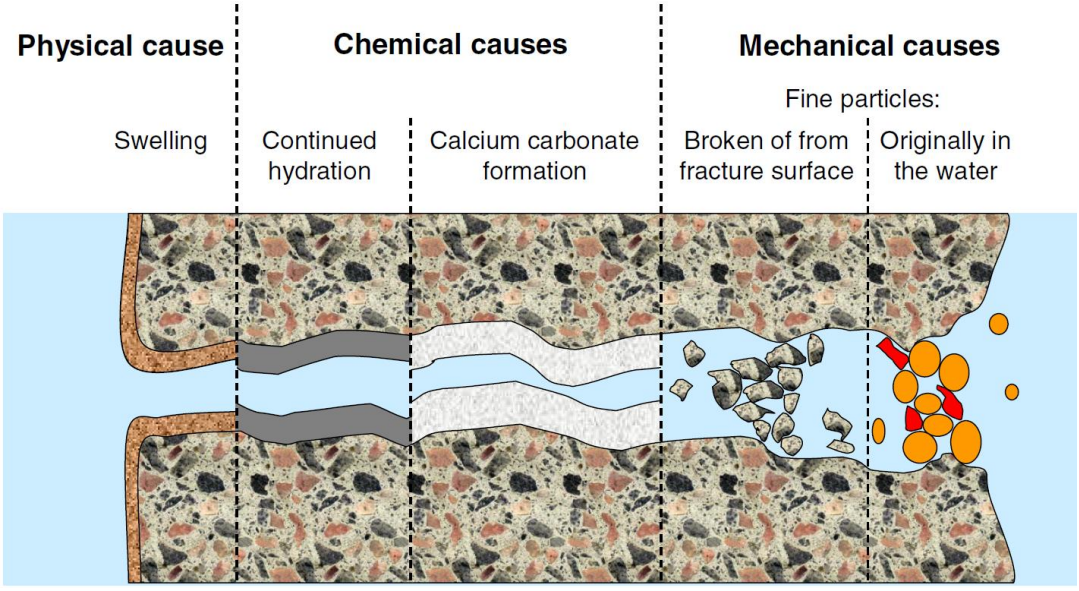

Figure 3 - Different healing mechanisms responsible for autogenous healing. Source: Rooij *et al.* (2013).

The first mechanism is physical, the matrix may expand due to swelling of calcium silicate hydrates (C-S-H). The second is the hydration of anhydrous cement grains, present on the surface of the crack. Part of this mechanism is also the reaction of supplementary cementitious materials, such as fly ash or blast furnace slag, which can react even more through pozzolanic or latent hydraulic activity. The third is the formation of calcium carbonate, the carbon dioxide dissolved in water reacts with Ca^{2+} ions, present in the concrete matrix, to form calcium carbonate crystals ($CaCO_3$).

The fourth and fifth mechanisms are mechanical, loose particles or impurities block the crack. These can occur in two ways; they can be debris originating from the crack or they can be fragments that come from the water that penetrates the crack.

According to Nishiwaki and Mihashi (2012), Rooij *et al.* (2013), Tittelboom and De Belie *et al.* (2013), Snoeck (2015) and De Belie *et al.* (2018), among these five mechanisms, two are more significant in the healing of cracks, which is the continuous hydration of non-hydrated cement forming C-S-H crystals and calcium carbonate formation. A white material that fills the crack, when the pH is above 8, the precipitation of calcium carbonate occurs through Equations 1 to 3 (EDVARSEN, 1999).

$$CO_2(\text{gaseous}) + 2\ OH^-(\text{aqueous}) \rightarrow CO_3^{2-}(\text{aqueous}) + H_2O(\text{liquid}) \quad (1)$$

$$Ca^{+2}(\text{aqueous}) + CO_3^{2-}(\text{aqueous}) \rightarrow CaCO_3(\text{solid}) \quad (2)$$

$$CO_2 + 2\ OH^- + Ca \rightarrow CaCO_3 + H_2O \quad (3)$$

For the pH between 7 and 8 (EDVARDSEN, 1999), $CaCO_3$ precipitation occurs according to Equation 4:

$$Ca^{2+} + HCO_3^- \rightarrow CaCO_3 + H^+ \quad (4)$$

According to Edvardsen (1999), crack closure is dependent on the width of the crack and the water pressure, but it is independent of the type of water. The crystallization of calcium carbonate is primarily controlled by the surface of the crack, nevertheless, the Ca^{2+} ions are consumed over time. This way, the precipitation becomes controlled by diffusion, therefore the Ca^{2+} ions need to migrate through the cementitious matrix. Because of that, the second phase is evidently much slower than the initial one. In the

case of a composite cement containing pozzolanic additions, part of the calcium hydroxide, identified as the main source of Ca^{2+} ions, is used in the pozzolanic reaction, specifically for the development of C-S-H, this leads to a slower and weaker carbonate calcium precipitation capacity.

From the studies by Mihashi and Nishiwaki (2012), Rooij *et al.* (2013), Tittelboom and De Belie *et al.* (2013), Snoeck (2015) and De Belie *et al.* (2018), it can be summarized that the autogenous healing mechanisms are efficient only for small cracks, smaller than 100μm. However, a wide range of crack sizes that can heal above 100 μm have been reported, sometimes up to 200 μm but less than 300 μm, and only in the presence of water. Autogenous self-healing is difficult to predict due to the dispersion of results, which are influenced by several factors and parameters. The main influencing factors are the age of the concrete, concrete composition, the presence of water during healing, the width, and the shape of the concrete crack.

For this research, crack size was established taking into account the high dispersion of the literature results, the difficulty to control crack opening, and the lack of technique that controls with precision the crack size. In the first stage of the present study, it was decided to work with cracks width from 100 μm to 200 μm. As for the second phase, a new technique to control crack opening and produce a uniform crack without the fiber reinforcement was developed, and the crack width of 200 μm was chosen.

2.2.2 Stimulated autogenous self-healing

Stimulated autogenous healing contains methods to improve the effectiveness of autogenous healing. Some of these methods are alternatives to restrict the size of cracks, such as the incorporation of fibers or reinforcement, additions that provide hydration and internal curing of the concrete, additions that stimulate the production of healing products.

Among these types of healing are the following: use of mineral additions; use of crystallizing additives; use of fibers to restrict crack width, and to cause the effect of multi-cracking; and use of the superabsorbent polymers. The last two techniques will be explained in detail in item 2.4 Self-healing of concrete reinforced with fibers and in item 3 State-of-the-Art.

Most studies on the effects of mineral additions on self-healing relate mainly to the use of blast furnace slag and fly ash. It is sought, through an increase in the content of additions, that there is enough material to promote healing at older ages, since significant amounts of these additions remain unhydrated for a long time. The pozzolanic reaction, specific to siliceous or siliceous and aluminous additions (fly ash, silica fume, calcined clay, etc.), as cementitious materials can complement the continuous hydration of cement grains in the long-term, also through the development of C-S-H products, and consequently, improving the level of autogenous self-healing (DE BELIE *et al.*, 2018).

Crystalline admixtures received particular attention as chemical additives to promote self-healing due to their availability and use in the construction industry. They have the primary function of reducing the permeability of concrete. However, the compositions of these additions are not disclosed. In general, crystalline admixtures are products formed by "active chemicals" generally mixed with cement and sand, with highly hydrophilic behavior. They react in the presence of water, forming insoluble precipitates that block pores, increasing C-S-H density, and resistance to water penetration (FERRARA, KRELANI and CARSANA, 2014; FERRARA, KRELANI and MORETTI, 2016; CUENCA and FERRARA, 2017).

2.2.3 Techniques to evaluate concrete self-healing

There are many ways to promote the self-healing of concrete, but these procedures differ significantly. According to Ferrara *et al.* (2018), it is necessary to evaluate the effectiveness of the different self-healing technologies concerning the material properties and the intended application. In order to have a basis for comparison and verify efficiency, it is necessary to standardize self-healing techniques. For this, three general approaches are used:

- Evaluation of the recovery of mechanical properties over time.
- Verification based on the recovery of durability properties.
- The observation of crack closure and characterization of the healing material.

These investigations must take into account a set of multiple experimental variables that include:

- The initial crack size opening and the age at which the cracks were formed.
- The healing conditions and its duration.
- The presence of sustained load throughout the healing period, which results in the crack under stress states during the healing process.
- The repeatability of the healing action and its effectiveness as a result of successive repeated cracking phenomena, in the same and/or in different places.

Regardless of the self-healing approach used, it is needed to perform a mechanical pre-cracking to induce one or more cracks that will be evaluated in the self-healing study. In order to do so, the most common techniques are a three-point bending test with or without a notch, four-point bending test without a notch, direct tensile test, tensile splitting test (Brazilian test) with or without a notch, and compression tests. Notching is a feature that can be used to induce the crack in a particular place of the specimen. Table 1 exhibits which tests are most suitable for the type of concrete concerning the fiber reinforcement.

Table 1 - Summary of pre-cracking techniques for different classes of cementitious composites. "Common" indicates that the test has been frequently reported in the literature. "Possible" indicates that the test is possible but insufficiently documented. Source: Ferrara *et al.* (2018).

Type of test	Plain Concrete	Fiber-reinforced Concrete (FRC)	High Performance Fiber-reinforced Cementitious Composites (HPFRCC)
Compression	Common	Possible	Possible
Direct tensile	Difficult, hardly ever employed	Possible but not commonly employed	Common due to strong tensile strain hardening behavior. Multiple cracks will form.
Tensile splitting	Common	Common	Possible
3- or 4-point bending	Common	Common	Four-point bending is most common. Allows formation of multiple cracks in the central part of the specimen
Pre-slip between fiber and matrix	Not applicable	Common	Possible

Methods that evaluate the crack closure are described in Table 2, which shows their advantages and disadvantages. Most of them only visually estimate of the crack closure. With visual observation, it is possible to detect hydrates formed on the surface, but not those formed inside where the crack may remain hollow, without any healing product. When this occurs, the images provide positive information about the self-healing phenomena, but the results of the strength recovery may diverge, as inside there is no material that interconnects the fractured surfaces.

Table 2 - Methods to evaluate crack closing. Source: Ferrara *et al.* (2018).

Method	Advantages	Disadvantages
Photographic cameras	- Largest area of visualization. - Allow acquisition of data during testing. - Easy continuous monitoring for fast self-healing methods.	- Generally, needs certain distance to cover the whole specimen. - Less detail for a specific crack.
Light microscopy (optical, digital and stereo)	- Cheap and easy to implement. Easy preparation of samples. - Visualization of the surface crack as seen by the eye but at improved resolution, while showing natural colors. - Larger area visualization. - Good results for 0.05–0.30 mm cracks.	- Not able to evaluate internal crack width. - Not able to evaluate composition of precipitates.
Polarized and fluorescence functions for light microscopy	- High contrast in the borders between matrix and voids or cracks. - Allows identification of crystalline solids from optical properties.	- Needs time-consuming preparation of samples with polarized epoxy or fluorescence filter sets
Electron microscopy	- Allows complementary tests of the composition of precipitates, e.g., by EDX. - Generally, focus on small size cracks. - Good for verifying autogenous healing.	- Expensive compared with light microscopy techniques. - Only in grey scale depending on the atomic number of the element.
Fibre optic sensing	- Predetermination of crack locations are not required. - Reveals time-variation of crack widths. - Non-destructive and absence of radiation risks.	- Delicate specimen preparation works with embedded Sensors. - Risk of damaging the sensors
Tomography and CT-scans (X rays and neutron)	- Internal crack evaluation, in the damage and healing stage. - Allows the differentiation by densities of the materials. - In the case of neutron tomography, high sensitivity for hydrogen detection, good for analysis of water uptake.	- Extremely expensive and low availability of equipment. - Health and safety hazard due to radiation risks. - Time consuming. - High resolution only for small samples.
Electrical methods	- Reveals time-variation of crack width. - Can be applied to specimens and structural elements under load. - Non-destructive	- May require dedicated and expensive equipment and suitable post-processing model to correlate electrical measure with crack width.

Nevertheless, for most structures, the goal of using the self-healing phenomena is to recover strength but to improve durability properties. For most structures, the desire is to improve the service life, and for that, it is necessary to prevent water and other agents

from entering the concrete. Even though the critique of the self-healing phenomena is mainly happening on the surface, it is still a good result and can prevent the concrete from deteriorating and the steel to corrode. Therefore, it is still essential to perform durability tests, such as described in Table 3.

Table 3 - Review of test methods to determine healing and recovery of durability properties after repairing (Source: Van Tittelboom and De Belie (2013), and Souradeep and Kua (2016) apud Ferrara *et al.* (2018)).

Test	Purpose	Limitations
Water permeability (low/high pressure)	Water permeability coefficient can be determined by flow of water through healed cracks	Effectiveness depends on how the cracks were formed
Sorptivity	Concrete's ability to absorb and transmit liquid through it by capillary suction	Needs a reference sample as water uptake happens also from the undamaged matrix. Absorption ''driving force" under debate (capillary forces in smaller cracks?). Multidimensional effects in water uptake not adequately taken into account.
Air permeability	The rate of air flow, after healing, is an indirect measure of resistance against moisture/foreign substance penetration through (healed) cracks.	Very sensitive to the specimen composition: methanol can dissolve organic polymers used as healing agents.
Chloride diffusion and penetration	Measurement of resistance against chloride penetration. Relevant and applicable for coastal structures or structures exposed to de-icing salts.	Good correlation between the water permeability and rapid chloride ion permeability so far demonstrated only for specimens with w/c higher than 0.40.

Among the techniques presented, to investigate the self-healing of high strength concrete to assess the recovery of strength, it was chosen the direct tensile test. Furthermore, to address the durability aspect, water permeability test, air permeability tests, and the evaluation of crack closure by optical microscope were chosen.

2.2.4 Self-healing of fiber reinforced concrete (FRC)

In self-healing research, it is necessary to restrict the crack size and to control its crack opening in order to know the level of damage formed in the concrete and, consequently, determine a size in which the crack can heal. Therefore, the first approach

of this study was to use fibers to control cracking. Later on, a new method to control the cracks was implemented in Chapter 7.

There are two main applications for the use of fibers in a conventional fiber reinforced concrete: to control the shrinkage cracking (if used in low volume percentages: for example, 0.2-0.3%), and partial or complete replacement of some type of traditional reinforcement, with the fiber volume percentages varying between 0.5 to 1%.

With high percentages of fiber volume (between 1% and 2%), improvements in mechanical performance can be obtained. Including obtaining a behavior called "strain hardening" defined by Naaman and Reinhardt (1995), under direct tension, with the formation of multiple cracks, characterized by the formation of an extra stretch in the stress-strain curve. In this phase, the increase in strain causes multiple cracks in the material. This is because the fibers are not being pulled out but transferring stresses to the concrete and causing new cracks.

The mechanism consists of the concrete suffering its rupture for stress (σ_{cc}), also called of first cracking stress. After formation of the first crack, in the weakest section, the stresses previously supported by concrete in this section are now supported by the fibers. With sufficient amounts of fibers, there is neither pull-out nor yielding in the fibers. Being able to withstand an additional stress, fibers transfer stresses to concrete, and a new crack is formed. The continuation of this process results in multiple cracks until a maximum point, where there is the maximum stress (σ_{pc}). At this point, the softening branch begins, where among the various cracks formed, only one will significantly open until the material breaks. In this branch, the deformation of the material is mainly controlled by the crack opening.

In the case of concrete reinforced with fibers, for the study of self-healing, there are three premises to be verified: the presence of self-healing agents, intrinsic or not, enough fiber volume to control cracking and the control of the fiber orientation, concerning the requesting efforts (FERRARA *et al.*, 2011).

Sell-healing in HPFRC is more attractive than in conventional fiber-reinforced concrete that is rarely used, although it is possible. The main reason for that is the multi-cracking characteristic led to high deformation capacity, keeping the width of a single

crack below 100 μm or less, improving ductility, increasing damage tolerance as well as increasing the capacity to dissipate energy (FISHER and LI, 2002); (FUKUYAMA and SUWADA, 2003) and (SAHMARAN and LI, 2008). The Rilem TC 208 - HFC committee gathered several studies proving the high durability of the HPFRC, published by Van Zijl and Wittmann (2010).

Within the HPFRC class, a new type of material called "Engineered Cementitious Composites" (ECC) was developed by Professor Victor Li of University of Michigan and his collaborators, Li and Stang (1997), Yang (2008) and Yang *et al.* (2009), which obeys micromechanical laws based on the work of Marshall and Cox (1988) specially developed to promote stable multi-cracking. The fundamental requirement for being an ECC is to have strain hardening behavior and stable propagation of micro-cracks arising from defects in the matrix under tension. The micromechanical theory is based on two criteria, strength and energy.

The strength criterion ensures that the fiber connects the microcracks and transfers the stresses of an imperfect section. Specifically, this criterion, shown in Equation 5, requires that the first crack stress (σ_{fc}), controlled by the matrix's toughness and the size of its defects, be less than the stress required to overcome the fiber's bonding capacity with the matrix (σ_0) in any cracking plane. This criterion is worth mentioning to choose the fiber type according to the tensile strength of the matrix.

$$\sigma_{fc} \leq \sigma_0 \tag{5}$$

The energy criterion is necessary to promote multiple cracking in a stable manner. To avoid rupture due to a single crack, which is a more complex mechanism and can be seen in the work of Li and Stang (1997), Yang (2008) and Yang *et al.* (2009).

Most of the ECCs produced in Professor Li's studies use PVA fibers, from the company Kuraray, with a 1.2% oil coating, with 2% of fiber content in volume. The objective was to increase the complementary energy by flattening the $\sigma(\delta)$ relation. The result was a moderate tensile strength, between 4-6 MPa, and extremely high ductility of 3-5% of deformation. In these composites, there is a synergic effect between fibers,

matrix, and interface, that maximizes the tensile ductility of the material. Usually, the crack size is 20 to 100 μm.

Several studies have already proven the self-healing effect on ECCs developed with PVA fibers with 1.2% oil coating. Among which the one that stands out is the work of Herbert and Li (2013), who managed to heal cracks under environmental conditions. Cracks smaller than 50 μm were healed entirely, while cracks larger than 150 μm showed partial healing.

As the ECC with PVA fibers presents stable multi-cracking, the PVA fiber was identified as the most used fiber in self-healing studies, in a total of 41% of all studies about self-healing with fibers. However, other types of fibers can also be used, according to Cuenca and Ferrara (2017): steel (12% of the total studies), natural fibers (12%) to promote internal cure, polypropylene (12%) and glass (5%).

For high-strength concretes, the steel fiber is more suitable due to the strength criterion shown in Equation 5. A stronger matrix requires a stronger fiber/matrix bond or greater fiber volume. The decrease in the bond between the PVA fibers and the cementitious matrix, in order to meet the energy criterion, is a limitation for the increase in the fiber/matrix bond. An increase in the volume of PVA fibers significantly decreases the workability of the material.

However, steel fiber presents a problem that still needs to be investigated, which is the corrosion of steel fibers when the crack is exposed to water under curing conditions (GARAS *et al.*, 2009; ROSSI *et al.*, 2014; FERRARA, 2015.)

2.2.5 Self-healing application in cementitious materials

The main challenge to investigate the self-healing of plain concrete is the pre-cracking technique. The original crack, without the filling material, must remain open in a specific width for the entire healing process, which can take months to years.

The use of plain concrete is mostly seen in autonomous self-healing studies, where they use the shape of the capsules containing the healing agent to control the crack width.

The capsules can be shaped like fibers, tubes, vascular network, or even wires that will be activated to reduce the size and close the crack.

Moreover, in some large-scale applications, for autonomous studies such as Van Mullen *et al.* (2020), Tsangouri *et al*. (2019), Davies *et al.* (2018) and Tittelboom *et al.* (2016), steel bars as reinforcement for slabs and large beams are used. The pre cracking is performed with three or four-point bending tests or with concentrated load in a slab.

However, these tests present the problem of producing cracks without a uniform width, forming a triangle, making it difficult to reach the targeted size and healing evaluation. Additionally, the autonomous mechanisms depend on the size and shape of the crack; therefore, this technique has limitations for the purpose of the present study and is not used in this research.

As explained in the previous section, the addition of fibers was considered the most common way to control the crack width for autogenous self-healing. Though fibers interfere in the self-healing results, they act as points of nucleation for the healing products (C-S-H, $CaCO_3$, and $Ca(OH)_2$), as shown in Figure 4. Because of that, fibers are classified as stimulated autogenous self-healing since they are beneficial for the self-healing phenomena. However, this classification may disguise the real results presented by other healing agents, such as SAP (RAJCZAKOWSKA *et al*., 2019).

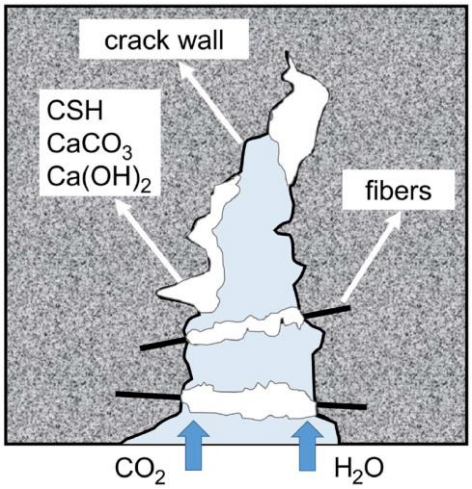

Figure 4 – Autogenous self-healing, fibers acting as stimulated self-healing, nucleation to form healing products. Source: Rajczakowska *et al.* (2019).

Besides, fiber reinforced concrete is not always suitable for all applications. In some cases, the concrete presents very low workability and mixing, spreading and compacting the concrete is difficult. To understand the real influence of the healing agent and evaluate its efficiency, it is necessary to study the plain concrete separately, without the fiber reinforcement. This allows to understand the real effect of the healing agent on the structures.

Some recent studies were found, after starting the experimental part of this research, namely Chindasiriphan, *et al*. (2020); Park and Choi (2018) and Sidiq *et al.* (2019), reflecting the tendency to understand the autogenous self-healing phenomena without the use of fiber-reinforced concrete. Two of them, Park and Choi (2018) and Chindasiriphan, *et al*. (2020), adapted the Brazilian splitting test to produce the crack. Sidiq *et al.* (2019) developed a compressive test to produce cracks without fiber reinforcement.

Park and Choi (2018) pre-cracked the concrete through the Brazilian splitting test, using copper wire and epoxy resin so that the crack remained at a certain width, to perform water permeability tests.

In their study, 50 mm x 25 mm disk specimens were prepared. Cracks were created with the inducing method shown in Figure 5 (a). The specimens were completely separated into two pieces, and 0.2 mm diameter copper wires were inserted into the crack surface, as shown in Figure 5 (a), to maintain the crack width. Then, the separated pieces were reassembled. The peripheral parts of the specimens were then sealed with epoxy to fix the crack width. The specimens were placed in a transparent acrylic pipe to prevent variations in the crack width during the experiment, and the space between them was fixed with an epoxy resin.

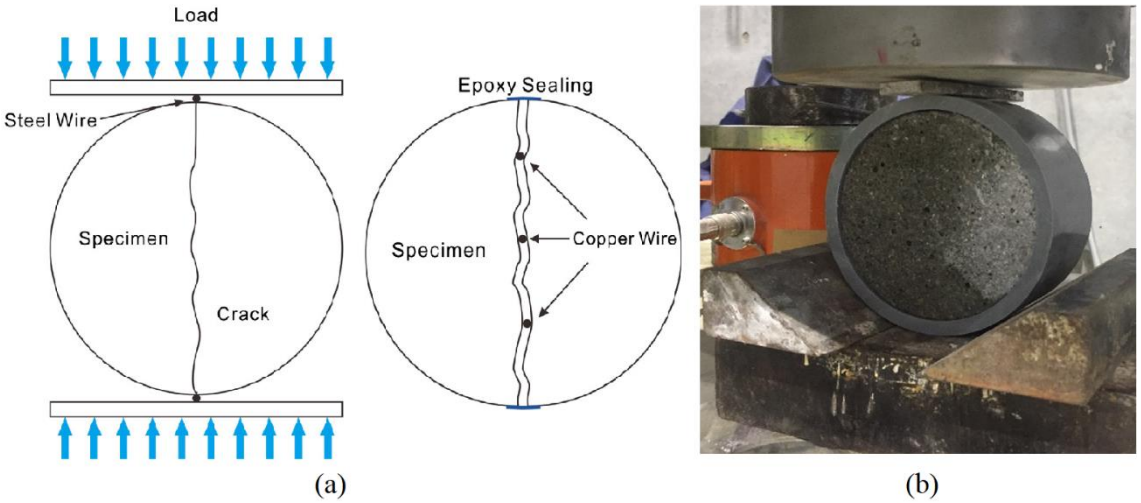

Figure 5 - Pre-cracking and preparation of the specimens to water permeability test by Park and Choi (2018). b) Splitting test with a PVC ring by Chindasiriphan, *et al.* (2020). Source: Park and Choi (2018); Chindasiriphan, *et al.* (2020).

Chindasiriphan, *et al*. (2020) also adapted the Brazilian splitting test for the pre-cracking phase, as seen in Figure 8 (b). The splitting load simultaneously deformed the PVC jacket and the specimen. The lateral confinement at failure generated pre-cracking that satisfied the control crack width of 0.2 ± 0.1 mm.

Sidiq *et al.* (2019) produced cracks by compression with an inhouse-fabricated steel mold that was used to generate internal crack patterns. Cracks were thus developed throughout the entire volume of the sample. Cracks were triggered by applying 70% of the maximum compressive strength as per initial measurement at 28 days.

Our research has developed a method based on a direct tensile test approach, using a single steel bar to ensure the intended crack size. The method developed can be used to evaluate self-healing of autogenous cementitious materials, and it is combined with water and air permeability tests.

2.3 Systematic literature review using the consolidated meta-analytical approach theory

This item aims to identify the state of the art of research on self-healing of concrete using superabsorbent polymers. For this, exploratory research with a quantitative approach was carried out through the Theory of the Consolidated Meta Analytical Approach - TEMAC, by Mariano and Rocha (2017).

There are three stages of the TEMAC method: Stage 1- Preparation of the research; Step 2 - Presentation and interrelation of data and Step 3 - Detailing, integrating model, and validation by evidence.

Step 1 was established by answering questions about the search term, time frame, and database. Search terms were: “healing”; “concrete”; “superabsorbent”; and “polymer”. The databases were Web of Science and Scopus. The timeframe was not defined in order to identify all studies, including the oldest ones.

Sixty-three articles were found in the Web of Science database and 50 articles in the Scopus database, combining a total of 80 different articles on the topic, indexed in the databases between 2012 and 2020. In the past two years, the number of papers has doubled, showing the growing interest in the subject.

Until the beginning of this research in 2017, the topic had about 30 papers predominantly publications from the Ghent University in Belgium.

However, when updating the search, there was an expansion of authors and diversity of institutions, also showing the increase of the interest in the subject but revealing new trends and divergent results.

With the VOSviewer software, heat maps were created, presented in Figure 6, Figure 7 and Figure 8, facilitating the visualization and the relationship between the main authors, the countries that most published, and the most relevant articles, respectively.

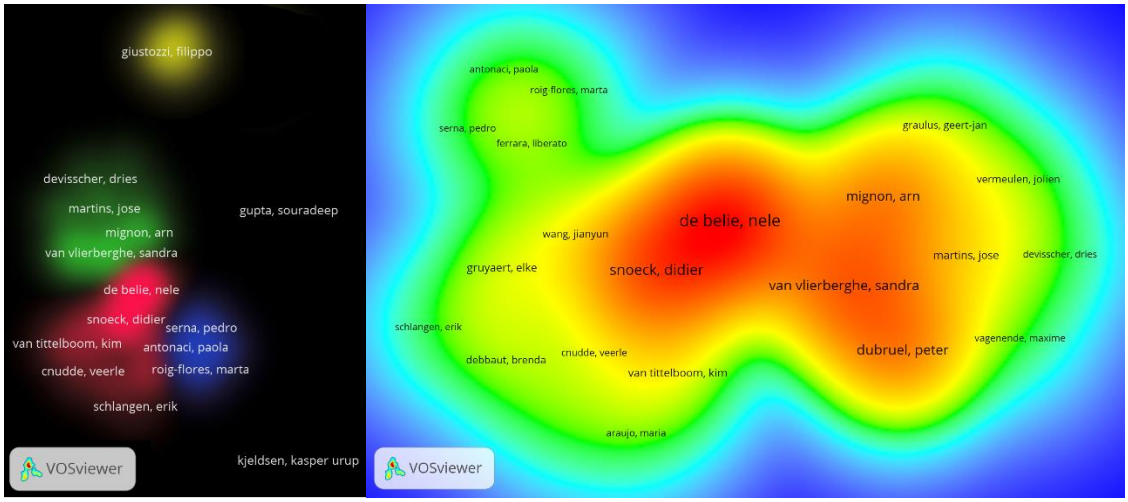

a) b)

Figure 6 - a) Global heat map listing the authors who most publish and the relationship as they publish together; b) Zoom at Europe heat map listing the authors who most publish and the relationship as they publish together. Source: The author himself. Extracted from VOSviewer.

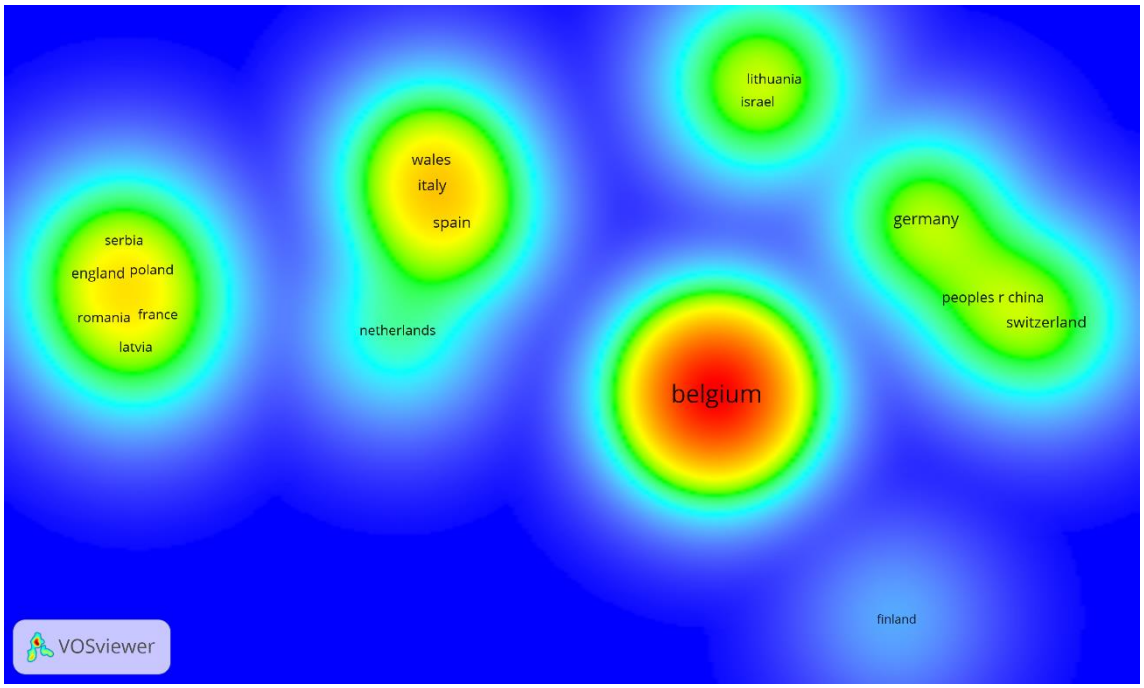

Figure 7 - Heat map listing the countries that most publish together. Source: The author himself. Extracted from VOSviewer.

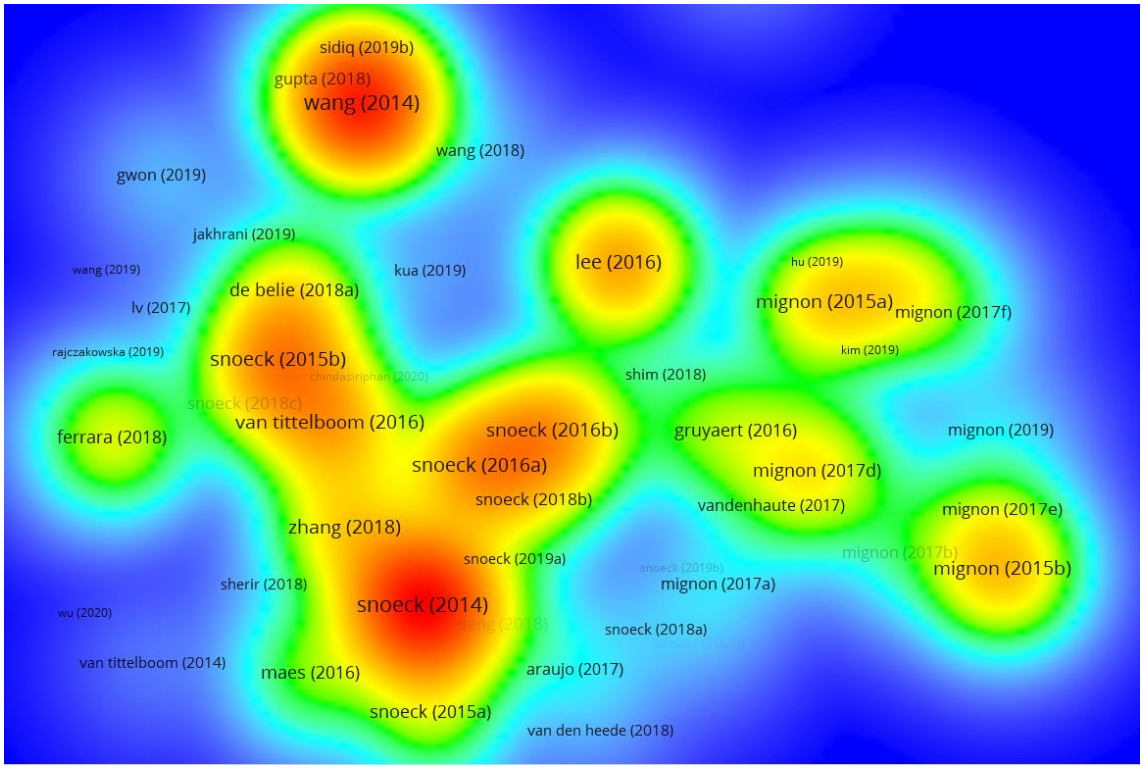

Figure 8 - Bibliographic coupling heat map. Source: The author himself. Extracted from VOSviewer.

The program created six clusters, presented in Figure 6 a. Three of them, the green, the red, and the blue, are formed by authors that presented interconnected publications. To better understand this relationship, Figure 6 b presents a zoom of these 3 clusters and shows the leading authors on the field, that are from European institutions, most of them participating in the SARCOS organization and the RILEM 221-SHC committee.

As for the three independent clusters showed in Figure 6 a, the yellow stands out for the research of Professor Filippo Giustozzi of the Royal Melbourne Institute of Technology - RMIT in Australia concerning modified polymers for asphalt pavement. This author's articles are out of the scope of the superabsorbent polymers for concrete. In the heat maps of Figure 7and Figure 8, there is no mention of Australia or any of his articles.

Concerning the other two independent authors, Gupta Souradeep and Kasper Urup Kjeldsen, are from Singapore and Denmark, respectively. Both of them are working with bacteria inserted in the superabsorbent polymers for self-healing purposes. Gupta (2018) presented relevant research that showed closure of cracks with 700 µm when the concrete is combined with biochar immobilized spores and SAP reinforced with PP fibers,

observing an improvement in strength by 38% and reduction in water penetration and absorption by 65% and 70%.

This line of research is presented in Figure 8, with the most cited paper by Wang (2014) from Belgium, that showed that concrete with spore bacteria and superabsorbent polymers exhibited maximum crack healing of 500 µm and water permeability decrease of 68% while using SAP without bacteria presented a maximum crack heal of 300 µm and an average water permeability decrease of 55%. Also, this nucleus displayed the review paper of Sidiq (2019), which analyzed the available self-healing approaches focusing on the efficiency of healing materials of biotechnological (bacteria), polymeric and chemical components for crack healing and improvement in strength. This approach represents one of the future research lines of using SAP in concrete with bacteria, showing prominent research, as shown in these papers.

Regarding Figure 6 a, the blue cluster presented the main authors: Pedro Serna, Marta Roig-Flores, Liberato Ferrara, and Paola Antonaci. The focus of this group was the general review of the self-healing phenomena, citing super-absorbing polymers as one of the techniques. The most relevant publication of this cluster is the Ferrara *et al*. (2018), also seen in a separated cluster in Figure 8. It can also be seen in Figure 7 that the countries of Spain, Italy, Netherlands, and Wales are presented together since they are the nationality of the authors of this review cluster since they are also SARCOS members.

As for the green and the red cluster (Figure 6 a), they are mostly from Ghent University in Belgium. However, they are distinguished in two clusters because they express two different approaches for the self-healing with superabsorbent polymers.

The red Clusters, with the authors: Nelie De Belie, Didier Snoeck, and Kim Van Tittelboom, exhibits the primary approach to understand the self-healing phenomena promoted by superabsorbent polymers. The principal author is Didier Snoeck, who developed the first thesis (Snoeck, 2015) of self-healing concrete using superabsorbent polymers, under the guidance of Prof. De Belie. Based on this investigation, the following works were presented: 23 articles in A1 journals; 2 in A2 journals; 1 in an A3 magazine; 3 book chapters, and 31 publications of C classification published. Some of these articles can be seen in Figure 8 and will be later detailed.

The study by Snoeck (2015) was extensive and exploratory. Its general objectives were to solve the problems regarding the mixing and workability of concrete when using superabsorbent polymers with PVA fibers; to develop an intelligent cementitious composite aimed at self-sealing and self-healing regardless of environmental conditions.

The study started with the selection of 10 SAPs, nine of them commercial products, and one produced by the University of Gent. The aim was to find or produce a polymer with a more pronounced response to changes in pH of the solution. Therefore, the SAP would absorb more water in an ion free medium and swallow less water in the cementitious medium. All SAPs were initially tested to verify autogenous healing, by means of strength recovery.

Among the ten selected polymers, two superabsorbent polymers were chosen to continue the study of healing and sealing properties, one of sodium acrylate acrylamide copolymer, particle size range 100.0 ± 21.5 μm; the second is cross-linked potassium polyacrylate, particle size range 477 ± 53 μm. The geometry of the polymers was not spherical, and both were produced by BASF.

The choice of the two polymers was based on two criteria: limited reduction on mechanical properties and optimal autogenous healing based on measurements of strength recovery after healing. For the chosen SAPs, the strength recovery was also investigated in repeatable cycles, reported in Snoeck and De Belie (2016), shown in Figure 8 as Snoeck (2016b). For comparative purposes, the investigation used concrete with SAP and PVA fibers, after being subjected to two load cycles under a four-point bending test. The healed specimens were able to regain up to 75% of their mechanical properties; the second reloading of those healed samples lead to up to 66% of regain in mechanical properties.

Snoeck (2015) also carried out studies to evaluate mineral additions with the purpose of achieving the best feature for self-healing. The additions used were fly ash and blast furnace slag, and the ideal proportions and type of fiber for self-healing were investigated. It was concluded that the best addition is fly ash, with a w/c ratio of 0.3 and the addition of PVA fibers in 2% (by volume) with 1.2% oil layer.

These findings were also reported in Snoeck *et al.* (2014), which is the most cited paper on the subject. It reported the evaluation of crack sealing and healing with permeability tests as also with the recovery of mechanical properties by performing four-point-bending tests. In an environment with a relative humidity of more than 60%, only samples with superabsorbent polymers showed healing. Introducing 1 m% of superabsorbent polymer of cross-linked potassium salt polyacrylate (particle size 477 ± 53 mm) gave the best results, with no reduction of the mechanical properties in comparison to the reference, and the superior self-sealing capacity.

Advanced techniques such as neutron radiography and X-ray computed microtomography, showed in Snoeck *et al.* (2016) and Snoeck *et al.* (2018), respectively (seen in Figure 8 as Snoeck 2016b and 2018b), were used to assess permeability on a small scale. They have shown that the 477 ± 53 μm cross-linked potassium polyacrylate SAP particles efficiently sealed the sample, proving that the SAP are able to prevent the movement of water through a crack, thereby reducing the absorption of harmful substances, which can lead to longer-term durability and extended life. Cracks of up to 130 μm were completely healed when subjected to wetting and drying cycles. The main healing products were calcium carbonate, controlled by the exposed surface at first, and then controlled by diffusion, decreasing the speed of $CaCO_3$ production.

Additionally, conclusions of both studies were: wet/dry cycles exhibit the best healing as a fair amount of water is available for autogenous healing. The healing was caused by further hydration, pozzolanic activity, and calcium carbonate crystallization. The SAP specimens showed pronounced healing and cracks larger than 500 μm also show some extent of healing. At relative humidity above 90%, but below saturation, the healing is far less compared to the healing in wet/dry cycles, since there is almost no liquid water. However, specimens with superabsorbent polymers do show partial healing. The extent of healing in wet/dry cycles depends on the position along the crack depth. SAP can completely heal a shallow region at about 0 to 800-1000 μm from the surface. In the interior of the specimen, the healing amount was less.

As two-dimensional neutron radiography and three-dimensional neutron tomography were techniques that showed good results to evaluate self-sealing and self-healing techniques with superabsorbent polymers. The potential for further research

based on this promising technology was outlined and discussed by Zhang (2018), that reviewed the specific aspects of durability and deterioration of cement-based materials. It was understood from this review that neutron imaging provides a solid basis for a better understanding of deterioration mechanisms of cement-based materials, as recent improvements in neutron imaging facilities have allowed unexpected possibilities to study complex processes in cement-based materials.

In Figure 8 it can be seen a nucleus with De Belie *et al.* (2018) next to Snoeck and De Belie (2015b) and Ferrara *et al.* (2018). These studies are together because they represent reviews in self-healing concrete, being De Belie *et al*. (2018) and Ferrara *et al.* (2018) broader reviews on self-healing. Snoeck and De Belie (2015b) published a review regarding the use of different microfibers in cementitious composites for improved autogenous healing, which highlighted the potential of the strain hardening material to keep the cracks small and enhance durability; they proposed, as a future research line, a study of natural fiber reinforced concrete.

Also included in this nucleus, Van Tittelboom *et al.* (2016) presented research on two self-healing mechanisms (large-scale specimens): the use of encapsulated polyurethane and the use of superabsorbent polymers. Real-scale concrete beams (150 mm x 250 mm x 3000 mm), with and without self-healing products, were made, and the self-healing efficiency was evaluated after crack creation using the four-point bending test.

Mixtures with SAP, 1% in mass, completely healed the medium-sized cracks (width of 105 um). For cracks with larger widths (width 198 um), the crack filling was almost complete by precipitates, but some gaps were detected. For wider cracks (width 607 um) some healing was also observed. From acoustic emission analysis, it was detected a glass capsule breakage upon crack formation. X-ray tomography, fluorescent light microscopy, and thin section analysis demonstrated that cracks were indeed partially filled with healing products, calcium carbonate crystals.

Snoeck and De Belie (2019) showed results with eight-year-old concrete, and the study included an SAP A (a copolymer of acrylamide and sodium acrylate with a particle size of 100.0 ± 21.5μm, BASF) and an SAP B (a cross-linked potassium salt polyacrylate

having a particle size of 477 ± 53μm, BASF). From these eight years, the study concluded that the healing and recovery of the mechanical properties decrease over time.

As being cracked at the age of 8 years, the healing in reference samples is only a third of the healing when specimens are cracked at the age of 7 days. SAPs in a cementitious matrix seem to be stable up to 8 years, showing almost no degradation, showing as they may be effective for sealing and healing purposes up to a minimum of 8 years of construction service life, showing an increased healing capacity compared to a reference sample without SAPs.

Concerning the second line of research of the Ghent University, showed in the green nuclei of Figure 6 a and b, with Arn Mignon, Peter Dubruel and Sandra Van Vlieberghe along other research, they are focused on the chemical level of the research, namely in finding and producing an ideal superabsorbent polymer for self-healing purposes.

The main papers produced by this line of research, displayed in Figure 8, are Mignon *et al.* (2015a), Mignon *et al.* (2015b), and Mignon *et al.* (2017), whit the focus of producing a pH-sensitive SAP, ideal for concrete self-healing purposes. The idea is to produce SAP whose swelling depends on the pH of the medium, being able to swell less in an alkaline medium and more in a neutral medium. In this way, during concrete mixing the SAP would swell less due to the presence of ions in the cementitious medium, keeping the SAP particles small in size. When the crack is formed, and the SAP comes into contact with ion-free clean water, the SAP would swell more and fill the crack. Thus, the empty space produced during the production of the concrete would be smaller and the swollen in the neutral medium would be larger. In this way, the voids produced by SAP would also be smaller, decreasing the loss of strength due to the introduction of SAP in the concrete mix.

The last addressed group in Figure 8, but very significant, is the nucleus of Lee *et al.* (2016), where the developed studies explained the self-sealing of concrete with SAP. Forty samples containing SAP, with through-thickness cracks, were subjected to 0.12 wt.% NaCl at 4 m/m hydrostatic pressure gradient to simulate groundwater seepage. The

investigation showed that SAP can re-swell and seal cracks of 0.3mm cracks reducing the peak flow rate and total flow by 85% and 98%, respectively.

It is clear that the research group at Ghent University has developed very important research in this field. Since the beginning of the research in 2017, most of the studies presented in the literature are based on the results of the Ghent research group.

Nevertheless, it is important to highlight some new information that was published from 2018 to 2020, that showed progress in the self-healing field by using superabsorbent polymers. The conclusions of the new results found confirmed that this kind of technology does not work alone. That outcome was also one of the main conclusions of this research, which is that SAP can improve the concrete behavior. However, to be efficient, a high amount of SAP is needed, superior to 1%, and, with this amount of SAP, the loss of strength is significant, unless the concrete without SAP is also a low strength concrete. Alternatively, self-healing can be reached with the use of combined technologies, such as fibers, fly ash, MgO, crystalline admixtures, or bacteria.

Chindasiriphan *et al*. (2020) examined eight mix proportions with varying fly ash and SAP replacement ratios of 0, 4%, 6%, and 8% in mass. The SAP had irregular shape, and the particle sizes ranged from approximately 10 to 500 μm. Self-healing efficiency was evaluated by water permeability tests and crack closure observation by stereomicroscope. The compressive strength with 0% of SAP was 55,4 MPa; 4 % of SAP reduced by 21%; 8% of SAP reduced by 34%. For healing analyses, the specimens were preloaded to generate a crack of 200 μm to 300 μm, and these pre-cracked specimens were healed either by continuous water immersion or exposure to wet-dry conditions. Crack width decreased with the increase in the fly ash replacement ratio, whereas the higher volume of SAP stopped the water discharge through the crack by the swelling of the SAP gel. These effects, in combination, achieved a maximum of 100% crack closure and permeability restoration by 28 days of healing. As a result, the medium-term self-healing ability of concrete can be enhanced by the coupling effect of fly ash and SAP. The crack closure was found to be associated with the development of self-healing products such as calcium carbonate and C-S-H.

Hu *et al.* (2019) prepared superabsorbent CaAlg hydrogels by crosslinking Ca^{2+} and sodium alginate (NaAlg). The compressive strength of the concrete without SAP was 28MPa; the addition of 0.5 m% CaAlg caused a negligible reduction (0.014%) in the compressive strength due to the limited swelling capacity in the pore solution of this polymer when compared to the commercial SAPs. However, with 1% in mass of SAP addition, the strength had a reduction of 19%. In order to evaluate the effect of CaAlg on the self-healing of the cement composites, samples were cracked, and fractured parts with approximately 150 μm wide were selected. The prepared CaAlg shows ion-sensitive behavior due to the crosslinking reaction with Ca2+, which promoted efficient self-healing in the sodium silicate system. In addition to the self-healing effects, the Ca2+ in CaAlg increases newly precipitated CASAH, which enhances the binding force between CaAlg and the cement matrix in healed areas.

Wu *et al*. (2019) developed an ECC with superabsorbent polymer and light-burned magnesium oxide (MgO) to enhance self-healing property. SAP showed a higher ductility effect but lowered the tensile strength. This effect was also reported in the First Stage of our research with the use of steel fibers. To evaluate self-healing, the permeability test, scanning electron microscopy (SEM), and X-ray diffraction (XRD) were used. Multiple cracks lower than 30 μm were produced. The results showed that the expansion induced by the hydration of MgO makes the cracks close, while SAP provides water for further hydration even under dry conditions. The two actions can both accelerate the self-healing process of ECC. The combined addition of MgO and SAP can reduce the healing time by about 50%.

Additionally, regarding ECC with SAP addition, Deng and Liao (2018) studied self-healing in ECC with different pre-cracked levels and different curing conditions (high/low relative humidity (RH) cycle and 95% RH). SAPs made of acrylamide and sodium acrylate, in two sizes of 550 and 75 μm, with additions of 2% and 4% by weight of cement. Compressive strength without SAP at 28 days was 52.4 MPa, with the addition of 2% and 4% of SAP reduced the strength by 5% and 13%, respectively. Water permeability tests and uniaxial tensile tests were conducted to evaluate the influence of self-healing.

Results confirmed that incorporating SAPs can enhance the ductility of ECC and decrease the crack width. SAPs can accelerate the self-healing process by providing internal curing and enhance the recovery effectiveness of the mechanical performance of ECC. Without internal water, SAPs can promote continuous hydration by absorbing water from the surrounding high RH conditions. Compared with room air curing, the high/low RH cycle provided faster self-healing. Also, with more SAP particles, the faster the self-healing behavior. The water permeability of the mixture with 4% of SAP was zero after three high/low RH cycles due to swollen. The results showed that SAP can heal completely a 550 μm wide crack. Calcium carbonate, produced by the chemical reaction between calcium hydroxide on the crack surface and CO_2 in the air, is a significant self-healing product.

Park and Choi (2018) investigated the self-healing properties of cementitious materials with crystalline admixtures (CAs) and super absorbent polymers. Three types of SAP of acrylic acid powders were used, with different crushed particle size. The mean particle sizes of SAP were 541 μm, 234 μm, and 83 μm, in the dry condition. The content of 0.5% of SAP was used. Specimens were pre-cracked with a crack width of 200 to 300 μm at 7 and 28 days. The self-healing capacity was evaluated with the water flow test and the crack closing test. The water flow of specimens containing CAs decreased significantly relative to that of the plain specimen after self-healing. Large SAP particles were able to seal the crack entirely during the water permeability tests; however, the small particle size was not able to seal the crack. The results indicate that using CAs with SAPs accelerated the crack sealing. SEM observation confirmed that CAs produced more self-healing products around SAPs.

Shim, Hong and Choi (2018) investigated the autogenous healing of cementitious materials with superabsorbent polymers exposed to eight cycles of wet/dry conditions. In each cycle, cracked cement paste specimens (300 μm wide) with different SAP dosages were exposed to wet conditions for one hour, during which capillary water absorption tests were conducted, and then exposed to dry conditions for 47 h. At 28 days, the compressive strength of the concrete was of 56.1 MPa for the mixture without SAP. For mixtures with SAP addition of 0.5%, 1% and 1.5%, the loss of strength was 17%, 37%, and 51%, respectively. The test results revealed that the initial sorptivity values after one

cycle of the reference, 0.5% SAP, 1.0% SAP, and 1.5% SAP specimens decreased by 22.9%, 36.8%, 42.8%, and 46.3%, respectively, after eight cycles. X-ray micro-computed tomography analysis showed that the crack volume percentages filled with healing products were 1.1%, 1.6%, 2.2%, and 2.9% in the reference, 0.5% SAP, 1.0% SAP, and 1.5% SAP specimens, respectively. As cycling was repeated, the reduction ratio, relative to the initial sorptivity, and the volume of healing products increased with increasing SAP dosages. This study demonstrated that the incorporation of SAPs in cementitious materials could enhance the autogenous healing performances of materials exposed to cyclic wet/dry conditions.

2.4 Mechanisms that promote self-healing and self-sealing of concrete with superabsorbent polymers

The first works on this subject were carried out by Tsuji *et al.* (1998) and Tsuji (1999), who proved that SAP is able to seal cracks. Soon after, the concept was better explained and developed by Lee *et al.* (2010) et al., Snoeck *et al.* (2012), Snoeck *et al.* (2014), Lee *et al.* (2016), Araujo *et al.* (2016) and Gruyaert *et al.* (2016).

As mentioned before, pioneering studies proposing SAP as a healing agent are promising. Through these studies, it is possible to understand the mechanism of SAP as a self-healing agent when incorporated into concrete. First, SAP swells right after being added to the mixture of the fresh concrete, absorbing mixing water from the fresh concrete.

However, the swelling of SAP is less than that induced by pure water, due to ions such as Ca^{2+}, K^{+}, Na^{+} and OH^{-}, dissolved in the water of the concrete mixture, resulting in a high ionic concentration in the water in the mixture, with a high pH, in the order of 12.5 to 13, decreasing the SAP's ability to swell. Over time, cementitious materials dry up, and SAP releases water into surrounding concrete, reducing in size, and leaving voids in the material. The initial voids created by the swelling are imperfections in the material, being regions more prone to the propagation of cracks.

When cracking occurs, the polymer is exposed on the crack surface. Thus, when water penetrates the crack, or when there is a high humidity environment, water molecules brought from outside, reduce the ionic concentration in the pore solution, causing a

swelling of the SAP, higher than that initially given by the interstitial solution of the cement paste. In this way, SAP has the potential to completely block the crack, quickly preventing the entry of other liquids, with the proposed mechanism illustrated in Figure 9.

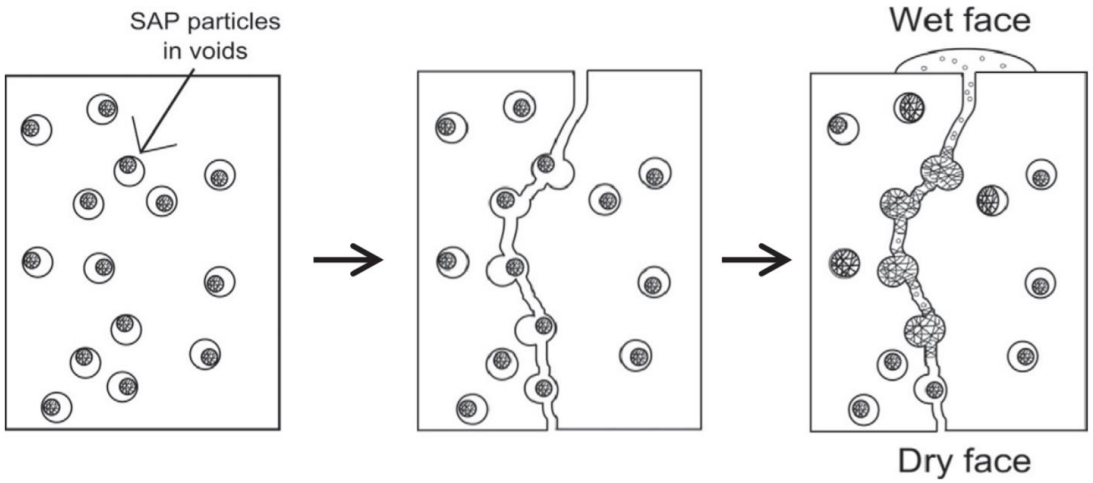

Figure 9 - Scheme of the self-sealing mechanism for cracks using SAP: SAP is added to the fresh concrete during mixing. The initial swelling is confined. As the concrete hardens, SAP shrinks and remains inactive in the microstructure. Then, the cracking of the concrete occurs that propagates through the SAP voids, exposing the polymer. Source: LEE *et al.* (2010).

More recent studies by Hong and Choi (2017) confirm this effect. They carried out swelling tests on different concrete mixtures with SAP particles, checking the time required to seal the crack, using permeability tests. They found that five minutes in contact with the water was enough for the crack to be completely sealed.

After sealing the cracks, under certain circumstances, the phenomenon of self-healing may also occur. When absorbing water through the interstitial solution, the SAP particles release this water when there is desiccation in the pores, enabling the hydration of cement grains that were not previously hydrated by the available water, and thus allowing the formation of new calcium silicates that promote precipitation of calcium carbonate. Therefore, self-healing occurs when these hydrates are sufficient to fill the crack, forming a more rigid structure and capable of restoring load capacity.

However, the effect of the hydration of the cement grains on crack sealing is closely linked to the crack size and the SAP grains size. An SAP with bigger particles has the potential to seal larger cracks, but larger cracks are more difficult to heal due to the effect of additional hydration of cement particles. This outcome was proved by Edvardsen

(1999), who studied in detail the autogenous self-healing of concrete without additions, where the necessary boundary conditions, the laws that govern nucleation, and the process of crystal growth were studied.

Edvardsen (1999); Granger *et al.* (2007); Ter Heide (2005); Yang *et al.* (2008); Homma *et al.* (2009) and Van Tittelboom *et al.* (2011) confirmed that the process of self-healing concrete, closing small cracks, is governed by two main mechanisms, the continuous hydration of cement grains, and the precipitation of calcium carbonate ($CaCO_3$). Another important conclusion of these works is that these processes are more likely to occur in small fissures. However, the precise maximum size is not yet defined.

To ensure that the crack after being sealed is healed, it is necessary to control the cracking process. One solution is to add fibers to the concrete. In the last 50 years, there has been a significant increase in the development and application of fiber reinforced concrete (FRC). This material was developed to improve the properties of conventional concrete, which is a brittle material with low tensile strength and low deformation capacity. Addition of fibers produces an improvement in the ductility and toughness of the concrete, making it able to work in the post-cracking phase.

The fibers, when correctly dosed, can provide a behavior called "strain-hardening" in the post-cracking phase, so the cementitious material can prevent the formation of large cracks, by presenting multiple cracks. For the same total deformation, one large crack is equivalent to several cracks of smaller size. In this way, it is possible that each small crack can heal itself. Combining different self-healing tactics, the use of SAP in conjunction with the use of fiber reinforcement, it is expected to obtain a durable concrete, with the ability to seal and heal cracks.

However, for high strength concrete the use of fibers has some limitations. This type of concrete usually presents very good mechanical and durability characteristics, in order to avoid large cracks, which may compromise the concrete behavior, strain-hardening response is required, and consequently the use of very high dosages of fibers is normally mandatory. This has a major negative effect on the workability of the concrete. Therefore, a way to investigate the self-healing of the high strength concrete

with superabsorbent polymers without the use of fiber reinforcement is presented in the second part of this research.

3 RESEARCH PROPOSAL

3.1 Conclusions from the literature review

After a comprehensive review of the literature, it can be concluded that superabsorbent polymers are capable of promoting healing and sealing cracks in certain cases. However, as the subject is relatively new, the number of studies carried out is limited and, consequently, there are several knowledge gaps. Some of the most important ones are identified below:

- Self-healing studies with the addition of superabsorbent polymers do not cover high-strength concretes.
- There are a few types of SAPs that have been studied for self-healing, but none have been suitable for mitigating autogenous shrinkage.
- In studies carried out to promote self-healing, SAPs with larger grain size were used, that is, the ones suitable for the phenomenon of crack sealing to occur quickly. However, one SAP that serves for both purposes has not yet been investigated.
- It is not yet clear what is the ideal volumetric fraction of SAP for complete self-healing in cracks of about 200μm. Few SAP volume fractions have been studied.
- Studies addressing the use of steel fibers in conjunction with SAP are rare; five articles and three conference papers from RILEM have been found, and the combination of the two subjects in self-healing has not yet been studied.
- It is believed that cracks up to 100 μm are healed autogenously. However, for larger cracks, the extent of the damage to be healed by stimulated autogenous healing is not yet known. Since the results are highly dispersed, further studies are needed to corroborate the results already obtained in the literature.

- There is no standardization of methods to assess healing, and the used techniques differ considerably. There is still no method capable of producing a crack with uniform width, to correctly define the size and depth to be analyzed, without fiber reinforcement.

- There is also a lack of methods that provide data that can be used in numerical models, to allow later use in structural applications.

- Durability studies, including cracks formed at different concrete ages, are required in order to assess the behavior of this technique over time.

- The ideal curing conditions recommended for autogenous healing with superabsorbent polymers is 28 wetting and drying cycles. However, it is known that the absorption and desorption of water in SAP depends on each type of polymer. As few polymers were used for this purpose, the effect of different curing conditions should be analyzed.

3.2 Problem definition

There are already studies that prove the efficiency of SAP as a self-healing agent. However, for high-strength concretes, where SAP is used primarily to mitigate autogenous shrinkage, there is a gap in the self-healing potential of these polymers. The studies so far have been carried out on concretes until normal strength (50MPa) and the commercial SAP used as a self-healing agent are not intended to mitigate autogenous shrinkage.

3.3 Research question

Based on the literature review, on the knowledge gaps identified and framed in the definition of the problem, this doctorate aims to answer the following question:

"What degree of healing does a superabsorbent polymer with the function of mitigating autogenous shrinkage achieve in a high-strength concrete?"

3.4 Hypothesis

Knowing that SAP mitigates autogenous shrinkage, acting as a water reservoir and thus minimizing the phenomenon of self-drying. It can also serve as sources of water for the hydration of anhydrous cement, always present in high-strength concrete. With the cracks, these water reservoirs can be replenished and swollen by capturing water from the external environment and, thus, providing self-healing, by slowly releasing water into the concrete.

3.5 Objectives

The general objective proposed for this work is to analyze the phenomenon of self-healing in high strength concrete, promoted by the use of superabsorbent polymers intended to mitigate autogenous shrinkage.

The focus is on high strength concrete and on verifying the SAP effectiveness of self-healing and self-sealing cracks, as well as the ideal amount of SAP needed to promote healing.

In the first stage of this research, the cracking control was achieved by using fiber reinforced concrete. For this, the following specific objective was proposed:

- Develop a concrete mixture, reinforced with steel fibers, that provide “strain hardening” behavior. The influence of different dosages of superabsorbent polymers should be evaluated. In the fresh state, the mixtures should present enough workability for usual applications. In the hardened state, the concrete must have high strength.

The results of the first stage were not satisfying due to the low workability and uncontrolled crack opening. Taking this into account, the objectives of the second stage were the followings:

- Develop a high-strength concrete mixture using superabsorbent polymers. This mixture should contain the highest dosage of SAP that allow high strength and enough workability for normal applications.

- Evaluate high strength concrete mixtures, with different contents of superabsorbent polymers, regarding the autogenous shrinkage properties.

- Develop a cracking methodology using steel reinforcement that does not affect the healing agent and healing products, that is able to produce cracks with uniform depth and width, being the geometry of the crack maintained during the healing process.

- Develop a water and air permeability methodology using the cracked specimens developed in the cracking methodology. In order to measure the crack closure by durability index.

- Quantify the self-healing capacity of the HSC developed with 200 µm of crack opening represented by three recovery indicators: mechanical recovery (load recovery index); of durability (determining the durability recovery index) and geometric (determining the crack closure index, by images taken of the cracks in the microscope).

3.6 Methodology

The study was divided into two stages: the first one regarding the use of fiber reinforcement, the pilot study, with fiber reinforced concrete; and the second one concerning the evaluation of the self-healing of reinforced concrete. In the second stage, the self-healing evaluation was divided into three sections, the mechanical recovery, the durability-related characteristics, and the crack closure. Figure 10 presents a flowchart with the steps and tests performed in each one. Some complementary studies concerning autogenous shrinkage and hydration were also carried out but are not presented in the flowchart.

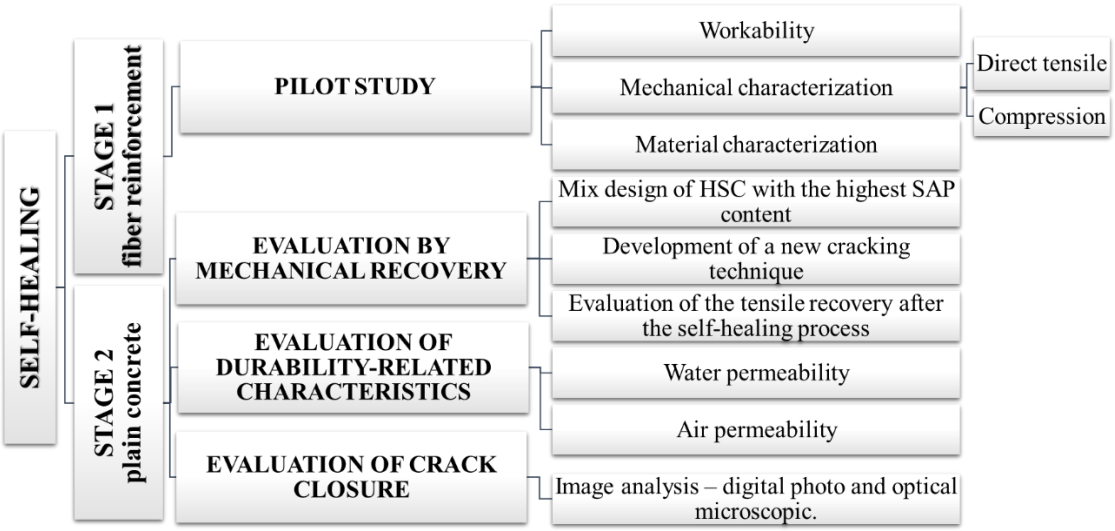

Figure 10 - Flowchart of the methodology used in this work.

These stages are briefly described below and detailed in the following chapters. The first stage of this work was the pilot study whose objectives were to experimentally formulate a mixture that simultaneously met four criteria:

- High compressive strength, above 60MPa.
- Strain-hardening behavior.
- High SAP content in the mixture (T_{max}), in order to promote the great self-healing capacity.
- Enough workability for molding specimens.

The pilot study was carried out in Brazil, at the Laboratory of the Federal University of Uberlândia (UFU).

The second stage of the investigation was carried out at the National Civil Engineering Laboratory (LNEC) in Portugal, within the scope of the sandwich doctorate.

The investigations initiated in Brazil had the purpose of experimentally determine the maximum content of SAP (T_{max}), compatible with high strength and sufficient workability. With this value, $T_{max,}$ an intermediate value, T_{int}= 0.5Tmax, was established.

In Portugal, the tests carried out in Brazil were repeated with local materials, making adjustments to the mixtures, in order to reach enough ductility for the cracking objectives. Strain-hardening behavior for 200 μm cracking required an increase on the fiber's dosages incompatible with the necessary consistency for practical applications. Consequently, in the second stage conducted in Portugal, it was developed a high strength concrete similar to the one produced in Brazil, but without the fiber reinforcement. It was confirmed that the T_{max} content of SAP could be used in the mixture. Compressive tests, hydration tests, and autogenous shrinkage tests of the new mixture were carried out.

Following the design of the concrete mix, it was developed a new cracking technique under direct tensile with the use of a steel bar for reinforcement of the high strength concrete. The steel bar allows strain-hardening behavior in high-strength concrete and facilitates obtaining the predefined crack opening, and preserving it during the healing process, but do not offers a spread of surface area for precipitation of hydration products in the healing process as the fibers do.

Compared to fibers, the use of a steel bar also allows a better assessment of mechanical recovery due to the healing process, since repeatable measurements are possible without distinct slips at the fiber-matrix interfaces.

The effect of self-healing on durability was indirectly evaluated by water and air permeability tests, using cracked specimens through this new technique, but then adapted to fit on the respective test device. An optical microscope monitored crack width before and after submitting to the self-healing procedure. These methods were required to calculate the durability index and the crack closure index.

Before starting the self-healing test campaign, the effect of two curing conditions on hydration and compressive strength was investigated. The concrete was subjected to two temperatures and tested at for several ages. The age of seven days was chosen to represent young concrete, when there is still a significant volume of anhydrous cement, and 28 days to represent old concrete, when almost all the available internal capillary water has already been consumed. Twenty-eight days is also a standard age for testing concrete.

At 28 days, with almost no water in the capillary pores, it is expected that the SAP particles are also empty. In this way, the SAP near the cracked concrete can absorb water from outside and provide conditions for additional hydration, the source for the healing effect. The negligible hydration between 28 days and 90 days shows that without external water no self-healing is possible. As cement paste of high strength concrete is very dense, the effectiveness of external water as source for additional hydration is very poor. Under these conditions, any self-healing that occurs in the cracking zone must be the result of the SAP effect. In this way, it is possible to assess the real effect of the SAP as a healing agent.

After the curing period, 7 or 28 days, the specimens were cracked. As a result of the literature review, it was concluded that the maximum crack size for complete autogenous self-healing is about 200 μm. This crack width is also a standard service limit for some structural applications. Nevertheless, the research on this subject is not consensual and diverging results are presented. The crack width is a parameter that influences the healing process. Therefore, it was initially planned to test concrete with cracks of 100 μm and 200 μm, to characterize the effect of crack size.

After carrying out preliminary crack tests with the new cracking method, it was concluded that, in order to achieve an exact crack of 100 μm, several samples would have to be withdrawn due to variations in the crack width, something that did not allow obtaining a sufficient number of valid tests, due to the limited availability of SAP. After considering cracks of 100-150 μm, instead 100 μm, the option was put aside, because with this variation, precise conclusions about the influence of crack width in the healing process would not be possible. However, for future studies, tests with the 100 μm crack size can be performed. Before the development of the cracking method, the crack width was one of the independent variables. Nevertheless, the method is more suitable and easier to perform with crack widths above, therefore the size of 200 μm was chosen as a fixed variable.

The healing condition chosen for this research was based on wetting and drying cycles, as it is the most efficient condition for sealing with SAP, according to the studies by Snoeck (2015). It was found that SAP does not present significant healing capability under high humidity or in a dry environment since the healing mechanism requires liquid

water. After the induction of cracks, the concrete remained four months under daily wetting and drying cycles.

The following is a brief description of the methodologies adopted in each one of the four chapters presented. Specific details of the materials, specimen's preparation and experiments carried out can be found within each chapter since they are self-contained.

Stage 1: Pilot Study - fiber reinforced concrete

- Chapter 5: Self-healing of high strength concrete with steel fibers and SAP

This chapter presents the first approach to produce concrete with self-healing properties, where steel fibers were used for control of the crack size. The objective was to produce a composite with strain-hardening behavior using the maximum superabsorbent content in the mixture compatible with high strength concrete. For that the following tests were carried out: slump tests to investigate workability; compressive test to determine the strength; direct tensile test with digital image correlation to produce and identify the crack opening.

Stage 2: Plain concrete

- Chapter 6: Autogenous shrinkage of high strength concrete with SAP for self-healing purposes.

This chapter focuses on validating the results of the Pilot Study, using Portuguese constituents, and checking the strain-hardening behavior of the high strength concrete. The reevaluation of the strain-hardening behavior was required due the strain necessary to produce the specified crack width, 200 μm. In fact, observing the stress-strain curve on direct tension, after reaching the first peak of the stress, the length of the strain-hardening line was very short, and then a deep decrease on tension was observed. So, after increasing the volume of fibers in order to avoid this deep stress decrease, it was concluded that the number of fibers needed to reach the required strain-hardening behavior was incompatible with the workability needed to mold the specimens. As a consequence, it was necessary to verify the maximum and intermediate SAP content without the use of fiber reinforcement and resume the study with crack control by steel bars. For the fresh state,

Slump tests were performed. At the hardened state, compressive strength, three-point bending, and Young's Modulus tests were carried out at the ages of 1, 3, 7, 28, and 60 days to characterize the concrete. Furthermore, to verify the hydration process with different temperatures of curing, at 20°C and 40°C, compressive tests and measurement of the mass gain in small specimens were performed at the ages of 1, 2, 3, 4, 7, 10, 14, 28, 60 and 90 days. Additionally, all Portuguese materials were chemically characterized. Finally, autogenous shrinkage using corrugated tubes was measured for the maximum and intermediate content of SAP, along with the reference one.

- Chapter 7: Evaluation of self-healing concrete by mechanical recovery

This chapter proposes a methodology to produce a single crack in direct tensile with uniform width and length, by using a single steel bar with a reduction on the diameter in the center of the bar. The bar was isolated from the concrete leading to no interference in the self-healing results. The methodology was developed and tested with a non-linear analysis using the finite element method with the program Ansys. Pre-cracking was conducted in the ages of 7 and 28 days. After the pre-cracking, samples were stored and subjected to wet and dry cycles for 4 months daily. Mechanical recovery was performed by doing the same direct tensile test, 4 months after the pre-cracking. In order to evaluate crack closure, microscope photos of the crack after the pre-cracking and before the verification of the mechanical recovery were taken.

- Chapter 8: Evaluation of self-healing concrete by oxygen and water permeability tests

This chapter introduces a methodology to evaluate durability-related characteristics by using oxygen and water permeability tests on pre-cracked samples through the direct tensile equipment. Samples were pre-cracked at the ages of 7 and 28 days, sawed and glued with silicon in a concrete cylinder base, and put to dry for 24h. Microscopy photos of the back and front of the sawed specimen were taken after the pre-cracking and after 4 months, before the re-done of the permeability tests. After the sample preparation, oxygen permeability tests were performed, using the time of the passage of the oxygen by the crack as a measure of the crack sealing. Next, water permeability tests were performed using PVC pipes glued to the base. The time, the volume of water, and

pressure passing through the crack were measured. After the oxygen and water permeability tests, samples removed from the base with toluene and stored for four months, while undergoing daily wet and dry cycles. At the end of that period, the tests were re-done to measure the self-healing effect.

3.7 Control Variables and Response or Dependent Variables

The independent or controlled variables are the parameters that can influence the behavior of the concrete. With the crack width as a fixed parameter, 200 µm, the present study had the following independent variables:

- SAP content in concrete - 0%; intermediate content (T_{int}) and maximum content (T_{max}).
- Pre-cracking at 7 days and at 28 days.

The combination of the SAP content and age of cracking resulted in 6 different study situations, shown in Table 4.

Table 4 - Combination of independent variables of the study.

Mix designation	Independent Variables		
	SAP content	Pre-cracking	Crack size
REF-7-200	Reference - 0%	7 days	200µm
INT-7-200	Intermediate content – 0.3%	7 days	200µm
MAX-7-200	Maximum content – 0.6%	7 days	200µm
REF-28-200	Reference - 0%	28 days	200µm
INT-28-200	Intermediate content – 0.3%	28 days	200µm
MAX-28-200	Maximum content – 0.6%	28 days	200µm

The response or dependent variables are the characteristics or properties related to the concrete behavior that can be determined experimentally. Consequently, independent variables influence response variables. In the present study, the response variables were the tests proposed to assess self-healing and the tests to characterize the concrete regarding the fresh and the hardened state. For self-healing assessment, the response variables were:

- Load recovery index by direct tensile test.

- Durability index due to air permeability.
- Durability index due to water permeability.
- Crack closure index by optical analysis.

The same approach can be used for the fresh and hardened concrete properties. In the fresh state, only the SAP content is an independent variable, and the chosen response variables are:

- Consistency
- Time Zero

In the hardened state, the chosen response variables are:

- Compressive strength.
- Flexural strength by three-point bending test.
- Young's Module.
- Autogenous shrinkage.

3.8 Materials

The materials constituting the concrete mixture for both Phase I in Brazil and Phase II in Portugal are presented in the following sub-items. They are also addressed in each independent Chapter.

3.8.1 Cement

In Phase I, Portland cement of high initial strength, CPV-ARI was used (ABNT NBR 16697, 2018). CPV cement was used because it contains a high clinker content and, consequently, low content of other mineral constituents, thus minimizing its effect on the properties evaluated. Besides, this type of cement has high employability in high-strength concrete (HSC), and it was manufactured in Brasília.

With the same purpose, in Portugal it was chosen the CEM I 42,5 following the EN 197-1 (2011) standard. Both binders presented high clinker content (≥95%). Chemical and physical properties are shown in Table 5.

Regarding the results, both types of cement fulfill the requirements of the Brazilian and Portuguese standards. It is important to highlight they present low insoluble residue content; and that there is no evidence of the presence of pozzolanic material. The levels of calcium oxide and magnesium oxide are at acceptable levels.

Table 5 - Chemical characterization of the types of cement used in the study.

Chemical Components		**CEM I 42,5 R**	**CP V ARI**	**Requirement of NBR 5733**	**Test Method**	
Loss on ignition (%)	**to 105°C**	0,2	1,82	≤ 4,5	EN 196-2 section 7	NBR NM 18/2012
	to 1050°C	4,1				
	to 950°C	4,1				
Insoluble residue (%)		1,11	0,79	≤ 1,0	EN 196-2 section 9	NBR NM 15/2012
Sulfur trioxide (SO_3) (%)		2,89	3,28	Not specified	EN 196-2 section 8	NBR NM 16/2012
Magnesium oxide (MgO) (%)		1,59	4,36	≤ 6,5	EN 196-2 section 13.13	NBR NM 11-2/2012
Silicon dioxide (SiO_2) (%)		18,36	24,41	Not specified	EN 196-2 section 13.4 and 13.9	
Iron oxide (Fe_2O_3) (%)		3,41	3,02	Not specified	LNEC E 406	
Aluminum oxide (Al_2O_3) (%)		5,06	7,09	Not specified	EN 196-2 section 13.11	
Calcium oxide (CaO) (%)		61,42	53,74	Not specified	EN 196-2 section 13.12	
Chloride content (%)		0,03		Not specified	EN 196-2 section 14	
Total alkalis (%)	**Sodium oxide (Na_2O)**	0,1	0,29	Not specified	EN 196-2 section 17	NBR NM 17/2012
	Potassium oxide (K_2O)	1,02	0,77	Not specified		
	Alkaline equivalent (Na_2O)	**0,8**	0,8	Not specified		
Blaine fineness (kg/cm^2)		384	5723	Not specified	EN 196-6	NBR NM 23:2001
Density (g/cm^3)		3,14	3,03	Not specified		NBR NM 23:2002

3.8.2 Silica fume

The silica fume used in Brazil was from the national company Silmix; the one from Portugal was produced as a residue. Both silica fume from Brazil and Portugal are

of the non-densified type, from one batch of each manufacture. Physical and chemical characterization tests were performed, and the results are shown in Table 6. The values found for both silica fume used in the production of micro concrete are within the specifications of ABNT NBR 13956: 2012.

Table 6 - Physical and chemical characterization of the Silica Fume.

Chemical Components		**Brazil**	**Portugal**	**Requirement of NBR 13956:2012**	**Test Method**	
Loss on ignition (%)		2,94	3,22	≤ 6,0	EN 196-2 section 7	NBR NM 15:2012
Magnesium oxide (MgO) (%)		0,86	0,49	Not specified	EN 196-2 section 13.13	NBR 13956-2:2012
Silicon dioxide (SiO_2) (%)		93,95	93,55	≥85	EN 196-2 section 13.4 and 13.9	
Iron oxide (Fe_2O_3) (%)		0,27	0,16	Not specified	LNEC E 406	
Aluminum oxide (Al_2O_3) (%)		0,16	0,15	Not specified	EN 196-2 section 13.11	
Calcium oxide (CaO) (%)		0,74	0,37	Not specified	EN 196-2 section 13.12	
Total alkalis (%)	**Sodium oxide (Na_2O)**	0,37	0,26	Not specified	EN 196-2 section 17	NBR NM 17:2004
	Potassium oxide (K2O)	0,84	0,85	Not specified		
	Alkaline equivalent (Na_2O)	0,91	0,82	≤ 1,5		
Blaine fineness (g/cm^2)		8584	-	Not specified	EN 196-6	NBR NM 23:2001
Density (g/cm^3)		3,33	2,21	Not specified		NBR NM 23:2001

3.8.3 Fine aggregate

The fine aggregate used in the production of the mixtures was natural sand from an alluvial deposit. The sand used in Brazil was from the Corumbá River, located about 220 km from Brasília, and the sand used in Portugal was from Rio Maior. The choice of the fine aggregate was based on grading requirements, particles with no discontinuity in size being preferred, within the usable zone and closest to the optimal zone according to the recommendations of the ABNT NBR 7211: 2011 standard, as shown in Figure 11. The fineness module is 2.73, the upper sieve size is 4.75 mm, and the specific weight is 2.65 kg/dm³ as for the Portuguese is 2.60 kg/dm³.

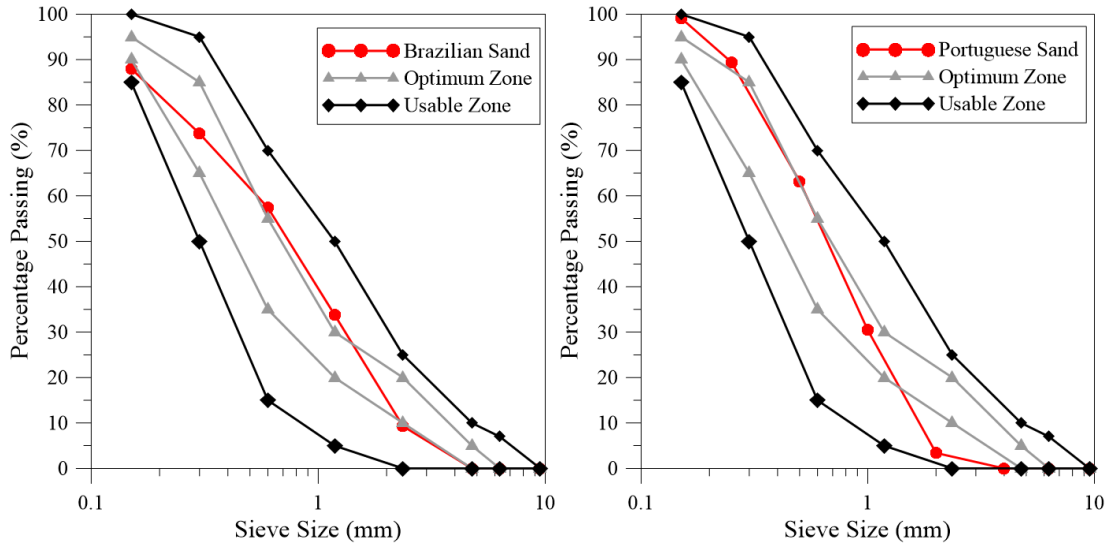

Figure 11 - Grading of the fine aggregate: a) Brazilian Sand; b) Portuguese Sand.

3.8.4 Superplasticizer

In Brazil, the superplasticizer ADVA CAST 129, from Grace Company, was used, this is a water reducer of high efficiency (superplasticizer type II - SPII-N), based on polycarboxylates, of normal setting time, according to the classification of ABNT NBR 11768: 2011. The technical data sheet indicates the following characteristics: density of 1,060 -1,100; orange color; pH of 5-7; solid content from 38,85 to 42,94%.

In Portugal, it was used the superplasticizer Glenium ACE 429 provided by BASF, classified as water reducer of high efficiency, also based on polycarboxylates. The technical data sheet indicates density of 1,04; dark orange color, pH of 6.

3.8.5 Superabsorbent polymers

The superabsorbent polymer was supplied by Prof. Ole Mejlhede Jensen, and it was developed at the Technical University of Denmark (DTU). The polymer is an acrylic acid/acrylamide with covalent cross-links produced by the reverse suspension polymerization technique (JENSEN and HANSEN, 2001). It was developed for a particular use in a high alkaline environment, such as the cement suspension. It is supplied in a dry, white powder with spherical particles. In Figure 12, the polymer is presented in the dry and swollen state, using the scanning electron microscope and digital microscope H1000X / S1000X, respectively.

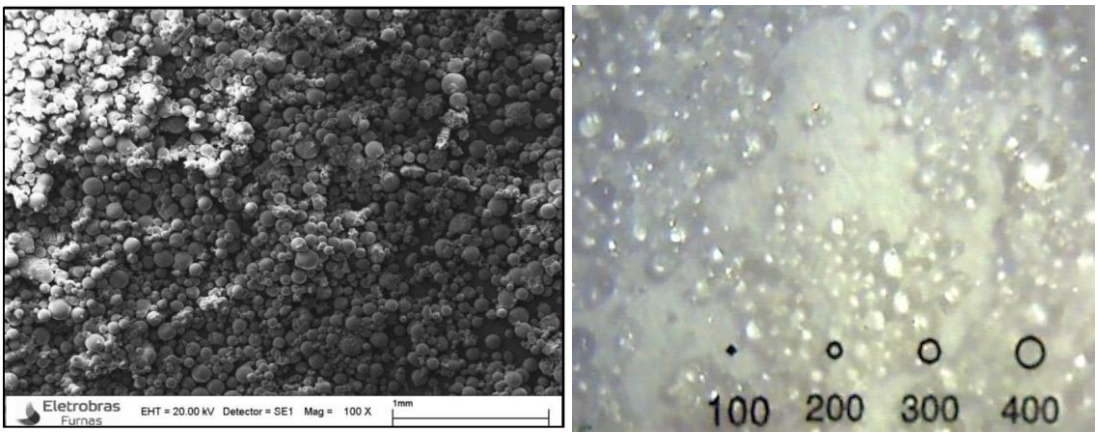

Figure 12 - Superabsorbent polymer: a) dry; b) swollen, the numbers indicate the diameter of the dark circumferences, in micrometers. Source: Manzano (2016) and own author.

This SAP has the following characteristics: an absorption in the alkaline cementitious medium of 18g of water for 1 g of SAP; density of 1.456; average dry diameter of 66.3µm; and average swollen diameter of 189.6µm. The particle size of the material was characterized by D_{10} = 27.3 µm, D_{50} = 66.3 µm and D_{90} = 101.7 µm.

The choice of SAP dosages was based on work by other authors and on preliminary tests. The initial levels of 0.2% and 0.3% were chosen because they were the best dosages obtained in the study by Manzano (2016) to mitigate autogenous shrinkage. For the purpose of self-healing, an upper limit of 0.6% was obtained in the Pilot study. Besides, this content was based on the work using fibers and SAP by Gupta, Kua and Pang (2017), who adopted this percentage of SAP as the maximum content. Snoeck (2015) used 1% SAP, however, the decrease in strength, regarding the reference mixture, was considered too high.

3.8.6 Fibers

In Snoeck (2015), PVA fibers were used, and their role was to produce multiple stable cracks, as extensively researched by Li (2001). In the present study, the hypothesis of using PVA fibers from the same company Kuraray, coated with a 1.2% oil layer, was evaluated. However, its use was discarded for two reasons, presented below.

According to the Micromechanical Law developed by Li (2001), and shown in Equation (5), the tension on the matrix must be lower than the tension of the fiber-matrix bonding for multiple cracking to occur. As the premise of the research was to study high-

strength concrete, this concrete requires high bonding capacity and high volume of fibers in order to fulfill this micromechanical law. In fact, immediately before cracking, the tensile stress on high-strength concrete is higher than the tensile stress on conventional concretes, and the bonding on oil-coated fibers is low. Thus, it was decided to discard the use of PVA fiber in favor of steel fibers.

The initial tested mix design refers to some concrete with strength of 80MPa, presenting higher tensile strength than the concrete presented in the studies by Snoeck (2015) and Li (2001). Thus, it was foreseen that the use of PVA fibers in this mix would not produce “strain hardening” behavior, which was considered mandatory to improve the durability of the composite and the repeatability of the tests on the healed cracks.

The second reason was due to information from the company Kuraray that the fibers are not sold in Latin America, or Portugal, and donations and imports are restricted in those regions.

Based on the Micromechanical theory and studies by Formagini (2000) and Moreira (2017), the steel fiber of DRAMIX OL 13/.16 mm from BEKAERT, made of smooth steel with 13 mm in length, 0.16 mm in nominal diameter, was considered able of providing strain-hardening behavior. The fiber presented Young’s modulus of 200GPa and tensile strength of 2750 MPa. According to the researchers, this steel fiber can cause multi-cracking in concrete with strength of 120 MPa. The aspect of the fibers is illustrated in Figure 13. The initial content of the fibers incorporated in the mixture was 1.28% by volume, the same used by Moreira (2017).

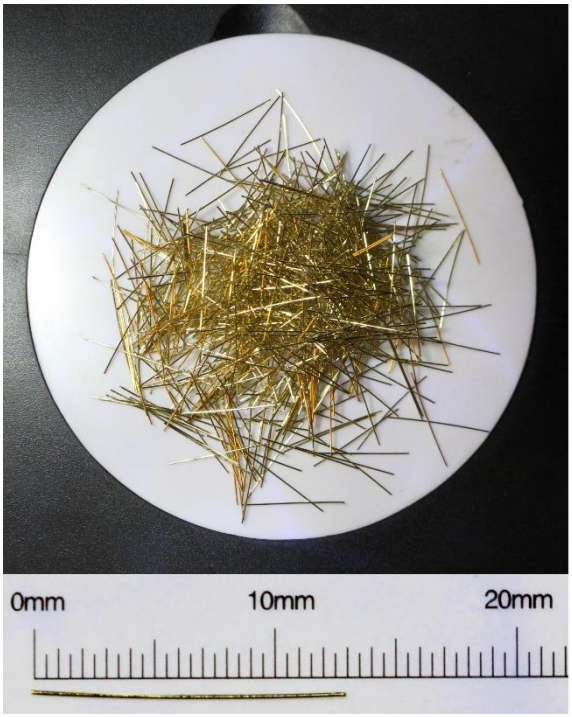

Figure 13 - Dramix Ol 13. /16 steel fiber from Bekaert Company. Source: Author.

3.8.7 Steel bars

Steel bars were of the nominal diameter of 6mm, a section of 283 mm^2, a mass of 0.22 kg/m, the spacing between ribs of 5 mm with a tolerance of 20%, and a maximum height of ribs of 0.39 mm. They were classified as MEGAFER 500SD-SEIXAL bars manufactured by hot rolling, satisfying LNEC specifications: E460: 2010. In the center of the bars, the diameter was reduced to 3 mm with a grinder, shown in Figure 14.

Figure 14 - Steel bar (6 mm), with reduced diameter (3 mm) in the central part.

STAGE I – Fiber reinforcement

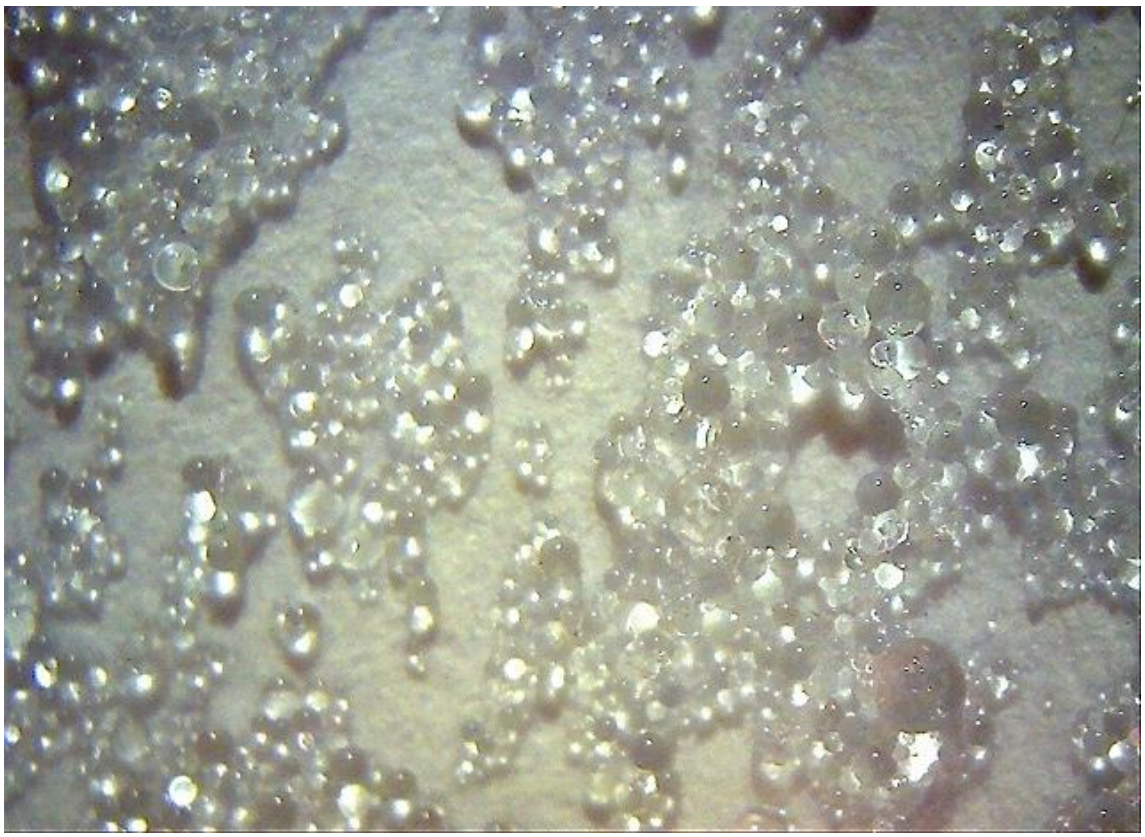

4 - PILOT STUDY

Effect of the Combination of Superabsorbent Polymers for Autogenous Shrinkage Control with Steel Fibers of High-Performance Concrete Under Uniaxial Tension Using DIC

Abstract

This chapter presents a study of the effect of a superabsorbent polymer (SAP) for autogenous shrinkage control on the uniaxial tensile behavior of steel fiber reinforced concrete (SFRC). This pilot study is based on the potential of using fibers and SAP to increase the durability of concrete, preventing large cracks due to autogenous shrinkage and improving post-cracking behavior. Furthermore, SAP can provide further hydration for self-healing purposes and improve the ductility of the SFRC. This chapter is already published in Materials Journal referenced as Santos *et al.* (2020).

In order to evaluate the effect of the addition of SAP in SFRC, dog-bone SFRC specimens with different dosages of polymer were cast and tested under uniaxial tension. The digital image correlation (DIC) technique was used to understand the effect of SAP on the steel fibers' crack-bridging mechanisms. Surface strains and crack openings were inferred using the DIC technique. The effect of SAP and fibers on fresh and hardened concrete was individually investigated by flow tests and compressive strength tests.

Autogenous shrinkage was measured in plain concrete to investigate the minimum SAP content required to mitigate autogenous shrinkage. The use of 0.3% SAP was sufficient to control the shrinkage and reach multiple cracking behavior. This content of SAP completely suppressed the autogenous shrinkage with minimal side effects on compressive strength.

An analytical formulation for the tensile behavior of SFRC was developed using the variable engagement model, presenting a mean correlation of R^2 of 0.97 with the experimental results.

4.1 Introduction

The present investigation focused on the tensile behavior of steel fiber reinforced concrete (SFRC) with superabsorbent polymer (SAP). In general, SAP is used to control autogenous shrinkage without significantly affecting strength and workability (HASHOLT *et al.*, 2012; JENSEN and HANSEN, 2001; JENSEN and HANSEN, 2002; MECHTCHERINE *et al.*, 2014 a, MECHTCHERINE *et al.* 2014 b; REIS *et al.*, 2020, SCHRÖFL *et al.*, 2012; SHEN *et al.*, 2016; WYRZYKOWSKI *et al.*, 2018). Fibers are used in concrete for cracking control (AFROUGHSABET *et al.*, 2016, DI PRISCO *et al.*, 2009; KWON *et al.*, 2009; NAAMAN and REINHARDT, 2006; NAAMAN, 2018; VAN ZIJL *et al.*, 2012).

The synergic effect of SAP and fibers has been mainly studied with synthetic fibers (MIGNON *et al.*, 2017; SHERIR *et al.*, 2015; SNOECK, 2016; SNOECK and DE BELIE, 2015; SNOECK *et al.*, 2014; TOSUN-FELEKOĞLU *et al.*, 2014; YAO *et al.*, 2012). The studies of concrete with synthetic fibers and SAP shows that the presence of the two constituents modifies the tensile behavior of the composite, and improvements on the durability of the material can be achieved (LI, 2003; LI *et al.*, 2001; WANG and LI, 2004). The main improvements are due to the reduction in the size of the crack by increasing the number of cracks. This multi-cracking behavior is obtained not only from the presence of fibers, but also by the multi-flaws provided by SAP (YAO *et al.*, 2012).

Studies of concrete with fibers and SAP are scarce in the literature. The study presented by Liu *et al.* (2020) showed promising results on the use of SAP to densify the interfacial transition zone and reduce micro-cracks around the fibers. Wang *et al.* (2019) conducted a study with splitting tensile tests on concrete with SAP and steel fiber for cellular concrete applications, but, therefore, the material is quite different from high strength concrete. None of these studies were performed using direct axial tension tests.

The present document intends to contribute to the understanding of the overall behavior of the composite subjected to direct tension by analyzing the development of the crack formation and the crack pattern with the digital image analysis technique. This technique allows for simultaneously observing the influence of the reinforcements and flaws provided, respectively, by the set of fibers and SAP particles, and the interaction

between them. This combined influence cannot be obtained when testing only one fiber in tension (LIU *et al.*, 2020) nor with the splitting test (WANG *et al.*, 2019).

The research also deals with inherent other specific subjects: (1) Investigate the maximum SAP content to be incorporated in high strength concrete (HSC) and steel fiber reinforced concrete (SFRC) compatible with a reduced loss of compressive strength and avoiding significant loss of workability; (2) Investigate the minimum SAP content that controls the autogenous shrinkage of HSC; (3) Correlate the tensile properties of SFRC with different SAP contents with the crack pattern and the full-field strain measurement using DIC; and (4) Develop an analytical model for the tension behavior of HSC with varying SAP dosage.

4.2 Materials

Portland cement of high initial strength conforming to (ABNT NBR 16697, 2018) Type CPV-ARI (CIPLAN, Brasília, Brazil) was used for all mixes in this study. A silica fume, of the non-densified type, meeting the requirements of the standard (ABNT NBR 13956, 2012) was supplied by the national company Silmix (Breu Branco, Pará, Brazil). Both products were already described in items 4.8.1 and 4.8.2. Locally available sand of the Corúmba River, shown in item 4.8.3, with maximum particle size of 4.75 mm and gradation conforming to (ABNT NBR 7211, 2009) standard usable zones, was used. A water reducer of high-efficiency, commercially available as superplasticizer ADVA CAST 129 from Grace Company (Sorocaba, São Paulo, Brazil), based on polycarboxylates, was used to maintain the fluidity of the mortar within a fixed range for all mixes.

Steel fibers of DRAMIX OL 13/.16 mm from BEKAERT (Zwevegem, Belgium), mentioned in item 4.8.6, with the content of 1.28% in volume, were used.

The superabsorbent polymer used was an acrylic acid/acrylamide (Technical University of Denmark, Lyngby, Denmark) with covalent cross-links produced by the reverse suspension polymerization technique, described in detail in item 4.8.4.

The water absorption capacity of SAP was measured by the slump flow consistency method and by means of graduated cylinders proposed by Jensen (2011).

Absorption of SAP was tested for deionized water and cement filtrate. Both results are useful for the present study, since the absorption of fluid by the SAP takes place initially in the fresh concrete mixture and afterwards, when the cracking occurs. In the first phase, the SAP absorption takes place in a highly active electrochemical environment, but after cracking the SAP particles are in contact with pure water. The absorption capacity in deionized water was 96 grams of water per 1 gram of SAP.

The smaller absorption of cement filtrate by the SAP particles, when compared to absorption of water, caused by calcium and magnesium ions present in the cementitious fluid (increase the cross-linking in SAP) is an advantage for self-healing purposes. This effect leads to a smaller void creation in the hardened paste and, after crack formation, when the SAP gets into contact with clean water, it swells and temporarily seal the crack. The saturated environment can then provoke self-healing of the crack by hydration of the remaining anhydrous cement, under certain conditions and quantities of SAP (SNOECK *et al*, 2014; VELASCO, *et al*., 2015; ROOIJ *et al.*, 2013),

In order to investigate the combined effect of the SAP and steel fibers, eight concrete mixtures were prepared according to Table 7. These included three reference compositions, two without SAP or fibers (REF-035 and REF-040), and another with fibers and without SAP (REF-035F). The remaining five mixtures included SAP or SAP and fibers.

All mixtures presented low w/c ratio and high strength. The total water–cement (w/c) ratio was set at 0.35 (water–binder of 0.32). A reference mixture with w/c of 0.4 was also prepared for comparison purposes, a mixture where additional water was placed in order to have the same total water content as the water content of mixture with 0.3% SAP. In the mixtures without fibers, the content of the superplasticizer was adjusted to reach the required workability.

All mortars with w/c=0.35 had the same contents of binder and aggregates, and the SAP dosage ranged from 0 to 0.6%. In the mixtures with fibers, the amount of superplasticizer was fixed at 2%, and the fibers content was set constant at 1.28% in volume.

Table 7 – Composition[1] of the concrete mixtures, values in kg/m³.

Mixture (kg/m³)	Cement	Silica	Sand	SAP	Fiber	Superplasticizer	$w/c_{(basic)}$	$w/c_{(total)}$[2]	Flow (mm)
REF-035	675.8	67.6	1306.5	0	0	11.15	0.35	0.35	183
REF-040	654.2	65.4	1264.5	0	0	8.50	0.40	0.40	200
SAP-0.2	675.8	67.6	1306.5	1.35	0	12.50	0.35	0.38	183
SAP-0.3	675.8	67.6	1306.5	2.03	0	12.50	0.35	0.40	180
REF-035F	675.8	67.6	1306.5	0	100	13.50	0.35	0.35	307
SAP-0.2F	675.8	67.6	1306.5	1.35	100	13.50	0.35	0.38	243
SAP-0.3F	675.8	67.6	1306.5	2.03	100	13.50	0.35	0.40	230
SAP-0.6F	675.8	67.6	1306.5	4.06	100	13.50	0.35	0.46	208

[1] The contents in kg/m³ refers to the sum of cement, silica, sand, basic water and superplasticizer, excluding the volumes of fibers, SAP, and water absorbed by the SAP; [2] Including water absorbed by SAP.

The mortars were prepared in a mechanical pan type mixer (Solotest, São Paulo, Brazil) under the following steps. The first step was the dry mixing of the cement, the SAP, and the sand, for 5 min at low speed. The second step was the water and superplasticizer addition for 2 min, and then the mixing speed was changed to high speed for 5 min. Then, the mixer was stopped, the edges of the bowl were scraped, and followed by mixing for another 3 min at high speed. In the correspondent mixtures, the fibers were then added constantly in motion for 5 min at slow speed, preventing the ball bearing effect, then the edges were scraped again for 3 min. Finally, the mortar was mixed for 5 min at high speed to ensure uniform dispersion of the fibers. For proper compaction, the mixes were cast into molds placed on a vibrating table. The specimens were then moved to a room with 100% relative humidity and 22 ± 1 °C. They were demolded after 24 h and stored in this room until the testing date.

4.3 Test methods

4.3.1 Flowability and Compressive Strength

Slump flow tests were carried out right after mixing, following the procedure (DIN 18555-2, 1982). The fresh mortar was poured into a Hagerman cone (base diameter of 100 mm, height of 60 mm, and top diameter of 70 mm) into two layers. Each layer was tamped 10 times evenly distributed, and then the cone was gently removed, and the spread was measured. The largest diameter was measured along with the diameter in the perpendicular direction.

Compressive tests were carried out according to the standard (ABNT NBR 5739, 2018). Cylinder specimens (Ø 50 mm × L 100 mm) were used, and an average of three tested samples was reported. The base of the specimens was ground to ensure a smooth and plane surface. The test adopted a Microcomputer-controlled electromechanical universal test system (MTS) of the Federal University of Uberlândia, and the loading rate was 0.4 MPa/s.

4.3.2 Autogenous Shrinkage

The autogenous shrinkage was assessed according to the methodology developed by Silva (2007), which is a modified method of Tawaza (1999) using the ASTM C490 (2000) apparatus, shown in Figure 15. The test consists in the measurement of the deformation of mortars, cast in a prismatic mold with nominal size of 7.5 × 7.5 × 28 cm. Each mold was previously prepared, with polystyrene layers inside to decrease friction, allowing the concrete to move almost freely. Additionally, two threaded metal pins were placed in the extremities of the mold aligned with the specimen's longitudinal axis. Strain gauges are coupled in these pins and connected to a computer to collect and store the data. The distance between these pins is called G, and the measurement of this distance determines the shrinkage.

After casting, to prevent the loss of water by evaporation, the mold with the mortar inside was wrapped with multiple layers of polystyrene and adhesive tape. The weight of the mold with mortar was measured, and they were stored in a chamber with 50 ± 2% of relative humidity and temperature of 21 ± 2 °C for 28 days, where the strain gauges continuously recorded the G distance.

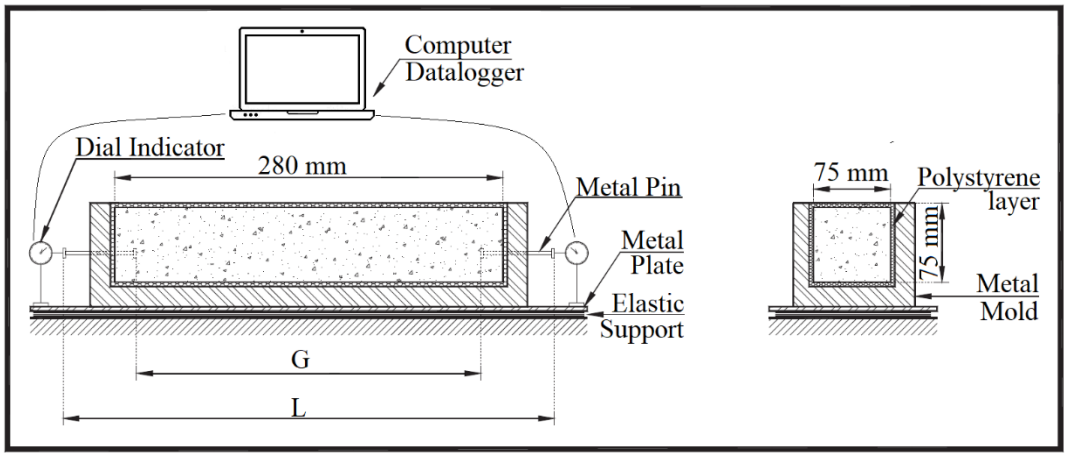

(a)

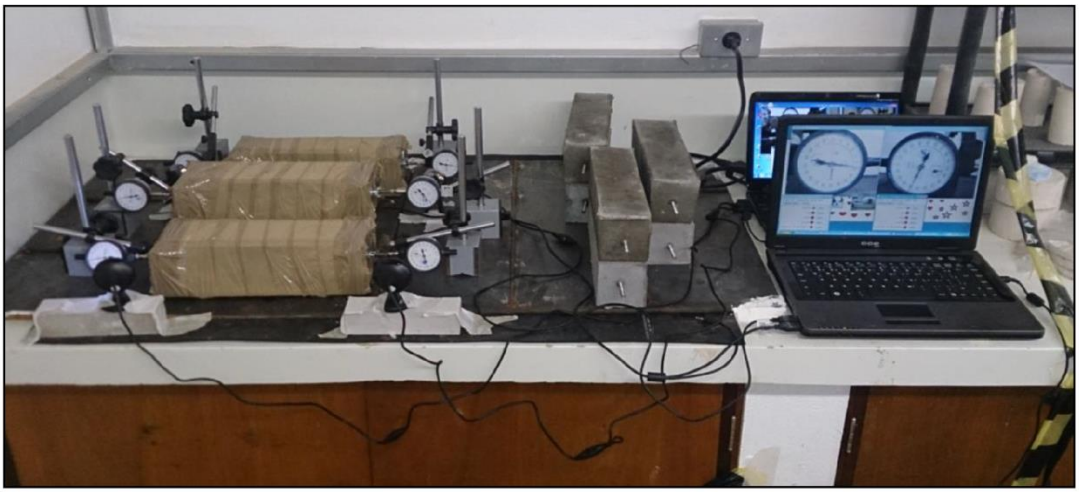

(b)

Figure 15 - Autogenous shrinkage test: (a) test setup scheme and (b) on going test.

4.3.3 Uniaxial Tensile Testing Equipment with Digital Image Correlation (DIC) Arrangement

In order to evaluate the stress-strain behavior of all HPC mixtures at 28 days, a series of direct tensile tests were performed following Yokota *et al.* (2008). An INSTRON (Instron, São José dos Pinhais, Paraná, Brazil) electronic universal testing machine with displacement control and load capacity of 100 kN of the Federal University of Uberlândia, was used at a constant speed of 0.3 mm/min. The loading force was measured on load cell by a computerized data recording system, and the strain was measured by two linear variable displacement transducers (LVDT, HBM, São Paulo, Brazil) placed on both sides of the specimen, the average of both was used to measure the strain, and the initial length

(l_0) was set at 70 mm. Additionally, the strain was also monitored by digital image correlation (DIC, Correlated Solutions, Irmo, United States of America). The tensile setup and geometry of the specimen are shown in Figure 16.

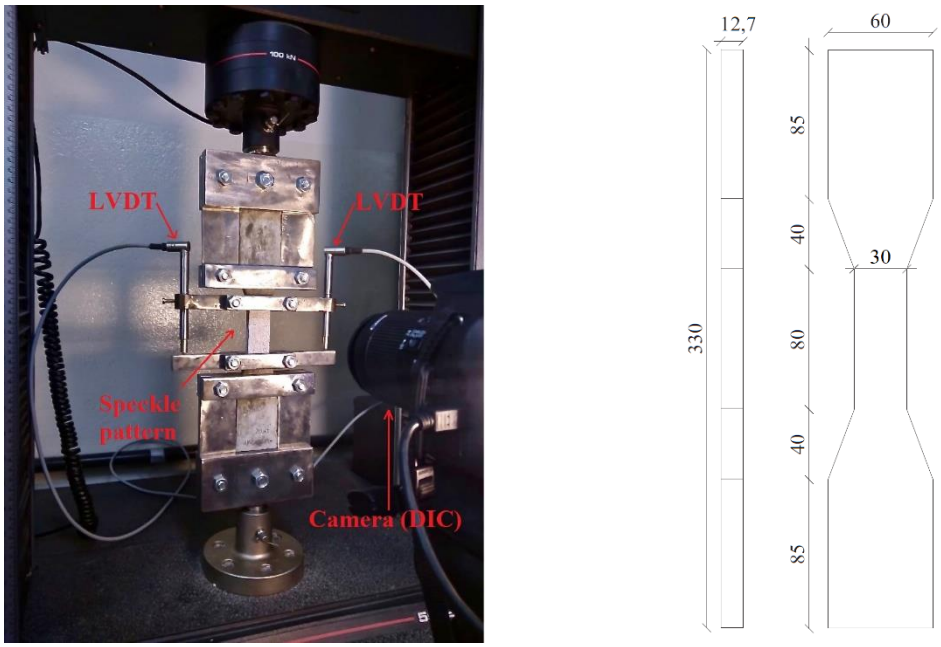

(**a**) (**b**)

Figure 16 - The direct uniaxial tensile test: (a) test setup with DIC and (b) specimen dimension (mm).

The DIC was used to analyze the crack pattern and the continuous deformation of the specimen. With this equipment, a step-by-step analysis is possible, concerning the applied load and the specimen behavior, a very valuable tool to assist the investigation of the strain hardening behavior with the addition of the SAP and steel fibers. The DIC setup included a digital camera, sufficient light in the specimen, and a careful prepared sample. The sample preparation consisted of painting the specimen with a white paint, forming a uniform white base, where aleatory and heterogeneously dark dots are impregnated to form distinct patterns that can be recognized by the image correlation program. The software used works well, when the dots, the camera configuration, and the camera position are adjusted for each dot to have four to six pixels in the picture. Before beginning each test, a calibration image is taken to convert the pixel scale to a millimeter scale. The camera, the testing machine and the data acquisition system for LVDT measurements started to operate simultaneously so that the data could be correlated later.

Image processing software VIC-2D was used in this study to correlate different images and obtain the corresponding deformations. The software relates the deformed images by dividing the area of interest (AOI) into many small regions, called subsets, where each subset is unique and identified by the program via the dots pattern. The program detects the change in the first image subset, set as a reference, with the images taken during the test and calculates the distance, which is used to calculate the full-field displacement and strains by interactive techniques (SCHREIER *et al.*, 2009).

Due to the brittle behavior, it is challenging to obtain the post-peak strain–stress curve of plain concrete specimens with the direct tension test with displacement control. In this case, the splitting tensile strength test was carried out based on EN 12390-6 (2009). This method was used mainly to evaluate the effect of SAP incorporation on tensile strength. Three cylindrical samples (Ø 100m × 200 mm) were used to measure the splitting tensile strength of concrete on the seventh and 28th day. The machine for testing the splitting tensile strength was an MTS microcomputer-controlled electromechanical universal test system, with the loading speed of 0.2 MPa/s.

4.4 Results and Discussions

4.4.1 Influence on Mortar Flow

The flow values of each mixture and the corresponding superplasticizer content are presented in Table 7. The results of mixtures REF-35 and SAP-02, without fibers, showed that to keep the same flow (183 mm) in both mixtures, 0.2% of SAP required an increase of 12% in the superplasticizer dosage. Mixture SAP-0.3, with the same superplasticizer dosage but more 0.1% of SAP, led to a small reduction in the flow (180 mm). This effect on flow is expected, as the incorporation of SAP particles increases the solid particle concentration in the fluid, but the effect was limited and manageable. Paiva *et al.* (2009) proposed that a water-reducing agent could be efficient at maintaining the flowability since SAP particles do not interfere with the plasticizer chains.

The adverse effects of steel fibers on workability of concrete have been widely discussed by (BAYASI and SOROUSHIAN, 1992), and by more recent publications dealing with high strength concrete such as (FERRARA and MEDA, 2006) and

(HOLSCHEMACHER *et al*., 2010). In order to have enough workability after the incorporation of fibers, the superplasticizer content was increased to 2% of the cement weight, which led to a reference flow of 307 mm (REF-035F).

The effect of SAP on the flow can be clearly seen in the last four mixtures of Table 7, since the water content and the superplasticizer dosage were kept constant. The flow progressively decreases as the addition of SAP increases. The reduction was 20.85%, 25.1%, and 32.2% for 0.2%, 0.3%, and 0.6% of SAP, respectively.

The decrease in the workability suggests that the additional water provided to fill the SAP is not enough to fully saturate the SAP, and the flow decrease is a consequence of lesser free water per unit of volume, due to extra water absorbed by the SAP. These findings were supported by Filho *et al*. (2012). The opposite effect was reported by Liu *et al*. (2020), Faping and Jiesheng (2019), and Dudziak and Mechtcherine (2008), which leads to a gap in the literature as the effect of the SAP in the workability is not entirely understood.

Jensen (2011), Zhao *et al.* (2020), and Hasholt *et al*. (2012) explained that the broad diversification of results would depend on the methodology used to accurately estimate the amount of water absorbed by SAP in the cementitious environment. The over or underestimated amount of additional water can affect the workability and the total w/c. Another hypothesis of the loss of workability was provided by Snoeck *et al*. (2014), who believed that the swollen SAP particles behaved as soft aggregates and offered a restraining effect in the rheology of the mortar. Nevertheless, all the mixtures maintained good workability and no signs of segregation.

4.4.2 Compressive Strength

A summary of the compressive strength results for the fiber reinforced concrete and the plain concrete at 28 days is provided in Figure 17 and Table 8. Each compressive strength result is the average of six specimens.

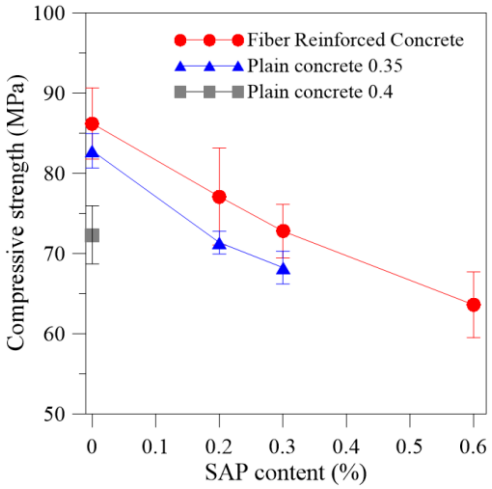

Figure 17 - Compressive strength results at 28 days of the fiber reinforced concrete of the $w/c_{(basic)}$ of 0.35; plain concrete without fiber reinforcement with the $w/c_{(basic)}$ of 0.35, and the plain concrete without fiber reinforcement with the $w/c_{(basic)}$ of 0.40.

Increases in SAP dosage for the same $w/c_{(basic)}$ tended to almost linearly decrease the compressive strength for both mixture series (with and without fiber reinforcement). However, comparing the compressive strength of mixtures with same $w/c_{(total)}$, REF-040, and SAP-0.3, the values were similar. This indicates the major role of the total volume of pores on strength, regardless of the presence or absence of SAP.

Table 8 - Mechanical properties of the high strength concrete and steel fiber reinforced concrete.

Mixture	Mean Compressive Strength (MPa)	Strength Reduction Considering the $w/c_{(basic)}$ (%)	Mean Tensile Stress (MPa– first cracking	Ratio of Tensile to Compressive Strength
REF-035	82.80 ± 2.1	-	5.39	0.065
REF-040	72.32 ± 3.6	-	4.92	0.068
SAP-0.2	71.36 ± 1.4	13.82	5.04	0.071
SAP-0.3	68.24 ± 2.0	17.58	5.07	0.074
REF-035F	86.20 ± 4.4	-	6.01 ± 0.45	0.070
SAP-0.2F	77.09 ± 4.8	10.57	4.59 ± 0.25	0.060
SAP-0.3F	72.78 ± 4.8	16.47	5.92 ± 0.04	0.081
SAP-0.6F	63.60 ± 4.1	26.22	3.23 ± 0.23	0.051

Strictly speaking, in order to individually evaluate the influence of the SAP, a specific reference mixture should be manufactured containing the same total w/c ratio, but for the purposes of the present work, this information was not considered necessary.

This subject leads to a discussion presented in the literature that has yet to be enlightened. Many authors have reported the loss of compressive strength in the literature. However, as published by Zhao *et al.* (2020), this loss of strength could be provoked by the excess of water addition due to a misleading measure of the SAP absorption in the

cementitious environment. Simple methods have been used to estimate the SAP absorption capacity and could be overestimating the water absorption, increasing the water in the mixture, and lowering the compressive strength. However, this hypothesis was not validated by the slump results obtained in this research. If there were an excess of water in the fresh state, the slump would not decrease since it would facilitate the workability.

Another explanation and more common for the loss of strength, supported by Hasholt *et al.* (2012), Chindasiriphan *et al.* (2020); Lee *et al.* (2010); Snoeck *et al.* (2014), and others, determined that the initial swelling of SAP creates a reasonable amount of macropores due to the SAP swelling. Snoeck *et al.* (2014) further explained that in the fresh mix, macropores spontaneously form and become occupied by swollen SAP particles. Following this, the concrete pore solution is consumed by cement hydration, which decreases the ambient moisture where the SAP is located. Afterward, SAP slowly releases the inside water, causing the SAP to shrink. After SAP voids form, they result in increases in the total porosity of the concrete system. However, some studies have reported a straight gain due to effective internal curing, where the later hydration of the cement provided by the SAP entrapped water densified the pore structure, which was not the case in this study.

The addition of steel fibers in the mixture increased the compressive strength in 4.11%, 8.03%, and 5.51% when compared with the reference without fiber reinforcement and $w/c_{(basic)}$ of 0.35 for the 0.2%, 0.3%, and 0.6% of SAP incorporation, respectively. The 0.6% of SAP was determined to be the highest SAP incorporation for this mix design. Given that, according to ACI COMMITTEE 363 (2010) and ABNT NBR 8953 (2015), the lower limit of strength to be classified as HSC is 55 MPa, for this research, it was stipulated to reach a minimum value of 60 MPa so that the concrete can be classified as high strength.

4.4.3 Autogenous Shrinkage

The deformation measured in the test was considered as autogenous shrinkage since minimum moisture exchange occurred between the specimens and the environment

due to the coat of aluminum and plastic tape applied to the specimens before starting the test.

The scope of the research was to find the content of SAP that could mitigate or control autogenous shrinkage. Therefore, the worst-case scenario was to carry out the test without fiber reinforcement, since the reinforcement is an obstacle to the free shrinkage. The autogenous shrinkage for the mixtures without fiber reinforcement up to 28 days are shown in Figure 18. Each value represents an average of three specimens. As displaced in Figure 18, the reference, REF-035, presented autogenous shrinkage much higher than that of ordinary concrete, and increased significantly in the first seven days due to the absence of coarse aggregate and the low water/binder ratio. REF-035 presented a maximum deformation of 424 μm/m and an initial expansion of 106 μm/m, which was overcome by autogenous shrinkage after 10 h.

As general trend in Figure 18, from 10 days onwards the shrinkage variation is relatively small. In the SAP-containing mixtures, the percentage of 0.3% completely mitigated the autogenous shrinkage and presented a maximum expansion of 248 μm/m at six hours after setting. The shrinkage did not counterbalance the expansion and, after 28 days, still presented 42 μm/m of expansion. The expansion phenomenon is not yet fully understood, but there are several attempts at explanation, for example, involving expansive pressure by forming hydration products (the high MgO content of the cement used may be a source of early expansion). This can be beneficial for some prestressed applications since the concrete compressive strength is higher than its tensile strength. The material is likely to withstand the maximum compression efforts induced by the expansion. Additionally, this expansion can be helpful and contribute to preventing cracking from drying shrinkage.

The use of 0.2% of SAP reduced 90% of the autogenous shrinkage compared to the reference at seven days, and it reduced 50% at 28 days. It also presented an expansion of 262 μm/m at four hours after time 0. The authors in Jensen and Hansen (2001), Jensen and Hansen (2002), and Lura, *et al*. (2003) described the water releasing mechanism of the SAP after setting of the cement-based material, which explained the reduction of autogenous shrinkage. The incorporation of SAP leads to the formation of controlled water-filled microscope inclusions, which prevent internal moisture evaporation from

compensating water loss for curing, promote the hydration of unhydrated cement, and reduce the autogenous shrinkage.

The use of more than 0.3% of SAP addition is considered to ensure autogenous shrinkage control, with beneficial properties such as the expansion, which can avoid cracking and produce a more durable concrete, as seen in Wyrzykowski *et al*., (2018).

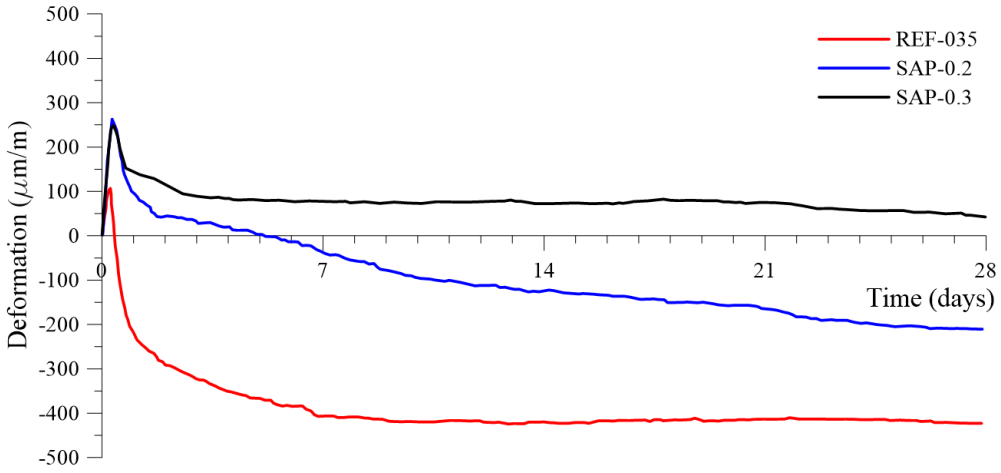

Figure 18 - Autogenous strain (um/m) for cement mortar mixtures without fibers w/$c_{(total)}$ of 0.35, with SAP additions of 0.2% and 0.3%, determined from time zero up to 28 days.

4.4.4 Tensile Properties

For the unreinforced specimens, the splitting tensile test was performed, and the tensile strength along with the ratio of tensile to compressive strength for all mixtures is presented in Table 9. The specimens failed, as expected, releasing almost all the energy soon after the peak load. The average tensile strength of the specimens without fiber reinforcement was 5.11 ± 0.2 MPa.

Typical stress-strain/load-displacement curves of the developed SFRC with SAP particles at 28 days are presented in Figure 19 a), all curves are displayed in Appendix A. A diagrammatic sketch of the strain-softening behavior presented by Naaman and Reinhardt (2006) is shown in Figure 19 b), who classified the composites based on their tensile response. The parameters regarding Naaman (2006), chosen to characterize the tensile behavior and to implement the analytical model described in the next section, were: first structural cracking stress (σ_{cc}) and force (F_{cc}); first structural cracking strain (ε_{cc}) and displacement (d_{cc}); maximum post-cracking stress (σ_{pc}) and force (F_{pc}); crack

opening (w_{pc}); and tension toughness index (TTI), as presented in Table 9. TTI is a measurement of toughness calculated by area under the stress x strain curve until the specimen ultimately failed.

Before the crack opening, the acquired displacement was used for computing the strain of the composite; after the first crack, the displacement is used for evaluation of the crack opening.

The main aspect to be highlighted by the SAP incorporation is the increase in the ductility of the composite. This behavior is not clearly seen in Figure 18Figure 19 but is distinctly observed by the DIC analysis shown in Figure 20, through the crack pattern of the SFRC. According to Naaman and Reinhardt (2006), the higher the strength, the lower the strain at the peak stress. Comparing the stress and the strain at the cracking point in the reference mixture with same point in the SAP mixtures, this rule applies. However, when comparing the mixtures with different SAP content, the mixture SAP-0.2F is an exception. Therefore, this suggests the general trade-off between strength and ductility also applies to the developed composites. The TTI values show, in general, higher tension toughness (or energy absorption) is tightly related to higher SAP content, except, again, for the SAP-0.2F mixture. Compared to the reference, the TTI for SFRC increased by 21% for SAP-03F, 12% for SAP-06F, and decreased 37% for SAP-02F.

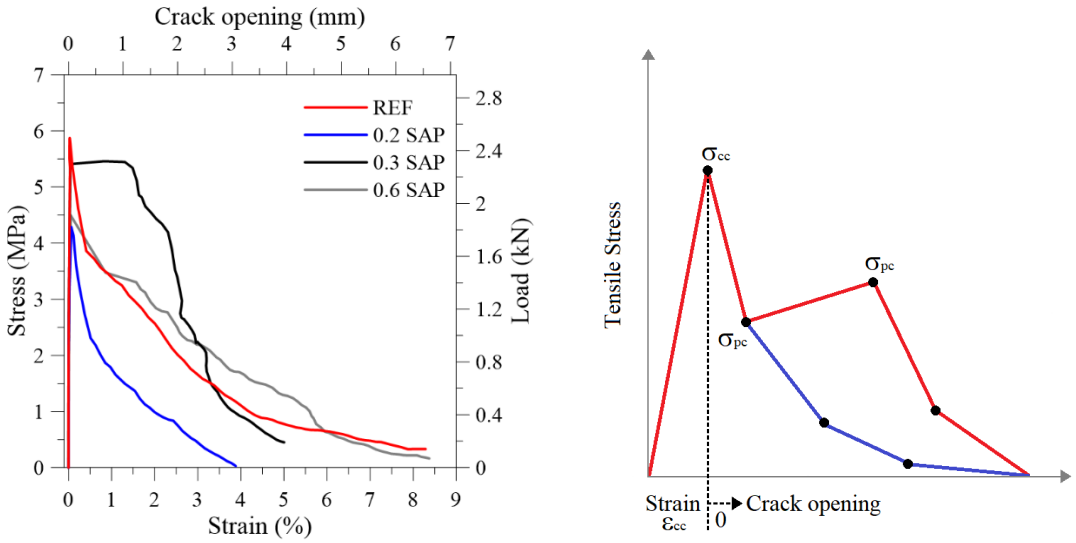

(a) (b)

Figure 19 - Stress x strain curves of: a) SFRC with different SAP content; b) typical curves of strain softening behavior.

Table 9 - Tensile properties of SFRC specimens at 28 days.

Mixture	F_{cc} (kN)	F_{pc} (kN)	σ_{cc} (MPa)	σ_{pc} (MPa)	d_{cc} (mm)	ε_{cc} (%)	w_{pc} (mm)	TTI (MPa)
REF-035F	2.45	1.63	5.87	3.86	0.023	0.029	0.325	0.1336
SAP-0.2F	1.85	0.99	4.29	2.31	0.050	0.064	0.404	0.0491
SAP-0.3F	2.38	2.26	5.62	5.35	0.035	0.044	1.169	0.1623
SAP-0.6F	1.92	1.41	4.50	3.31	0.038	0.048	1.235	0.1491

In Figure 20 images of the DIC are presented. Each image corresponds to a camera snapshot. The corresponding instant is shown in the stress-strain curve in the right column of the Table 9. Two instants are presented: point (A), when occurs the first crack, in the second column in the table; a point soon after the cracking occurrence (B), in the third column of the table. These points were obtained correlating the camera and the data acquisition times. It is possible to observe that at the first cracking stress (σ_{cc}), point A, the composite without SAP produced one transverse localized crack, which is also seen in point (B), but propagated. As for the composites with SAP, they produced a different damage mode. At point (A), first peak stress (σ_{cc}), several zones of the specimen present high stress, which are potential first cracks, showing smaller gradient of stresses. Indeed, at point (A) the reference specimen shows a large pink area (very low stresses) and a narrow yellow/red area (higher stresses) with some blue stains (low stresses). On the contrary, AT point (A), SAP mixtures show several yellow-red areas and only small pink

areas. It is interesting to note that the yellow-red pattern grows as the SAP content increases. At same time, the pink tint turns to green tint. This clearly shows more homogenous stress distribution.

The information obtained from images taken in point (B) also reveals a different behavior of the mixtures with SAP. Comparing the images of points (A) and (B), in the reference mixture, from (A) to (B) we can see an increase of the stresses in the neighborhood of the first crack, and the disappearance of the blue zones. In the SAP mixtures, from (A) to (B) we can see a decrease of yellow-red zones in the neighborhood of the first crack (meaning a decrease of the stress concentration), and some blue zones remain.

When a first crack crosses the specimen, the link between the two parts of the specimen is done through the steel fibers. This implies a release of stresses in the surrounding concrete, and an increase in the extent of the steel in the fibers that connect the two parts of the specimen. These changes necessarily imply a high stress rearrangement, which depends on the type and quantity of fibers, but for which the stress state prior to the formation of the first crack also contributes. The more homogenous stress distribution is favorable for a ductile behavior.

The TTI results show the trend of higher ductility with more homogenous stress distribution but fails to detect the multi-cracking behavior seen in images of SAP-0.2F. However, this is not an unexpected finding. In fact, the value of TTI depends on the stress of cracking and on the stress distribution after cracking. After cracking, the tensile test is in fact testing two different specimens, that result from the fracture produced by the first crack. The stress-softening branch of the curve depends on the behavior of the two parts of the specimen and on the configuration of the link (bridge) provided by the steel fibers. SAP-0.2F shows the smaller value of first structural cracking stress (σ_{cc}), and the smaller value of the maximum post-cracking stress (σ_{pc}). This cannot be explained by the low dosage of SAP. The narrower yellow-red area in the point (B) of SAP-0.2F, when compared with remaining mixtures with SAP, is an indication of higher stress concentration in the neighborhood of the first crack, which may result from heterogeneity of steel-fibers/SAP-particles distribution, but this was not further explored.

Yao *et al.* (2012) incorporated SAP to control and improve the performance of fiber-reinforced concrete with polyvinyl alcohol (PVA) fibers. SAP improved the ductility of the material by the insertion of mechanical flaws. According to the micromechanical theory developed by Wang and Li (2004) and Li *et al.* (2001), one of the criteria to increase the toughness and multiple cracking in the cementitious composite is fulfill the condition $\sigma_{cc} \leq \sigma_{pc}$. This criterion can be meet by decreasing the strength of the matrix by inserting flaws in the matrix. The matrix tensile strength does not exceed the stress required to break the bond between the fiber and matrix, and the composite develops a more ductile behavior.

This type of behavior was intensely studied with PVA fibers. However, for composites with steel fibers, it was observed that as soon as the specimen cracked on reaching the σ_{cc}, there was a sudden drop in stress, leading to large crack widening. A large amount of steel fibers is required to avoid this behavior, with consequences on cost and workability.

Nevertheless, it was also noted from Figure 20 that the SAP incorporation enhanced the toughness of the composite as it increased the multiple-cracking behavior when the difference of σ_{cc} and σ_{pc} was lower. The mixture with 0.3% SAP addition achieved the best behavior due to the small loss of strength after the first cracking. The difference between the two stresses, σ_{cc} and σ_{pc}, was 0.3 MPa.

The stable multiple-cracking behavior is achieved when σ_{pc} is higher than σ_{cc}, allowing different sections of the specimen to reach σ_{cc}. For the developed SFRC, the σ_{pc} was not higher than the σ_{cc}, and the multiple-cracking behavior was not achieved. Still, the fibers fulfilled their purpose to increase the toughness and produce a progressive, yet gradual decrease in the load-carrying capacity.

As already mentioned, as the SAP addition increased, there was a tendency to the tensile strength decrease. The mixture with a content of 0.2% SAP was the exception. The exception is relevant in the concrete with fiber reinforcement, since only two mixtures were prepared with SAP (0.2% and 0.3%) and without fibers, with similar tensile strength.

Liu, Farzadnia and Shi (2020) along with Wang *et al.* (2019), are the few articles found in the literature investigating the tensile behavior of steel fiber reinforced concrete with superabsorbent polymers. Wang *et al.* (2019) focused on investigating different types and contents of steel fibers, with an established SAP content in the mixture, as opposed to our research that fixed the fiber type and content to investigate the influence of different SAP content.

As reported by Liu, Farzadnia and Shi (2020), the addition of SAP increased the flexural to compressive strength ratio of their ultra-high-performance concrete (UHPC). For the UHPC with small size SAP, the increase in the ratio regarding the reference was 8% with 0.3% of SAP and 22% with 0.6% of SAP. Despite the difference in the test method, flexural strength is an indirect measure of the tensile strength. The increase of the ratio tensile to compressive strength could also be observed for the concrete without fiber reinforcement (Table 8).

The ratio increased by 9% for 0.2% SAP and 14% for 0.3% SAP. The increment in the tensile to compressive strength ratio means that the SAP's internal cure is more beneficial for the development of tensile than compressive strength. Liu, Farzadnia and Shi (2020) raised the hypothesis that the addition of SAP increased the interstitial bonding strength of steel fibers. Additionally, this could be one of the critical factors in increasing the tensile to compressive results. However, for SFRC, only the 0.3% of SAP addition showed an improvement in the ratio of 16%; as for the other content, no improvement was observed.

Mix	First Crack (A)	Crack Propagation (B)	Moment in the graphic
REF-035F	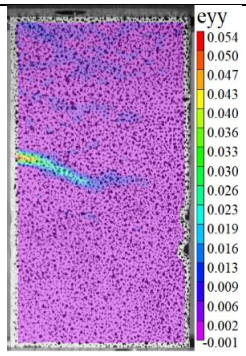	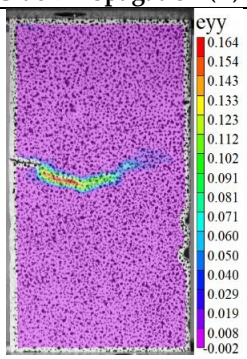	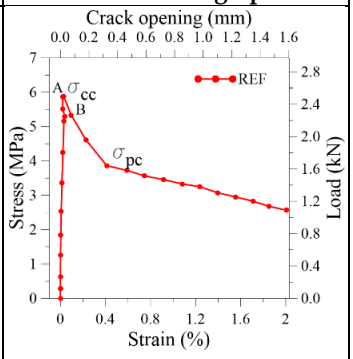
	f_a = 2.45 kN, d_a = 0.023 mm σ_a = 5.87 MPa, ε_a = 0.00029	f_b = 2.25 kN, d_b = 0.075 mm σ_b = 5.33 MPa, ε_b = 0.00095	σ_{cc} = 5.87 MPa, ε_{cc} = 0.00029 σ_{pc} = 3.86 MPa, w_{pc} = 0.325 mm
SAP-0.2F	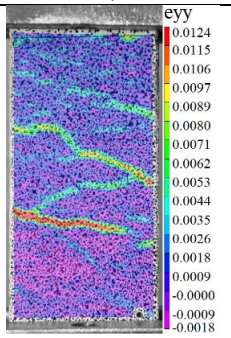	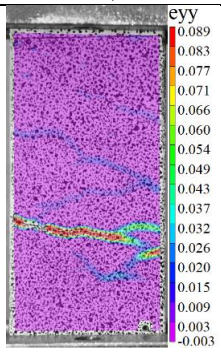	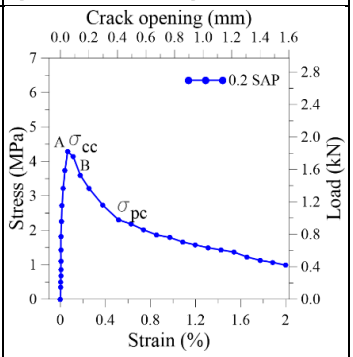
	f_a = 1.84 kN, d_a = 0.050 mm σ_a = 4.29 MPa, ε_a = 0.00064	f_b = 1.54 kN, d_b = 0.139 mm σ_b = 3.60 MPa, ε_b = 0.00177	σ_{cc} = 4.29 MPa, ε_{cc} = 0.00064 σ_{pc} = 2.31 MPa, w_{pc} = 0.404 mm
SAP-0.3F	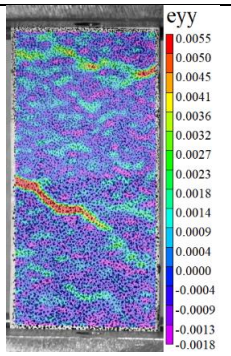	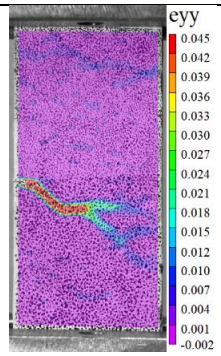	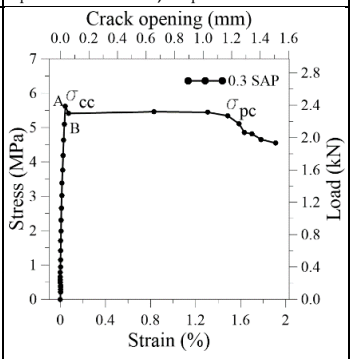
	f_a = 2.38 kN, d_a = 0.035 mm σ_a = 5.62 MPa, ε_a = 0.00044	f_b = 2.29 kN, d_b = 0.056 mm σ_b = 5.41 MPa, ε_b = 0.00071	σ_{cc} = 5.62 MPa, ε_{cc} = 0.00044 σ_{pc} = 5.35 MPa, w_{pc} = 1.169 mm
SAP-0.6F	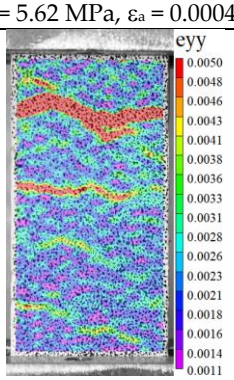	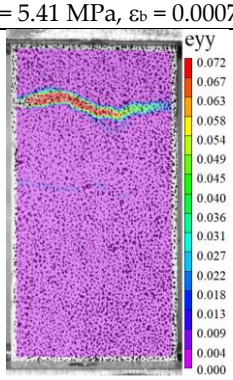	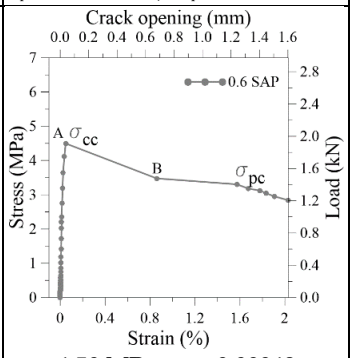
	f_a = 1.92 kN, d_a = 0.038 mm σ_a = 4.50 MPa, ε_a = 0.00049	f_b = 1.48 kN, d_b = 0.674 mm σ_b = 3.48 MPa, ε_b = 0.00859	σ_{cc} = 4.50 MPa, ε_{cc} = 0.00048 σ_{pc} = 3.31 MPa, w_{pc} = 1.235 mm

Figure 20 - Morphology of cracking apparent on the face of a specimen of SFRC, where A is the first cracking point, and B is the crack propagation, both presented in the respective graphic for each mix.

4.4.5 Analytical Tensile Evaluation of SAP Incorporation

There are many analytical models to describe the behavior of fiber reinforced concrete, especially regarding steel fiber reinforcement, for example, Aveston and Kelly (1973), Gray (1984), and Rossi (1987). It was not within the scope of this work to evaluate the best analytical model to describe the experimental obtained curves. Instead, a more contemporary and consolidated model was chosen to describe and predict the SFRC. The variable engagement model (VEM) has been extensively used to investigate fiber reinforcement, even in DIC analyses of direct tensile test such as in Rasheed and Prakash (2018), more details of the model can be found in Voo and Foster (2004) and Lei *et al.* (2005). This model gives an approach for modeling strain softening behavior on uniaxial tension, where the fibers are randomly orientated in three dimensions.

For modeling the developed SFRC, as the fibers were straight the mechanical anchorage was dismissed. The total tensile stress computed by the model, f_t, was composed by the sum of the stress carried by the matrix, f_{ct}, and the stress carried by the fibers, f_{st}. The stress in the fibers is mobilized through frictional stresses between the fiber and the matrix. The stress balance is outlined in Figure 21 a) and Equation (10).

$$f_t = f_{ct} + f_{st} \tag{10}$$

VEM considers that the embedded fiber is pulled out from the crack's side with a short-embedded fiber length and ignores the axial elastic deformation of the fibers. An exponential tension softening relationship on the matrix is provided as:

$$f_{ct} = f'_t \cdot \exp(-c \cdot w) \tag{11}$$

where f'_t is the tensile strength of the specimens without fibers; w is the crack width on the specimen at a given load; and c is an attenuation factor for the concrete matrix undergoing tension decay after cracking. The c parameter is a variable to the model, which should determine through experimental curves.

The stress carried by the fiber is given by:

$$f_{st} = K_f \alpha_f \rho_f \tau_b \tag{12}$$

where K_f is the global orientation factor; α_f is the aspect ratio; ρ_f is the volumetric ratio; and τ_b is the mean shear stress between the fiber and the matrix.

The aspect ratio is given by:

$$\alpha_f = \frac{l_f}{d_f} \tag{13}$$

where l_f is the length of the fiber and df the diameter, and the global orientation factor is given by:

$$K_f = \frac{(\tan^{-1}(w/\alpha))}{\pi}\left(1 - \frac{2w}{l_f}\right)^2 \tag{14}$$

where α is the engagement parameter, which for fiber composites with straight or end hooked steel fibers is of $\alpha = d_f/3.5$.

The presented model is not valid when the fiber fracture, so, the Equation (15) must be satisfied.

$$l_f < l_c = \frac{d_f}{2}\frac{\sigma_{fu}}{\tau_b} \tag{15}$$

where lc is the critical fiber length and σ_{fu} is the ultimate tensile strength of the fiber.

In the present case, by observing the cracked section, after the tensile test was performed, no fiber fracture was detected, so the model is applicable. The analytical model presented using Equations (10) – (15) was plotted with the experimental results in Figure 21 b), where EXP designates the experimental and ANA represents the analytical curves of the tensile stress, f_t, of the composite (matrix + fibers).

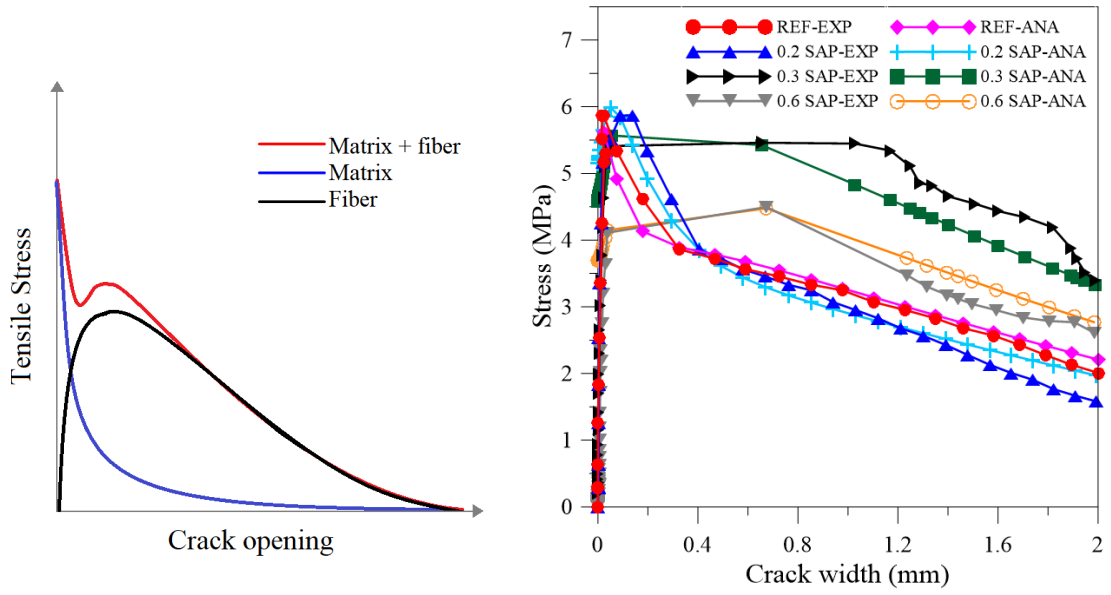

(a) **(b)**

Figure 21 - a) Typical stress versus crack opening after cracking for the fiber–matrix composite. b) Analytical model with experimental results for the SFRC with SAP additions.

Since all the composites had the same type of fiber and at equal content, only three parameters of the model vary: the parameter c that is dependent of the type of concrete; the stress at the fiber bond; and the tensile strength of each composite at 28 days. The tensile strength was provided by the results obtained in the tests. The other parameters were adjusted to the experimental curves, using the values presented in the literature as first approach.

The values obtained by fitting these parameters revealed that the bond between the fiber and the matrix was enhanced with the SAP addition, except for the 0.2% content, which is again an exception, due to uncertain causes. The initial value set for the bond strength was 10 MPa, value given by Orange *et al.*, (2000). The interpolation to better fit the experimental curve to the model led the following results: for the reference mixture, the stress bond was 9 MPa; mixtures with SAP, SAP-0.2F, SAP-0.3F, and SAP-0.6F, the stress bond was 8.0, 13.5, and 11.2 MPa, respectively.

The bound results can indicate that SAP-0.3F provide superior bond between the fiber and the matrix, and, consequently, enhance the toughness and present the best behavior. Results from the SAP-0.6F mixture are also in agreement with the assumption that the SAP addition enhance the bond between the matrix and the steel fibers.

The VEM is designed for strain-softening cementitious materials. Other explanations for the increased bonding resulting from fitting can rely on the Micromechanical Law of Li and Leung (1992) strength criteria. SAPs decreased the tensile strength and presented a slight strain-hardening behavior that can be interpreted as the increased bounding. The same amount of fibers due to the loss of tensile strength for the sap voids increases the effective fiber volume, increasing the multiple cracking effects observed in the DIC images and showing the result of a higher bonding value.

The parameter c can be physically interpreted as expressing the level of tension decay after cracking; the typical value for concrete is 15 and it is 30 for mortar (VOO and FOSTER, 2004). The fitting values revealed that the SAP addition increased the value of c, which means that changed the material to be more likely to usual mortar than to usual concrete. The values obtained were the following: for REF-035, c was 15, which is the typical value for concrete; for SAP-0.2F, SAP-0.3F, and SAP-0.6F, c was 6, 18, and 22, respectively. The very low value of c for SAP-0.2F, also reveals some abnormality of the test of this mixture, in agreement with the exceptions previously mentioned.

In summary, this work showed that the analytical model can be used to describe the behavior of the SFRC with SAP under uniaxial tension. The adjusted parameters presented a good correlation, indicated by a mean correlation R^2 of 0.97. Future work should be performed to better investigate the pull-out behavior and evaluate the robustness of the indicated values.

4.5 Conclusions

This study established the framework to investigate the tension behavior of a durable steel fiber reinforced concrete with increasing dosage of SAP and to develop an HSC with SAP to mitigate autogenous shrinkage. It shows that an analytical model can be used for predicting the tension behavior of HSC with varying SAP dosage. Based on the results presented, the following conclusions can be drawn:

- HSC can incorporate a dosage of 0.6% of SAP, keeping high strength and workability.

- Autogenous shrinkage can be adequately mitigated using a content of 0.3% SAP.

- The use of 0.3% SAP was also beneficial in different aspects. It has minor influence on workability, it is compatible with high strength concrete, and significantly enhance the SFRC's ductile performance.

- The variable engagement model used was capable of describing the behavior of the SFRC with SAP. This model can be used in finite element applications.

- The use of fiber reinforcement, in a content of 1.28%, was not sufficient to provide considerable multiple cracking behavior. A higher volume of fibers is required to promote considerable strain-hardening behavior.

In order to resume the investigation using SFRC, the crack control was not achieved for the 1,28% of fiber content with the testing conditions carried out. An experimental campaign was initiated with a higher percentage of fibers, 1.5%, to achieve the strain-hardening behavior. However, the very low workability obtained prevented the study from moving forward.

STAGE II –Plain Concrete

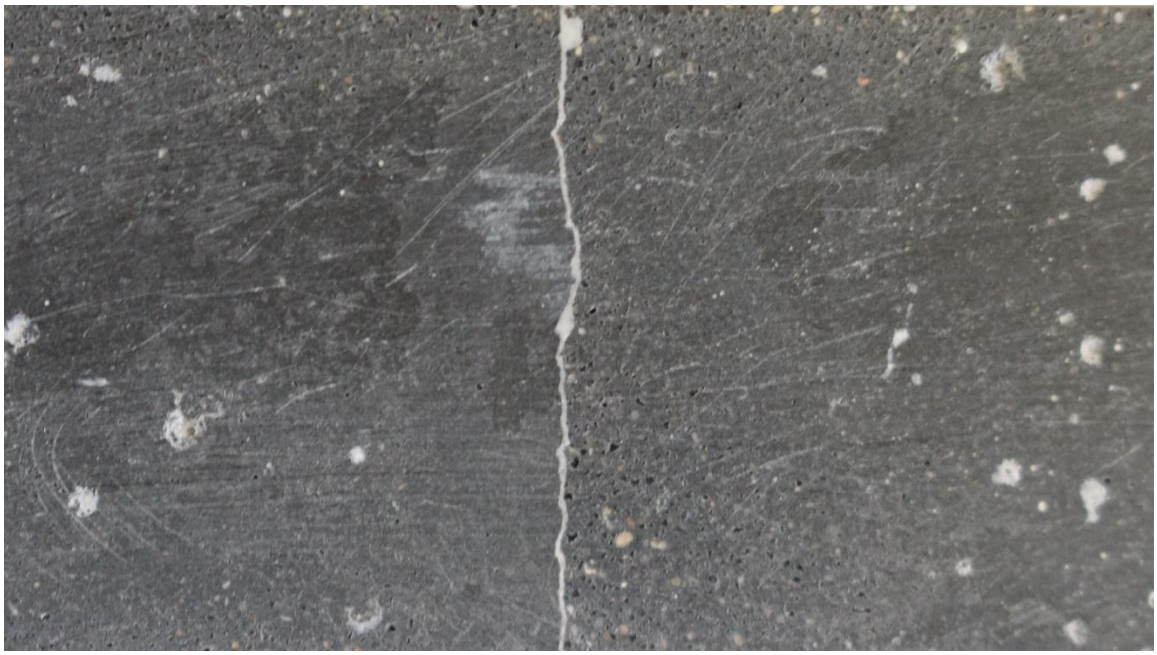

5 – AUTOGENOUS SHRINKAGE

Autogenous Shrinkage of high strength concrete with SAP for self-healing purposes.

Abstract

Cracking due to autogenous shrinkage (AS) on high strength concrete (HSC) has become a significant problem to the structures' durability. SAP has been pointed out as one of the principal alternatives to control AS. This chapter presents the results of autogenous shrinkage tests on a HSC with superabsorbent polymers (SAP) as an option for AS control and potential self-healing purposes, studying mixtures with 0.3% and 0.6% of SAP. The investigation showed that both contents were enough to suppress autogenous shrinkage, without compromising the high compressive strength. The AS RILEM Model B4, updated by Rasoolinejad *et al*. (2019), and experimental results obtained from the literature were used as benchmark for the experimental findings. It was concluded that, despite the different formulation, the test results are in accordance with the values obtained by others, and present a good correlation with the model, when expressed through a coefficient of correlation (R^2 of 0.95).

5.1 Introduction

Autogenous shrinkage (AS) became a significant issue after the development of high strength concrete (HSC). The low water/cement (w/c) of the cement pastes on HSC implies that hydration leads to a formation of a fine, dense microstructure with a decrease of internal relative humidity, which significantly increases the autogenous shrinkage and could lead to cracking of the concrete (TAZAWA, and MIYAZAWA, 1995; LOUKILI *et al.*, 1999; IGARASHI *et al.*, 2000; YANG *et al.*, 2005). Several alternatives to solve the problem have been addressed (WEBER and REINHARDT, 1997; JENSEN and HANSEN, 2001 a, BENTUR *et al.* 2001; CRAEYE *et al.*, 2011;). The one with more promising results is the use of superabsorbent polymers (SAP) to mitigate autogenous shrinkage (JENSEN and HANSEN, 2001 b; JENSEN and HANSEN, 2002;

WYRZYKOWSKI *et al*., 2011; HASHOLT *et al.*, 2012; MECHTCHERINE *et al.*, 2014; LIN and PANG, 2019; DE MEYST *et al*., 2020; REIS *et al*., 2020; SANTOS *et al.*, 2020).

Some attempts to model the autogenous shrinkage of HSC and the influence of the use of SAP were investigated as a function of cement hydration (WYRZYKOWSKI *et al*., 2011; SHEN *et al*., 2015; RAHIMI *et al*., 2019; LU *et al*., 2020). The models developed are often complex and challenging to use in the currently available computer models for structural analysis since they require knowledge of the water migration in the inner structure of cement paste and sophisticated mathematical functions. Simple analytical models are the most used since they are easy to implement and often have the required accuracy to crack control. Some of them are presented on standards: Eurocode (EN 1992-1-1, 2004), JSCE code (2007), CEB MC90-99 (CEB-FIP Model, 2010). According to Hubler *et al*. (2015), the B4 model (BAZANT *et al*., 2015) gave the best predictions when compared with results from different standards.

As the hydration of cement can continue for decades, the B4 model highlights the importance of autogenous shrinkage over a long period since most research results are focused on values obtained over a few months. Having a model that predicts AS in the long term, like Model B4, is of great interest since the results found in the literature of HSC are scarce and for a maximum of six months (JENSEN and HANSEN, 2002; SCHRÖFL *et al*., 2012; MECHTCHERINE *et al*., 2014; SNOECK *et al*., 2015; URGESSA *et al*., 2018; WYRZYKOWSKI *et al*., 2020).

5.2 Materials and Methods

The mix design was developed to obtain an HSC using Portuguese constituents. The proportions and the strength of the mixture used for the tests were similar to the mix design developed for the RILEM Interlaboratory Tests implemented by the RILEM Committee 225, published in Mechtcherine *et al.* (2014) and Mechtcherine *et al.* (2012). However, to adjust to the materials available in Portugal, some modifications were made. A lower content of silica was used, in order to improve workability, therefore changing the overall composition. The reference composition of the high strength concrete is shown in Table 10.

Table 10 – Reference composition of the HSC, values in kg/m^3.

Cement	Silica	Sand	Superplasticizer	Water	w/b
860	43	1032	13.50	271	0.30

SAP incorporation in the reference mix design implies changes in the dosages of the constituents since the introduction of SAP demand extra water that will be absorbed by the SAP particles. The added water will change the total water/binder ratio but keeping constant the water/binder ratio called basic. In order to achieve the corrected dosages of the SAP mixtures, the volume of the materials presented in Table 10 (1 m^3) and the volume (V_{abs}) of the added water was summed, and the final dosages, per cubic meter, of each constituent was computed using this correction factor (dosage of Table 10 reduced by the factor $1+V_{abs}$). The composition after the adjustment used in the research is presented in Table 11. These HSC were used to evaluate the influence of a superabsorbent polymer on AS.

Table 11 – Composition of the HSC mixtures, values in kg/m^3

Mixture (kg/m^3)	0% SAP	0.3% SAP	0.6% SAP
Cement	860	822	786
Silica	43	41	39
Sand	1032	986	943
Water	271	259	247
SAP (dry)	0.0	2.58	5.16
Added water	0.0	46.4	51.6
Superplasticizer	25.8	24.7	23.6
Water	271	259	247
Water Basic / Cement	0.31	0.31	0.31
Water Basic / Binder	0.30	0.30	0.30
Added water / Binder	0.00	0.05	0.11
Water total / Binder	0.30	0.35	0.36
Binder / Aggregate	0.88	0.88	0.88

All the HSC compositions have the same relative proportions of binder and siliceous sands aggregate (0.88), and used the same cement, with Blaine fineness of 5760 cm^2/g. The water-binder (w/b) ratio was set at 0.30. The content of the superplasticizer was adjusted to reach the required workability.

The sand particle size distribution (grading curve) was chosen in order to comply with the usable zone, preferably to reach the optimum zone, of the recommendations of the NP EN 933-1 (2014) standard, as shown in Figure 11 in item 4.8.3. The fineness module was 2.73, the nominal maximum particle size was 4.75 mm, and the density is 2.65

kg/dm³. The content of SAP is presented item 4.8.5, and was set to 0.0%, 0.3%, and 0.6 % of the cement dosage.

The mortars were prepared in a mechanical pan mixer with 3 liters of capacity from ELE International (Bedfordshire, UK) under the following steps. The first step was a dry mix of the cement, sand, and SAP (if used) for 5 min at slow speed. The second step was the addition of water and superplasticizer, mixing for more 2 min at the same speed, and then the velocity was increased to high speed for 5 min. Then the mixer was stopped, the edges of the bowl were scraped, followed by a mixing phase for 3 min at high speed.

Pastes and mortars were cast into the corrugated tubes (WYRZYKOWSKI *et al*., 2017) using a vibrating table for proper compaction. The filling process was performed with the help of a syringe, carefully adjusting the filling rate and the vibration amplitude in order to avoid the formation of large air bubbles in the tube. When filled, each tube was firmly capped and glued with epoxy to avoid air exchanges with the surroundings. Subsequently, the external surface of the tube was cleaned, and the specimen was weighed and put on the steel frame of the test equipment. The room temperature was 22 ± 1 °C during all tests. Additionally, prismatic specimens were cast for compressive strength and Young´s Modulus tests, also prepared in the vibrating table. The size of the prisms was 40 x 40 x 160 mm for the compressive strength tests and 50 x 50 x 200 mm for Young's Modulus tests.

5.2.1 Autogenous shrinkage

The autogenous shrinkage was assessed according to the ASTM C1698 - 09 (2009) standard using the corrugated tube method, shown in Figure 22. The test consists of the continuous measurement of the deformation of the cement-based material, cast in a corrugated tube with nominal dimensions of 28.5 mm of diameter (minimum of 25.4 mm and 28 mm in the corrugation) and a length of 440 mm.

As mentioned, after casting, each tube was placed on the steel frame shown in Figure 22. The longitudinal deformation of the corrugated tube was recorded by an electronic comparator of the brand Mitutoyo Europe (Neuss, Germany), with ± 3 μm of precision (resolution of 1 μm), logged at a data acquisition system that record the

deformation initially every 5 minutes. From 4 to 10 days onwards, depending on each mixture, when the deformation rate is small, the records were performed manually.

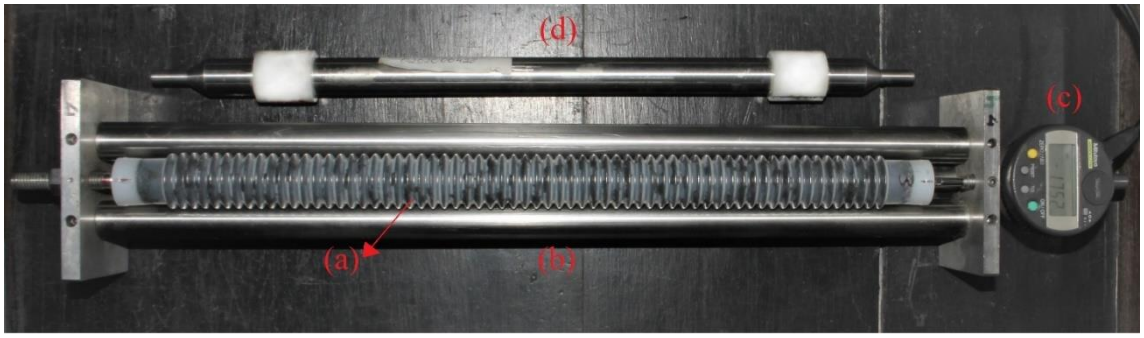

Figure 22 - Setup used for the measurements of autogenous deformation: (a) corrugated tube adequately filled and sealed, ready for the first measurement; (b) steel frame, (c) electronic comparator linked to the data logger and (d) reference bar with the length of 474 mm.

5.2.2 Compressive strength and Young´s Modulus of HSC

Compressive tests were carried out according to the standard NP EN 191-1 (2017) in mortar specimens, using an electromechanical testing device, Form Test Seidner (Riedlingen, Germany), with 200 kN load cell, with a loading rate of 2,55 kN/s. The Young's Modulus was assessed in agreement with the standard NP 12390-13, (2014), using the electromechanical testing device Form Test Seidner (Riedlingen, Germany), with 600 kN of load cell and a testing rate of 1,25 kN/s. Three measurements per mortar type were performed in the specimens with 7, 28, and 60 days of curing.

5.3 Autogenous shrinkage model

The model developed by Rasoolinejad *et al*. (2019) improved the RILEM B4 model significantly, and here is designated by the updated B4 Model. It added 417 autogenous shrinkage test measurements in the existing database and made statistical comparisons with the prediction models of the Eurocode (EN 1992-1-1, 2004), JSCE code (2007), CEB MC90-99 (CEB-FIP Model, 2010). It is expected that the B4 updated model to give significantly better data fits.

The updated B4 Model predicts an increase of the autogenous shrinkage with time without a fixed final value. The use of a power-law function characterizes the model, generally represented by Equation 16.

$$f(x) = ax^b \tag{16}$$

where a and b are constants, x is the time, and f(x) is the autogenous shrinkage.

The updated B4 Model, which predicts AS based on the concrete composition, is described in the following Equations (17) to (24). The total autogenous shrinkage is obtained from Equation 17, which takes into account the pure autogenous shrinkage, ε_{au}, obtained from Equation 19, and a swelling deformation occurring simultaneously, ε_{sw}, which is considered an intrinsic phenomenon due to hydration, is expressed in Equation 18. (BAŽANT *et al*., 2015; RAHIMI-AGHDAM *et al*., 2019).

$$\varepsilon_{au\,total} = \varepsilon_{au} + \varepsilon_{sw} \tag{17}$$

$$\varepsilon_{sw} = -\frac{k\,t^{0.2}}{1 + t^{0.2}} \tag{18}$$

where t is the time expressed in days, and k is a constant assumed to be 250 due to the lack of data.

Pure AS is a phenomenon caused by self-desiccation. The two phenomena, ε_{au} and ε_{sw}, are opposed, therefore the negative sign in Equation 18. The model considers that self-desiccation neutralizes the expansion but does not prevail in the beginning. As mentioned, the swelling is computed with Equation 18 (RASOOLINEJAD, *et al*., 2019) (used when the concrete is sealed right after it is cast, as specified in the ASTM C1698 standard (ASTM, 2009)). The pure autogenous shrinkage is obtained using information from the mixture proportioning, Equation 19.

$$\varepsilon_{au} = k_\gamma k_s C \left(\frac{t}{1\ day}\right)^n \tag{19}$$

where C and n are empirical dimensionless parameters obtained from the concrete composition; k_γ depends on the cement type, as presented in Table 12, and k_s considers the effect of supplementary cementitious materials.

Table 12 - Values of kγ

Cement type factor	N	H	M	L
k_γ	1.0	1.2	0.85	0.4

In Table 12, N is the Ordinary Portland cement, H is the high-strength Portland cement M is the moderate-heat Portland cement, L is high-early-strength Portland cement.

Parameter C is obtained from Equation 20, based on results from a database, minimizing the sum of squared errors. This equation is valid for the w/c ratio in the range of 0.2-0.8 and the aggregate/cement (a/c) ratio from 0 to 7. The aggregate to cement ratio in this formula includes both coarse and fine aggregates.

$$C = \frac{100}{\left(\frac{w}{c}\right)^{2.5} + \left(\frac{a/c}{10}\right)^{1.5}} \tag{20}$$

Parameters n and C are mutually correlated and depend on the aggregate-cement ratio (a/c). Power n of Equation 19 is obtained from Equation 21, and parameters *p* and *q* of Equation 21 are determined from Equations 22 and 23.

$$n = p + q \ln C \tag{21}$$

$$p = 1.2 - 0.1(a/c) \tag{22}$$

$$q = -0.14 + 0.005\ (a/c) \tag{23}$$

The parameter k_s of Equation 19 is given in Equation 24 and considers the presence of silica fume (SiO_2) and slag in the mixture through mass ratios per unit volume of concrete.

$$k_s = \left\{1 + 3\left(\frac{SiO_2}{Cement}\right)\right\}\left\{1 + 2\left(\frac{Slag}{Cement}\right)\right\} \tag{24}$$

The measurements taken in this study, using the corrugated tube method, according to the standard ASTM C1698-09 (2009), started nearly 30 minutes after mixing and the results show a typical curve shape shown in Figure 23. There are several

approaches for the choice of time zero (time from which the deformation is relevant), this is, when AS should begin to be recorded. As deformation of concrete as a fluid is not important for computing stresses, at time zero some solid networks should also exist. The theme is under discussion, and sometimes the value is defined based on other tests, such as the Vicat setting time or ultrasonic tests (DARQUENNES *et al*., 2010; SEDDIK MEDDAH and TAGNIT-HAMOU, 2011; WYRZYKOWSKI *et al*., 2017; HUANG and YE, 2017; FILHO *et al*., 2019).

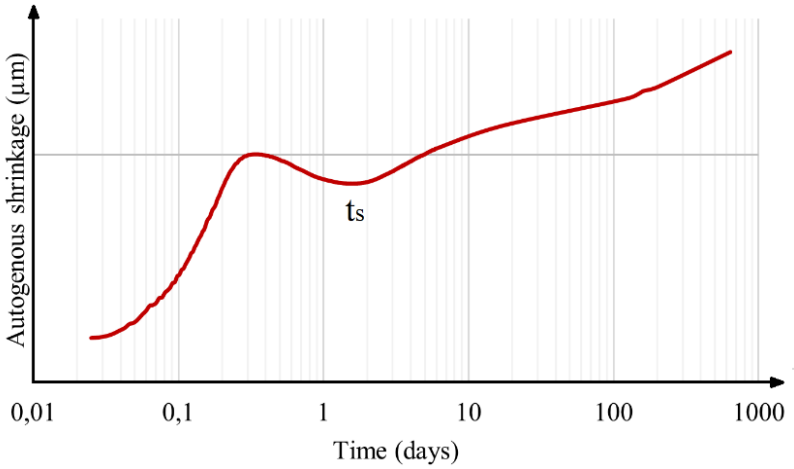

Figure 23 - Typical autogenous shrinkage curve obtained from the corrugated tube method.

This discussion is not in the scope of this work, so to fit our data into the B4 updated model, it was taken into consideration the method proposed by Rasoolinejad *et al*. (2019), that is, using the "ts" shown in Figure 23, where the curve is deflected. The autogenous shrinkage $\varepsilon_{au}(t\text{-}ts)$ is obtained by Equation 25. Also, Equation 25 is used in the model to adjust the model with the experimental data.

$$\varepsilon_{au}(t - t_s) = \varepsilon_{au}(t) - \varepsilon_{au}(t_s) \tag{25}$$

where $\varepsilon_{au\ total}$ is the total autogenous shrinkage, t is the time, and t_s is the time indicated in Figure 23.

5.4 Results and discussion

5.4.1 Compressive strength and Young's modulus

A summary of the compressive strength and Young's modulus results for HSC with 0%, 0.3% and 0.6% of SAP is provided in Figure 24. Each compressive strength result is the average of six specimens and Young's modulus an average of three specimens.

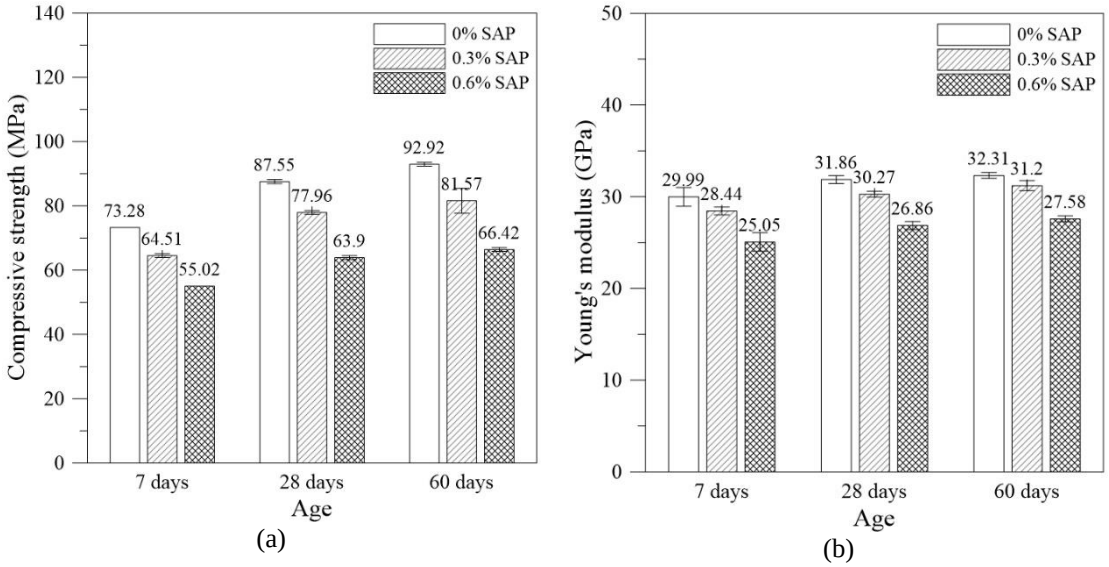

Figure 24 – Compressive strength (a) and Young´s modulus (b) of mortars with 0 %, 0.3 % and 0.6 % of SAP addition.

In accordance with literature results of Hasholt *et al.* (2012), Chindasiriphan *et al.* (2020), Lee *et al.* (2010) and Snoeck *et al.* (2014), the compressive strength and Young's modulus decrease with SAP inclusion. This phenomenon occurs due to the increase of voids in the matrix, inherent to the SAP insertion (voids in the space previously filled with the added water). In the fresh mix, SAP swell with the mixing water, and macropores spontaneously form and become occupied by swollen SAP particles. After setting, the swollen SAP leaves the water into the cementitious environment and decreases in size living voids in the matrix. The result is an increase in the concrete system's total porosity.

The loss of compressive strength increases over time, showing a maximum loss of 25%, 27%, and 29% for 7, 28, and 60 days respectively, for the mixture with 0.6% of SAP content. Young's modulus showed a medium loss of 16% for all texting dates for the mixture with 0.6% of SAP, not increasing over time. The content of 0.6% was found as

the highest SAP content that could be used in this mixture, keeping it as HSC. Following ACI 363R (2005) and ABNT NBR 6118 (2014) standards, the lower limit of strength to be classified as HSC is 55 MPa. With this criterion, all mixtures are classified as HSC. Still, the higher limit determined in the ABNT NBR 6118 (2014) is 90 MPa, therefore, the concrete strengths of mixtures used in this work are in the range accepted for structural applications.

5.4.2 Autogenous shrinkage of HSC with SAP

Figure 25 exhibits results for the autogenous shrinkage of HSC with 0, 0.3%, and 0.6% of SAP incorporation and studies with the same w/c ratio of 0.3 from Schröfl *et al*. (2012), Mechtcherine *et al*. (2014) and Wyrzykowski *et al*. (2020). The B4 updated model was applied in HSC and gave a correlation of R^2 of 0.95.

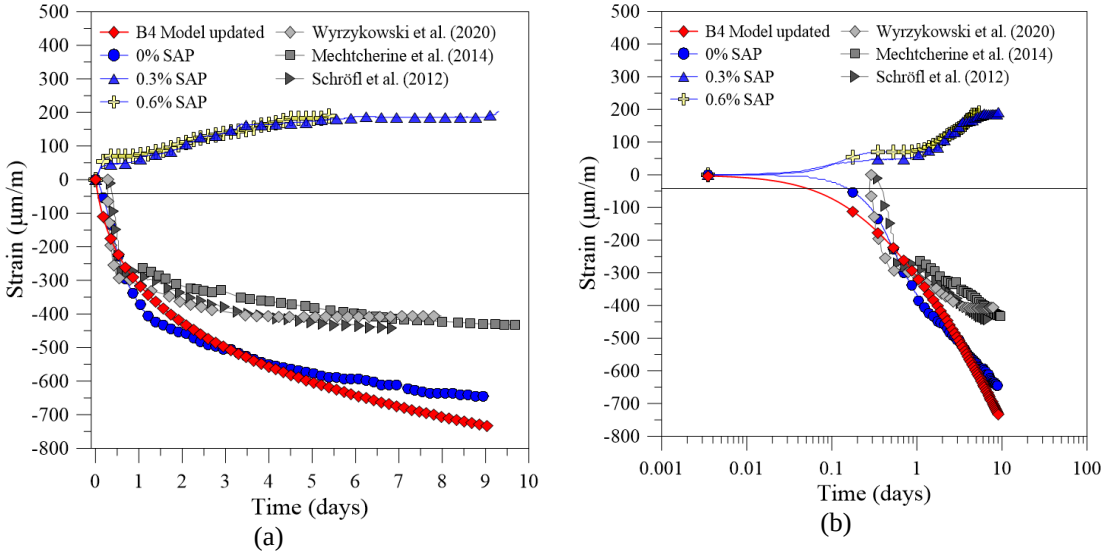

Figure 25 – Autogenous shrinkage of HSC with w/c of 0.3 (a) plot in linear time and (b) logarithm base 10 time.

The AS experimental result for 0% SAP was higher than the ones from the literature, but more in accordance with the model. The higher AS of the reference mixture, when compared with the values from others, may be related with the high Blaine fineness of the cement used. However, it is possible to see in Figure 25 that the model is well-adjusted with the experimental data obtained in this study.

Figure 25 also shows absence of autogenous shrinkage by using 0.3% or 0.6% of SAP, and an expansion of almost the same magnitude for both SAP contents, being the 0.6% SAP slightly above. Studies Hansen (2001), Jensen and Hansen (2002), and Lura,

et al. (2003) described a water releasing mechanism from SAP particles, which explains the reduction of autogenous shrinkage. The incorporation of SAP leads to the formation of microscopic inclusions filled with water, which is available to prevent the internal moisture decay, reducing autogenous shrinkage. Later, this water source also promotes hydration of the anhydrous cement particles. The expansion on Figure 25 is about 200 μm, a small value that does not cause relevant stresses for HSC.

5.5 Conclusions

An experimental investigation on the role of superabsorbent polymers of a high strength concrete, in mechanical properties and autogenous shrinkage was performed. The following conclusions were drawn:

- Using 0.3% or 0.6% of SAPs in a HSC mixture can control the autogenous shrinkage, still being high strength concrete.
- In terms of mechanical performance, the use of 0.3% is recommended since it is enough to control autogenous shrinkage and presents higher strength than the use of 0.6%.
- For self-healing purposes, the use of 0.6% may be a better option, since increases the water available for self-healing purposes, and still presents high strength.
- The B4 updated model presented a good estimation for the autogenous shrinkage results obtained with our HSC reference mixture.

6 EVALUATION OF SELF-HEALING CONCRETE BY MECHANICAL RECOVERY

New cracking methodology to evaluate self-healing by mechanical recover without fiber reinforcement

Abstract

This chapter proposes a methodology to produce a single crack in direct tension with uniform width and length using a single steel bar with a reduction in its diameter at the center. The bar is isolated from the concrete leading to no interference in the self-healing results. The methodology was developed and tested with a non-linear analysis using the finite element method with the program Ansys.

Compressive strength tests were carried out on the high strength concrete (HSC) to evaluate the concrete maturity cured at temperatures of 20°C and 40°C. This information was used to define the pre-cracking age and conditions. Pre-cracking was produced at the ages of 7 and 28 days at 20°C to evaluate the self-healing phenomena for different hydration degrees of the cement particles. The early age is more suitable to reproduce conditions when more anhydrous material is available and the cracking at 28 days intends to reproduce conditions where the concrete has older ages when cracking. After the pre-cracking, samples were stored and subjected to daily wet and dry cycles for four months.

Mechanical recovery was performed by doing the same direct tensile test, four months after the pre-cracking. In order to evaluate crack closure, microscope photos of the crack after the pre-cracking and before the verification of the mechanical recovery were taken.

6.1 Introduction

As presented before in chapters 2, 3, and 4, one of the main challenges to study self-healing is to produce the crack in the concrete, especially since the crack width, length, and location will influence the self-healing result.

As discussed previously in item 2.4, there are several techniques for assessing self-healing, and the procedures differ significantly. The study started using fibers to control the crack opening, but the results showed the need of a very high amount of fibers to achieve strain-hardening behavior, with not enough workability for molding the specimens.

Therefore, it was needed to create a new method to evaluate the self-healing behavior, without fiber reinforcement. At the beginning of this research, there was no recognized method for producing a single crack, with controlled crack width, available for plain concrete in autogenous self-healing.

As already reported in item 2.5, the studies Chindasiriphan *et al*. (2020), Park and Choi (2018), and Sidiq *et al.* (2019) were published after the beginning of the experimental campaign. Moreover, they are used to understand the autogenous self-healing phenomena without fiber-reinforcement, but the presence of a reinforcement affects the self-healing, enhancing the phenomena.

Another challenge is to produce a crack as uniform as possible and keep the same width (200 µm) during the self-healing process. Producing a crack through a notch is also a limitation, since it does not reproduce the rupture conditions when a crack forms in the structure. As better explained in item 3.2 and shown in Figure 12, SAP will create voids, and these voids will lead to a loss of strength at these points, and the crack will form where there are more SAPs and voids. Using a notch would induce the crack in a specific section that would not necessarily have the representative content of SAPs.

The method to produce a single crack was developed, which is explained later on, based on the direct tensile test used to evaluate fiber reinforced concrete. The initial attempts used usual steel reinforcement bars, since concrete and steel are mainly used in everyday applications. With the results obtained, the method was developed, reaching the

defined purposes. A non-linear analysis was conducted, and the method was applied in the variables of 0, 0.3%, and 0.6% of SAP. Another variable to be defined was the pre-cracking age. Therefore, an independent study in the HSC without SAP was conducted with 1, 2, 3, 7, 10, 14, 28, and 60 days cured at 20°C and 40°C. The mechanical self-healing assessment, using the new pre cracking technique, was done, and the analysis was complemented with the evaluation of crack closure by microscopic images.

6.2 Modeling the cracking methodology

As a brittle material, after cracking plain concrete there is an uncontrolled crack opening, leading to a sudden separation of the two parts of the specimen. A challenge when studying self-healing under reproducible conditions is to maintain the crack width at a certain size throughout the test period.

In the first attempts, the fiber reinforcement was replaced by a steel bar, and the test was carried out using the direct tensile setup used in the pilot study, shown in Figure 16. It was aimed for a single crack to appear in the middle of the specimen. The steel bar would act as anchoring bar, keeping very close the two parts of the specimen after cracking. The NP EN 1992-1-1 (2010) standard was used to design the steel rebar for the specimen, shown in Figure 16, using the cross section of the specimen, but disregarding its geometry. A single steel bar with 6 mm diameter was placed in the center of the specimen. As a result, one crack formed at the center, but another longitudinal crack also formed in the specimen's center due to the bonding between steel and concrete, as shown in Figure 26.

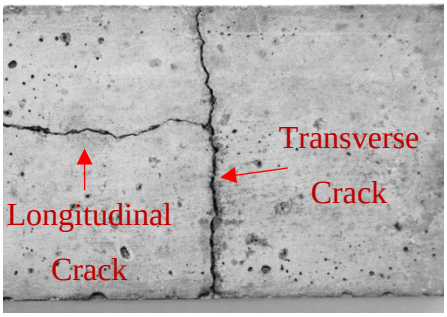

Figure 26 - Cracking pattern from one single rebar of 6 mm.

As steel has higher strength and Young's modulus than concrete (NEVILLE and BROOKS, 1987; COUTINHO and GONÇALVES, 1997; ISAIA, 2007), after unloading the crack was formed, but the two parts of the specimens were very close, with almost no evidence of crack. Since the steel was still in the growing linear branch of its tensile stress x strain curve, represented in Figure 27, two significant problems needed to be addressed to solve the cracking procedure. One is to isolate the steel bar from the concrete and avoid the longitudinal crack due to bonding.

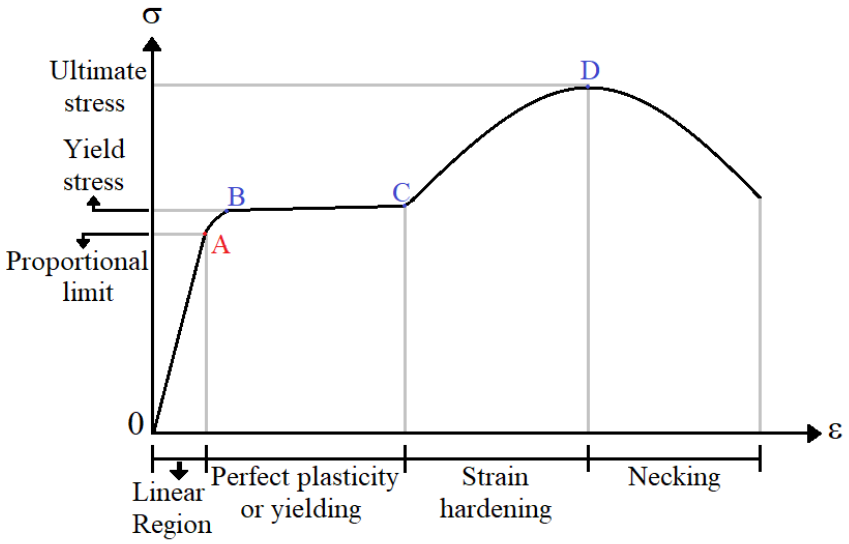

Figure 27 – Typical steel tensile stress x strain curve. Adapted from Neville and Brooks (1987); Coutinho and Gonçalves (1997); Isaia (2007).

The second one concerned the steel bar, which should be stressed until reaching the plastic branch, between points B and C in Figure 27. So, the steel would stretch in the plastic phase, and when the specimen was unloaded, the crack size should decrease, but the plastic strain should remain, representing the crack width at that size for the self-healing conditioning.

To reach the predefined crack opening, ≈ 200 μm, it was required a section of the rebar disconnected from the concrete. Hence, a small box made of Styrofoam was used in the center of the specimen, with 25 x 15 x 5 mm, coated with plastic adhesive tape to avoid adherence between the box and the concrete. The box also reduces the force required to crack the specimen and the tensile stresses in the specimen. This procedure induces the formation of a crack in all cross section, due to a uniform stress field, avoiding stress gradients as the notch would do. This way, the crack will form in the weaker cross

section, consequently where there are more voids due to SAP particles absorption, as already discussed before.

The second problem involving the maintenance of the crack's size was addressed by doing four nonlinear analysis solutions using the Workbench platform of the program ANSYS, shown in Figure 28. The overall problem was that the concrete specimen should resist the steel bar's load to enter the plastic stage between points B and C of Figure 27.

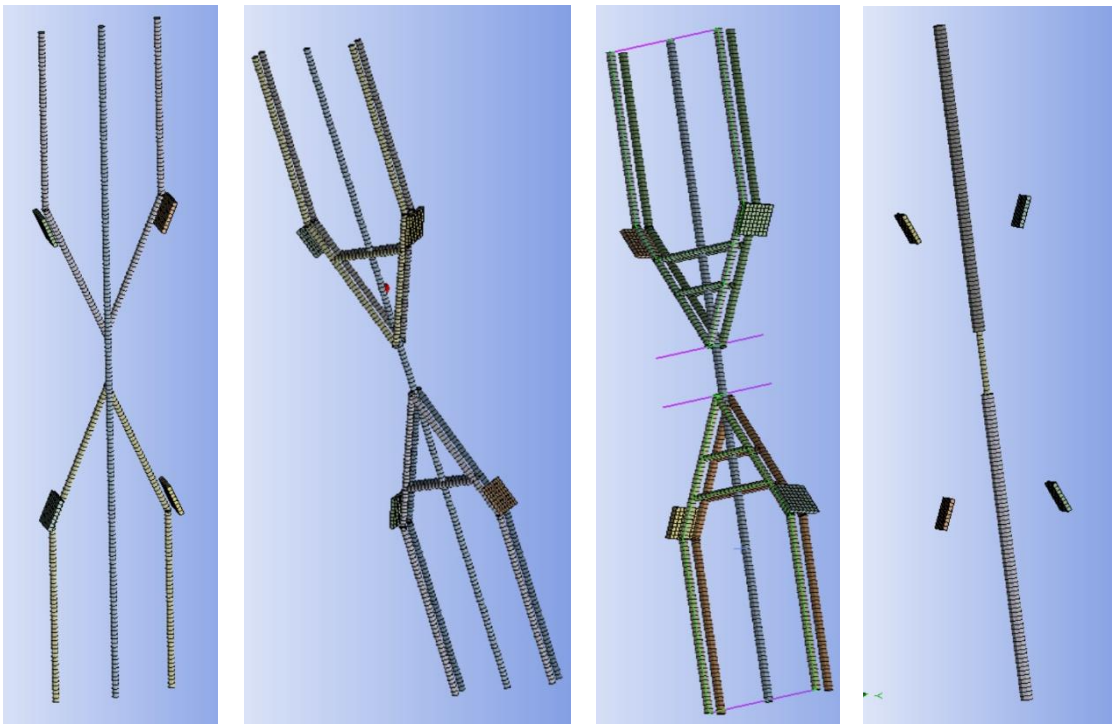

a) b) c) d)

Figure 28 – Proposed solutions for the cracking method: a) one single bar of 300 mm with 8 bars aligned according to the specimen geometry; b) one single bar of 300 mm with 16 bars aligned according to the specimen geometry and 4 transversal reinforcing bars; c) one single bar of 300 mm with 16 bars aligned according to the specimen geometry and 8 transversal reinforcing bars; d) one single bar of 300 mm of 6 mm of diameter and a reduction to 3 mm in the center.

Three approaches a), b) and c) of Figure 28 intend to reinforce tensile zones in the stress field, represented by the four squares in each picture, increasing the number of steel bars in the specimen. The adopted solution was the one represented by d) in Figure 28. This option, which reduces the steel cross-section in the middle of the specimen, allows decreasing the tensile stresses on the specimen, since it requires a lower load to reach the established crack width.

The non-linear analysis was assessed by using the Workbench from ANSYS. The package "static structural" was selected, the geometry of the concrete was set as in Figure 29. A hole in the middle of the specimen in the square format of 25 x 15 x 5mm shown in the green part was created. As shown in Figure 29 in yellow, four impactors drawn as squares were designed to apply the distribution load. The impactors were frozen for the geometry to be separated from the specimen. This initial geometry of the concrete represented in Figure 29 was equal for all four solutions. The difference relies on rebar's addition, which was done following the described below steps and according to Figure 28.

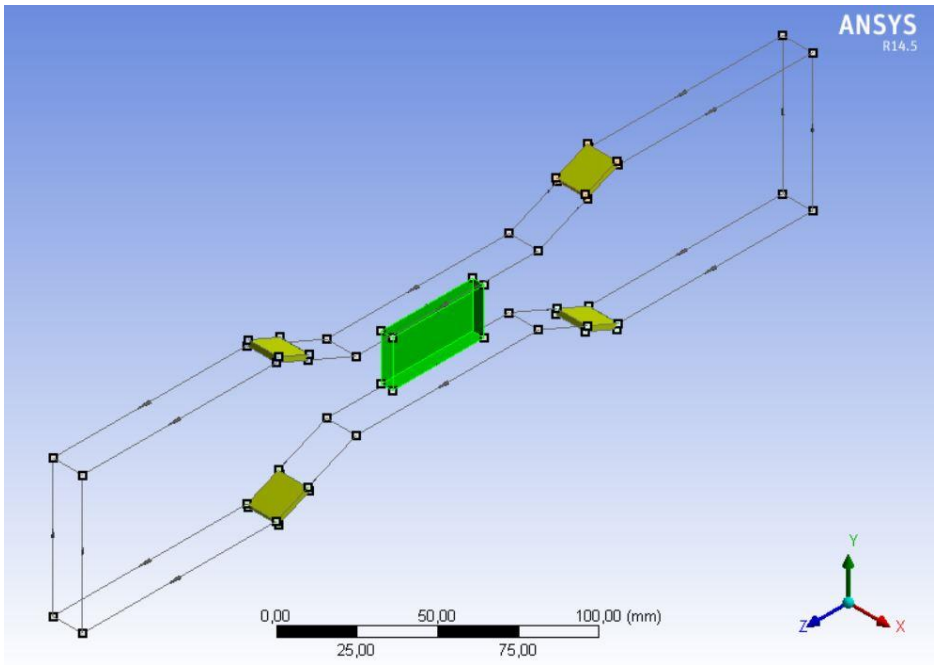

Figure 29 - Geometry of the specimen made of concrete.

The 6 mm rebars were created by drawing one line and extruding a body through this line with a circular cross-section of 6 mm in diameter. After creating all rebars for each solution, the rebars are grouped to simplify each case's calculation.

At the end of drawing all elements, there are three solids in the geometry workspace, the specimen in concrete, the rebars, and impactors. Each one will be designated with a code to specify the material.

The concrete properties were inserted in the Workbench platform by the code described in Appendix A.1 to overwrite the input material, which is structural steel,

SOLID65 was the defined element, and its characteristics are shown in Appendix A.2. Also, the multilinear isotropic hardening (MISO) was chosen in the code. Furthermore, the table data for the compressive stress versus strain curve for a 90 MPa concrete, shown in Figure 50 in Appendix A.3, was inserted in the code. As for the rebar, the code was also rewritten with the one described in Appendix A.4. The element chosen was LINK180. The impactor was set as the ANSYS's default material, that is, structural steel.

After the geometry was done, setting the connections was the next step. There were four contacts where the load is to be applied by the impactor, the type of asset as "no separation", the formulation was set at multi point constraint (MPC), which connected the nodes. Following, the elements were meshed with the size of 0.50 mm.

Subsequently, the option "Static Structural" was chosen, and the load and boundary conditions were added. It was necessary to define the contact and adhesion between concrete and rebar; to do so in the "command object" in the preprocessor it was placed the code in Appendix A.5.

Then, the load was added as a pressure in the face of the impactors. For each solution of the four presented in Figure 28, seven analyses were done, each analysis with a different load. The load began with 0.5 kN and was incremented with 0.5kN for each analysis until the final load, 3.5 kN.

Toward the solution, the Von Mises stress (equivalent stress) and maximum principal stress were chosen as output. Additionally, to evaluate the cracking and crushing plots for a determined load, it was needed to insert a code described in Appendix A.6 in the "command object". Then to solve, moreover, to have the result just for the concrete, the data is cleared, and instead of all bodied, it was chosen just the part of the concrete, and all results are evaluated.

From a simple calculation of the stress obtained by force applied divided by the cross-section area, it is obtained the required load for the rebar of 6 mm and 400 MPa of yield stress, 460 MPa of tensile strength. The required force for the 6 mm rebar to enter in the plastic mode was 11.3 kN. The concrete should hold this load at the loading point where the impactors were placed. The modeling revealed similar results for cases a), b), and c) of Figure 28, showed in Figure 30. The specimen's center showed a failure and

crack pattern transversal to the cross-section of the middle of the specimen, where it should reveal the crack opening. Besides, the stress field showed high stresses where the impactor was placed, increasing the risk of concrete failure at the loading area.

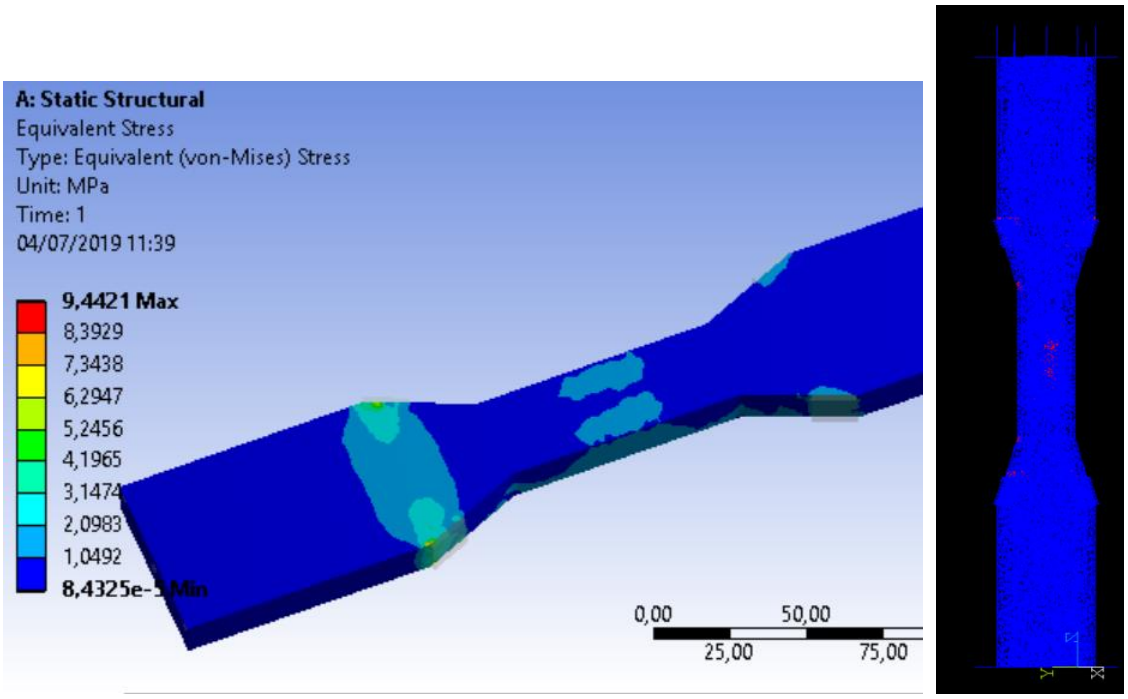

(a) **(b)**

Figure 30 – a) Equivalent Stress for solution 1 for the load of 1.5 kN; b) Crack crushing plot for solution 1. Source: Author extracted from Workbenck (ANSYS).

The fourth, and final, solution d) in Figure 31 approached the problem from a different perspective. In order to decrease the tensile stresses outside the central part of the specimen, the cross-section of the rebar at the center of the specimen was reduced, to decrease the force required for reaching the plastic mode.

From the three first simulations, it was known that the specimen would fail between 3 to 3.5 kN. The inverse calculation showed that a 3 mm diameter need a load of 2.8 kN to reach plasticity. Therefore, the simulation was done and showed the crack formation at the center, as illustrated in Figure 31. Where different from Figure 30 the crack formation, red dots are formed majorly in the center and the cross-section direction. Therefore, this solution solved the two major cracking problems and was chosen to be implemented in the experimental program.

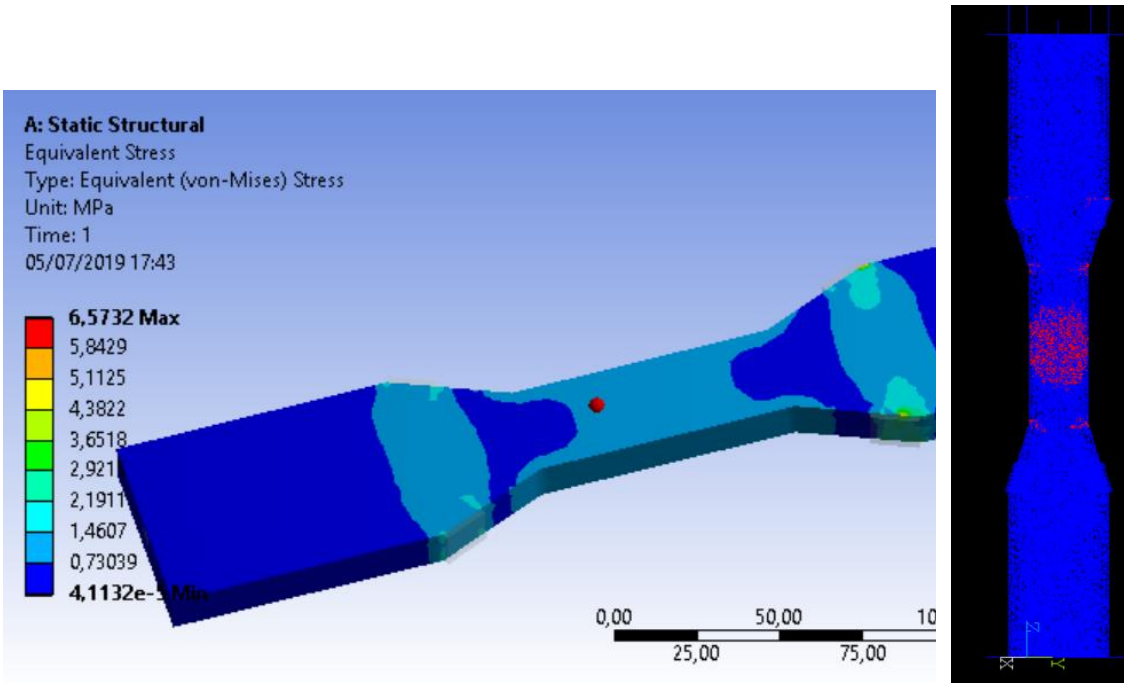

(a) **(b)**

Figure 31 - a) Equivalent Stress for solution 4 for the load of 1 kN; b) Crack crushing plot for solution 4. Source: Author extracted from Workbenck (ANSYS).

6.3 Materials

The HSC developed was the one presented in the item 6.2, Table 10. A cement with Blaine fineness of 576 m^2/kg was used, with a fixed content of siliceous sands as fine aggregates. The sand particle size distribution (grading curve) was chosen in order to comply with the usable zone, preferably to reach the optimum zone, of the recommendations of the NP EN 933-1 (2014) standard, as shown in Figure 11 in item 4.8.3. The fineness module was 2.73, the nominal maximum particle size was 4.75 mm, and the density is 2.65 kg/dm^3.

The SAP is the one presented in item 4.8.5, and the content was set to 0.0%, 0.3%, and 0.6 % of the cement dosage. The rebar was of the nominal diameter of 6 mm, a section of 28.3 mm^2, a mass of 0.22 kg/m, the spacing between ribs of 5 mm with a tolerance of 20%, and a maximum height of ribs of 0.39 mm. They were classified as MEGAFER 500SD-SEIXAL bars manufactured by hot rolling, satisfying LNEC specifications: E460: 2010 of 400 MPa of yield stress and 460 MPa of tensile strength.

6.4 Methods

In order to implement in practice, the solution tested through numerical analysis, the steel bar needs to suffer a reduction in the cross-section, which was done by manually grinding the steel bar. The process was done slowly, and the steel was cooled during the griding, to avoid changes in its properties. A smooth transition between the 6 mm and 3 mm was done to avoid any undesired stress concentration. The final result is shown in Figure 32 a). Figure 32 b) shows the position of the steel bar in the mold, involved with the Styrofoam box covered with plastic adhesive tape before casting, and Figure 32 c) shows the central part of the sample after filling the mold with concrete hardening, and cutting.

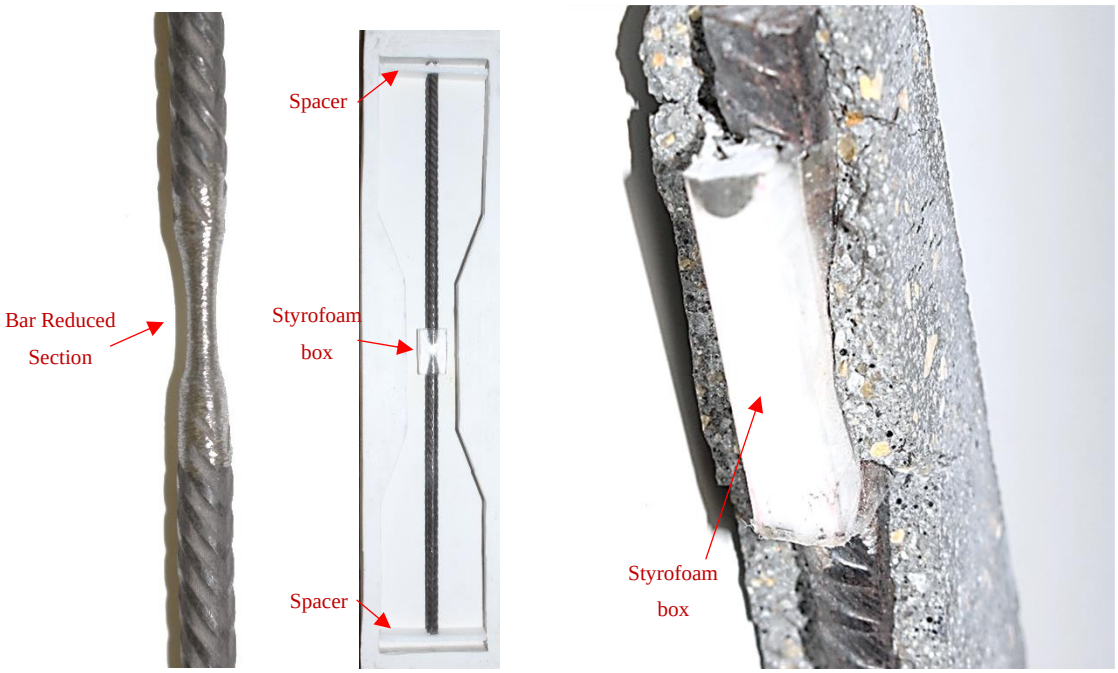

Figure 32 - a) Steel bar with cross-section reduction to 3 mm; b) Specimen's mold; c) Inside of the concrete specimen.

The concrete was prepared in a mechanical pan mixer with 3 liters of capacity from ELE International (Bedfordshire, UK) under the following steps. The first step was a dry mix of the cement, sand, and SAP (if used) for 5 min at a slow speed. The second step was the addition of water and superplasticizer, mixing for more than 2 min at the same speed, and then the velocity was increased to high speed for 5 min. Then the mixer

was stopped, the edges of the bowl were scraped, followed by a mixing phase for 3 min at high speed.

Concrete was cast into the silicone molds, where the steel bar as placed through spacers on both end sections to avoid the bar to get in touch with the bottom of the silicone base, as shown in Figure 32 b). The casting was done in three steps to better fill the mold without voids, especially in the central part; the first step was filling half the mold with concrete, without steel inside (raising the rebar with spacers shown in Figure 32 b); then the rebar with spacers were placed; and finally, the mold was completely filled with concrete.

Given the small dimensions of the specimen, it was necessary to be very careful in filling the mold, being required that, when filling the mold, the upper face was slightly above the level of the mold, to achieve symmetry in the cross section of the specimen (in order to avoid influence of any curvature, due to surface tension, on surface shape). Symmetry was obtained by polishing the molding surface, making the surface perfectly flat, like the surface in contact with the mold, on the opposite side of the specimen.

The specimens prepared for self-healing tests were stored in the silicone mold for 48h, in controlled humidity chamber, with relative humidity above 90% and temperature of 20 ± 1 °C. Then they were demolded and stored in a laboratory room with the same average temperature, 20 ± 2 °C, until the pre-cracking age, 7 and 28 days. These testing ages were chosen based on the compressive strength test results, shown in item 7.5.1.

The objective was to assess the self-healing potential for young and mature concrete. Since the concrete's hydration enhances the strength, compressive strength was chosen as an indicator of the degree of hydration of the cement particles. In a graph expressing the strength versus the age (or equivalent age, when using different temperatures) of a cementitious material, in saturated conditions, the slope of the curve gives an indication about the stage of the hydration process. When the curve reaches a plateau, this in an indication of mature concrete, and difference between the strength at a specific age and the strength reached at the plateau gives an indication of the youth of concrete.

The pre-cracking age was chosen based on the compressive strength of 48 prisms (40 x 40 x 160 mm). Those were cast following the NP EN 196-1 (2017). The specimens were demolded 24 hours after casting, half of them were stored in a tank with water at 20 ± 1 ºC, and the other half was stored in a tank with water at 40 ± 1 ºC. Compressive tests at the ages of 1, 2, 3, 7, 10, 14, 28, and 60 days were carried out according to the standard NP EN 196-1 (2017) in mortar specimens, using an electrohydraulic testing device, Form Test Seidner (Riedlingen, Germany), with 200 kN load cell, with a loading rate of 2,55 kN/s.

The new cracking technique was applied using the direct tensile setup performed for fiber-reinforced concrete developed by Yokota *et al*. (2008). Few changes were made to adapt to the new method, shown in Figure 33. A linear variable displacement transducer (LVDT) was placed in the specimen's back to record the displacement. Furthermore, a magnifying camera was placed where the crack was formed to monitor the crack opening when the crack was formed.

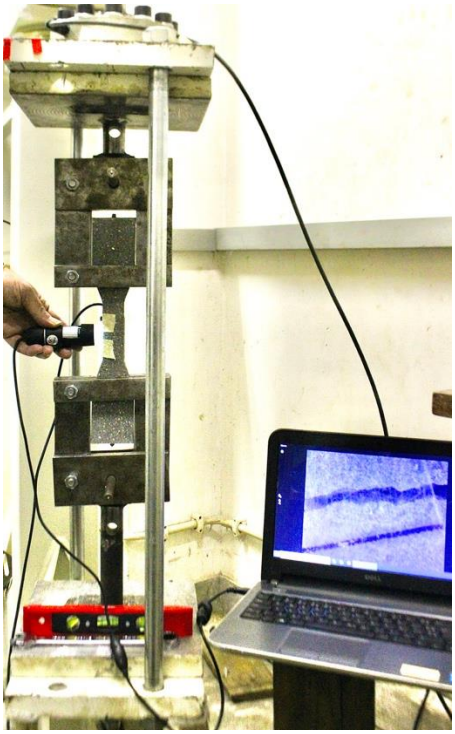

Figure 33 - Pre-cracking of the specimen, controlled by LVDT and microscopic camera.

Another change was the replacement of the electronic universal testing machine with a hydraulic jack to apply the load. The loading force was measured on the load cell

by a computerized data recording system. The use of a hydraulic jack made it easier to adjust the crack width at a desired size. The use of the electronic universal testing machine was time consuming, implying also heating risks for the device. With the jack, the loading-stopping-unloading testing phases are more flexible, and the absence of control of the rate deformation after cracking is not relevant for the objective of this study.

The procedure consisted of applying load to the specimen at a constant speed of 0.1 kN/min until the crack appears, or until 2 kN, then the specimen was unloaded as shown in Figure 34 in the blue line. This procedure was used for determination of the tensile stiffness of the concrete, before (E_{pre}) and after (E_{SH}) the specimens were subjected to the self-healing phase.

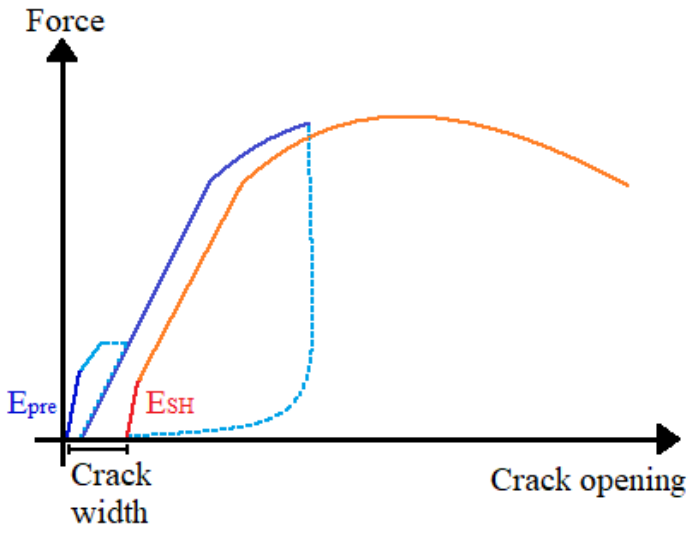

Figure 34 – Typical force x crack opening curve for the method.

After unloading, in the first cycle of the pre-cracking phase (light blue line on the left of Figure 34), it is visually verified the almost complete closure of the crack (steel bar in elastic mode). A microscopic camera with a scale was placed where the crack was formed. The LVDT was set at zero. The second loading began with no concrete interference in the cross section of the crack, only with the steel bar linking the two parts of the specimen. In the second cycle the loading rate was set as 0.1 kN/min, but the load could be stopped for some time at any value of the load.

In the second cycle, during the loading phase, the crack opening measured by the LVDT corresponds to the sum of elastic and plastic deformation of the steel. Subtracting

the elastic component for the corresponding load level, we obtain the crack opening after unloading. When the desired crack width was reached at the unloading, shown by the light blue line in Figure 34, measured in combination with the LVDT and digital microscope, the specimen was taken from the testing machine, and it was photographed by a digital microscope.

After the pictures were taken, the specimen was put in a chamber with 20 ±1 ºC temperature and above 60% RH. Cycles of wetting and drying were done, by daily spraying a high amount of water on both sides of the specimens for four months. This part of the methodology was called conditioning. The objective of wetting and drying cycles, instead of submerging the specimen in water, was to analyze the efficiency of the SAP in the process of self-healing due to the cement hydration. When SAP is filled with external water, it slowly releases water to hydrate the anhydrous cement particles of concrete, and the hydration is promoted by the SAP mechanism. Immersing the specimens in water would not allow highlighting the SAP influence.

After four months of wetting and drying cycles, the specimens were taken from the chamber and were observed by microscopic images. This observation makes it possible to compare the cracked section before and after the self-healing cycles. Then, the specimens were submitted again to the tensile tests, at the same loading rate of 0.1kN/min, until complete failure. With the broken specimen, it was also possible to observe the cross section, inspecting the surface for the presence of any healing product and, when necessary, to look at the healing products at a microscope.

Based on the crack width measurements taken before and after the conditioning, the crack Closing Ratio used by Flores (2018) and Oliveira (2018), shown in Equation 26, was used to quantify the self-healing. For each specimen, more than 20 pictures were taken from the front and back of the crack, using the maximum zoom capacity of the microscope. The pictures were manually fitted, so each ending point matched the next photo. This way, the creation of a big picture of the real crack was done with minimum distortion. With the program Image J, the crack width of each crack side (front and back) was measured over 50 points. With this information, statistical parameters were computed: average, standard deviation, maximum and minimum crack width.

$$\text{Closing Ratio} = 1 - \frac{\alpha_{\text{final}}}{\alpha_{\text{initial}}} \tag{26}$$

where: α_{final} is the average crack width taken after the wetting and drying cycles, and α_{initial} is the average crack width before wetting and drying cycles.

The cracking method was experimentally validated using three specimens without SAP, called reference specimens (REF). All of them were cracked at 7 days with a crack width of around 200 µm. After producing the crack, the opening was filled with cement grout as repair material, simulating the perfect self-healing, and the results were compared, before and after the repair, as shown further in item 7.5.2.

Self-healing efficiency was measured by comparing the tensile stiffness (kN/mm) obtained during the pre-cracking, here denominated pre-cracking stiffness (E_{pre}), and the tensile stiffness after the conditioning, here denominated self-healing stiffness (E_{SH}). Equation 27 gives the self-healing index (SHEMR) through the stiffness recovery. If SHEMR is lower than 0.10, the self-healing index is to be considered 0. The stiffness is a linear response of the material. When no self-healing has occurred, the response is an artifice of the alignment of the specimen. The response is exclusive of the steel bar, and instead of a linear behavior, a curve is observed. By visually observing the crack and seeing that no self-healing has occurred, the maximum value recorded to this initial phase corresponded to SHEMR of 0.10. When the two parts of the specimen showed any bonding, the response is linear, and the value is above 0.10. Figure 34 illustrates an expected curve where total stiffness recovery is obtained, SHEMR=1.

$$\begin{gathered}\text{SHEMR} = \frac{E_{SH}}{E_{pre}} \text{ ; valid for SHEMR} \geq 0.1; \\ \text{if SHEMR} < 0.1, \text{then SHEMR} = 0\end{gathered} \tag{27}$$

The variables studied are presented in Table 13. They were the content of SAP 0.0%, 0.3%, and 0.6%, and the pre-cracking age of 7 and 28 days. Each variable was cast six specimens, and the best ones were chosen to go to the wetting and drying cycles.

Table 13 – Label of the variables used for self-healing.

Label	SAP content	Pre-cracking age (days)
REF	0.0	7
MR1-0.0-7d	0.0	7
MR2-0.3-7d	0.3	7
MR3-0.6-7d	0.6	7
MR4-0.0-28d	0.0	28
MR5-0.3-28d	0.3	28
MR6-0.6-28d	0.6	28

6.5 Results and discussion

6.5.1 Compressive strength results

The compressive strength results for 1, 2, 3, 7, 10, 14, 28, and 60 days at the 20ºC and 40 ºC are displayed in Figure 35. At 28 days, the strength of the specimens cured at 20 ºC and 40 ºC are similar. The strength increase from 28 to 60 days is also small, despite half of the prisms were subjected to 40 ºC of temperature. This is an indication that the specimens cured at 28 days under 20 ºC temperature, produced with the HSC developed for this study, may be considered as being in mature state. The 7 days age was chosen as representing a younger concrete, with significant amount of anhydrous cement particles (from 7 days to 60 days the strength increased more than 30 %).

Based on these results, the chosen temperature of cure was 20°C, and the pre-cracking testing ages were 7 and 28 days. It was considered that there was no significant advantage in waiting for a longer period of time, in order to obtain greater maturation of the concrete, as this would have excessive implications in extending the required experimental period. On the other hand, starting the tests at an age younger than 7 days would have limitations in the procedures for preparing the specimens, without achieving a significant reduction in the degree of hydration.

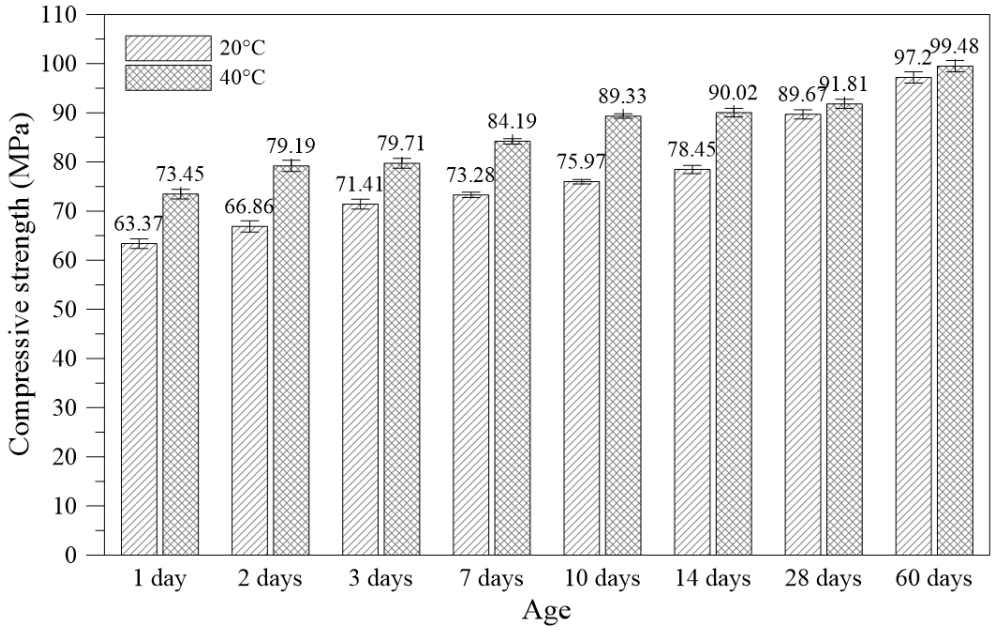

Figure 35 – Compressive strength results for HSC concrete subjected to 20ºC and 40ºC cure for the ages of 1, 2, 3, 7, 10, 14, 28, and 60 days.

6.5.2 Validation of the method

All three specimens of the reference mixture (REF) presented a similar aspect and mechanical behavior. The typical aspect is shown in Figure 36. The mechanical behavior is presented through the average values of the direct tensile Force versus the Displacement, in the curves of Figure 37. The crack shown in Figure 36 fulfilled the requirement of being located in the middle of the specimen, with a linear shape, transverse to the specimen alignment, as expect for nearly uniform stresses, and with average crack width of 196 μm.

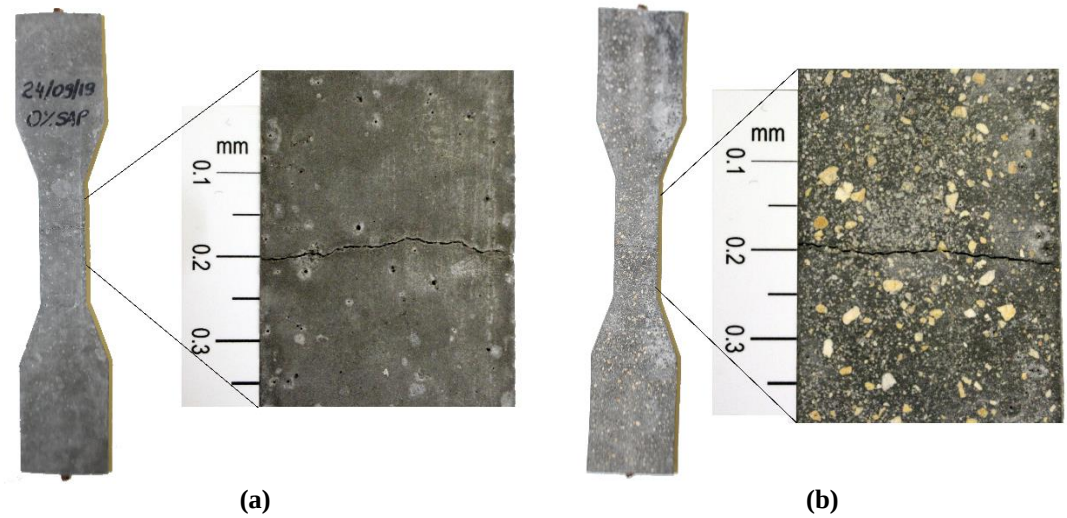

(a) **(b)**

Figure 36 - Specimen after cracking: a) Front and b) Back

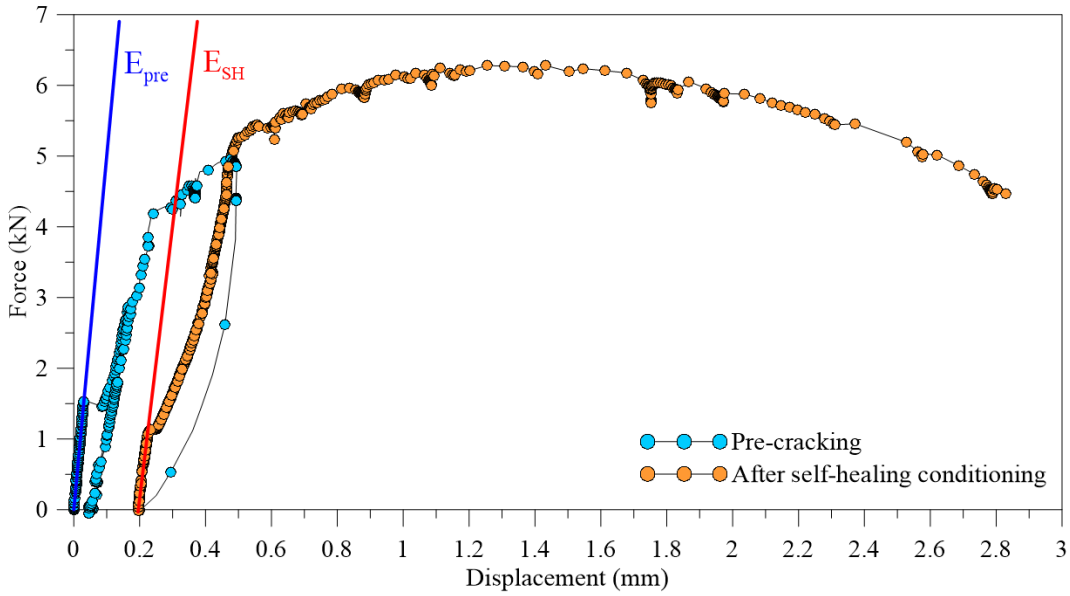

Figure 37 – Typical force x crack opening curve of the method.

After filling the crack with a cement paste, and submitting again the specimens to direct tension test, the pre cracking stiffness (E_{pre}) and the stiffness after cracking and conditioning (E_{SH}) presented similar results. The E_{pre}, represented by the dark blue line shown in Figure 37, presented the average of 34.3 kN/mm and a standard deviation of 11.8 kN/mm. The E_{SH}, represented by the red line in Figure 37 presented an average of 33.4 kN/mm and a standard deviation of 10.3 kN/mm. It showed a full self-healing potential with a SHEMR of 0.97, indicating that the self-healing evaluation by the mechanical recovery method is valid.

In Figure 37, the light blue dots showed the first cycle of the test representing the pre-cracking phase. After the concrete cracking (load of ≅ 1.5 kN), the displacement increases suddenly, due to stress transference from the concrete to the steel. The second cycle, showed also in light blue dots, represents the phase where the steel bar enters in plastic mode (≈ 4 kN) and then returns to the displacement of 0.2 mm, the defined crack size, average value latter confirmed by observation through microscopic camera. The load to enter the plastic mode will depend on the diameter of the bar that, during manually grinding could vary between 3 to 4 mm, therefore the load can vary from 3 to 5kN.

The orange dots represent the test after the conditioning. If perfect self-healing occurs, the two parts of the specimen are reunited, but the plastic deformation on the steel remains. In this case, the stiffness before cracking in the orange dots (E_{SH}) is similar to the stiffness before cracking in the light blue dots (E_{pre}), and the two lines, blue and orange, come together when the load in the orange phase reaches the highest load reached in the blue phase.

Figure 37 shows this typical behavior of perfect healing, obtained by cement past repair. However, if the self-healing phenomena does produce any bind of the two parts, when the specimen is reloaded the resulting stiffness obtained from the measurements on the LVDT sensors is conditioned mainly by the strain of the steel in the section of the rebar disconnected from the concrete. In this case, if the alignment of the rebar is perfectly linear, the stiffness when reloading is expected to correspond to the stiffness of the steel.

However, this is not the case due to geometric imperfections of the steel bar and due to handling specimens during conditioning and positioning the specimens in the tension machine. In the absence of self-healing, shown in Figure 38, the displacement in the reloading phase has a first branch for almost zero load, represented by the E_{SH}, correspondent to steel deflection to reach the position of alignment of the applied force with the alignment of the rebar, and then, when increasing load, the second branch corresponds to the stiffness of the steel.

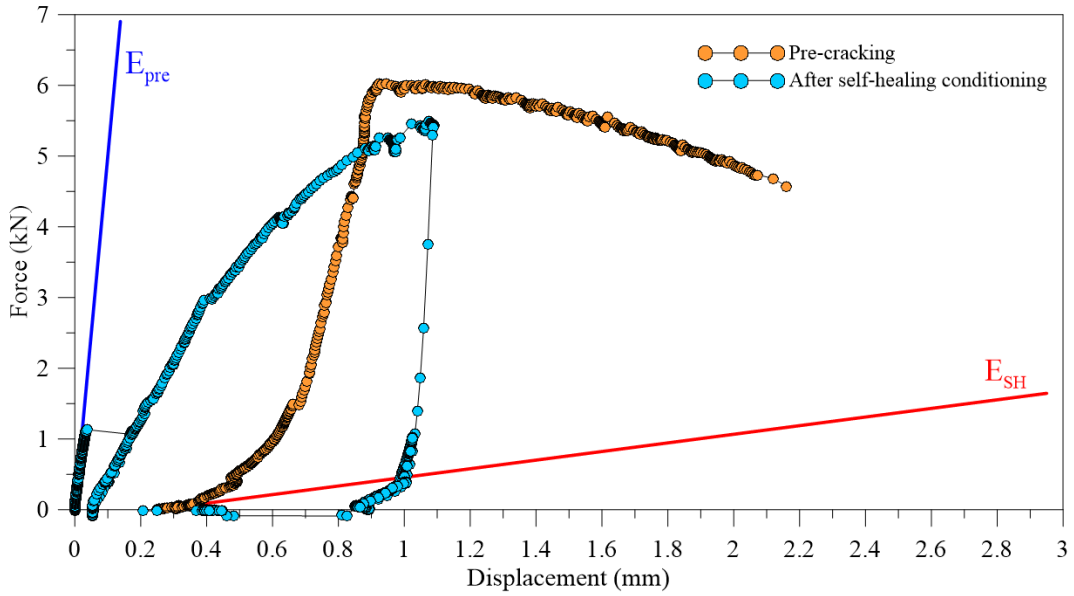

Figure 38 – Typical force x crack opening curve of the method when there is no self-healing.

In cases where there is binding of the two parts of the specimen due to self-healing, the healing products has influence in the first branch of the reloading phase, increasing the load required for the same displacement. This load increase is expressed through the stiffness value (E_{SH}), and this parameter is used to quantify the healing degree.

6.5.3 Self-healing results

Figure 39 and Table 1Table 14 exhibit the stiffing results for the pre-cracking phase (E_{pre}) and after the conditioning (E_{SH}) of the HSC with 0, 0.3%, and 0.6% of SAP incorporation cracking ages of 7 and 28 days. The SHEMR was calculated from Equation 27 for all the specimens, and it is displayed the average of the results in Table 14 and in Figure 40.

The photos of the back and front of each specimen's crack, taken from the digital microscope, are presented in Appendix B. The average, the standard deviation, maximum, and minimum of the crack width measurements are displayed in the legend for each one. The crack Closing Ratio is an average calculated from Equation 26 for each specimen and is presented in Table 14 and Figure 40.

Table 14 – Mechanical recovery results for variables used for self-healing.

HSC	E_{pre} (kN/mm)	E_{SH} (kN/mm)	SHEMR	Closing Ratio
MR1-0.0-7d	34.6 ± 2.4	1.63 ± 0.09	0	0.26 ± 0.09
MR2-0.3-7d	27.5 ± 1.9	2.61 ± 0.05	0	0.26 ± 0.07
MR3-0.6-7d	21.9 ± 4.7	1.53 ± 0.07	0	0.38 ± 0.08
MR4-0.0-28d	48.0 ± 5.6	1.88 ± 0.09	0	0.25 ± 0.15
MR5-0.3-28d	27.9 ± 1.4	3.36 ± 0.05	0.15	0.25 ± 0.10
MR6-0.6-28d	22.8 ± 1.4	4.20 ± 0.13	0.17	0.35 ± 0.12

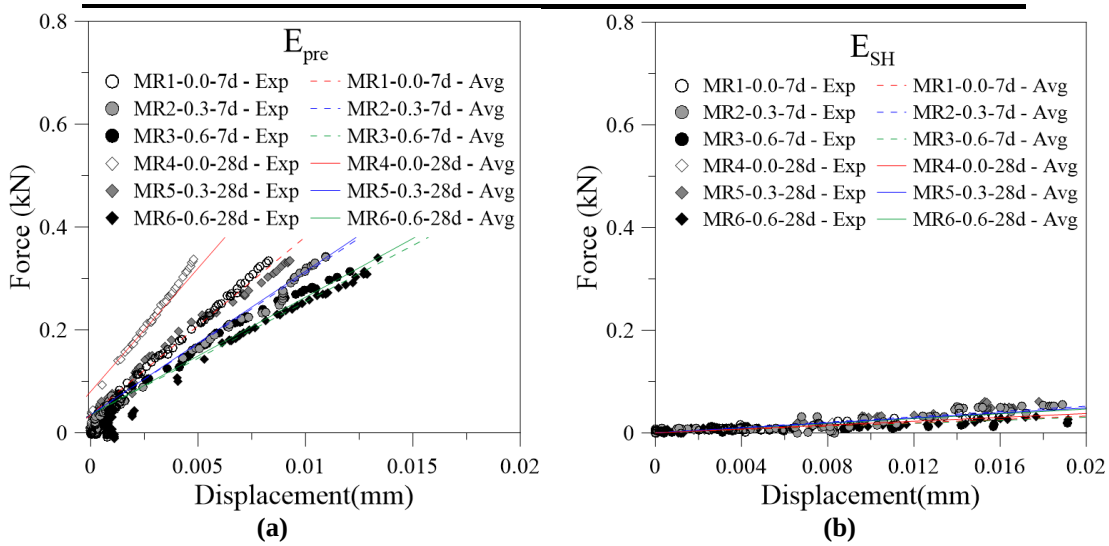

(a) **(b)**

Figure 39 - Stiffening results: a) pre-cracking phase and b) after wetting and drying cycles. Where Exp represents experimental results, and Avg represents the average of the experimental results

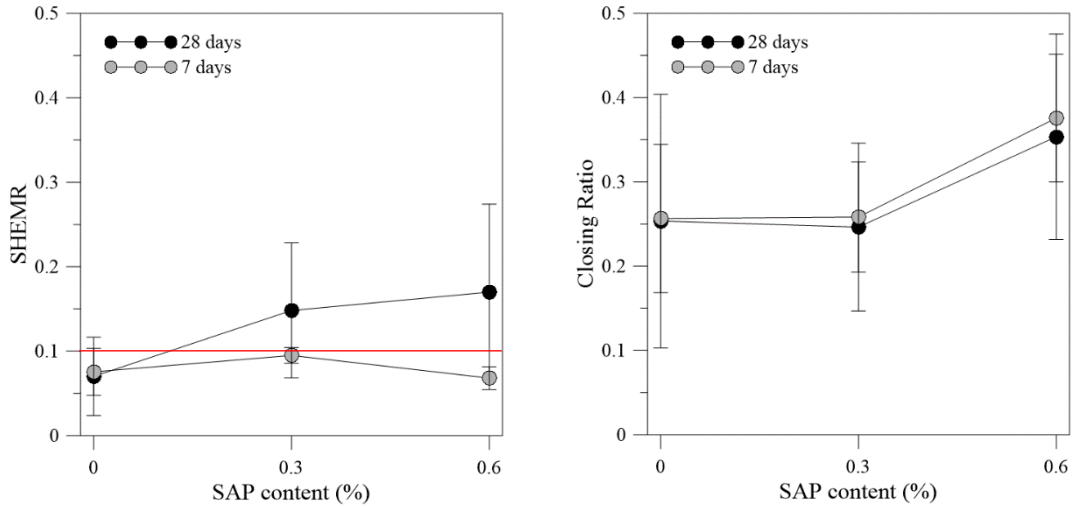

(a) **(b)**

Figure 40 – Results of a) the SHEMR coefficient and b) Closing Ratio coefficient.

It should be also mentioned that, due to the low strain values obtained before cracking, and the level of accuracy of the strain measurement device, the analysis of the results is performed trough the average results obtained for the same condition, and with a comparative purpose. In fact, it is expected a significant scatter on the individual results,

since, beyond the equipment's precision issues in relation to the specimen dimensions, the influence of the self-healing process on mechanical properties is largely dependent on constitution of the cracking surface and on the relative geometrical position of the healing products that bind the two parts of the specimen.

The results are presented in Table 14, which shows that SAP, as expected, decreases the apparent tensile stiffness for both the ages of 7 and 28 days. At the younger age, 7 days, compared to the 0% SAP reference, the 0.3% SAP mixture presented a decrease of 21%, and the 0.6% SAP mixture decreased 37 %. At 28 days compared to the reference, the loss was 42% and 53% for the contents of 0.3% and 0.6%, respectively.

The loss on the apparent tensile stiffness can be attributed to the SAP inclusion, as already explained for compressive strength of Young's modulus in item 6.2.2, due to the increase of voids in the matrix, as mentioned by Hasholt *et al*. (2012), Chindasiriphan *et al*. (2020), Lee *et al*. (2010) and Snoeck *et al.* (2014).

These results also indicate that the apparent tensile stiffness loss is more preeminent in later ages. This trend is similar for results of 0.3% and 0.6% and is in agreement of the expected higher relative influence of internal defects (voids) in more closed matrices.

The reference apparent tensile stiffness increased in time, presenting an increase of 38% when comparing 7 with 28 days. The gain is due to the cement hydration and, consequently, C-S-H formation. The relative increase in this stiffness parameter is higher than the relative increase on the compressive strength Young's Modulus, shown in Figure 24, contrary to what normally occurs between variations in strength and stiffness, but as mentioned, the apparent tensile stiffness was obtained through a non-uniform stress filed, which includes non-linear material behavior.

The obtained high loss of stiffness due to SAP is a result against the expected from the results seen in the literature, since it was believed that SAP would have a positive effect on hydration of the anhydrous cement, and consequently a positive effect in the overall mechanical performance, compensating, at least partially, for the initial loss of strength due to void formation.

The conclusions drawn were for the apparent tensile stiffness obtained in the pre-cracking phase. Looking now for the stiffness after the conditioning (E_{SH}), it can be seen that the values are much lower than E_{pre}, with no evident correlations between them.

In order to have a better insight into the phenomena, the SHEMR for each specimen was calculated, and the values are shown in Figure 40 a) and Table 14. The results pointed to zero self-healing for almost all conditions. The red line shows that values under it are considered as zero in Table 14. The exceptions were the mixture with 0.6% of SAP tested at 28 days, which showed the best result, with nearly 17 % of the mechanical recovery, and the mixture with 0.3 % of SAP, also tested at 28 days presenting, with 15 % of the mechanical recovery.

These results are still low, and it can be understood that at some point of the two parts of the specimen were bonded by the self-healing products, although at a minimum content. The other variables under 0.10 showed values that can be inferred as no bonding was achieved between the specimen's two parts. Besides, the SHEMR variability was high. The conclusion drawn is that no mechanical recovery can be inferred by the SAP addition in the conditions of four months of wetting and drying cycles.

In addition to the mechanical evaluation, it is important to evaluate the filling of the space by hydration products. In this evaluation, and concerning the role of SAP particles, more promising results were found when using the crack Closing Ratio, Figure 40 b) and Table 14. The results showed that the crack Closing Ratio with the SAP addition of 0.6%, in 7 days, presented 38% of crack closure and 35% for the 28 days. The reference of 0.0% SAP and the content of 0.3% of SAP showed no significant difference, resulting in no relevance for obtaining self-healing properties.

Observing the images and the average width of the crack in Appendix B, it is possible to detect a partial crack closure, probably due to cement hydration. However, since there are no fibers linking the two parts of the specimen, the nucleation effect displayed in Figure 7 is not present. The efficiency of the SAP particles in closing the crack is reduced. Clear bridges between the two parts of the specimen cannot be seen.

The smaller efficiency of the SAP particles in HSC, when compared with ordinary concrete with fibers, can also be related to water migration properties. Indeed, HSC has

a very closed pore structure, making it very difficult for the water to penetrate the space where anhydrous material exists. Even when this happens, the diffusion of calcium hydroxide to the outside, filling the crack, will always be very slow. This limitation was expected since the beginning of the study, but the scope of its magnitude was greater than expected.

6.6 Conclusions

This study developed a new method to investigate self-healing by mechanical recovery. The self-healing of HSC with the increasing dosage of SAP at different ages for pre-cracking was investigated. Based on the results presented, the following conclusions can be drawn:

- The methodology developed can be used to evaluate self-healing in cement-based materials.
- The methodology produced a single crack at the desired size, in a linear and uniform pattern, showing minimum influence with the material.
- The crack produced in the methodology managed to stay with the same crack width for the self-healing conditioning phase.
- The use of 0.6 % of SAP showed self-healing, although not sufficient to regain the material's strength or stiffness.
- The addition of SAP at the conditioning of four months with wetting and drying cycles does not produce sufficient or relevant self-healing properties.
- The SAP used to control autogenous shrinkage at the optimum content of 0.3% does not promote mechanical recovery.

7 EVALUATION OF SELF-HEALING CONCRETE BY AIR AND WATER PERMEABILITY TESTS

Permeability tests of oxygen and water with new cracking methodology to verify self-healing of cementitious materials and self-sealing

Abstract

This chapter proposes a methodology to study self-healing properties by durability parameters obtained using water and air permeability tests in samples cracked by the method presented in Chapter 7. A single crack of about 200 μm was produced by direct tension, with nearly uniform width and length, using a single steel bar with a reduction in its diameter at the central section.

HSC mixtures with the contents of 0.0, 0.3 % and 0.6 % of SAP were prepared and tested. Pre-cracking was produced at the ages of 7 and 28 days on specimens cured at 20°C to evaluate the self-healing phenomena at early and older ages. After the pre-cracking, samples were daily subjected to wet and dry cycles for four months.

Water permeability tests were carried out on specimens immediately after pre-cracking to evaluate SAP sealing capacity, through reduction of the water flow provided by the swelling of SAP particles. Permeability tests were also carried out after the conditioning period to evaluate the self-healing capacity.

Air permeability tests were conducted before water permeability tests to evaluate the self-healing capacity apart from the swelling effect. In order to evaluate crack closure, microscope photos of the crack after the pre-cracking and before the verification of both air and water permeability tests were taken.

7.1 Introduction

Despite the existence of several laboratory methods to evaluate self-healing properties by gain in strength or mechanical recovery, this particular characteristic is rarely applicable in models of real-life situations. The gain in strength is a proper parameter because it is a reliable indicator that the self-healing has occurred in a large extent. It is doubtful whether the autogenous healing technique is efficient for structural reinforcement, since it takes a long time to occur. Therefore, it cannot be used as a solution for urgent repair cases.

A much more interesting use of the self-healing properties is regarding durability since healing can improve significantly concrete resistance to water penetration without any intervention. The clack closure can, even if it happens mainly on the surface, delay the entry of harmful agents into the concrete and prevent the progress of its deterioration.

As already discussed in Chapter 3, especially in item 3.2, there are at least two mechanisms through which SAP can improve durability. One is the self-sealing, described by Lee *et al*. (2010), represented in Figure 12, in which SAP swallows and prevents water from entering into the concrete; this phenomenon happens in a few minutes. The second is self-healing, where SAP provide water for cement hydration and promoting the crack closure through hydration products. This later one takes a longer time.

In order to evaluate the presence of both mechanisms, water and air permeability tests are proposed to assess self-sealing and self-healing, being the results used as durability parameters. However, as already discussed in Chapter 2, in the beginning of this experimental research, there was no available method to evaluate permeability by water or air without fiber reinforcement. Therefore, it was needed to create a new method to assess it using the cracking method developed in Chapter 7.

Adaptations were performed to the standard permeability (NP EN 12390-8 and LNEC specification E392). The air and water permeability tests were carried out immediately after the pre-cracking, in specimens with crack of about 200 μm widths, and after four months of wetting and drying daily cycles, for the mixtures containing 0.0 %, 0.3%, or 0.6% of SAP, for the pre-cracking ages of 7 and 28 days. Also, as complementary

information for durability assessment, crack closure was measured by microscopic images.

7.2 Materials

The HSC prepared was the one presented in the item 6.2, Table 10. Cement with Blaine fineness of 576 m2/kg was used, with a fixed ratio of siliceous sands as fine aggregates. The sand particle size distribution (grading curve) was chosen in order to comply with the usable zone, preferably to reach the optimum zone, of the recommendations of the NP EN 933-1 (2014) standard, as shown in Figure 11 in item 4.8.3. The fineness module was 2.73, the nominal maximum particle size was 4.75 mm, and the density is 2.65 kg/dm³.

The SAP used was the one presented in item 4.8.5, and the content was set to 0.0%, 0.3%, and 0.6 % of the cement dosage. The nominal diameter of the steel rebar used was 6 mm, section of 283 mm2 and mass of 0.22 kg/m, with spacing between ribs of 5 mm (tolerance of 20%), and maximum height of ribs of 0.39 mm. The steel rebars were classified as MEGAFER 500SD-SEIXAL, manufactured by hot rolling, satisfying LNEC specification: E460: 2010.

7.3 Methods

To evaluate durability using the permeability test, the cracked specimen produced using the method of item 7.4, shown in Figure 41 – Specimen preparation for the permeability tests: a) Cracked and cut specimen, b) specimen with masking tape, c) base for the permeability tests, d) cracked specimen glued to the base. Figure 41 a), was adapted to the standardized permeability tests of LNEC, adjusting it to fit into the equipment of air permeability used in the LNEC specification E 392 (CEMBUREAU permeability test). For this standardized test, the specimen used is a cylinder with a high of 50 mm and a diameter of 100 mm. Additionally, this cylinder can be used for water permeability tests as suggested by SARCOS in an interlaboratory test campaign, yet to be published.

In order to fit the specimen to the equipment, the concrete was sawed in the region where the steel bar was firmly bond with the concrete, so the specimen does not follow apart. The approximate size of the specimen after cutting was 80 x 30 x 13 mm, as shown in Figure 41 a). A cylinder base of 50 mm high and a diameter of 100 mm was cast with a prismatic void in the center, designed to fit the sawed specimen. Besides, the base had a hole in the center so the air would pass freely, and the base does not interfere with the passing air. The base was cast with high strength concrete and is shown in Figure 41 c).

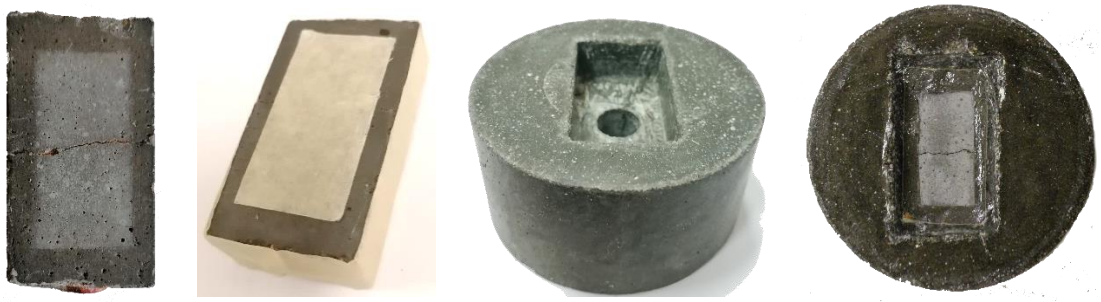

(a) **(b)** **(c)** **(d)**

Figure 41 – Specimen preparation for the permeability tests: a) Cracked and cut specimen, b) specimen with masking tape, c) base for the permeability tests, d) cracked specimen glued to the base.

The sawed specimen Figure 41 a) was glued into the base with sealant silicone glue, named Poly-Max Crystal Express of the brand UHU (Bühl/Baden, Germany), as shown in Figure 41 d). Before gluing the cracked specimen to the base, the specimen's lateral surface was coated with masking tape Figure 41 b). Additionally, in front of the crack, a masking tape of a size defined by 20 x 40 mm was placed, as shown in Figure 41 b), which was removed after applying the glue, when the glue is still fresh. In this way, a constant permeable surface area of 800 mm^2 is obtained.

The complete test procedure consisted of cracking the specimen, saw and let the base dry for 24 hours in a closed chamber at 20°C. Then the cracked specimen was coated with masking tape, the glue was applied, and the sample was kept in this condition for more than 12h (period to obtain sufficient hardening of the glue). The specimen was then placed in the oxygen permeability test equipment, shown in Figure 42 composed of three pieces, the steel chamber where the samples are placed under lateral pressure, an oxygen cylinder, and a permeameter (Testing bubble counter).

Figure 42 – CEMBUREAU air permeability equipment.

After the specimens were subjected to the oxygen permeability test, a pipe of 1 m high and a diameter of 90 mm was glued into the specimen for the water permeability tests, as seen in Figure 43. This water permeability test is a simple method developed by SARCOS for the interlaboratory test campaign, yet to be published, to measure the volume of water that passes through the specimen during a fixed period of time.

Figure 43 - Water permeability test, proposed by SARCOS.

The adaptation of standard permeability tests for healing assessment is challenging since the existing tests for cement-based material were developed for uncracked specimens. In uncracked concrete, the air and water flow measurements are made in samples that require high pressure and time for the flow to be measured. To enable readings on cracked specimens with similar methods, the pressure must be low enough to reach the flow measurement range of the equipment. The value was set as 0.1 Bar, the lowest reliable value for the air permeability equipment used in this work. With higher pressures, the flow was too high, and it was not possible to accurately record the elapsed time. For the oxygen permeability test, an extra care was taken in recording the time since the test was very fast, even with low pressure. To report the results with more precision, a digital camera filmed the bubble, and the time was recorded for a fixed gas volume of 100 ml, with millisecond resolution.

According to Equation 28 (Hagen-Poiseuille), for laminar gas flow, allow the determination of a coefficient of permeability, Grube *et al.* (1984).

$$K = \frac{2 \cdot P_2 \cdot L \cdot \eta \cdot Q}{A \cdot (P_1^2 - P_2^2)} \qquad 28)$$

where: K is the intrinsic permeability, P_1 is the absolute applied pressure (water or air permeability was 10 kN/m^2), P_2 is the atmospheric pressure (0,1 kN/m^2); η is the viscosity of the gas at 20 ºC ($2{,}075 \cdot 10^{-5}$ kg/m·s); A is the cross-section area defined by $8 \cdot 10^{-4}$ m^2.

The test conditions are not those considered in the Equation (28), laminar flow flowing through a long cylindrical pipe of constant cross section, but the formula give a coefficient that relates flow with pressure, which depends on the pore connectivity. The presence of a crack in the specimens largely increases the flow rate, when compared with uncracked concrete, and the wider the crack the greater the gas flow.

For the water permeability, the Darcy law may be applied. However, the scope of the research is to evaluate the self-healing and not the crack permeability. As the crack is filled with liquid or solid phases, the flow rate decreases. The Healing Ratio proposed by

Flores (2018) in Equation 29, was calculated. Since values of pressure (P1 and P2), specimen width (L), cross-section (A), and viscosity of the gas (η) are fixed for all samples, they are not needed in Equation 29.

$$\text{Healing Ratio} = 1 - \frac{\text{Final Flow}}{\text{Initial Flow}} \tag{29}$$

where Healing Ratio of 1 means complete healing and 0 means no healing. The Final Flow is the final air/water flow measured after the healing period, and the initial Flow is the air/water flow measured after pre-cracking.

Consequently, in Equation 29 the permeability after self-healing specimen is divided by the permeability before self-healing, leading to a nondimensional value. The Healing Ratio is determined by the flow measured (Q), volume versus time (m^3/s), also used for the water permeability test.

Comparing the values obtained in uncracked specimens with the ones cracked is unrealistic. The order of magnitude of the flow is not comparable, and uncracked samples will display a value that can be considered zero. Therefore, the variables studied are presented in Table 15. They were the content of SAP 0.0%, 0.3%, and 0.6%, and the pre-cracking age of 7 and 28 days. For each variable, six specimens were cast, and the specimens without defects after preparation were chosen to procced with the wetting and drying cycles.

Table 15 – Label of the variables used for self-healing.

Label	SAP content	Pre-cracking age (days)
P8-0.0-7d	0.0	7
P10-0.3-7d	0.3	7
P12-0.6-7d	0.6	7
P14-0.0-28d	0.0	28
P16-0.3-28d	0.3	28
P18-0.6-28d	0.6	28

After performing the initial permeability test, the specimen was removed from the base and cleaned. The silicon glue was also removed from the specimen with a razor, and the specimen was photographed by a digital microscope. Then, the pictures were taken and afterwards the specimen was put in a chamber. Wetting and drying cycles were done

daily by spraying a high amount of water on both sides for four months. Subsequently, the specimens were taken out for crack closure evaluation by microscopic images. Then they were submitted again to the permeability tests.

Based on the crack width taken before and after the four months of wetting and drying cycles, the crack Closing Ratio used by Flores (2018) and Oliveira (2018), shown in Equation 29, was also used to quantify the self-healing. For each specimen more than 20 pictures were taken, from both sides of the specimen, enabling the maximum zoom of the microscope. The pictures were manually fitted, so each ending point matched the next photo. This way, the creation of a big picture of the real crack was done with minimum distortion. With the program Image J, each crack side (front and back) was measured over 50 points. With this information, statistical values were determined: average, standard deviation, maximum and minimum crack width.

7.4 Results and discussion

7.4.1 Permeability results

Table 16 presents the results of air and water permeability tests. It displays: the flow; indicated by the letter Q, after pre-cracking indicated by “pre”, and after self-healing conditioning (four months of wetting and drying cycles) represented by “SH”; the Healing Ratio; Closing Ratio and the average crack width of the specimens of the HSC with 0.0%, 0.3%, and 0.6% of SAP incorporation cracking ages of 7 and 28 days.

Figure 44 a) shows the Healing Ratio obtained with the air permeability tests. Figure 45 exhibits the water permeability results, the Healing Ratio, and water flow after pre-cracking. Both Healing Ratios were calculated from Equation 29 for all the variables presented in Table 15.

Table 16 – Permeability average results for variables used for self-healing.

HSC	Q air pre (ml/min)	Q air SH (ml/min)	Q water pre (ml/min)	Q water SH (ml/min)	Healing Ratio air	Healing Ratio water	Closing Ratio	Average crack width (µm)
P8-0.0-7d	2897.3	2585.1	78.3	66.3	0.13	0.15	0.14	208
P10-0.3-7d	3189.7	2351.9	61.6	39.4	0.31	0.36	0.33	210
P12-0.6-7d	1237.8	794.2	60.0	32.7	0.34	0.46	0.32	158
P14-0.0-28d	2430.1	1800.9	51.1	28.6	0.26	0.44	0.21	189
P16-0.3-28d	3090.9	2286.4	54.6	30.8	0.28	0.44	0.28	192
P18-0.6-28d	3211.8	2259.1	61.5	32.1	0.30	0.48	0.28	192

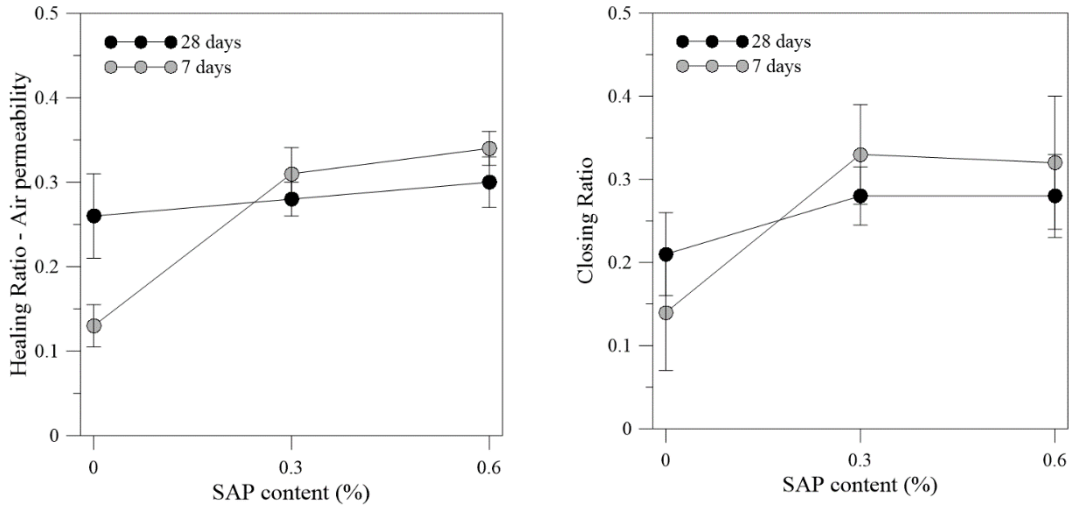

(a) **(b)**

Figure 44 – Results of a) Healing Ratio of the air permeability, and b) Closing Ratio of the permeability specimens.

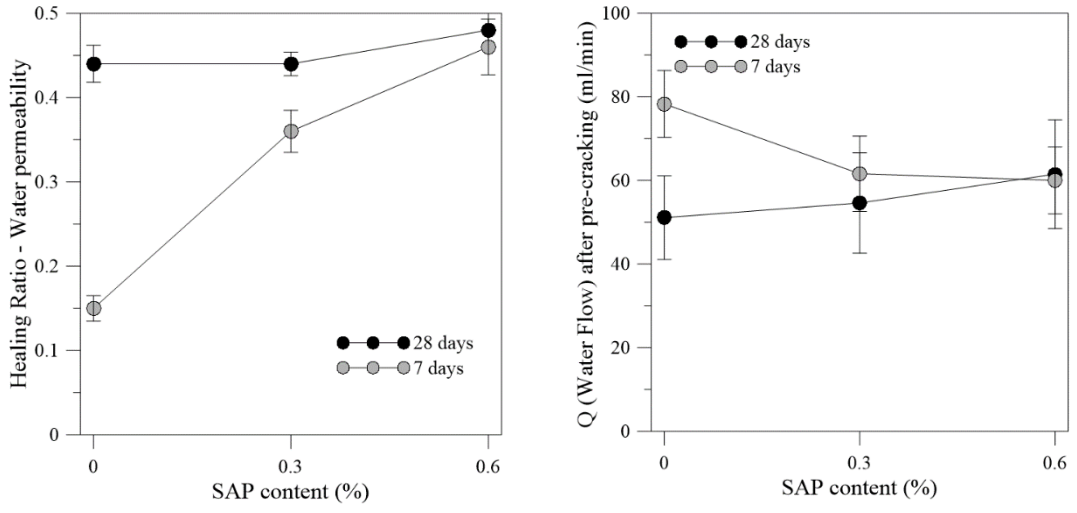

(a) **(b)**

Figure 45 – Results of a) Healing Ratio for the water permeability, and b) Water flow immediately after pre-cracking.

The photos of the back and front of each specimen's crack, taken from the digital microscope, are presented in Appendix C. The average, the standard deviation, maximum, and minimum of the crack width measurements are displayed in the caption of the figure for each one. The crack Closing Ratio is an average calculated from Equation 29 for each specimen and is presented in Table 16 and Figure 44 b).

As general trend, the results presented show that SAP increases the self-healing phenomena, as expected, however, with lower relevance than expected from the data found in literature. The air flow from permeability tests and crack closure from the images show self-healing effect.

The results of air permeability healing ratio and crack closing ratio follow the same tendency, presenting a higher Healing Ratio for the pre-cracking age of 7 days. Moreover, compared to the reference of 0.0% SAP, SAP additions of 0.3% and 0.6% presented a more pronounced Healing and Closing Ratio for the seven days, showing an increase of more 20% of the healing for both cases 0.3 and 0.6% of SAP. The SAP quantity did not significantly interfere in the results of the seven days age. For the 28 days, all mixtures presented similar results, although a slight increase of the healing and closing ratio is observed with higher SAP content.

The water permeability shows the self-sealing effect combined with self-healing, indicating higher values of Healing Ratio than those obtained with the air permeability test. The higher values found with the water permeability test can be understood by the concrete swelling phenomenon indicated in Figure 3 in item 2.2.1. In order to isolate the self-sealing effect, the water flow immediately after the pre-cracking is plotted in Figure 46 b.

The water permeability results shows that the healing effect described in the literature of Snoeck (2015), Snoeck *et al.* (2016), Snoeck *et al.* (2018), for lower strength concrete, is not observed in HSC. With lower strength concrete and polymer fibers, it was reported in the literature the healing of large cracks up to 500 μm. Knowing that the SAP used in this study was a smaller one and that HSC provides high resistance to permeation it was established to use specimens with cracks of 200μm, two and a half times smaller

than 500 μm. The results show that the self-healing, for cracks of this order of magnitude in HSC, is reduced.

The little efficiency of the SAP is attributed to the low water permeation of the high strength concrete, which can prevent the water from reaching the anhydrous phases in sufficient quantity and then migrate to the surface as an alkaline solution, therefore reducing the healing capacity.

The results obtained from the water permeability tests showed an increase of the healing ratio for the age of 7 days, showing that SAP can contribute for the self-healing comparing to the reference mixture. The self-healing effect increased more than 20% for the mixture with 0.3 % of SAP and more 30% for the mixture with 0.6 % of SAP. The results at 28 days showed a high self-healing ratio compared to seven days with minor effect with the SAP addition. At 28 days the healing was about 45%. The better healing at 28 days was unexpected since it was believed that the healing would be higher at younger ages since at 7 days more anhydrous phases are available.

In order to analyze the self-sealing capacity, and give some insight in surface phenomena, the water flow in the specimens prepared with SAP was compared to the flow of reference mixture (0.0% of SAP). At seven days, the addition of 0.3 % SAP decreased the flow by 18%, and the addition of 0.6% SAP reduced the flow by 21%. The results were in accordance with the literature, which indicates that SAP addition contributes to reducing the flow by a swelling phenomenon. However, for the 28 days, all mixtures presented similar results, and the presence of SAP slightly increased the water flow.

Putting together the results of the various tests carried out, the influence of the presence of anhydrous cement particles on HSC seems not relevant for the self-healing phenomenon.

7.5 Conclusions

This study developed a new method to investigate self-healing by durability parameters of air and water permeability tests. The self-healing of HSC with the

increasing dosage of SAP at different ages for pre-cracking was investigated. Based on the results presented, the following conclusions can be drawn:

- The permeability tests developed can be used to evaluate self-healing in cement-based materials.
- The water permeability results are higher than in the air permeability test due concrete swelling and self-sealing effect.
- Self-healing observed by the air permeability and crack closure results showed similar results of about 30% healing for both contents of 0.3% and 0.6% of SAP, independent of pre-cracking age.
- Self-sealing can be observed by the reduced water flow of about 20% due to SAP incorporation, for both contents 0.3% and 0.6% SAP.
- The addition of 0.3% and 0.6% of SAP presented similar healing ratio and crack closure results. No significant increase was observed due to the higher amount of SAP.
- The addition of SAP at the conditioning of four months with wetting and drying cycles does not produce sufficient or relevant self-healing properties regarding durability

8 SUMMARY AND FINAL CONCLUSIONS

This thesis aimed to analyze the phenomenon of self-healing in high strength concrete, promoted by the use of superabsorbent polymers intended to control autogenous shrinkage. Therefore, two main stages were proposed, the first with the evaluation of SAP combined with a fiber reinforced concrete, and the second stage, without fiber, using reinforced concrete. After analysis of the results of the first stage, the second stage aimed two main goals: 1) to study and develop an experimental procedure in order to efficiently evaluate self-healing phenomena regarding mechanical recovery and durability; and 2) to evaluate experimentally the self-healing efficiency of the superabsorbent polymer used to control autogenous shrinkage in high strength concrete.

The work presented proposed and validated a cracking methodology for cementitious materials with no use of fibers that can be easily implemented in other laboratories. The methodology developed makes a contribution to assess the self-healing phenomena by isolated effects, without the fiber contribution and synergic effect that enhances the phenomena. With this, it is possible to evaluate the self-healing efficiency by four means: mechanical recovery, air permeability, water permeability, and crack closure by images.

This Chapter summarizes this thesis's contribution and presents a list of conclusions drawn from the results herein. Since the thesis was written in independent pieces, each Chapter already has its conclusions at the end of it. Therefore, it was intended to join the overall work conclusions, which have been arranged in two sections the "9.1 Summary of Stage I" and "9.2 the Summary of Stage II". Item "9.3 Final conclusions" intends to answer the research question proposed in item 4.3. Finally, Section "9.4 Future perspectives" ends the Chapter with possible future research lines that could be initiated from the results of this thesis.

8.1 Summary of Stage I

Stage I intended to use steel fibers to control the crack width, with the premises of high strength concrete, super absorbent polymer in a minimum content to control

autogenous shrinkage in a maximum content to be defined until the concrete reached the strength of 60 MPa. The experimental campaign of this stage concluded that fiber reinforcement, in a content of 1.28%, was not sufficient to control to provide strain-hardening behavior or control the crack width at a desirable size, leading to an uncontrolled opening. A higher volume of fibers was required to control the crack width on high strength concrete. Though a higher content of 1.5% was initially investigated, the concrete consistency was unsuitable for practical application, preventing the study from moving forward. Another direction to control the crack width was developed.

Other conclusions were drawn:

- The content of 0.6% was defined as the maximum content to be incorporated to keep the concrete's high strength.
- Autogenous shrinkage can be adequately mitigated using the content of 0.3% SAP and subsequently 0.6%.
- The use of 0.3% SAP was also beneficial in different aspects. It has a minor influence on workability, it is compatible with high strength concrete, and significantly enhance the SFRC's ductile performance.
- The variable engagement model used was capable of describing the behavior of the SFRC with SAP, and it can be used in finite element applications.

8.2 Summary of Stage II

Stage II succeeded in developing a high-strength concrete mixture using superabsorbent polymers to control autogenous shrinkage and develop a methodology to evaluate self-healing by mechanical recovery, durability, and crack closure. The conclusions for the methodology developed of the overall work were:

- The methodology developed can be used to evaluate self-healing in cement-based materials regarding mechanical recovery, durability, and crack closure. The methodology is simple and easy to be implemented in other laboratories,

low cost, and can be highly repeatable. It can isolate the effect of the healing agent without the interference of fiber reinforcement.

- The limitations rely on the size of the specimens, being difficult to avoid some bending for low forces, at the beginning of the test.

- The cracking methodology managed to produce a single crack at the desired size, in a linear and uniform pattern, showing minimum influence with the material and maintaining the crack width during the healing process.

Relate to the evaluation of the SAP used for autogenous shrinkage control. The following conclusions were drawn from the overall self-healing evaluation:

- The content of 0,6% of SAP addition is the major content introduced in the mix design, while the concrete can still be classified as high strength.

- The 0.3% and 0.6% of SAP addition in an HSC mixture can successfully control the autogenous shrinkage. However, the use of 0.3% is recommended since it is enough to control autogenous shrinkage and presents higher strength than the use of 0.6%.

- The different pre-cracking ages of 7 and 28 days showed diverged results and comparing the healing performance of the two ages. It can be concluded that overall results were not significantly different, and the pre-cracking age in the cases studied is not a relevant variable. Though, concerning the mechanical recovery and water permeability tests, the 28 days showed slightly higher results. As regarding air permeability and crack closing ratio, the results for seven days presented higher results. Nevertheless, both results are not notable.

- Evaluating the SAP content, both addition of 0.3% and 0.6% showed similar results in all evaluations, independent of pre-cracking age. The difference between the results was in the range of the standard deviation. Both were showing the content of about 30% of healing regarding air and crack closing ratio. As for water permeability, the content was higher due to swelling and

SAP self-sealing. No mechanical recovery gain was observed, except for the 0.6 % SAP at 28 days that showed self-healing, although not relevant.

- The addition of SAP at the conditioning of four months with wetting and drying cycles does not produce sufficient or relevant self-healing properties.

- Self-sealing can be observed by the reduced water flow of about 20% due to SAP incorporation, for both contents 0.3% and 0.6% SAP.

8.3 Final conclusions

This thesis aimed to answer the question: "What degree of healing does a superabsorbent polymer with the function of mitigating autogenous shrinkage achieve in a high-strength concrete?".

Based on several analyses done on mechanical recovery, water and air permeability, crack closure evaluation, with the purpose for autogenous shrinkage control, the content of 0.3% of SAP can be introduced without significant loss of strength and workability, complete mitigation of autogenous shrinkage and the degree of self-healing of a crack of 200 μm under four months of daily wetting and drying cycles was of about 30%. In addition, the higher amount of SAP introduced (0.6%) led to a not significant increase in the self-healing properties.

8.4 Future perspectives

Several research lines can be proposed after the work developed in this thesis, such as:

- Use the mechanical recovery and durability methods to evaluate self-healing in other cement base material.

- Based on the methodology developed for mechanical recovery, make a larger specimen to evaluate concrete, using the principle of a single bar used in the center with a reduced section.

- Evaluate self-healing in steel bar reinforced concrete utilizing a single bar without the Styrofoam box to reduce cross-section, with a smaller crack width, and enlarging the size of the specimen

- Study other superabsorbent polymers that could control autogenous shrinkage and promote self-healing, maintaining the high strength, with other contents.

- Investigate autogenous self-healing by different healing conditions, such as water immersion. As also investigate smaller crack widths, smaller than 100 µm.

- Autogenous healing is a phenomenon with high dispersion results, and further studies are needed to corroborate a statistically reliable response to the phenomena.

- Studies including cracks formed at early concrete ages, can enhance the potential of the superabsorbent polymer and maybe improve the healing capacity.

In addition, studying self-healing is challenging as standards are still being developed, the techniques used to quantify healing most of the time are not comparable. The provided methodology is one solution, and it can be improved by: adding an evaluation on 3D mode; as implement the mechanical recovery in numeral models; investigating the self-healing under constant and cycling loads.

9 BIBLIOGRAPHY

ABNT NBR 13956-1, Sílica ativa para uso com cimento Portland em concreto, argamassa e pasta Parte 1: Requisitos. Rio de Janeiro: ASSOCIAÇÃO BRASILEIRA DE NORMAS TÉCNICAS, 2012.

ABNT NBR 5738, Concreto - Procedimento para moldagem e cura de corpos-de-prova. Rio de Janeiro: ASSOCIAÇÃO BRASILEIRA DE NORMAS TÉCNICAS, 2003.

ABNT NBR 5739, Concreto - Ensaios de compressão de corpos de prova cilíndricos. Rio de Janeiro: ASSOCIAÇÃO BRASILEIRA DE NORMAS TÉCNICAS, 2007.

ABNT NBR 6118, Projeto de estruturas de concreto - procedimento. Rio de Janeiro: ASSOCIAÇÃO BRASILEIRA DE NORMAS TÉCNICAS, 2014.

ABNT NBR 7211:2011, Agregados para concreto – Especificação Rio de Janeiro: ASSOCIAÇÃO BRASILEIRA DE NORMAS TÉCNICAS, 2011.

ABNT NBR 8953, Concreto para fins estruturais-Classificação pela massa específica, por grupos de resistência e consistência. Rio de Janeiro: ASSOCIAÇÃO BRASILEIRA DE NORMAS TÉCNICAS, 2015.

ABNT NBR 9775, Agregado miúdo – Determinação do teor de umidade superficial por meio do frasco de Chapman – Método de ensaio. Rio de Janeiro: ASSOCIAÇÃO BRASILEIRA DE NORMAS TÉCNICAS, 2011.

ACI COMMITTEE 211 - Standard practice for selecting proportions for normal, heavyweight and mass concrete, AMERICAN CONCRETE INSTITUTE, 1998.

AGOSTINHO, L. B. **Estudo Reológico de Pastas de Cimento Contendo Polímero Superabsorvente e Nano Partículas de Sílica**. Dissertação de Mestrado em Estruturas e Construção Civil, Departamento de Engenharia Civil e Ambiental, Universidade de Brasília, Brasília, DF, 128p., 2017.

ARAUJO, M.; VAN VLIERBERGHE, S.; FEITEIRA, J.; GRAULUS, G. J.; VAN TITTELBOOM, K.; MARTINS, J. C.; DUBRUEL, P.; e DE BELIE, N. **Cross-linkable polyethers as healing/sealing agents for self-healing of cementitious materials**. Materials & Design, v. 98, p. 215-222, 2016.

ASMARO, W. P. **Identification of concrete fracture parameters using digital image correlation and inverse analysis.** Doctoral thesis, Universty of Windsor, Windsor, Ontario, Canada, pp.284, 2013.

ASSMANN, A. **Physical Properties of Concrete Modified with superabsorbent polymers**. Tese doutorado, Universidade de Stuttgart, Faculdade de Engenharia Civil e Ambiental. Stuttgart - Alemanha, 213p. 2013.

ASTM C1698-09, **Standard Test Method for Autogenous Strain of Cement Paste and Mortar**, ASTM International, West Conshohocken, PA, 2009.

ASTM C1698-09, **Test Method for Autogenous Strain of Cement Paste and Mortar**. ASTM International, West Conshohocken, PA, 2009.

ASTM, C. 597, **Standard test method for pulse velocity through concrete**. ASTM International, West Conshohocken, PA, 2009.

BANG, S. S.; GALINAT, J. K.; RAMAKRISHNAN, V. **Calcite precipitation induced by polyurethane-immobilized Bacillus pasteurii**. Enzyme and microbial technology, v. 28, n. 4-5, p. 404-409, 2001.

BAŽANT, Z. P. **Concrete fracture models: testing and practice. Engineering fracture mechanics,** v. 69, n. 2, p. 165-205, 2002.

BAŽANT, Z. P. E OH, B. H. **Crack band theory for fracture of concrete**. Materials and Structures, p.155-177, 1983.

BAZANT, Z. P.; HUBLER, M. H.; WENDNER, R. **Model B4 for creep, drying shrinkage and autogenous shrinkage of normal and high-strength concretes with multi-decade applicability**. RILEM Technical Committee TC-242-MDC, 2015.

BENTUR, A., IGARASHI, S., KOVLER, K. **Prevention of autogenous shrinkage in high-strength concrete by internal curing using wet lightweight aggregates**. Cement and concrete research, v.31.11, p.1587-1591, 2001.

BROEK, D. **Elementary engineering fracture mechanics**. Springer Science & Business Media, 2012.

CEN, BS EN 1992- 1-1. Eurocode 2: Design of concrete structures–Part 1-1: General rules and rules for buildings, European Committee Standard, 2004.

CEZARIO, N. S. **Desempenho de bacillus sp. na biocimentação de materiais cimentícios**. Dissertação de Mestrado em Estruturas e Construção Civil, Departamento de Engenharia Civil e Ambiental, Universidade Estadual de Londrina, Londrina, PR, 2017.

CHINDASIRIPHAN, P., YOKOTA, H., PIMPAKAN, P. **Effect of fly ash and superabsorbent polymer on concrete self-healing ability**. Construction and Building Materials, p.233: 116975, 2020

CODE, CEB-FIP Model. **Fib Model Code for Concrete Structures 2010**; Ernst & Sohn. Wiley: Berlin, Germany, 2013.

COUTINHO, A. de S.; GONÇALVES, A. **Fabrico e propriedades do betão**. Lisboa: Laboratório Nacional de Engenharia Civil, 1997.

COUTO, P. B. **Caracterização reológica de pastas de cimento Portland de alta resistência contendo diferentes tipos de polímeros superabsorventes pela técnica de reometria rotacional.** Dissertação de Mestrado em Estruturas e Construção Civil, Departamento de Engenharia Civil e Ambiental, Universidade de Brasília, Brasília, DF, 2016.

CRAEYE, B., GEIRNAERT, M., DE SCHUTTER, G. **Super absorbing polymers as an internal curing agent for mitigation of early-age cracking of high-performance concrete bridge decks**. Construction and building materials, v.25.1: p.1-13, 2011.

CUENCA, E. e FERRARA, L. **Effects of Crystalline Admixtures on the Repeatability of Self-Healing in Fiber Reinforced Concrete**. Construction materials and systems, v. 5, p. 163, 2017.

D.P. BENTZ, O.M. JENSEN - **Mitigation strategies for autogenous shrinkage cracking**. Cement & Concrete Composites v.26 , p.677–685, 2004.

DARQUENNES. A, STAQUET. S, ESPION. B, **Determination of time-zero and its effect on autogenous deformation evolution**, Eur. J. Environ. Civ. Eng. v.15, p.1017–1029, 2010.

DAVIES, R., et al. **Large scale application of self-healing concrete: design, construction, and testing**. Frontiers in Materials, v.5: p.51, 2018.

DE BELIE, N.; GRUYAERT, E.; AL-TABBAA, A.; ANTONACI, P.; BAERA, C.; BAJARE, D.; DARQUENNES, A.; DAVIES, R.; FERRARA, L. JEFFERSON, T.; LITINA, C.; MILJEVIC B.; OTLEWSKA, A.; RANOGAJEC, J.; ROIG-FLORES M.; PAINE, K.; LUKOWSKI, P.; SERNA, P.; TULLIANI, J. M.; VUCETIC, S.; WANG, J. e JONKERS, H. M. **A Review of Self-Healing Concrete for Damage Management of Structures**. Advanced Materials Interfaces, p. 1800074, 2018.

DE MEYST, L., et al. **The Use of Superabsorbent Polymers in High Performance Concrete to Mitigate Autogenous Shrinkage in a Large-Scale Demonstrator**. Sustainability, v.12.11: p.4741, 2020.

DE MEYST, L., KHEIR, J., TENÓRIO FILHO, J. R., VAN TITTELBOOM, K., & DE BELIE, N. **The Use of Superabsorbent Polymers in High Performance Concrete to Mitigate Autogenous Shrinkage in a Large-Scale Demonstrator**. Sustainability, v.12(11), p.4741, 2020.

DE ROOIJ, M.; TITTELBOOM K. V.; DE BELIE N. e SCHLANGE E. (Ed.). **Self-healing phenomena in cement-Based materials: state-of-the-art report of RILEM technical committee 221-SHC: self-Healing phenomena in cement-Based materials**. Springer Science & Business Media, 2013.

DRY, C. **Matrix cracking repair and filling using active and passive modes for smart timed release of chemicals from fibers into cement matrices.** Smart Materials and Structures, v. 3, n. 2, p. 118, 1994.

DRY, C. **Procedures developed for self-repair of polymer matrix composite materials.** Composite structures, v. 35, n. 3, p. 263-269, 1996.

E392. "BETOES – Determinação da permeabilidade ao oxigénio." Especificação LNEC, Lisboa, 1993

EDVARDSEN, C. **Water permeability and autogenous healing of cracks in concrete.** Materials Journal, v. 96, n. 4, p. 448-454, 1999.

EN, T. S. 12504-4. **Testing concrete–Part 4: determination of ultrasonic pulse velocity**. British Standards Institution, p. 18, 2004.

ESTEVES, L. P. **On the absorption kinetics of Superabsorbent Polymers**. Int. RILEM Conference on Use of Superabsorbent Polymers and Other New Additives in Concrete, Technical University of Denmark, Lyngby, Denmark, 2010.

FERRARA, L. Tailoring the orientation of fibres in high performance fibre reinforced cementitious composites: part 1-experimental evidence, monitoring and prediction. International Journal of Materials and Structural Integrity, v. 9, n. 1-3, p. 72-91, 2015.

FERRARA, L.; KRELANI, V.; CARSANA, M. A "fracture testing" based approach to assess crack healing of concrete with and without crystalline admixtures. **Construction and Building Materials**, v. 68, p. 535-551, 2014.

FERRARA, L.; KRELANI, V.; MORETTI, F. **On the use of crystalline admixtures in cement-based construction materials: from porosity reducers to promoters of self-healing.** Smart Materials and Structures, v. 25, n. 8, p. 084002, 2016.

FERRARA, L.; OZYURT, N.; DI PRISCO, M. **High mechanical performance of fibre reinforced cementitious composites: the role of "casting-flow induced" fibre orientation**. Materials and Structures, v. 44, n. 1, p. 109-128, 2011.

FERRARA, L.; TIM VAN MULLEM T. V.; ALONSO M. C; ANTONACI P.; BORG R. P; CUENCA E.; JEFFERSON A.; NGG P. L.; PELED A.; ROIG-FLORES M.; SANCHEZ M.; SCHROEFL C.; SERNA P.; SNOECK D.; TULLIANI J. M e DE BELIE. N. **Experimental characterization of the self-healing capacity of cement-based materials and its effects on the material performance: A state of the art report by COST Action SARCOS WG2**. Construction and Building Materials, v. 167, p. 115-142, 2018.

FERREIRA, L. E. T. **Elementos de Mecânica da Fratura Aplicada à Engenharia Estrutural: aspectos analíticos, computacionais e experimentais**. Águas da Prata, São Paulo, 2015.

FISCHER, G.; LI, V. C. **Influence of matrix ductility on tension-stiffening behavior of steel reinforced engineered cementitious composites (ECC)**. Structural Journal, v. 99, n. 1, p. 104-111, 2002.

FORMAGINI, S. **Dosagem científica e caracterização mecânica de concretos de altíssimo desempenho.** Tese de doutorado. COPPE, Universidade Federal do Rio de Janeiro, Rio de Janeiro, RJ, 259 p, 2005.

FREYERMUTH, Clifford L. Life-Cycle Cost Analysis for Large Bridges. **Concrete International**, v. 23, n. 02, p. 89-95, 2001.

FRIEDRICH, S. V. **Superabsorbent Polymers (SAP).** In: RILEM TC 225-SAP. Application of superabsorbent polymers in concrete construction. London: Ed. Springer, Cap. 3, 2012.

FUKUYAMA, H.; SUWADA, H. **Experimental response of HPFRCC dampers for structural control.** Journal of Advanced Concrete Technology, v. 1, n. 3, p. 317-326, 2003.

GALI, S.; SUBRAMANIAM, K. V. L. **Multi-linear stress-crack separation relationship for steel fiber reinforced concrete: Analytical framework and experimental evaluation.** Theoretical and Applied Fracture Mechanics, v. 93, p. 33-43, 2018.

GARAS, V. Y.; KAHN, L. F.; KURTIS, K. E. **Short-term tensile creep and shrinkage of ultra-high-performance concrete.** Cement and Concrete Composites, v. 31, n. 3, p. 147-152, 2009.

GONZALEZ, M. L. S.; SILVA, E. F. e LOPES, A. N. M. **Polímeros Superabsorventes para Mitigar Retração Autógena de Concretos de Alta Resistência – Estado da Arte**. In: 56º Congresso Brasileiro do Concreto - CBC2014 – 56CBC. 2014.

GRANGER, S.; LOUKILI, A.; PIJAUDIER-CABOT, G.; CHANVILLARD, G. **Experimental characterization of the self-healing of cracks in an ultra-high performance cementitious material: Mechanical tests and acoustic emission analysis.** Cement and Concrete Research, v. 37, n. 4, p. 519-527, 2007.

GRUBE, H. & LAWRENCE, C. D. **Permeability of concrete to oxygen.** Cement and Concrete Association, 1984.

GRUYAERT, E.; DEBBAUT, B.; SNOECK, D.; DÍAZ, P.; ARIZO, A.; TZIVILOGLOU, E.; SCHLANGEN, E. e DE BELIE, N. **Self-healing mortar with pH-sensitive superabsorbent polymers: testing of the sealing efficiency by water flow tests**. Smart Materials and Structures, v. 25, n. 8, p. 084007, 2016.

GUPTA, S.; KUA, H. W.; PANG, S. D. **Combination of polypropylene fibre and superabsorbent polymer to improve physical properties of cement mortar.** Magazine of Concrete Research, v. 70, n. 7, p. 350-364, 2017.

GUPTA, S.; KUA, HARN W., DAI PANG, S. **Healing cement mortar by immobilization of bacteria in biochar: An integrated approach of self-healing and carbon sequestration**. Cement and Concrete Composites, v.86: p.238-254, 2018.

H. HUANG, G. Ye, **Examining the "time-zero" of autogenous shrinkage in high/ultra-high performance cement pastes**, Cement, Concrete, Research. v.97: p.107–114, 2017.

HASHOLT, M. T., JENSEN, O. M., KOVLER, K., & ZHUTOVSKY, S. **Can superabsorbent polymers mitigate autogenous shrinkage of internally cured**

concrete without compromising the strength?. Construction and Building Materials, v.31, p.226-230, 2012.

HEARN, N. **Self-sealing, autogenous healing and continued hydration: what is the difference?**. Materials and structures, v. 31, n. 8, p. 563, 1998.

HERBERT, E. N.; LI, V. C. **Self-healing of microcracks in engineered cementitious composites (ECC) under a natural environment.** Materials, v. 6, n. 7, p. 2831-2845, 2013.

HILLERBORG, A. **The theoretical basis of a method to determine the fracture energyG F of concrete.** Materials and structures, v. 18, n. 4, p. 291-296, 1985.

HILLERBORG, A.; MODÉER, M.; PETERSSON, P. E. **Analysis of crack formation and crack growth in concrete by means of fracture mechanics and finite elements.** Cement and concrete research, v. 6, n. 6, p. 773-781, 1976.

HILSDORF, H. K.; BRAMESHUBER, W. **Code-type formulation of fracture mechanics concepts for concrete.** International Journal of Fracture, v. 51, n. 1, p. 61-72, 1991.

HOMMA, Daisuke; MIHASHI, Hirozo; NISHIWAKI, Tomoya. Self-healing capability of fibre reinforced cementitious composites. **Journal of Advanced Concrete Technology**, v. 7, n. 2, p. 217-228, 2009.

HONG, G.; CHOI, S. **Rapid self-sealing of cracks in cementitious materials incorporating superabsorbent polymers.** Construction and Building Materials, v. 143, p. 366-375, 2017.

HUBLER, M. H., WENDNER, R., BAŽANT, ZDENĚK P. **Statistical justification of Model B4 for drying and autogenous shrinkage of concrete and comparisons to other models**. Materials and Structures, v.48.4: p.797-814, 2015.

IGARASHI, S. BENTUR, A., KOVLER, K. **Autogenous shrinkage and induced restraining stresses in high-strength concretes**. Cement and Concrete Research, v.30.11: p.1701-1707, 2000.

IGARASHI, S.; KUNIEDA, M. e NISHIWAKI, T. **Technical committee on autogenous healing in cementitious materials**. Japan: JCI. TC075B, 2009.

ISAIA, G. C. (ed.). **Materiais de construção civil e princípios de ciências e engenharia de materiais**. Ibracon, 2007.

J.R.T. FILHO, M.A.P.G. DE ARAÚJO, D. SNOECK, N. DE BELIE, **Discussing different approaches for the time-zero as start for autogenous shrinkage in cement pastes containing superabsorbent polymers**, Materials (Basel). V.12, 2019.

JEFFERSON, T., et al. **Research progress on numerical models for self-healing cementitious materials**. Advanced materials interfaces, v.5.17: p.1701378, 2018.

JENSEN, O. M., HANSEN, P. F. **Water-entrained cement-based materials: II. Experimental observations**. Cement and Concrete Research, v.32.6: p.973-978, 2002.

JENSEN, O. M.; HANSEN, P. F. **Autogenous deformation and RH-change in perspective**. Cement and Concrete Research, v.31.12: p.1859-1865, 2001.

JENSEN, O. M.; HANSEN, P. F. **Water-entrained cement-based materials I. Principles and theoretical background**. Cement and Concrete Research, v. 31, n. 6, p. 647-654, 2001.

JENSEN, O. M.; HANSEN, P. F. **Water-entrained cement-based materials II. Experimental observations**. Cement and Concrete Research, 32, 973–978, 2002.

JENSEN, O. M.; HANSEN, P. F. **Water-entrained cement-based materials: I. Principles and theoretical background**. Cement and concrete research, v.31.4: p.647-654, 2001.

JONKERS, H. M.; THIJSSEN, A.; MUYZER, G.; COPUROGLU, O.; SCHLANGEN, E. **Application of bacteria as self-healing agent for the development of sustainable concrete**. Ecological engineering, v. 36, n. 2, p. 230-235, 2010.

JSCE CONCRETE COMMITTEE. **Recommendations for design and construction of high performance fiber reinforced cement composites with multiple fine cracks.** Japan Society of Civil Engineers, Tokyo, Japan, 2008.

JSCE, Standard specification for concrete structures. Structural performance verification, Japan Society Civil Engineering. 2007.

KARIHALOO, B. L. **Fracture Mechanics and Structural Concrete (Concrete Design and Construction Series).** Ed. Longman Scientific & Technical. United States, 1995.

KAZEMI, M. T.; GOLSORKHTABAR, H.; BEYGI, M. H. A.; GHOLAMITABAR, M. **Fracture properties of steel fiber reinforced high strength concrete using work of fracture and size effect methods.** Construction and Building Materials, v. 142, p. 482 489, 2017.

KUMAR, Shailendra; BARAI, Sudhirkumar V. **Concrete fracture models and applications.** Springer Science & Business Media, 2011.

KUMM, T.C. **Influência do emprego de polímeros superabsorventes nas propriedades de materiais à base de cimento Portland.** Dissertação de mestrado. Universidade Federal de Santa Catarina, 159p. 2009.

LEE, H. X. D.; WONG, H. S.; BUENFELD, N. R. **Potential of superabsorbent polymer for self-sealing cracks in concrete**. Advances in Applied Ceramics, v. 109, n. 5, p. 296-302, 2010.

LEE, H. X. D.; WONG, H. S.; BUENFELD, N. R. Self-sealing of cracks in concrete using superabsorbent polymers. **Cement and Concrete Research**, v. 79, p. 194-208, 2016.

LEE, H. X. D.; WONG, H. S.; BUENFELD, N. R. **Self-sealing of cracks in concrete using superabsorbent polymers**. Cement and Concrete Research, v. 79, p. 194-208, 2016.

LI, V. C. **Durable overlay systems with engineered cementitious composites (ECC)**. 2003.

LI, V. C. **On engineered cementitious composites (ECC).** Journal of advanced concrete technology, v. 1, n. 3, p. 215-230, 2003.

LI, V. C.; LEUNG, C. K. Y. **Steady-state and multiple cracking of short random fiber composites.** Journal of engineering mechanics, v. 118, n. 11, p. 2246-2264, 1992.

LI, V. C.; STANG, H. **Interface property characterization and strengthening mechanisms in fiber reinforced cement based composites.** Advanced cement based materials, v. 6, n. 1, p. 1-20, 1997.

LIN, R., PANG, L. **Influences of superabsorbent polymers on the strength and shrinkage properties of low water-to-binder ratio expansive concrete**. Journal of Ceramic Processing Research, v.20.3: p.231-240, 2019.

LOPES, A. N. M.; SILVA, E. F.; DAL MOLIN, D. C. C. e TOLEDO FILHO, R. D. **Shrinkage-Reducing Admixture: Effects on Durability of High-Strength Concrete**. ACI Materials Journal; Vol. 110 Issue 4, p365, 2013.

LOPES, A.N. M.; SILVA, E. F.; TOLEDO FILHO, R. D. e DAL MOLIN, D. S. C. **Propriedades Mecânicas, Retração Autógena e por Secagem de Concretos de Alta Resistência contendo Aditivo Redutor de Retração.** In: XXXV – Jornadas Sul Americanas da Engenharia Estrutural. Rio de Janeiro, 2012.

LOPES, A.N. M.; SILVA, E. F.; TOLEDO FILHO, R. D. e DAL MOLIN, D. S. C. **Propriedades Mecânicas, Retração Autógena e por Secagem de Concretos de Alta Resistência contendo Aditivo Redutor de Retração.** In: XXXV – Jornadas Sul Americanas da Engenharia Estrutural. Rio de Janeiro, 2012.

LOUKILI, A., KHELIDJ, A., RICHARD, P. **Hydration kinetics, change of relative humidity, and autogenous shrinkage of ultra-high-strength concrete**. Cement and Concrete Research, v.29.4: p.577-584, 1999.

LU, T., LI, Z., VAN BREUGEL, K. **Modelling of autogenous shrinkage of hardening cement paste**. Construction and Building Materials, v.264: p.120708, 2020.

LURA, P. e JENSEN, O.M. **Measuring Techniques for Autogenous Strain of Cement Paste**, Materials and Structures. Vol. 40 (4) 431-440, 2007b.

LURA, P., **Autogenous deformation and internal curing of concrete**. Doctoral thesis, Delft, Netherlands, April., 2003.

LURA, P.; DURAND, F.; JENSEN, O.M. **Autogenous strain of cement pastes with superabsorbent polymers**. in International RILEM Conference on Volume Changes of Hardening Concrete: Testing and Mitigation, O.M. Jensen, P. Lura, and K. Kovler, Editors. Technical University of Denmark, Lyngby, Denmark, 2006a.

LURA, P.; FRIEDEMANN, K.; STALLMACH, F.; MÖNNIG S; WYRZYKOWSKI, M. e ESTEVES; L. P. **Kinetics of Water Migration in Cement-based Systems containing Superabsorbent Polymers**. In: RILEM TC 225-SAP. Application of superabsorbent polymers in concrete construction. London: Ed. Springer, Cap. 4, 2012.

LURA, P.; JENSEN, O. M.; IGARASHI, S. I. **Experimental observation of internal water curing of concrete**. Materials and Structure 40: 211–220, 2007a.

LURA, P.; JENSEN, O.M.; BREUGEL K. V., **Autogenous shrinkage in high performance cement paste: An evaluation of basic mechanisms**. Cement and Concrete Research, 33, p. 223–232, 2003.

LURA, P.; MAZZOTTA, G.B.; RAJABIPOUR, F.; WEISS, J. **Evaporation, settlement, temperature evolution, and development of plastic shrinkage cracks in mortars with shrinkage-reducing admixtures**, International RILEM-JCI Seminar ConcreteLife'06, Pro 46, pp. 203-214, 2006b.

M. SEDDIK MEDDAH, A. TAGNIT-HAMOU, **Evaluation of Rate of Deformation for Early-Age Concrete Shrinkage Analysis and Time Zero Determination**, J. Materials Civil Engineering. v.23, p.1076–1086, 2011.

M. WYRZYKOWSKI, Z. HU, S. GHOURCHIAN, K. SCRIVENER, P. LURA, **Corrugated tube protocol for autogenous shrinkage measurements: review and statistical assessment**, Materials and Structures. V.50, p.1–14, 2017.

MANZANO, M. A. R. **Estudo Experimental de Materiais Cimentícios de Alta Resistência modificados com Polímeros Superabsorventes (PSAs) como Agentes de Cura Interna**. Tese de Doutorado - Universidade de Brasília. Faculdade de Tecnologia.

Departamento de Engenharia Civil e Ambiental. Brasília, 2016, 324p.

MANZANO, M. A. R.; NETO, W. N. A.; SILVA, E. F. e LOPES, A. N. M. **Análise da Caracterização de um Polímero Superabsorvente Utilizado em Materiais Cimentícios**. In: XIII Congresso Latino-Americano de Patologia da Construção. Lisboa, Portugal, 2015.

MANZANO, M. A. R.; TRALDI, C. L.; SILVA, E. F. e LOPES, A. N. M. **Mecanismo de Atuação dos Polímeros Superabsorventes na Hidratação de Materiais Cimentícios**. In: 56º Congresso Brasileiro do Concreto - CBC2014 – 56CBC. 2014.

MARIANO, A. M.; ROCHA, M. S. **Revisão da Literatura: Apresentação de uma Abordagem Integradora.** In: XXVI Congreso Internacional de la Academia Europea de Dirección y Economía de la Empresa (AEDEM), Reggio Calabria (Italia). 2017.

MARSHALL, D. B.; COX, B. N. **A J-integral method for calculating steady-state matrix cracking stresses in composites.** Mechanics of materials, v. 7, n. 2, p. 127-133, 1988.

MECHTCHERINE, V.; DUDZIAK, L.; SCHULZE, J. **Internal curing by superabsorbent polymers (SAP) - Effects on material properties of self-compacting fibre-reinforced high performance concrete.** in International RILEM Conference on Volume Changes of Hardening Concrete: Testing and Mitigation, O.M. Jensen, P. Lura, and K. Kovler, Editors. Technical University of Denmark, Lyngby, Denmark, 2006.

MECHTCHERINE, V.; GORGES, M.; SCHROEFL, C.; BRAMASHUBER, W.; RIBEIRO, A.B.; CUSSON, D.; SILVA, E. F; ICHIMIYA, K.; IGARASHI, S.; KOVLER, K.; LOPES, A. N. M.; LURA, P.; REINHARDT, H. W.; FILHO, R. D. T; WEISS, J.; YE, G. **Effect of internal curing by using superabsorbent polymers (SAP) on autogenous shrinkage and other properties of a high-performance fine-grained concrete: results of a RILEM round-robin test**. In: Materials and Structures. 47, 541-562, 2013.

MECHTCHERINE, V.; REINHARDT, H. W. **Application of super absorbent polymers (SAP) in concrete construction: state-of-the-art report prepared by Technical Committee 225-SAP**. Springer Science & Business Media, 2012.

MECHTCHERINE, Viktor; REINHARDT, Hans-Wolf (Ed.). **Application of super absorbent polymers (SAP) in concrete construction: state-of-the-art report prepared by Technical Committee 225-SAP**. Springer Science & Business Media, 2012.

MIHASHI, H.; NISHIWAKI, T. **Development of engineered self-healing and self-repairing concrete-state-of-the-art report.** Journal of Advanced Concrete Technology, v. 10, n. 5, p. 170-184, 2012.

MÖNNIG, S. **Superabsorbing additions in concrete – applications, modelling and comparison of different internal water sources**. Tese doutorado, Universidade de Stuttgart, Faculdade de Engenharia Civil e Ambiental. Stuttgart - Alemanha, 164pp, 2009.

MOREIRA, M. M. **Efeito do aditivo redutor de permeabilidade em concretos com diferentes tipos de cimento Portland – contribuição aos processos de auto cicatrização**. Dissertação de Mestrado em Estruturas e Construção Civil, Departamento de Engenharia Civil e Ambiental, Universidade de Brasília, Brasília, DF, 166p., 2016.

MOREIRA, T. N. C. **Investigação do fenômeno de auto-cicatrização de fissuras em microconcreto de alta performance reforçado com fibras de aço e sisal.** Dissertação de Mestrado em Estruturas e Materiais, COPPE, Universidade Federal do Rio de Janeiro, Rio de Janeiro, RJ, 153p., 2017.

NAAMAN, A. E.; REINHARDT, H. W. **Characterization of high performance fiber reinforced cement composites—HPFRCC**. In: High performance fiber reinforced cement composites, p. 1-24,1995.

NEVILLE and BROOKS, 1987; COUTINHO e GONÇALVES, 1997; ISAIA, 2007;

NEVILLE, A. **Autogenous healing—a concrete miracle?**. Concrete international, v. 24, n. 11, p. 76-82, 2002.

NEVILLE, A. M., BROOKS, J. J. **Concrete technology**. England: Longman Scientific & Technical, 1987.

NISHIWAKI, T.; MIHASHI, H.; JANG, B. K.; MIURA, K. **Development of self-healing system for concrete with selective heating around crack.** Journal of Advanced Concrete Technology, v. 4, n. 2, p. 267-275, 2006.

NP EN 12390-13. Ensaios do betão endurecido; Parte 13: Determinação do módulo de elasticidade secante à compressão, Instituto Português Da Qualidade. 2014.

NP EN 12390-13. Ensaios do betão endurecido; Parte 13: Determinação do módulo de elasticidade secante à compressão, Instituto Português Da Qualidade. 2014.

NP EN 1992-1-1:2010. Eurocódigo 2- Projecto de estruturas de betão Parte 1-1: Regras gerais e regras para edifícios. Instituto Português Da Qualidade, 2010.

NP EN 933-1:2014. Ensaios das propriedades geométricas dos agregados; Parte 1: Análise granulométrica; Método da peneiração. Instituto Português Da Qualidade, 2014.

NP, EN 196-1. Métodos de ensaio de cimentos; Parte 1: Determinação das resistências mecânicas, Instituto Português Da Qualidade. 2017.

ORDÓÑEZ, S. T. L. **Mitigação da Retração Autógena em Microconcretos de Alta Resistência com Adição de Polímeros Superabsorventes e Aditivo Redutor de Retração**. Dissertação de Mestrado em Estruturas e Construção Civil, Departamento de Engenharia Civil e Ambiental, Universidade de Brasília, Brasília, DF, 160p. 2013.

ORDOÑEZ, S. T. L.; SILVA, E. F.; BAUER, E. e LOPES, A. N. M. **Mitigação da Retração Autógena em Microconcretos de Alta Resistência com adição de Polímeros Superabsorventes**. In: 4o Congresso Nacional da Construção. Coimbra – Portugal, 2012.

ORDOÑEZ, S. T. L.; SILVA, E. F.; BAUER, E. e LOPES, A. N. M. **Mitigação da Retração Autógena em Microconcretos de Alta Resistência com adição de Polímeros Superabsorventes**. In: 4o Congresso Nacional da Construção. Coimbra – Portugal, 2012.

ORDOÑEZ, S. T. L.; SILVA, E. F.; BAUER, E. e LOPES, A. N. M. **Utilização de polímero superabsorvente e aditivo redutor de retração no combate à retração**

autógena em microconcretos de alta resistência. In: 55º Congresso Brasileiro do Concreto IBRACON. Gramado, Rio Grande do Sul. 2013.

ORDOÑEZ, S. T. L.; SILVA, E. F.; BAUER, E. e LOPES, A. N. M. **Utilização de polímero superabsorvente e aditivo redutor de retração no combate à retração autógena em microconcretos de alta resistência**. In: 55º Congresso Brasileiro do Concreto IBRACON. Gramado, Rio Grande do Sul. 2013.

PARK, B., CHOI, Y. C. **Self-healing capability of cementitious materials with crystalline admixtures and super absorbent polymers (SAPs)**. Construction and Building Materials, v.189: p.1054-1066, 2018.

PIÉRARD, J., POLLET, V.; CAUBERG, N. **Mitigating autogenous shrinkage in HPC by internal curing using superabsorbent polymers.** In: International RILEM Conference on Volume Changes of Hardening Concrete: Testing and Mitigation, O.M. Jensen, P. Lura, and K. Kovler, Editors. Technical University of Denmark, Lyngby, Denmark, 2006.

RAHIMI-AGHDAM, S., et al. **Century-long expansion of hydrating cement counteracting concrete shrinkage due to humidity drop from self desiccation or external drying**. Materials and Structures, v.52.1: p.11, 2019.

RAJCZAKOWSKA, M., et al. **Autogenous Self-Healing: A Better Solution for Concrete**. Journal of Materials in Civil Engineering, v.31.9: p.03119001, 2019.

RAMACHANDRAN, V. S.; BEAUDOIN, James J. **Handbook of analytical techniques in concrete.** 2001.

RECOMMENDATION, RILEM Draft. **Determination of the fracture energy of mortar and concrete by means of three-point bend tests on notched beams.** Materials and structures, v. 18, n. 106, p. 285-290, 1985.

REDDY, K. C.; SUBRAMANIAM, K. V. L. **Analysis for multi-linear stress-crack opening cohesive relationship: Application to macro-synthetic fiber reinforced concrete.** Engineering Fracture Mechanics, v. 169, p. 128-145, 2017.

REIS, P. F, EVANGELISTA JR, SILVA, E. F. **Profile of internal relative humidity and depth of drying in cementitious materials containing superabsorbent polymer and nano-silica particles**. Construction and Building Materials, v.237: p.117412, 2020.

RILEM, T. C. 187-SOC. **Experimental determination of the stress-crack opening curve for concrete in tension",** Final report, 2007.

RILEM, TC89. 89-FMT, **Fracture mechanics of concrete-test methods. Size-effect method for determining fracture energy and process zone size of concrete**. Mater. Struct, v. 23, p. 461-465, 1990.

ROSSI, P.; CHARRON, J. P.; BASTIEN-MASSE, M.; TAILHAN, J. L.; LE MAOU, F.; RAMANICH, S. **Tensile basic creep versus compressive basic creep at early ages: comparison between normal strength concrete and a very high strength fibre reinforced concrete.** Materials and structures, v. 47, n. 10, p. 1773-1785, 2014.

S. RAHIMI-AGHDAM, E. MASOERO, M. RASOOLINEJAD, Z.P. BAŽANT, **Century-long expansion of hydrating cement counteracting concrete shrinkage due to humidity drop from self desiccation or external drying**, Materials and Structures. V.52, 2019.

ŞAHIN, Y. e KÖKSAL, F. **The influences of matrix and steel fibre tensile strengths on the fracture energy of high-strength concrete**. Construction and Building Materials, v. 25, n. 4, p. 1801-1806, 2011.

ŞAHMARAN, M.; LI, V. C. **Durability of mechanically loaded engineered cementitious composites under highly alkaline environments.** Cement and Concrete Composites, v. 30, n. 2, p. 72-81, 2008.

SANTOS, K. F.D., RIBEIRO, A. C. B. S., SILVA, E. F. D., MANZANO, M. A. R., MOTTA, L. A. D. C.,TOLEDO FILHO, R. D. **Effect of the Combination of Superabsorbent Polymers for Autogenous Shrinkage Control with Steel Fibers of High-Performance Concrete under Uniaxial Tension Using DIC**. Materials, v.13.20: p.4638, 2020.

SANTOS, T. A. C. **Estudo da adição de polímero superabsorvente e de nano partículas de sílica para melhorar propriedades de concretos de alta resistência**. Dissertação (Mestrado), Programa de Pós-Graduação em Estruturas e Construção Civil, Universidade de Brasília, 144 p., 2016.

SANTOS, T. A. C.; AIDAR, L. A. G.; BORGES, J. G.; FRANCINETE JR., P.; MANZANO, M. A. R.; SILVA, E. F. **Determinação do Tempo de Transição Suspensão-Sólido (Tempo Zero) em Microconcretos de Alta Resistência Contendo Polímero Superabsorvente e Nanossílica**. Anais do Congresso Brasileiro de Patologia das Construções - CBPAT 2016, Belém-PA, 2016.

SCHRÖFL, C., MECHTCHERINE, V., GORGES, M. **Relation between the molecular structure and the efficiency of superabsorbent polymers (SAP) as concrete admixture to mitigate autogenous shrinkage**. Cement and concrete research, v.42.6: p.865-873, 2012.

SHAH, S. P.; SWARTZ, S. E.; OUYANG, C. **Fracture mechanics of concrete: applications of fracture mechanics to concrete, rock and other quasi-brittle materials.** John Wiley & Sons, 1995.

SHEN, D., et al. **Effect of internal curing with super absorbent polymers on autogenous shrinkage of concrete at early age**. Construction and Building Materials, v.106: p.512-522, 2016.

SIDIQ, A., et al. **Microstructural analysis of healing efficiency in highly durable concrete**. Construction and Building Materials, v.215: p.969-983, 2019.

SILVA JUNIOR, F. P. **Estudo da estabilidade dimensional de concretos de alta resistência com adição de polímero superabsorvente e nanopartículas de sílica**. Tese de Doutorado - Universidade de Brasília. Faculdade de Tecnologia. Departamento de Engenharia Civil e Ambiental. Brasília, 2017, 345p.

SILVA, E. F. **Variações dimensionais em concretos de alto desempenho contendo aditivo redutor de retração**. Tese de doutorado. COPPE, Universidade Federal do Rio de Janeiro, Rio de Janeiro, RJ, 307 p, 2007.

SILVA, E. F.; CLARO, G. P.; SARAIVA, L. M. e LOPES A. N. M. **O polímero superabsorvente como estratégia mitigadora da retração autógena em microconcretos de alta resistência**. In: 55º Congresso Brasileiro do Concreto IBRACON. Gramado, Rio Grande do Sul. 2013a.

SILVA, E. F.; LOPES, A. N. M. e CHATER, L. **Metodologia para determinação da retração autógena unidirecional em concretos de alto desempenho (CAD) por capturas de imagens**. In: 6º Congresso Luso-Moçambicano de Engenharia. Maputo - Moçambique. 2011a.

SILVA, E. F.; LOPES, A. N. M.; CLARO, G. P. e SARAIVA, L. M. **Técnica do Ultrassom para determinar o Tempo-Zero de Microconcretos de Alta Resistência**. In: 55º Congresso Brasileiro do Concreto IBRACON. Gramado, Rio Grande do Sul. 2013b.

SILVA, E. F.; LOPES, A. N. M.; REGO, P. I. A. e AKITAYA, T. A. **Técnica da propagação de pulso ultrassônico para determinação do tempo-zero (t0) em concretos de alto desempenho (CAD**). In: 6º Congresso Luso-Moçambicano de Engenharia. Maputo - Moçambique. 2011b.

SILVA, E. F.; LOPES, A.N. M.; TOLEDO FILHO, R. D. e FAIRBAIRN, E. M. R**. Aditivo Redutor de Retração: Efeito na Retração Autógena, Propriedades Reológicas, Mecânicas e Térmicas, em Concretos de Alto Desempenho**. In: XXXIII Jornadas Sul Americanas da Engenharia Estrutural. Santiago - Chile. 2008.

SILVA, E. F.; LOPES, A.N. M.; TOLEDO FILHO, R. D. e FAIRBAIRN, E. M. R. **Uso de Onda Ultra-Sônica para determinar o Tempo-Zero em Concretos de Alto Desempenho (CAD) contendo Aditivo Redutor de Retração (ARR**). In: XXXIV - Jornadas Sul Americanas da Engenharia Estrutural. San Juan - Argentina. 2010.

SILVA, E. F.; LOPES, A.N. M.; TOLEDO FILHO, R. D. e FAIRBAIRN, E. M. R. **Resistência à tração direta de concretos de alto desempenho contendo aditivo redutor de retração**. In: 53º Congresso Brasileiro do Concreto IBRACON. Florianópolis, Santa Catarina. 2011c.

SILVA, E. F.; LOPES, A.N. M.; TOLEDO FILHO, R. D. e FAIRBAIRN, E. M. R. **Módulo de Elasticidade de Concretos de Alta Resistência (CAR) contendo Aditivo Redutor de Retração (ARR)**. In: XXXV – Jornadas Sul Americanas da Engenharia Estrutural. Rio de Janeiro. 2012.

SILVA, E. F.; R. MANZANO, M. A. R. LOPES, A.N. M. e TOLEDO FILHO, R. D. **Effect of SAP on the Autogenous Shrinkage and Compressive Strength of High-Strength Fine-Grained Concrete**. In: International RILEM Conference on Application of Superabsorbent Polymers and Other New Admixtures in Concrete Construction, Dresden, p. 211-219, 2014.

SKARŻYŃSKI, Ł.; SUCHORZEWSKI, J. **Mechanical and fracture properties of concrete reinforced with recycled and industrial steel fibers using Digital Image Correlation technique and X-ray micro computed tomography**. Construction and Building Materials, v. 183, p. 283-299, 2018.

SNOECK, D., **Self-Healing and Microstructure of Cementitious Materials with Microfibres and Superabsorbent Polymers.** Doctoral thesis, Ghent University, Belgium, 2015.

SNOECK, D.; STEUPERAERT, S.; VAN TITTELBOOM, K.; DUBRUEL, P.; E DE BELIE, N. **Visualization of water penetration in cementitious materials with superabsorbent polymers by means of neutron radiography**. Cement and Concrete Research, v. 42, n. 8, p. 1113-1121, 2012.

SNOECK, D.; VAN TITTELBOOM, K.; STEUPERAERT, S.; DUBRUEL, P., e DE BELIE, N. **Self-healing cementitious materials by the combination of microfibres and superabsorbent polymers**. Journal of Intelligent Material Systems and Structures, v. 25, n. 1, p. 13-24, 2014.

SNOECK, D.; VELASCO, L. F.; MIGNON, A.; VAN VLIERBERGHE, S.; DUBRUEL, P.; LODEWYCKX, P.; e DE BELIE, N. **The influence of different drying techniques on the water sorption properties of cement-based materials**. Cement and Concrete Research, v. 64, p. 54-62, 2014.

SOUZA, A. F. **Influência de aditivos cristalizantes e sal na cristalização de fissuras de pastas de cimentação para poços de petróleo.** Qualificação de Doutorado em Estruturas e Materiais, COPPE, Universidade Federal do Rio de Janeiro, Rio de Janeiro, RJ, 271p., 2017.

SOUZA, L. O. **Mecanismos de Fissuração e Autocicatrização de Compósitos Cimentícios Reforçados com Tecidos de Curauá**. Dissertação de Mestrado em Engenharia Civil, Pontifícia Universidade Católica do Rio de Janeiro, Rio de Janeiro, RJ, 166p., 2016.

SUAREZ, M. L. G. **Polímeros Super Absorventes (PSA) como agente de cura interna para prevenir fissuração em concretos de alta resistência**. Dissertação de mestrado, Programa de Pós-Graduação em Estruturas e Construção Civil, Universidade de Brasília, p.82, 2015.

TAKAGI, E. M. **Concretos autocicatrizantes com cimentos brasileiros de escória de alto-forno ativados por catalisador cristalino**. Dissertação de Mestrado, Instituto Tecnológico de Aeronáutica, São José dos Campos, SP, 130 p., 2013.

TASDEMIR, C.; TASDEMIR, M. A.; LYDON, F. D.; BARR, B. I. **Effects of silica fume and aggregate size on the brittleness of concrete.** Cement and Concrete Research, v. 26, n. 1, p. 63-68, 1996.

TAYLOR, H.F.W. **Cement Chemistry**. 2. Ed. London: Thomas Tellford, 1997.

TAZAWA, E., MIYAZAWA, S. **Experimental study on mechanism of autogenous shrinkage of concrete**. Cement and Concrete Research, v.25.8: p.1633-1638, 1995.

TENÓRIO FILHO, J. R., et al. **Discussing Different Approaches for the Time-Zero as Start for Autogenous Shrinkage in Cement Pastes Containing Superabsorbent Polymers**. Materials, v.12.18: p.2962, 2019.

TER HEIDE, Nynke. **Crack healing in hydrating concrete.** Delft University of Technology, 2005.

TOLEDO FILHO, R.D.; SILVA, E.F.; LOPES, A.N.M.; MECHTCHERINE, V. e DUDZIAK, L. **Effect of Superabsorbent Polymers on the Workability of Concrete and Mortar.** In: RILEM TC 225-SAP. Application of superabsorbent polymers in concrete construction. London: Ed. Springer, Cap. 5, 2012.

TRALDI, C. L.; AGUIRRE, L. M.; SILVA, E. F.; LOPES, A. N. M. **Polímero superabsorvente como agente de cura interna para prevenir fissuração em concretos**. In: Jornadas Sul Americanas de Engenharia Estrutural, 2014, Montevidéu. Anais Jornadas Sul Americanas de Engenharia Estrutural, 2014.

TRALDI, C.L.; AGUIRRE; L.M.; SILVA, E.F. e LOPES, A.N.M. **Polímero Superabsorvente como Agente de Cura Interna para prevenir fissuração em Concretos**. In: XXXVI – Jornadas Sul Americanas da Engenharia Estrutural. Montevideo – Uruguai. 2014.

TRIVEDI, N.; SINGH, R. K.; CHATTOPADHYAY, J. **Investigation on fracture parameters of concrete through optical crack profile and size effect studies.** Engineering Fracture Mechanics, v. 147, p. 119-139, 2015.

TSANGOURI, Eleni, et al. Feasibility study on real-scale, self-healing concrete slab by developing a smart capsules network and assessed by a plethora of advanced monitoring techniques. Construction and Building Materials, 2019, 228: 116780.

TSUJI, M.; OKUYAMA, A.; ENOKI, K.; e SUKSAWANG, S. **Development of new concrete admixture preventing from leakage of water through cracks**. JCA Proc. of Cement & Concrete (Japan Cement Association), v. 52, p. 418-423, 1998.

TSUJI, M.; SHITAMA, K. e ISOBE, D. **Basic studies on simplified curing technique, and prevention of initial cracking and leakage of water through cracks of concrete by applying superabsorbent polymers as new concrete admixture**. Journal of the Society of Materials Science, Japan, v. 48, n. 11, p. 1308-1315, 1999.

VAN BREUGEL, K. **Is there a market for self-healing cement-based materials**. In: Proceedings of the first international conference on self-healing materials, p. 1-9, 2007.

VAN MULLEM, T., *et al*. **First Large Scale Application with Self-Healing Concrete in Belgium: Analysis of the Laboratory Control Tests**. Materials, v.13.4: p.997, 2020.

VAN OSS, Hendrik G. **Background facts and issues concerning cement and cement data**. 2005.

VAN TITTELBOOM, K., et al. **Comparison of different approaches for self-healing concrete in a large-scale lab test**. Construction and building materials, v.107: p.125-137, 2016.

VAN TITTELBOOM, K.; DE BELIE, N. **Self-healing in cementitious materials—A review.** Materials, v. 6, n. 6, p. 2182-2217, 2013.

VAN TITTELBOOM, K.; DE BELIE, N.; DE MUYNCK, W.; VERSTRAETE, W. **Use of bacteria to repair cracks in concrete.** Cement and Concrete Research, v. 40, n. 1, p. 157-166, 2010.

VAN TITTELBOOM, K.; DE BELIE, N.; ZHANG, P.; WITTMANN, F. H. **Self-healing of cracks in concrete**. In: International workshop (ASMES) 2011: basic research on concrete and applications, p. 303-314, 2011.

VAN ZIJL, G. P. A. G.; WITTMANN, F. H. (Ed.). **Durability of strain-hardening fibre-reinforced cement-based composites (SHCC)**. Springer Science & Business Media, 2010.

WANG, J. Y., SNOECK, D., VAN VLIERBERGHE, S., VERSTRAETE, W., & DE BELIE, N. **Application of hydrogel encapsulated carbonate precipitating bacteria for approaching a realistic self-healing in concrete**. Construction and building materials, v.68, p.110-119, 2014.

WANG, J. Y.; DE BELIE, N.; VERSTRAETE, W. **Diatomaceous earth as a protective vehicle for bacteria applied for self-healing concrete.** Journal of industrial microbiology & biotechnology, v. 39, n. 4, p. 567-577, 2012b.

WANG, J. Y.; SOENS, H.; VERSTRAETE, W.; DE BELIE, N. **Self-healing concrete by use of microencapsulated bacterial spores.** Cement and Concrete Research, v. 56, p. 139-152, 2014.

WANG, J.; VAN TITTELBOOM, K.; DE BELIE, N.; VERSTRAETE, W. **Use of silica gel or polyurethane immobilized bacteria for self-healing concrete**. Construction and building materials, v. 26, n. 1, p. 532-540, 2012a.

WEBER, S.; REINHARDT, H. W. **A new generation of high performance concrete: concrete with autogenous curing**. Advanced cement based materials, v.6.2: p.59-68, 1997.

WEISS, J. **Experimental determination of the "time-zero" t0 (maturity M0)**. In: K. Kovler, A. Bentur (Eds.), International RILEM Conference on Early Age Cracking in Cementitious Systems—EAC', RILEM TC 181-EAS, Haifa, pp. 195–206, 2002.

WHITE, S. R.; SOTTOS, N. R.; GEUBELLE, P. H.; MOORE, J. S.; KESSLER, M.; SRIRAM, S. R.; BROWN, E. N.; VISWANATHAN, S. **Autonomic healing of polymer composites.** Nature, v. 409, n. 6822, p. 794-797, 2001.

WITTMANN, F. H. **Crack formation and fracture energy of normal and high strength concrete**. Sadhana, v. 27, n. 4, p. 413-423, 2002.

WYRZYKOWSKI, M., et al. **Corrugated tube protocol for autogenous shrinkage measurements: review and statistical assessment**. Materials and Structures, v.50.1: p.57, 2017.

WYRZYKOWSKI, M., et al. **Modeling of internal curing in maturing mortar**. Cement and Concrete Research, v.41.12: p.1349-1356, 2011.

WYRZYKOWSKI, M., LURA, P. **Controlling the coefficient of thermal expansion of cementitious materials–A new application for superabsorbent polymers**. Cement and Concrete Composites, v.35.1: p.49-58, 2013.

XIE, Z. L.; Zhou, H. F.; Lu, L. J.; Chen, Z. A. **An investigation into fracture behavior of geopolymer concrete with digital image correlation technique.** Construction and Building Materials, v. 155, p. 371-380, 2017.

YANG, E. **Designing Added Functions in Engineered Cementitious Composites**. University of Michigan, Ann Arbor, pp.293, 2008.

YANG, En-Hua. **Designing Added Functions in Engineered Cementitious Composites**. Doctoral thesis, University of Michigan, Ann Arbor, pp.293, 2008.

YANG, Y., SATO, R., KAWAI, K. **Autogenous shrinkage of high-strength concrete containing silica fume under drying at early ages**. Cement and Concrete Research, v.35.3: p.449-456, 2005.

YANG, Y.; LEPECH, M. D.; YANG, E. H.; LI, V. C. **Autogenous healing of engineered cementitious composites under wet–dry cycles.** Cement and Concrete Research, v. 39, n. 5, p. 382-390, 2009.

YU, J. H.; CHEN, W.; YU, M. X.; HUA, Y. E. **The microstructure of self-healed PVA ECC under wet and dry cycles**. Materials Research, v. 13, n. 2, p. 225-231, 2010.

YUNOVICH, M., THOMPSON, N. G. **Corrosion of highway bridges: Economic impact and control methodologies**. Concrete International, v. 25, n. 1, p. 52-57, 2003.

Z. BAŽANT, A. DONMEZ, E. MASOERO, S.A. **Interaction of concrete creep, shrinkage and swelling with water, hydration, and damage**: Nano-macro-chemo, Ascelibrary.Org., 2015

ZHOU, F. P.; BARR, B. I. G.; LYDON, F. D. **Fracture properties of high strength concrete with varying silica fume content and aggregates**. Cement and concrete research, v. 25, n. 3, p. 543-552, 1995.

ZHU, Y.; YANG, Y.; YAO, Y. **Autogenous self-healing of engineered cementitious composites under freeze–thaw cycles.** Construction and Building Materials, v. 34, p. 522-530, 2012.

ZIA, P. **High performance concretes: a state-of-the-art report**. Vol. 91. Strategic Highway Research Program, National Research Council, 1991.

APPENDIX A

A.1 FULL DATA OF THE UNIAXIAL TENSILE TEST

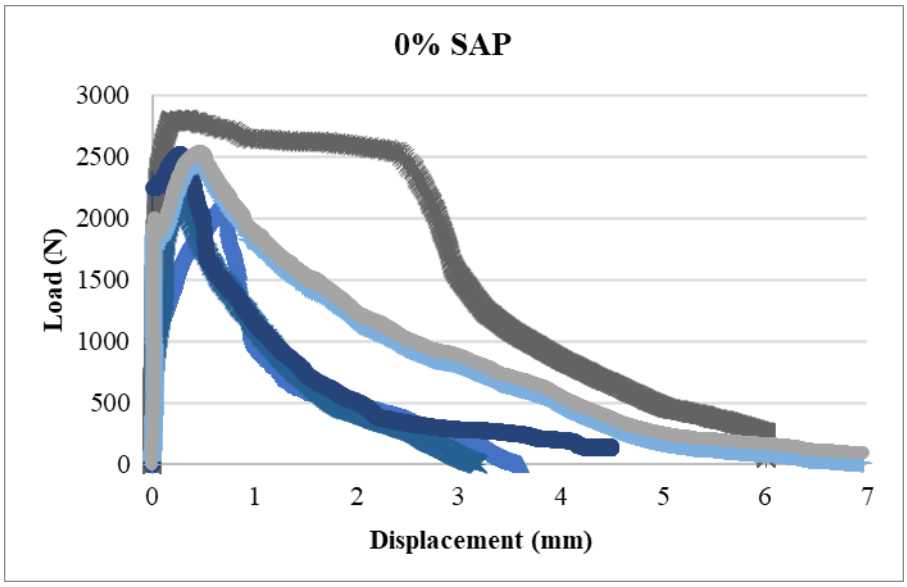

Figure 46 - Load vs. Displacement Curve for the 0.0% SAP content.

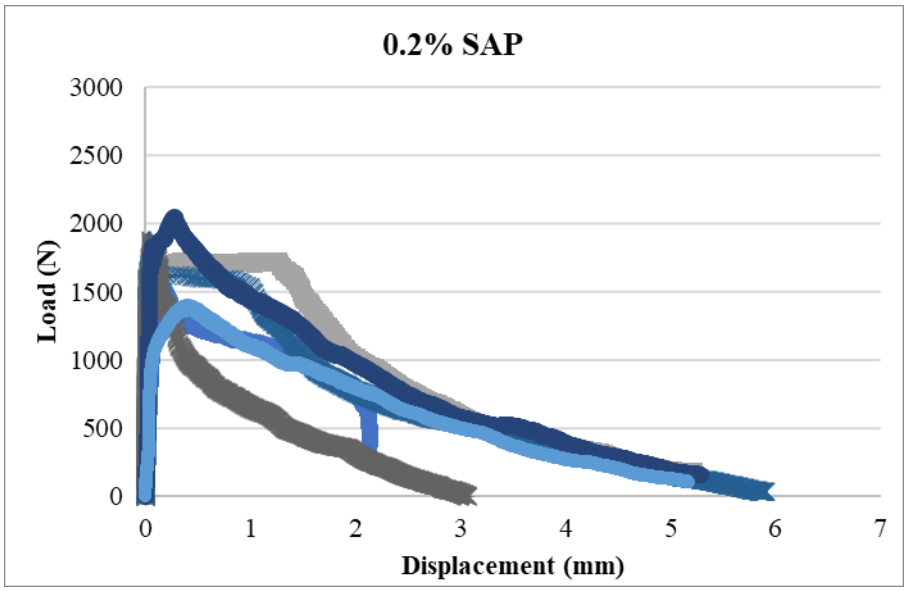

Figure 47 - Load vs. Displacement Curve for the 0.2% SAP content.

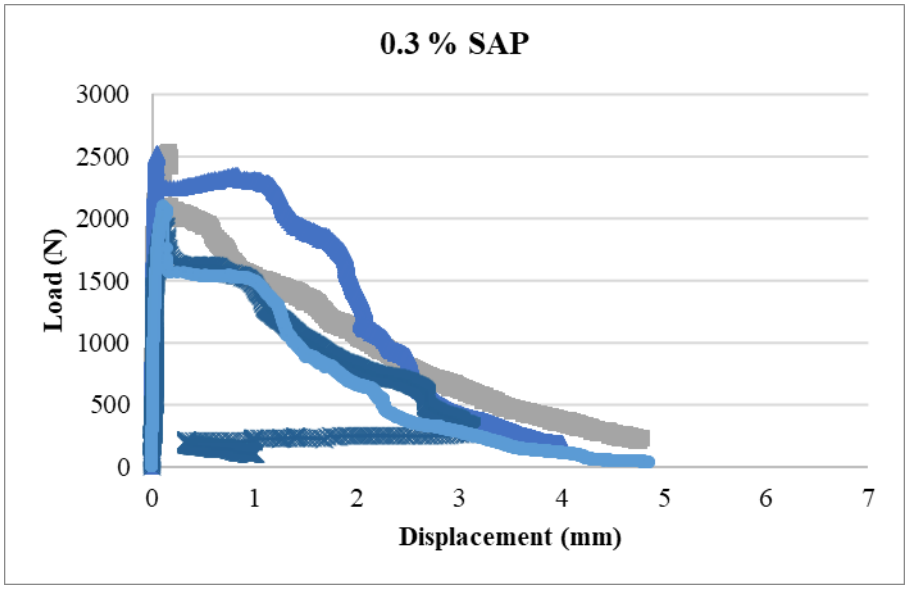

Figure 48 - Load vs. Displacement Curve for the 0.3% SAP content.

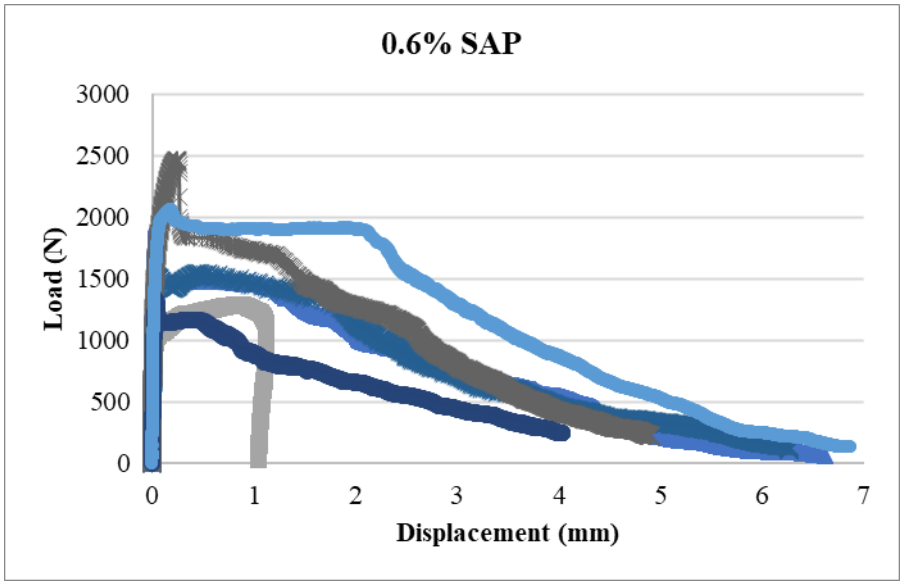

Figure 49 - Load vs. Displacement Curve for the 0.6% SAP content.

APPENDIX B – Modelling Data.

B.1 CODE inserted in the Workbench for concrete

```
ET,MATID,SOLID65
R,MATID,0,0,0,0,0,0
RMORE,0,0,0,0,0

MP,EX,MATID,35000
MP,PRXY,MATID,0.2
MPTEMP,MATID,0

TB,CONCR,MATID,1,9
TBTEMP,22
TBDATA,1,0.3,0.8,1.5,25

TB,MISO,MATID,1,35,0
TBTEMP,22
TBPT,,0.0001,2.925
TBPT,,0.0002,17.1
TBPT,,0.0003,24.975
TBPT,,0.0004,32.4
TBPT,,0.0005,39.375
TBPT,,0.0006,45.9
TBPT,,0.0007,51.975
TBPT,,0.0008,57.6
TBPT,,0.0009,62.775
TBPT,,0.0010,67.5
TBPT,,0.0011,71.775
TBPT,,0.0012,75.6
TBPT,,0.0013,78.975
TBPT,,0.0014,81.9
TBPT,,0.0015,84.375
TBPT,,0.0016,86.4
TBPT,,0.0017,87.975
TBPT,,0.0018,89.1
TBPT,,0.0019,89.775
TBPT,,0.0020,90
TBPT,,0.0021,90
TBPT,,0.0022,90
TBPT,,0.0023,90
TBPT,,0.0024,90
TBPT,,0.0025,90
TBPT,,0.0026,90
TBPT,,0.0027,90
```

```
TBPT,,0.0028,90
TBPT,,0.0029,90
TBPT,,0.0030,90
TBPT,,0.0031,90
TBPT,,0.0032,90
TBPT,,0.0033,90
TBPT,,0.0034,90
TBPT,,0.0035,90
```

B.2 Concrete Data provided by ANSYS (2014)

Table 17 – SOLID65 Concrete Material Data. Source: ANSYS (2014)

Constant	Meaning
1	Shear transfer coefficients for an open crack.
2	Shear transfer coefficients for a closed crack.
3	Uniaxial tensile cracking stress.
4	Uniaxial crushing stress (positive)
5	Biaxial crushing stress (positive).
6	Ambient hydrostatic stress state for use with constants 7 and 8.
7	Biaxial crushing stress (positive) under the ambient hydrostatic stress state (constant 6)
8	Uniaxial crushing stress (positive) under the ambient hydrostatic stress state (constant 6)
9	Stiffness multiplier for cracked tensile condition, used if KEYOPT(7)=1 (defaults to 0.6)

B.3 Stress versus strain curve for concrete with 90 MPa of compressive strength

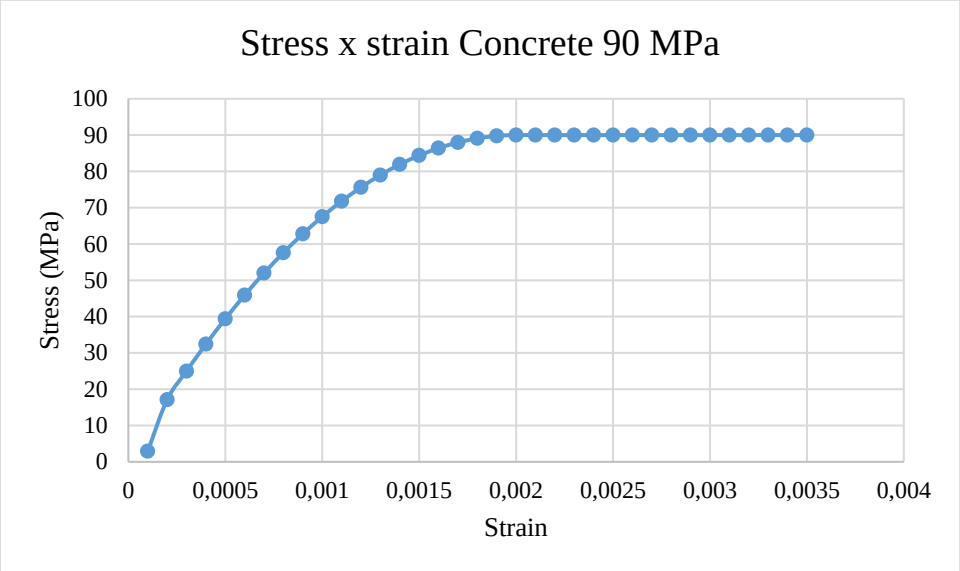

Figure 50 - Stress versus strain curve of a typical Concrete with 90 MPa. Source: ANSYS (2014).

B.4 CODE inserted in the Workbench for rebar

```
ET,MATID,LINK180
MPDATA,EX,MATID,,2e5
MPDATA,PRXY,MATID,,0.3
TB,BISO,MATID,1,2
TBDATA,,460,2100
R,MATID,6,,0
```

B.5 CODE inserted to join concrete with rebar

```
/PREP7
ESEL,S,ENAME,,65
ESEL,A,ENAME,,180
ALLSEL,BELOW,ELEM
CEINTF,0.001,
ALLSEL,ALL
/SOLU
OUTRES,ALL,ALL
```

B.6 CODE solution for crack and crush plots

```
/SHOW,png
/ANG,1,
/VIEW,1,0,0,0
SET,1,1
/DEVICE,VECTOR,ON
!PLNSOL,s,eqv
!SET,Lstep,1
SET,Last
PLCRACK
```

APPENDIX C – Crack photos of mechanical recovery tests

MR1-0.0-7d 176 - Back - Mean: 219.4; Std.Dev: 11.3; Min: 136.3; Max: 260.7.
a)

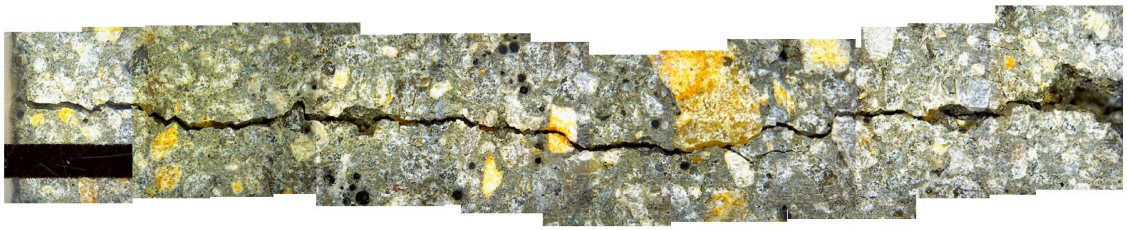

MR1-0.0-7d 176 – Front - Mean: 209.9; Std.Dev: 142.4; Min: 85.2; Max: 610.3.
b)
Figure 51 – M1 176 – After pre-cracking, before wetting drying cylcles.

MR1-0.0-7d 176 – Back - Mean: 184.7; Std.Dev: 42.7; Min: 80.1; Max: 324.0.
a)

MR1-0.0-7d 176 – Front - Mean: 166.8; Std.Dev: 147.9; Min: 66.8; Max: 795.2.
b)

Figure 52 – M1 176 – After wetting drying cylcles.

MR1-0.0-7d 177 - Back - Mean: 289.2; Std.Dev: 51.3; Min: 222.8; Max: 501.2.

a)

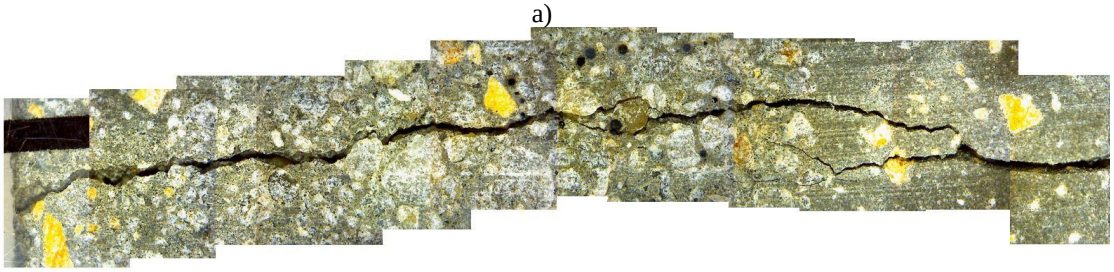

MR1-0.0-7d 177 – Front - Mean: 203.7; Std.Dev: 65.1; Min: 97.9; Max: 431.7.

b)

Figure 53 – M1 177 – After pre-cracking, before wetting and drying cylcles.

MR1-0.0-7d 177 – Back - Mean: 220.5; Std.Dev: 59.5; Min: 84.7; Max: 394.7.

a)

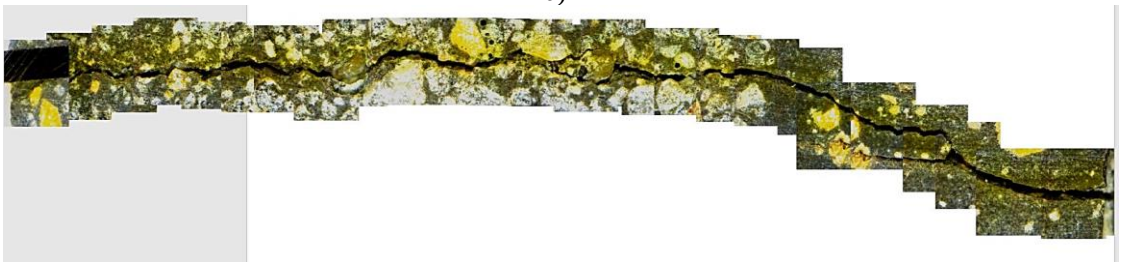

MR1-0.0-7d 177 – Front - Mean: 151.0; Std.Dev: 58.7; Min: 67.8; Max: 300.8.

b)

Figure 54 – M1 177 – After wetting and drying cylcles.

MR1-0.0-7d 178 - Back - Mean: 258.8; Std.Dev: 61.8; Min: 123.5; Max: 466.8.

a)

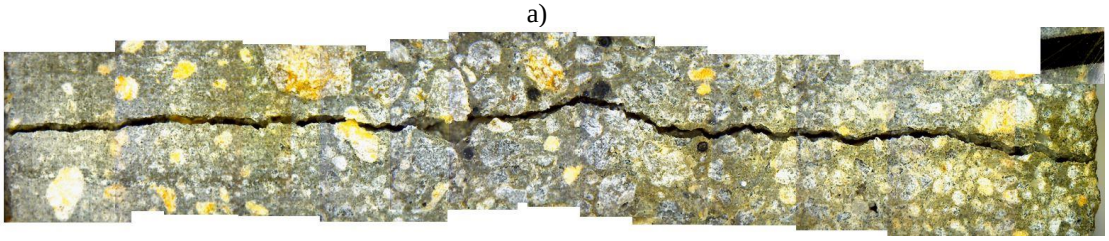

MR1-0.0-7d 178 – Front - Mean: 219.4; Std.Dev: 55.9; Min: 157.5; Max: 435.6.

b)

Figure 55 – M1 178 – After pre-cracking, before wetting and drying cylcles.

MR1-0.0-7d 178 – Back - Mean: 218.0; Std.Dev: 58.0; Min: 106.9; Max: 432.0.

a)

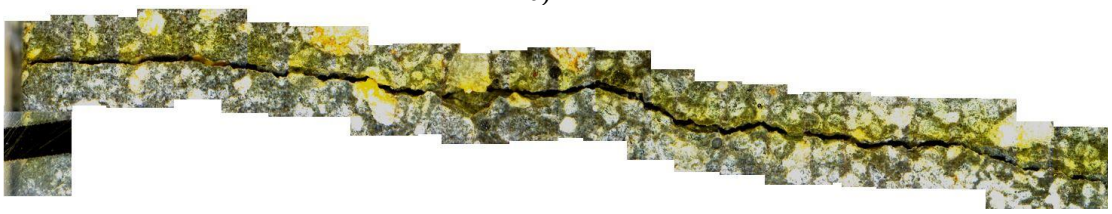

MR1-0.0-7d 178 – Front - Mean: 132.6; Std.Dev: 29.2; Min: 86.7; Max: 188.0.

b)

Figure 56 – M1 178 – After wetting and drying cylcles.

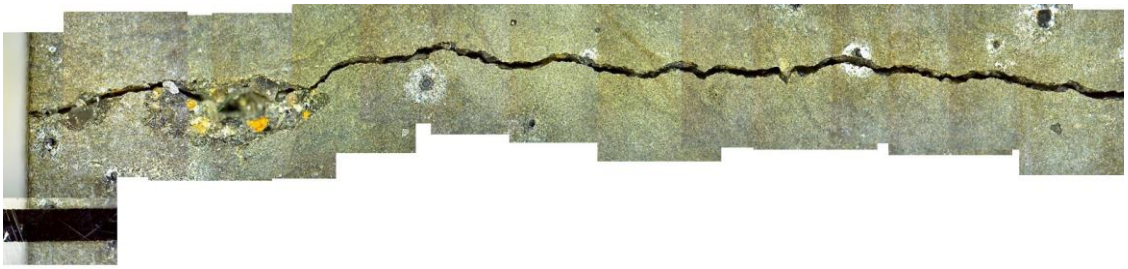

MR1-0.0-7d 179 - Back - Mean: 170.7; Std.Dev: 38.2; Min: 80.6; Max: 255.6.

a)

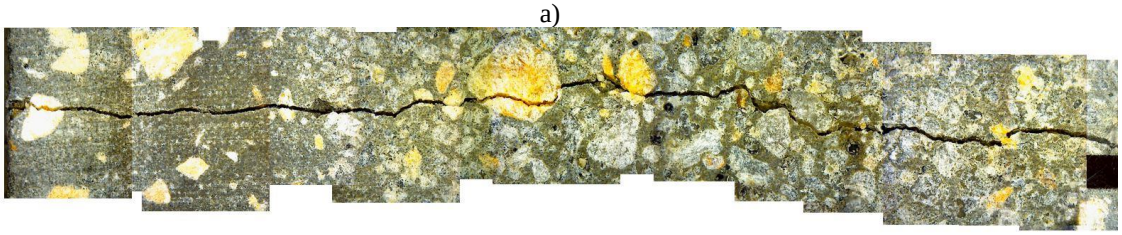

MR1-0.0-7d 179 – Front - Mean: 99.0; Std.Dev: 39.9; Min: 27.6; Max: 260.5.

b)

Figure 57 – M1 179 – After pre-cracking, before wetting and drying cylcles.

MR1-0.0-7d 179 – Back - Mean: 116.4; Std.Dev: 32.5; Min: 32.6; Max: 174.6.

a)

MR1-0.0-7d 179 – Front - Mean: 77.8; Std.Dev: 23.5; Min: 24.2; Max: 125.2.

b)

Figure 58 – M1 179 – After wetting and drying cylcles.

M2 180 - Back - Mean: 199.8; Std.Dev: 27.0; Min: 130.6; Max: 237.5.

a)

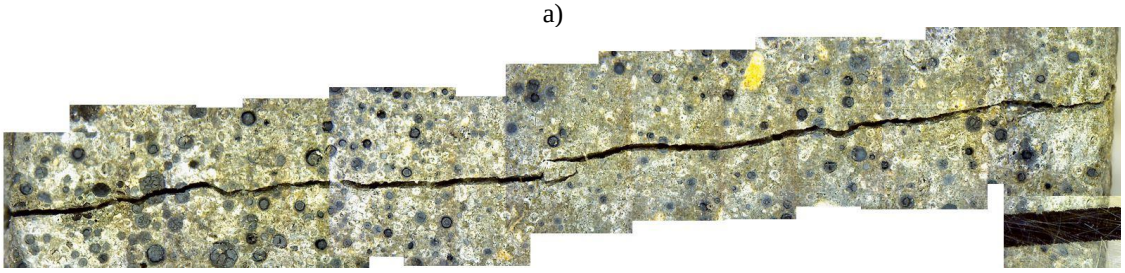

M2 180 – Front - Mean: 163.4; Std.Dev: 27.7; Min: 108.1; Max: 234.6.

b)

Figure 59 – M2 180 – After pre-cracking, before wetting and drying cylcles.

M2 180 – Back - Mean: 188.0; Std.Dev: 35.0; Min: 130.9; Max: 252.7.

a)

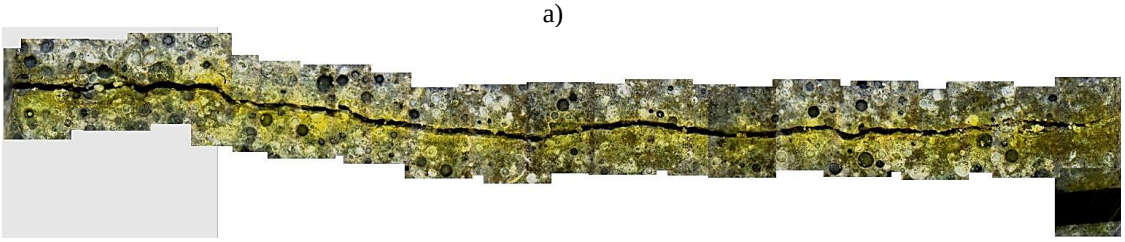

M2 180 – Front - Mean: 161.6; Std.Dev: 50.6; Min: 37.9; Max: 232.6.

b)

Figure 60 – M2 180 – After wetting and drying cylcles.

M2 183 - Back - Mean: 172.0; Std.Dev: 50.3; Min: 70; Max: 487.7.

a)

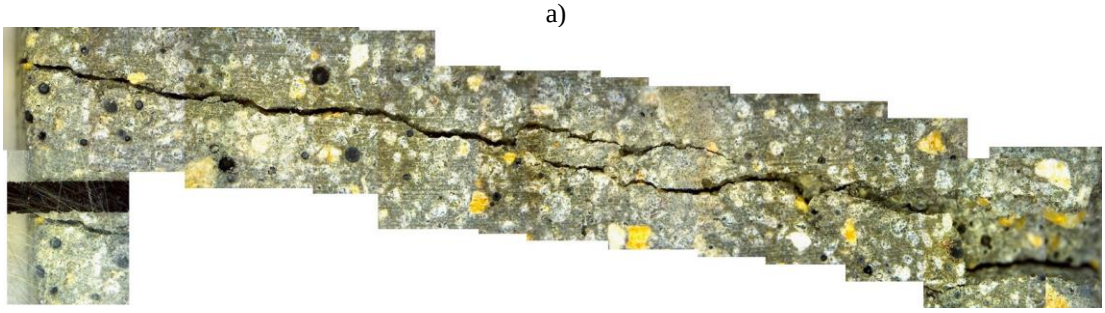

M2 183 – Front - Mean: 164.8; Std.Dev: 102.8; Min: 86.7; Max: 487.7.

b)

Figure 61 – M2 183 – After pre-cracking, before wetting and drying cylcles.

M2 183 – Back - Mean: 127.9; Std.Dev: 43.5; Min: 50.9; Max: 224.7.

a)

M2 183 – Front - Mean: 107.7; Std.Dev: 27.7; Min: 62.3; Max: 156.7.

b)

Figure 62 – M2 183 – After wetting and drying cylcles.

M2 184 - Back - Mean: 203,9; Std.Dev: 31,7; Min: 144,4; Max: 256,0.
a)

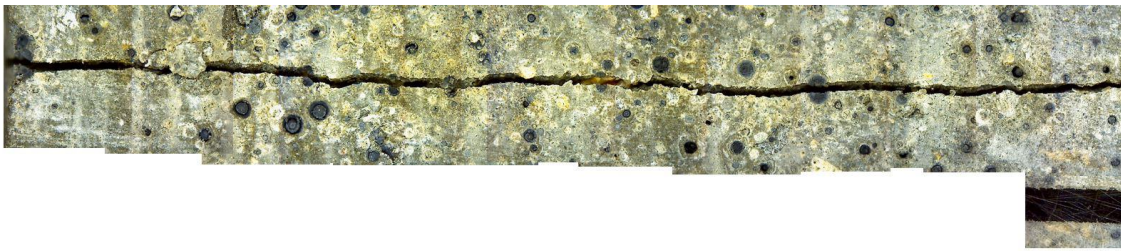

M2 184 – Front - Mean: 206,5; Std.Dev: 37,5; Min: 101,6; Max: 254,9.
b)
Figure 63 – M2 184 – After pre-cracking, before wetting and drying cylcles.

M2 184 – Back - Mean: 182,9; Std.Dev: 57,4; Min: 73,8; Max: 304,4.
a)

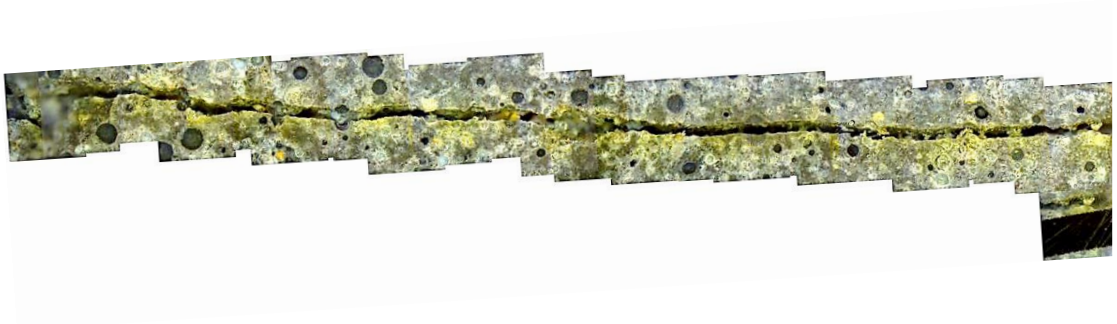

M2 184 – Front - Mean: 177,4; Std.Dev: 46,9; Min: 95,0; Max: 256,8.
b)
Figure 64 – M2 184 – After wetting and drying cylcles.

M2 185 - Back - Mean: 182,4; Std.Dev: 48,8; Min: 116,4; Max: 363,6.

a)

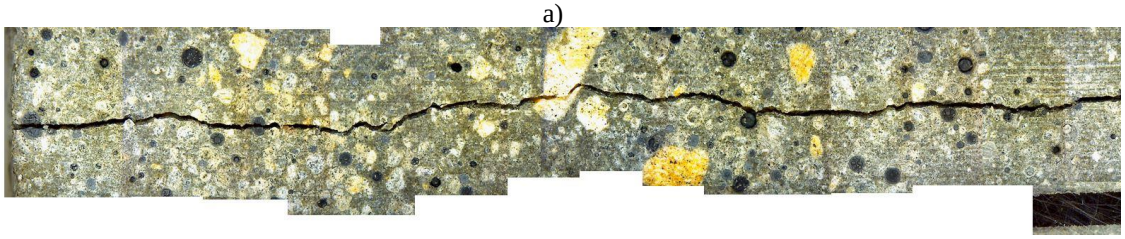

M2 185 – Front - Mean: 127,4; Std.Dev: 13,9; Min: 98,7; Max: 151,6.

b)

Figure 65 – M2 185 – After pre-cracking, before wetting and drying cylcles.

M2 185 – Back - Mean: ; Std.Dev: ; Min: ; Max: . 138,8 25,4 78,0 167,9

a)

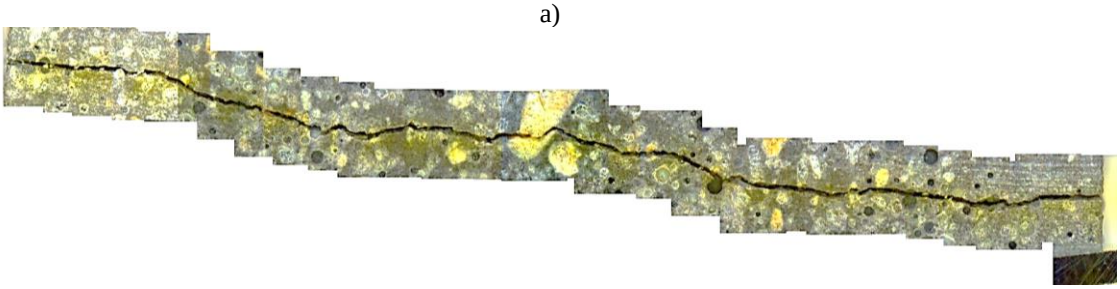

M2 185 – Front - Mean: 116,8; Std.Dev: 27,4; Min: 59,0; Max: 147,7.

b)

Figure 66 – M2 185 – After wetting and drying cylcles.

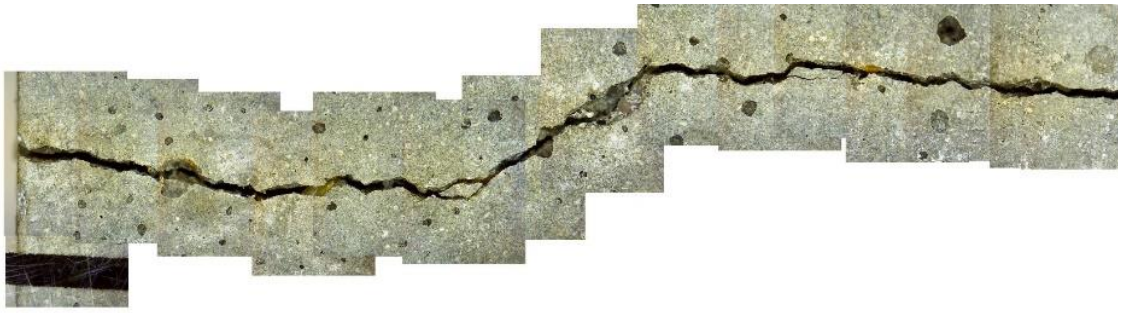

M3 169 - Back - Mean: 224,0; Std.Dev: 40,5; Min: 174,5; Max: 359,7.
a)

M3 169 – Front - Mean: 188,6; Std.Dev: 44,7; Min: 116,0; Max: 278,1.
b)
Figure 67 – M3 169 – After pre-cracking, before wetting and drying cylcles.

M3 169 – Back - Mean: 156,9; Std.Dev: 66,7; Min: 41,5; Max: 287,7.
a)

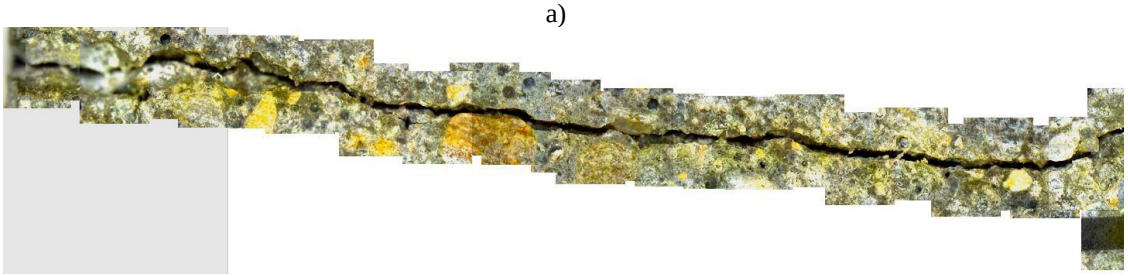

M3 169 – Front - Mean: 161,1; Std.Dev: 50,0; Min: 67,4; Max: 244,9.
b)
Figure 68 – M3 169 – After wetting and drying cylcles.

M3 172 - Back - Mean: 288.7; Std.Dev: 57.2; Min: 136.2; Max: 357.1.

a)

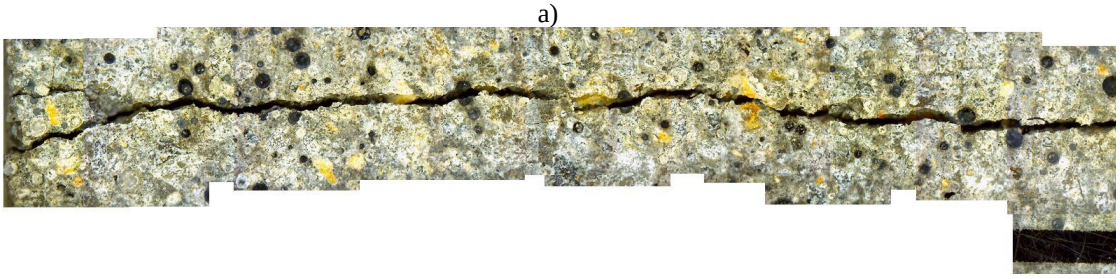

M3 172 – Front - Mean: 200.0; Std.Dev: 54.7; Min: 55.6; Max: 286.3.

b)

Figure 69 – M3 172 – After pre-cracking, before wetting and drying cylcles.

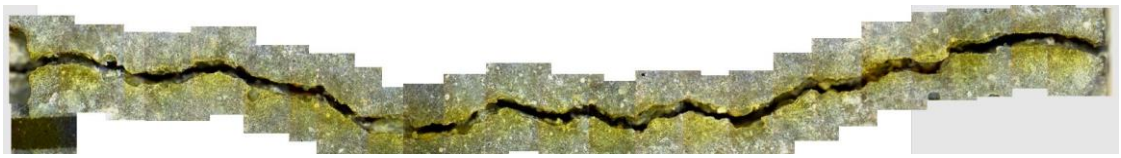

M3 172 – Back - Mean: 244.0; Std.Dev: 73.9; Min: 118.2; Max: 355.3.

a)

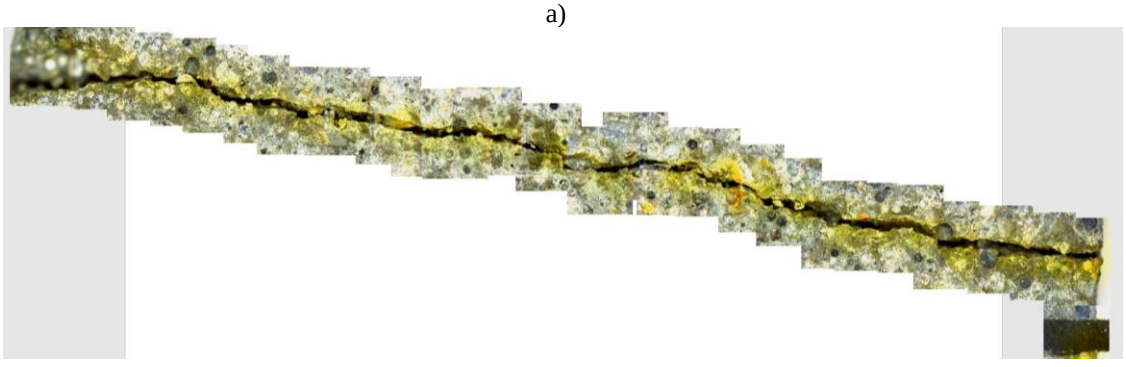

M3 172 – Front - Mean: 180.7; Std.Dev: 63.5; Min: 52.5; Max: 299.1.

b)

Figure 70 – M3 172 – After wetting and drying cylcles.

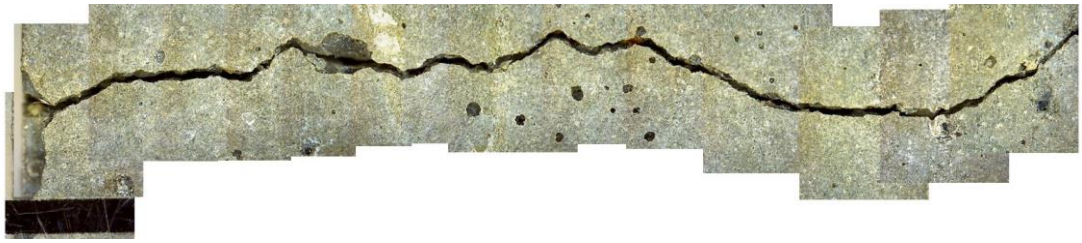

M3 173 - Back - Mean: 180.0; Std.Dev: 45.5; Min: 53.6; Max: 245.7.

a)

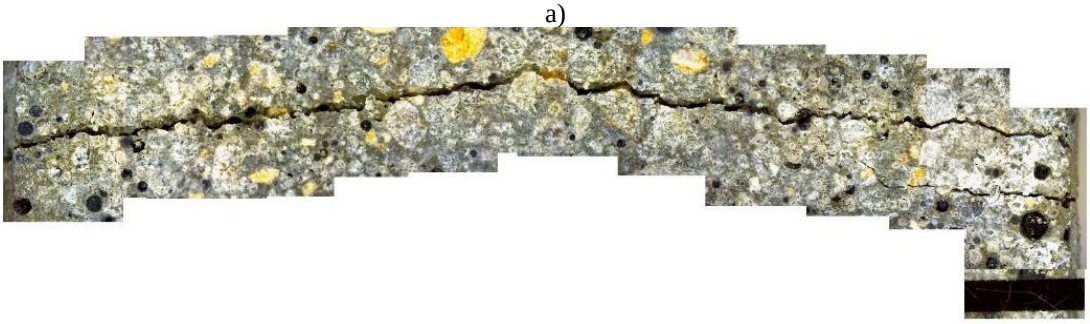

M3 173 – Front - Mean: 136.3; Std.Dev: 65.0; Min: 33.9; Max: 279.3.

b)

Figure 71 – M3 173 – After pre-cracking, before wetting and drying cylcles.

M3 173 – Back - Mean: 98.9; Std.Dev: 47.9; Min: 16.4; Max: 196.9.

a)

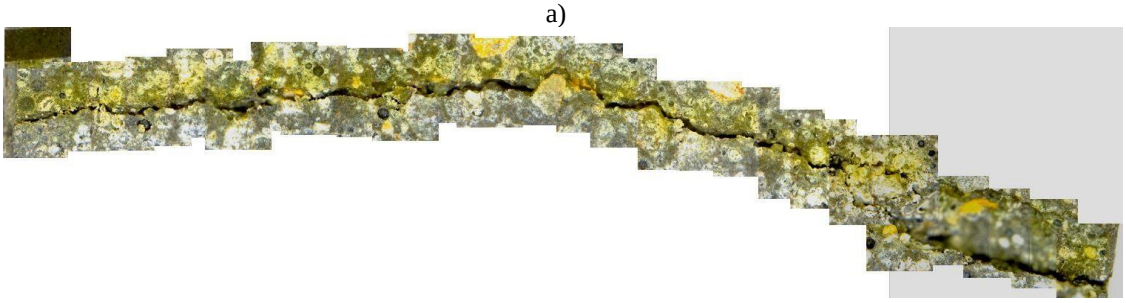

M3 173 – Front - Mean: 85.0; Std.Dev: 34.2; Min: 38.1; Max: 172.7.

b)

Figure 72 – M3 173 – After wetting and drying cylcles.

M4 96 - Back - Mean: 254.3; Std.Dev: 49.6; Min: 130.1; Max: 347.7.

a)

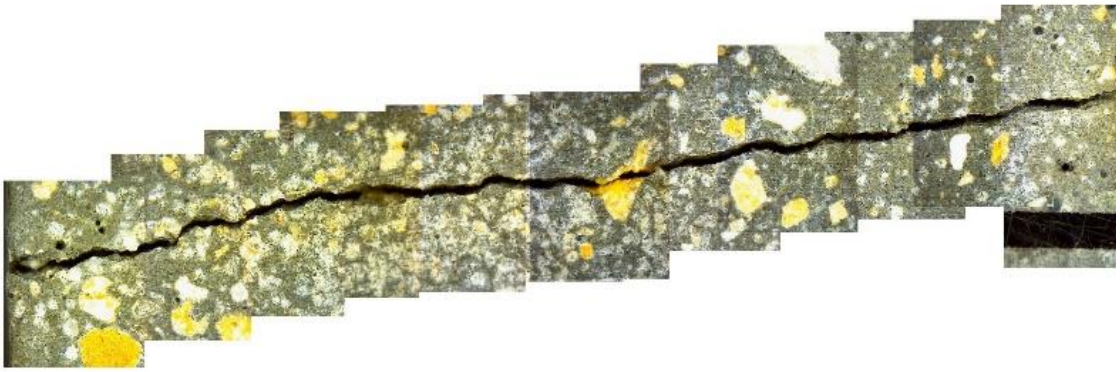

M4 96 – Front - Mean: 198.2; Std.Dev: 40.4; Min: 109.6; Max: 249.8.

b)

Figure 73 – M4 96 – After pre-cracking, before wetting and drying cylcles.

M4 96 – Back - Mean: 229.1; Std.Dev: 59.1; Min: 115.0; Max: 358.3.

a)

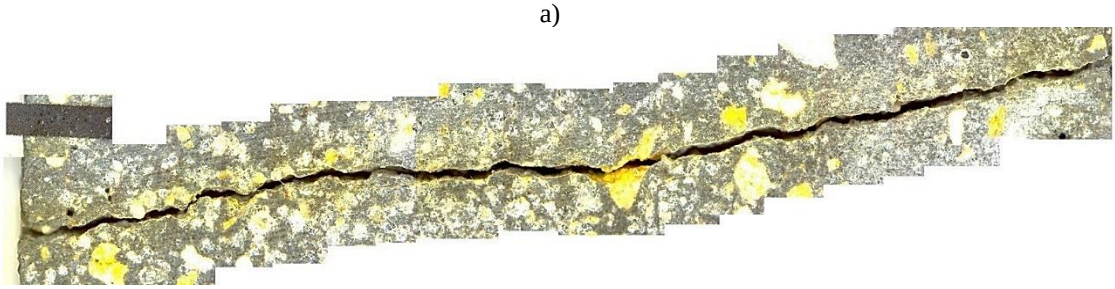

M4 96 – Front - Mean: 171.5; Std.Dev: 43.1; Min: 80.3; Max: 254.1.

b)

Figure 74 – M4 96 – After wetting and drying cylcles.

M4 98 - Back - Mean: 251.1; Std.Dev: 37.3; Min: 170.1; Max: 323.1.
a)

M4 98 – Front - Mean: 173.7; Std.Dev: 30.6; Min: 121.8; Max: 213,9.
b)
Figure 75 – M4 98 – After pre-cracking, before wetting and drying cylcles.

M4 98 – Back - Mean: 173.6; Std.Dev: 56.3; Min: 60.7; Max: 267.0.
a)

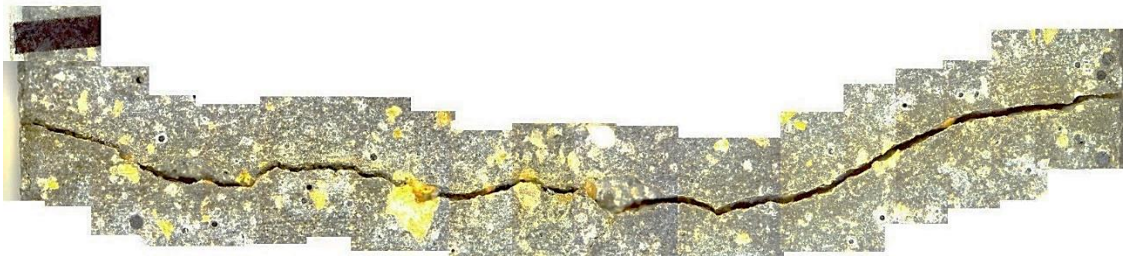

M4 98 – Front - Mean: 151.2; Std.Dev: 33.9; Min: 68.0; Max: 202.9.
b)
Figure 76 – M4 98 – After wetting and drying cylcles.

M4 100 - Back - Mean: 280.2; Std.Dev: 54.8; Min: 167.1; Max: 356.1.

a)

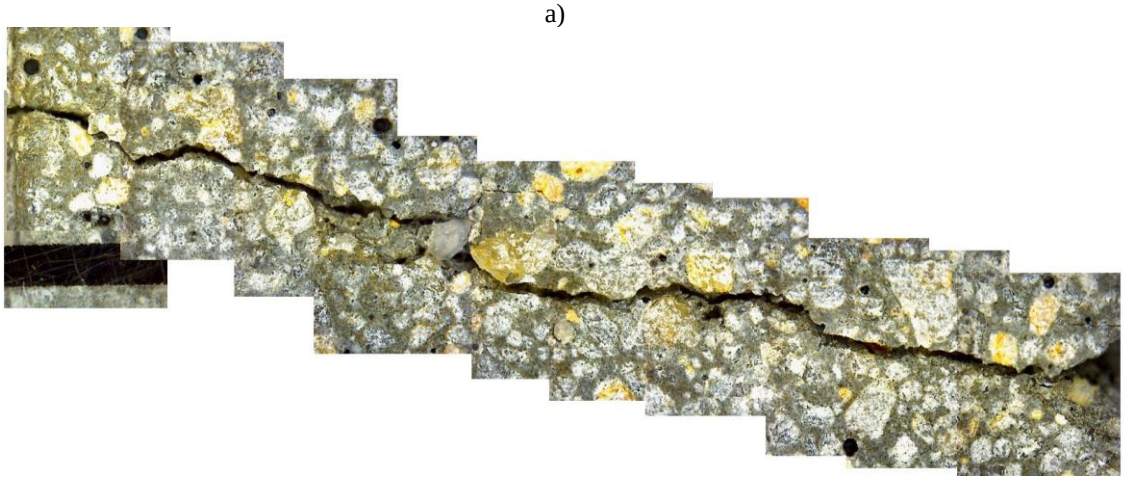

M4 100 – Front - Mean: 230.3; Std.Dev: 80.8; Min: 137.3; Max: 468.2.

b)

Figure 77 – M4 100 – After pre-cracking, before wetting and drying cylcles.

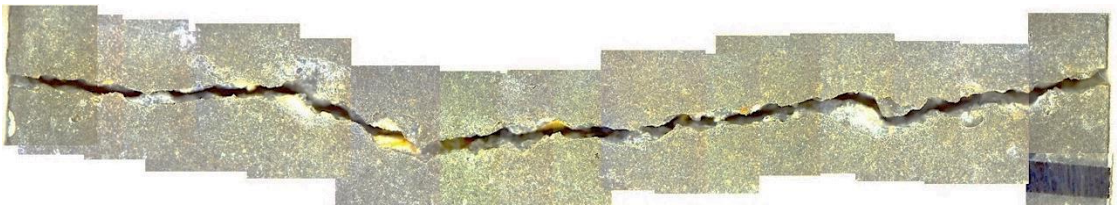

M4 100 – Back - Mean: 228.6; Std.Dev: 50.1; Min: 95.2; Max: 308.5.

a)

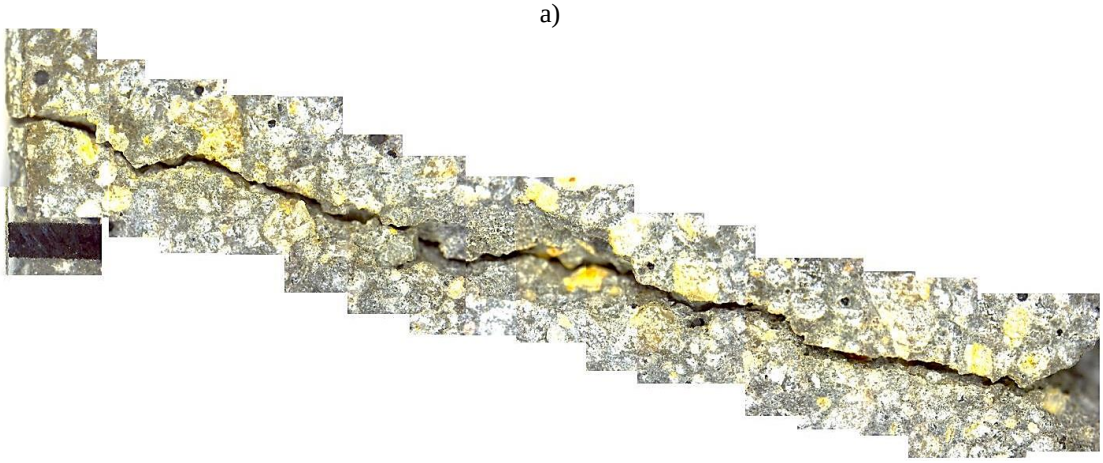

M4 100 – Front - Mean: 156.2; Std.Dev: 57.7; Min: 72.2; Max: 252.6.

b)

Figure 78 – M4 100 – After wetting and drying cylcles.

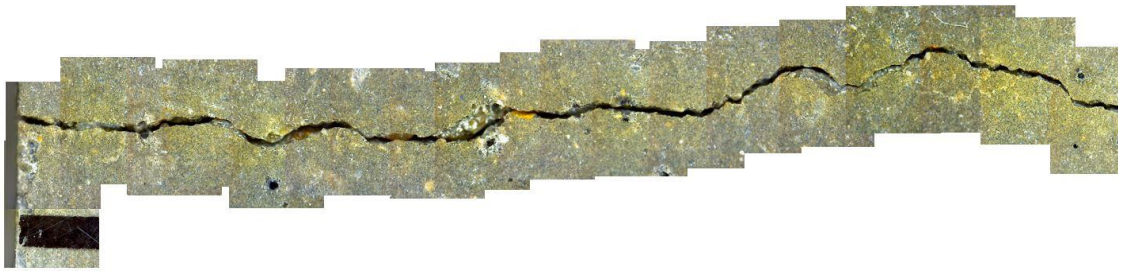

M5 126 - Back - Mean: 165.3; Std.Dev: 64.3; Min: 112.0; Max: 437.4.

a)

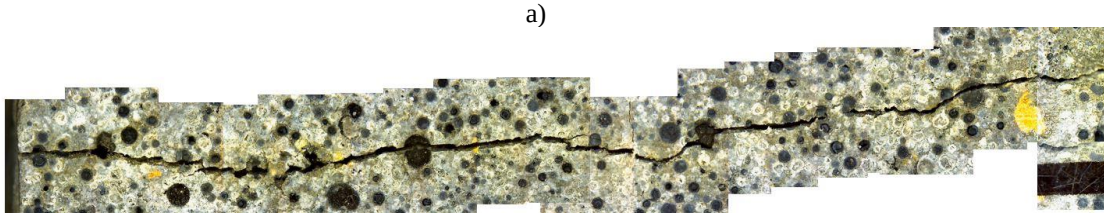

M5 126 – Front - Mean: 126.9; Std.Dev: 26.9; Min: 84.5; Max: 186.2.

b)

Figure 79 – M5 126 – After pre-cracking, before wetting and drying cylcles.

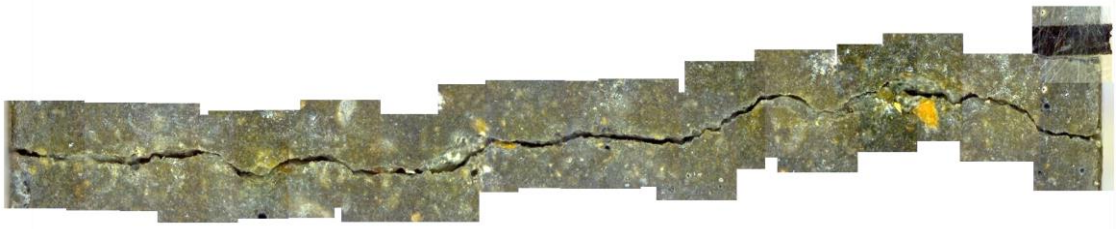

M5 126 – Back - Mean: 107.6; Std.Dev: 38.0; Min: 36.6; Max: 200.2.

a)

M5 126 – Front - Mean: 111.0; Std.Dev: 32.0; Min: 56.1; Max: 168.1.

b)

Figure 80 – M5 126 – After wetting and drying cylcles.

M5 127 - Back - Mean: 251.1; Std.Dev: 59.7; Min: 105.6; Max: 382.9.
a)

M5 127 – Front - Mean: 281.7; Std.Dev: 29.1; Min: 236.4; Max: 329.2.
b)
Figure 81 – M5 127 – After pre-cracking, before wetting and drying cylcles.

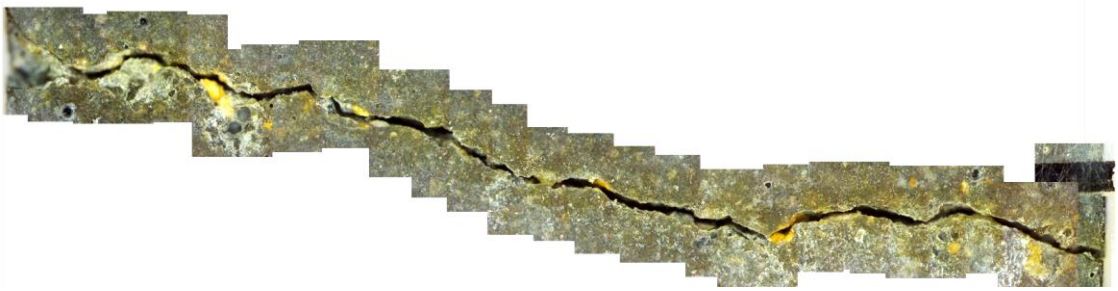

M5 127 – Back - Mean: 175.2; Std.Dev: 68.6; Min: 84.5; Max: 313.1.
a)

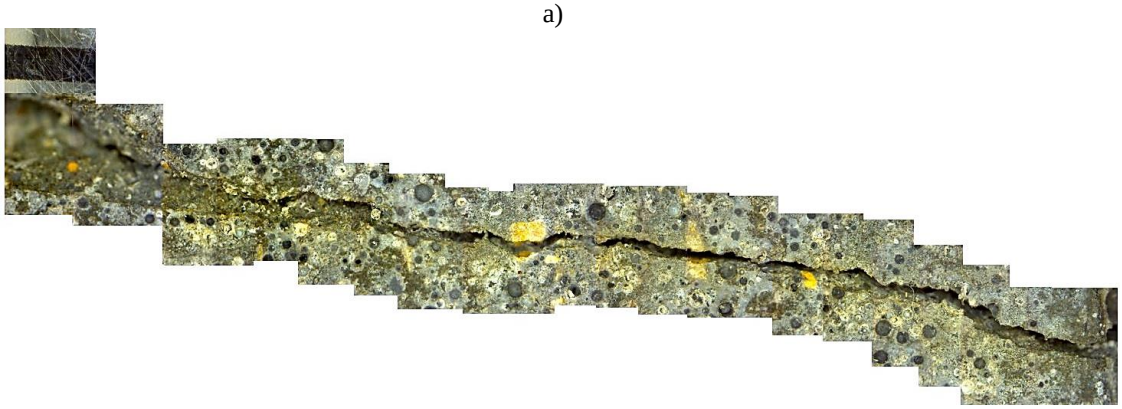

M5 127 – Front - Mean: 215.8; Std.Dev: 91.0; Min: 92.0; Max: 467.7.
b)
Figure 82 – M5 127 – After wetting and drying cylcles.

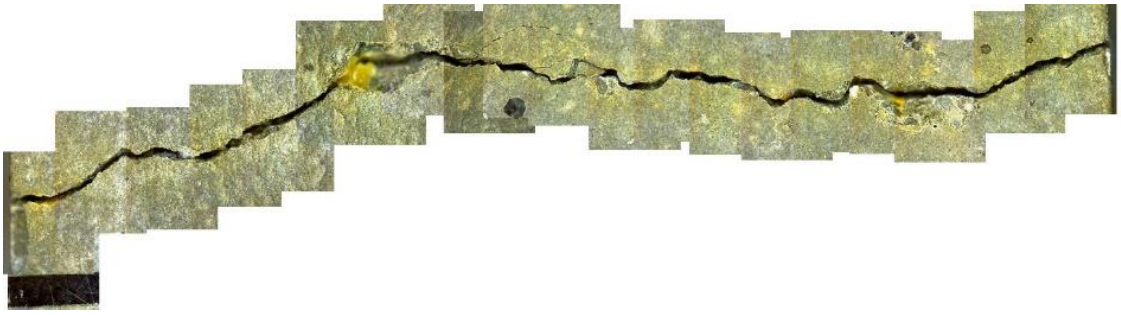

M5 128 - Back - Mean: 181.9; Std.Dev: 39.5; Min: 97.0; Max: 266.8.
a)

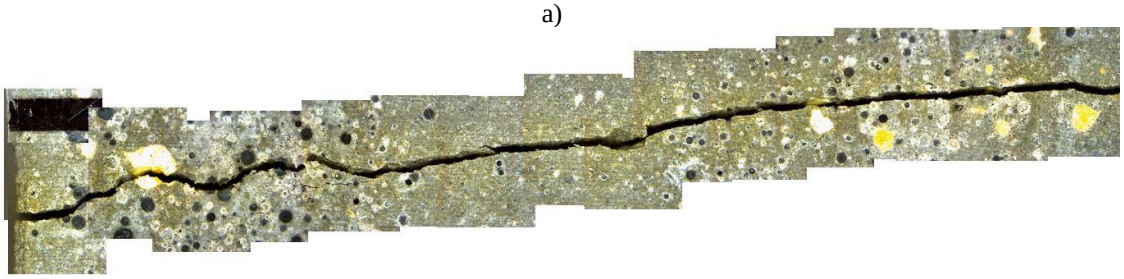

M5 128 – Front - Mean: 187.5; Std.Dev: 33.6; Min: 110.9; Max: 240.5.
b)
Figure 83 – M5 128 – After pre-cracking, before wetting and drying cylcles.

M5 128 – Back - Mean: 162.3; Std.Dev: 50.5; Min: 74.0; Max: 265.9.
a)

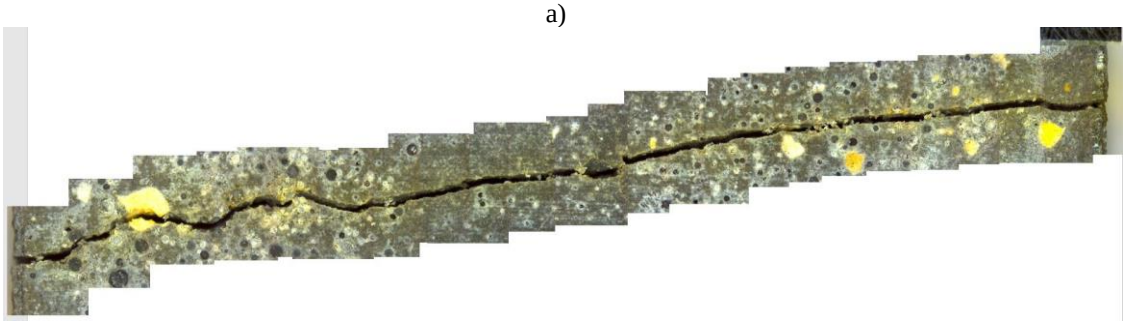

M5 128 – Front - Mean: 148.3; Std.Dev: 56.3; Min: 38.7; Max: 222.2.
b)
Figure 84 – M5 128 – After wetting and drying cylcles.

M6 114 - Back - Mean: ; Std.Dev: ; Min: ; Max: . 203,9 30,9 157,4 269,9

a)

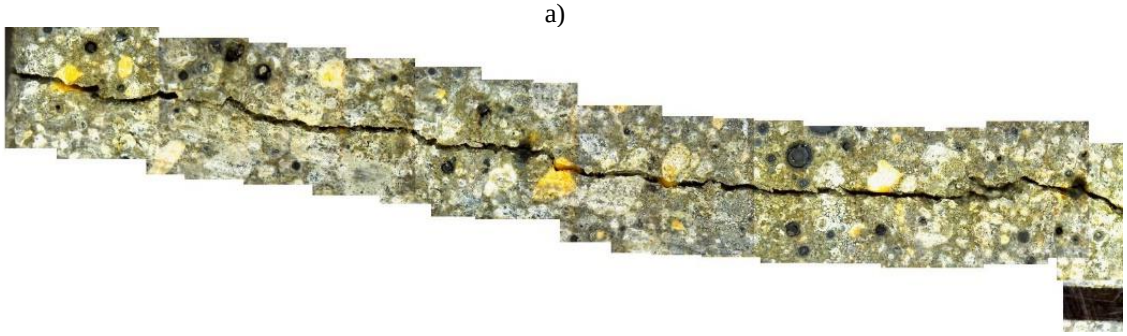

M6 114 – Front - Mean: ; Std.Dev: ; Min: ; Max: . 133,2 33,2 75,8 196,7

b)

Figure 85 – M6 114 – After pre-cracking, before wetting and drying cylcles.

M6 114 – Back - Mean: 146.5; Std.Dev: 44.4; Min: 89.5; Max: 234.6.

a)

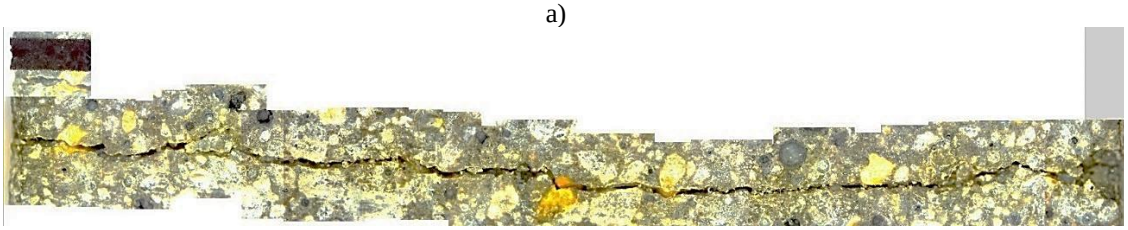

M6 114 – Front - Mean: 111.0; Std.Dev: 47.7; Min: 10.0; Max: 164.3.

b)

Figure 86 – M6 114 – After wetting and drying cylcles.

M6 115 - Back - Mean: 178.7; Std.Dev: 44.2; Min: 62.7; Max: 254.4.

a)

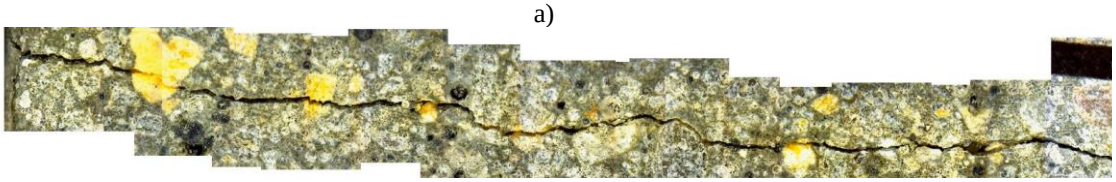

M6 115 – Front - Mean: 100.4; Std.Dev: 47.0; Min: 51.4; Max: 291.1.

b)

Figure 87 – M6 115 – After pre-cracking, before wetting and drying cylcles.

M6 115 – Back - Mean: 176.1; Std.Dev: 70.4; Min: 9.7; Max: 300.2.

a)

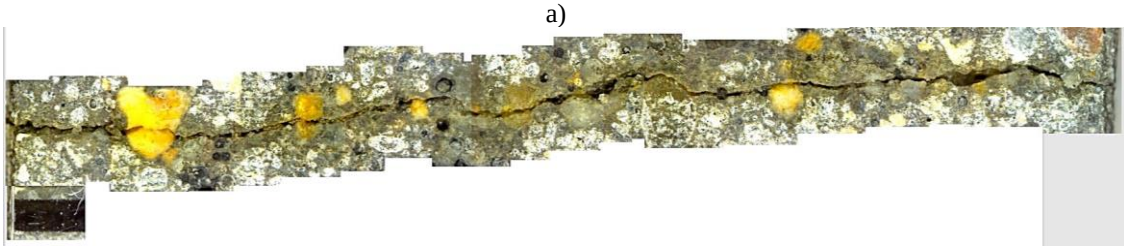

M6 115 – Front - Mean: 84.2; Std.Dev: 60.6; Min: 8.8; Max: 249.9.

b)

Figure 88 – M6 115 – After wetting and drying cylcles.

M6 119 - Back - Mean: 201.2; Std.Dev: 49.8; Min: 48.5; Max: 277.8.

a)

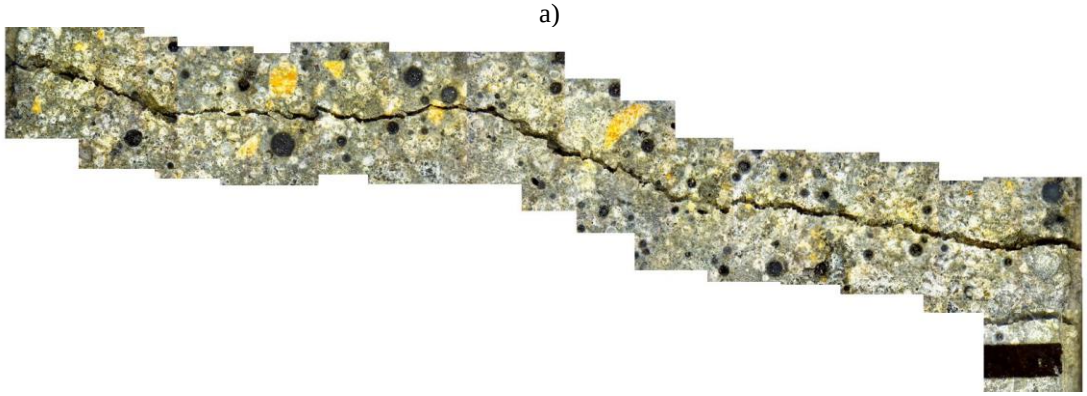

M6 119 – Front - Mean: 124.7; Std.Dev: 34.5; Min: 63.2; Max: 185.1.

b)

Figure 89 – M6 119 – After pre-cracking, before wetting and drying cylcles.

M6 119 – Back - Mean: 144.0; Std.Dev: 78.3; Min: 17.7; Max: 273.1.

a)

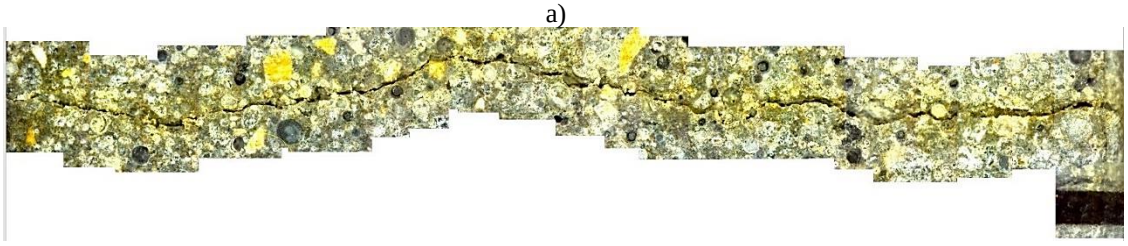

M6 119 – Front - Mean: 63.0; Std.Dev: 45.3; Min: 8.6; Max: 195.4.

b)

Figure 90 – M6 119 – After wetting and drying cylcles.

APPENDIX D – Crack photos of the permeability tests

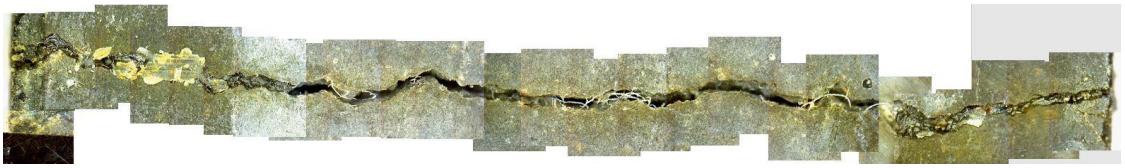

P8-0.0-7d 144 – Back - Mean: 270,4; Std.Dev: 75,0; Min: 13,4; Max: 398,5.

a)

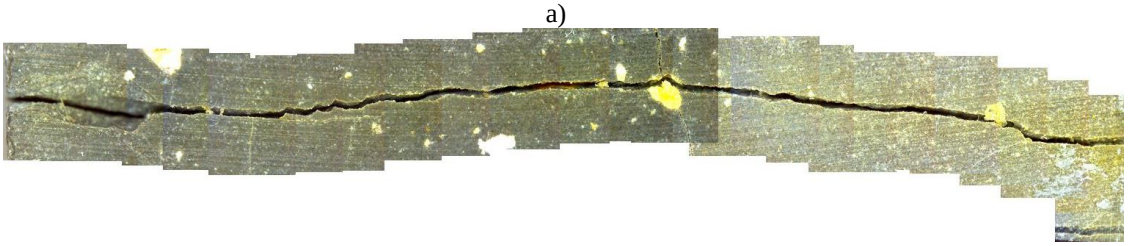

P8-0.0-7d 144 – Front - Mean: 165,2; Std.Dev: 26,7; Min: 79,3; Max: 214,8.

b)

Figure 91 – P8-0.0-7d 144 – After wetting and drying cylcles.

P8-0.0-7d 144 – Back - Mean: 269,8; Std.Dev: 49,2; Min: 118,2; Max: 378,9.

a)

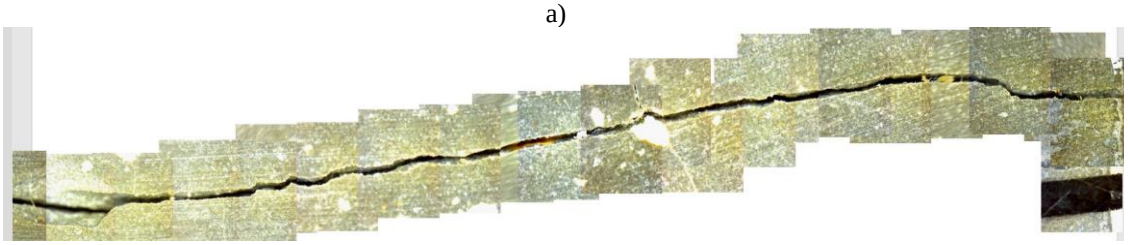

P8-0.0-7d 144 – Front - Mean: 156,2; Std.Dev: 32,8; Min: 70,2; Max: 204,1.

b)

Figure 92 - P8-0.0-7d 144 – After wetting and drying cylcles.

P8-0.0-7d 148 – Back - Mean: 228,8; Std.Dev: 85,1; Min: 149,8; Max: 646,3.
a)

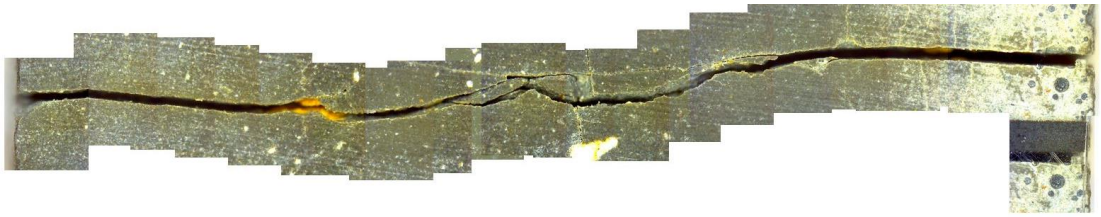

P8-0.0-7d 148 – Front - Mean: 252,7; Std.Dev: 51,1; Min: 164,6; Max: 363,2.
b)
Figure 93 - P8-0.0-7d 148 – After wetting and drying cylcles.

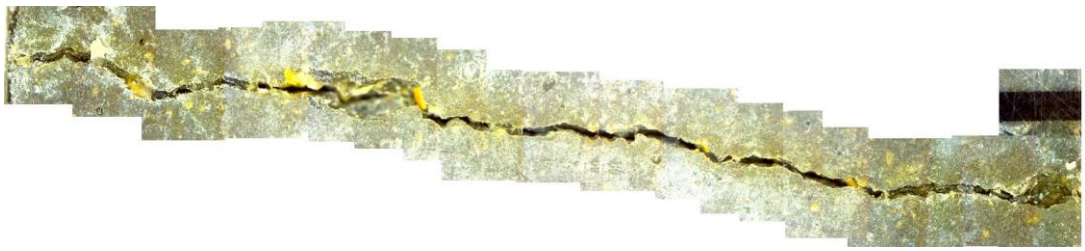

P8-0.0-7d 148 – Back - Mean: 190,7; Std.Dev: 35,1; Min: 137,7; Max: 249,0.
a)

P8-0.0-7d 148 – Front - Mean: 215,3; Std.Dev: 62,7; Min: 102,8; Max: 350,9.
b)
Figure 94 – P8-0.0-7d 148 – After wetting and drying cylcles.

P8-0.0-7d 149 – Back - Mean: 166,9; Std.Dev: 30,0; Min: 97,3; Max: 214,8.
a)

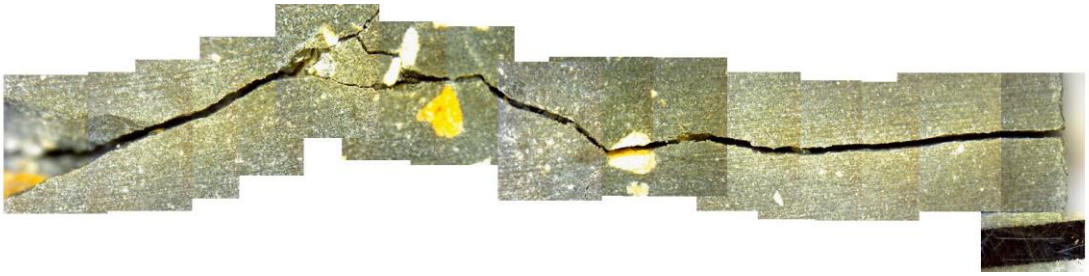

P8-0.0-7d 149 – Front - Mean: 162,9; Std.Dev: 28,3; Min: 91,8; Max: 213,3.
b)
Figure 95 - P8-0.0-7d 149 – After wetting and drying cylcles.

P8-0.0-7d 149 – Back - Mean: 132,3; Std.Dev: 37,0; Min: 68,2; Max: 235,2.
a)

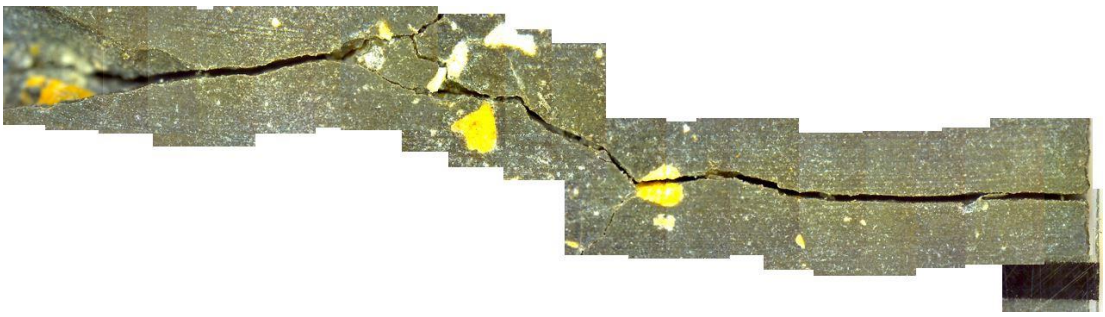

P8-0.0-7d 149 – Front - Mean: 124,9; Std.Dev: 28,1; Min: 65,9; Max: 196,0.
b)
Figure 96 – P8-0.0-7d 149 – After wetting and drying cylcles.

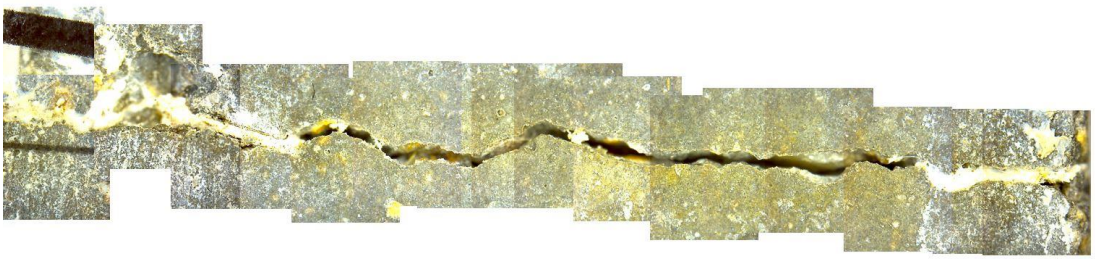

P10-0.0-7d 132 – Back - Mean: 277,2; Std.Dev: 66,1; Min: 100,6; Max: 378,1.
a)

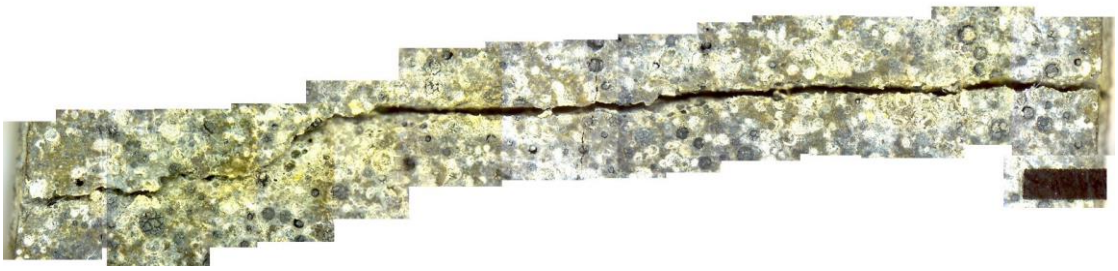

P10-0.0-7d 132 – Front - Mean: 229,7; Std.Dev: 42,7; Min: 146,4; Max: 304,6.
b)
Figure 97 – P10-0.0-7d 132 – After wetting and drying cylcles.

P10-0.0-7d 132 – Back - Mean: 208,3; Std.Dev: 63,4; Min: 86,2; Max: 309,5.
a)

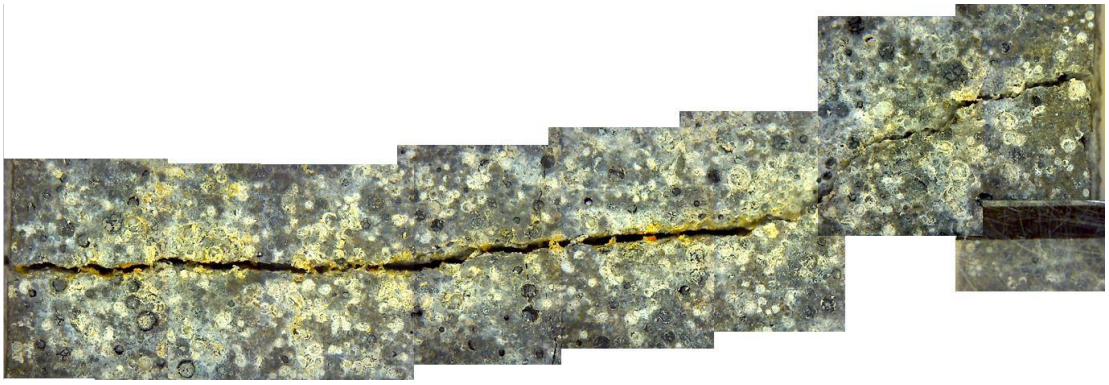

P10-0.0-7d 132 – Front - Mean: 123,5; Std.Dev: 51,7; Min: 27,9; Max: 228,1.
b)
Figure 98 – P10-0.0-7d 149 – After wetting and drying cylcles.

P10-0.0-7d 135 – Back - Mean: 172,2; Std.Dev: 38,9; Min: 91,6; Max: 222,4.
a)

P10-0.0-7d 135 – Front - Mean: 75,9; Std.Dev: 33,1; Min: 17,9; Max: 150,6.
b)
Figure 99 – P10-0.0-7d 135 – After wetting and drying cylcles.

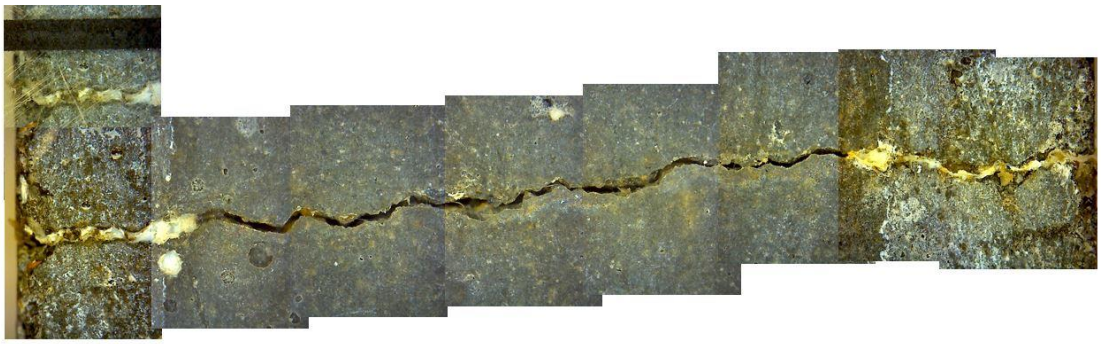

P10-0.0-7d 135 – Back - Mean: 134,0; Std.Dev: 38,1; Min: 60,9; Max: 179,3.
a)

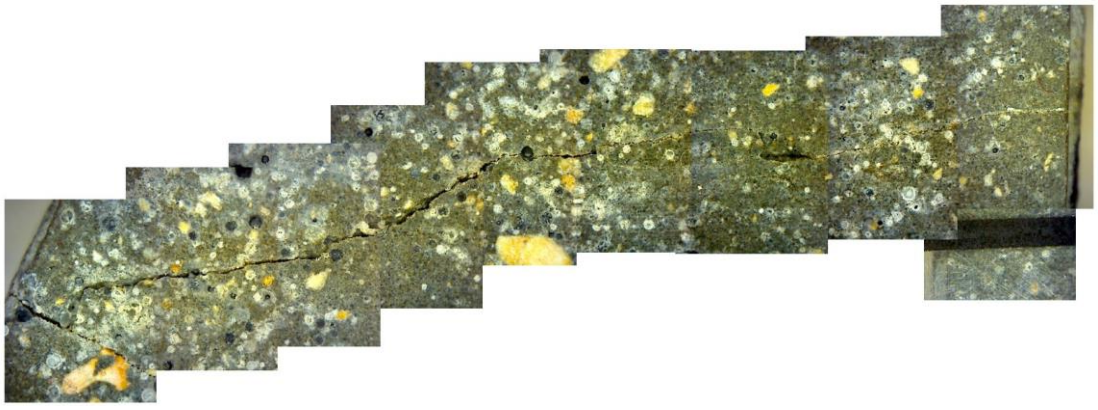

P10-0.0-7d 135 – Front - Mean: 36,4; Std.Dev: 24,5; Min: 6,6; Max: 80,0.
b)

Figure 100 – P10-0.0-7d 135 – After wetting and drying cylcles.

P10-0.0-7d 136 – Back - Mean: 293,3; Std.Dev: 52,8; Min: 198,5; Max: 422,2.
a)

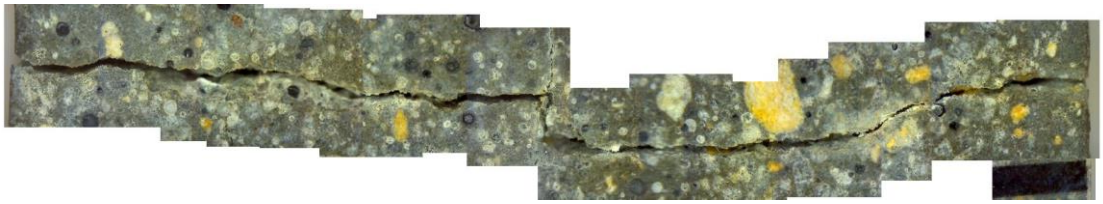

P10-0.0-7d 136 – Front - Mean: 210,2; Std.Dev: 66,1; Min: 75,5; Max: 350,1.
b)
Figure 101 – P10-0.0-7d 136 – After wetting and drying cylcles.

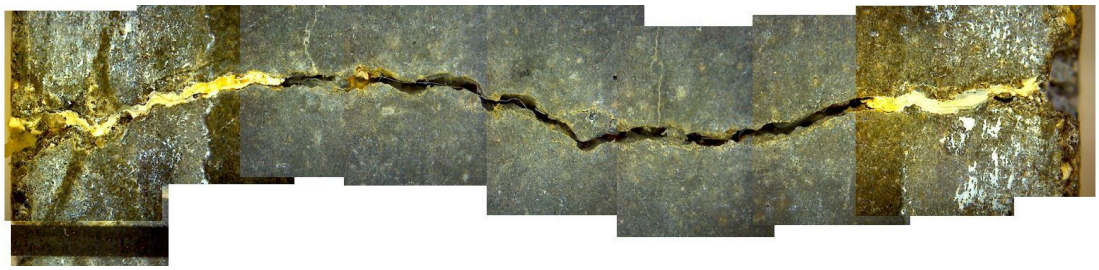

P10-0.0-7d 136 – Back - Mean: 218,6; Std.Dev: 81,9; Min: 59,3; Max: 359,5.
a)

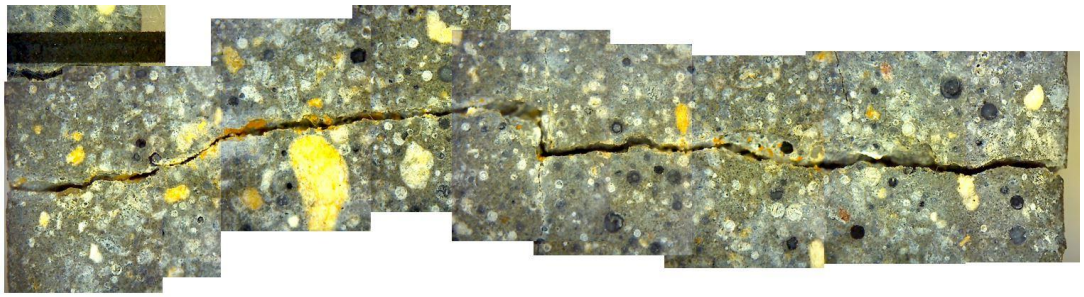

P10-0.0-7d 136 – Front - Mean: 152,3; Std.Dev: 70,3; Min: 21,5; Max: 256,4.
b)
Figure 102 – P10-0.0-7d 136 – After wetting and drying cylcles.

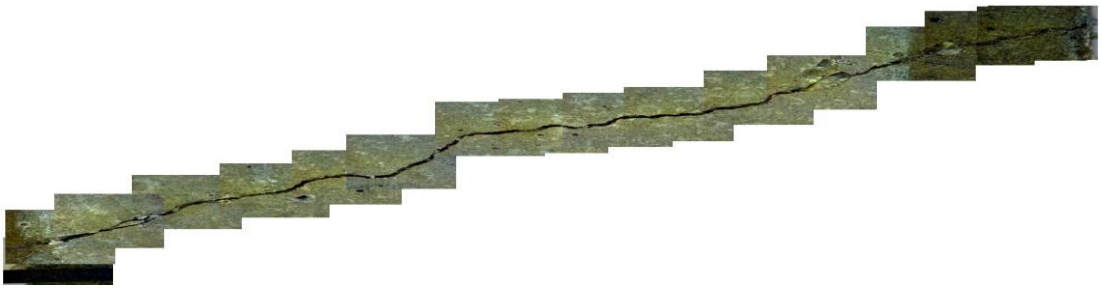

P12-0.0-7d 162 – Back - Mean: 160,4; Std.Dev: 20,4; Min: 135,0; Max: 221,1.
a)

P12-0.0-7d 162 – Front - Mean:87,9; Std.Dev: 38,3; Min: 33,6; Max: 165,8.
b)
Figure 103 – P12-0.0-7d 162 – After wetting and drying cylcles.

P12-0.0-7d 162 – Back - Mean: 116,5; Std.Dev: 33,5; Min: 28,1; Max: 169,7.
a)

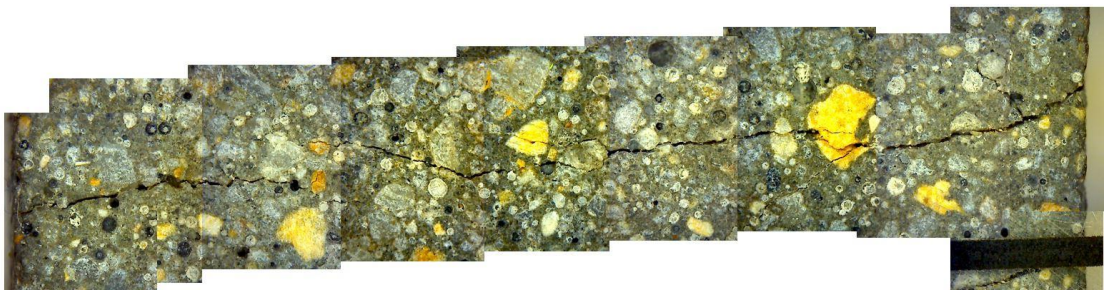

P12-0.0-7d 162 – Front - Mean: 62,4; Std.Dev: 33,3; Min: 15,6; Max: 138,9.
b)
Figure 104 – P12-0.0-7d 162 – After wetting and drying cylcles.

P12-0.0-7d 163 – Back - Mean: 153,6; Std.Dev: 75,6; Min: 34,4; Max: 334,1.
a)

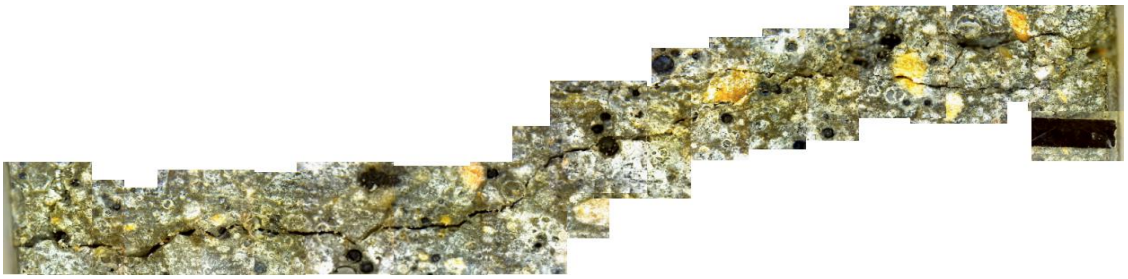

P12-0.0-7d 163 – Front - Mean: 111,4; Std.Dev: 79,5; Min: 31,2; Max: 394,7.
b)
Figure 105 – P12-0.0-7d 163 – After wetting and drying cylcles.

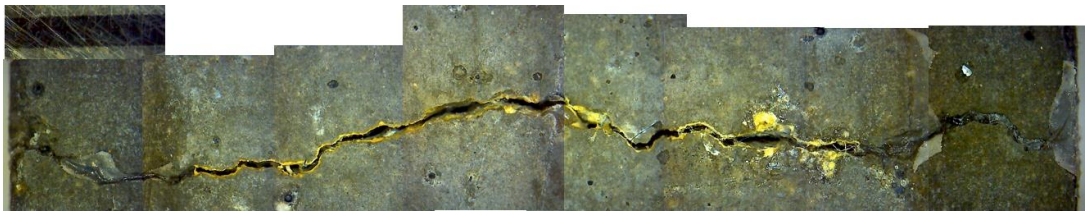

P12-0.0-7d 163 – Back - Mean: 116,7; Std.Dev: 53,7; Min: 23,8; Max: 267,6.
a)

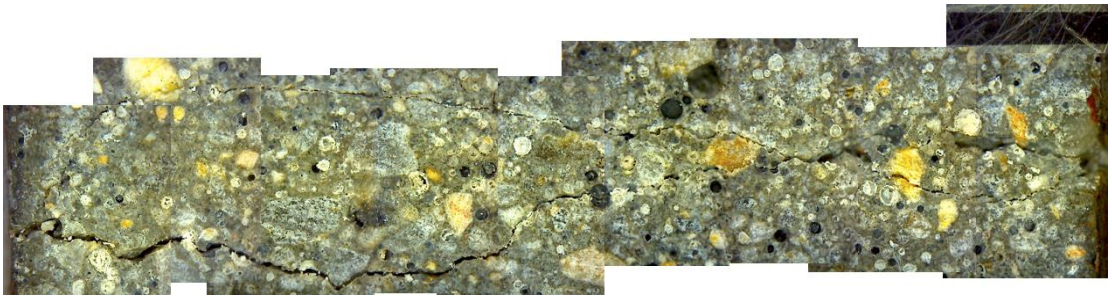

P12-0.0-7d 163 – Front - Mean: 63,7; Std.Dev: 40,3; Min: 8,8; Max: 136,3.
b)

Figure 106 – P12-0.0-7d 163 – After wetting and drying cylcles.

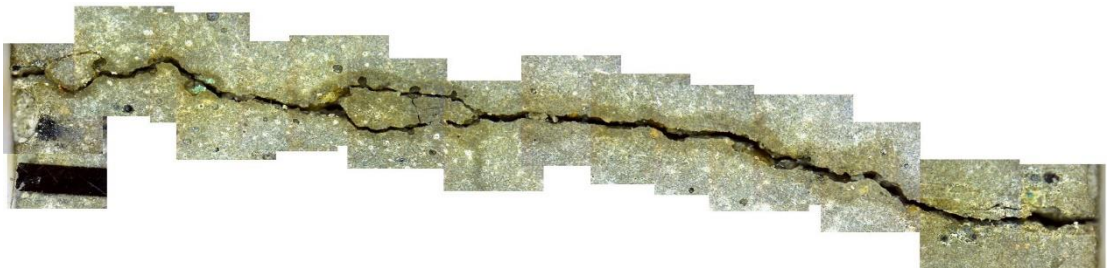

P12-0.0-7d 164 – Back - Mean: 160,7; Std.Dev: 54,4; Min: 79,2; Max: 295,4.

a)

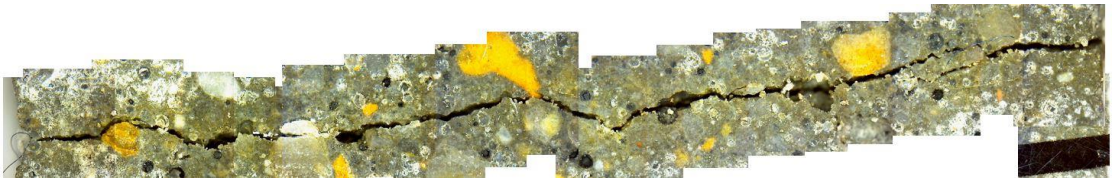

P12-0.0-7d 164 – Front - Mean: 135,1; Std.Dev: 23,3; Min: 92,1; Max: 181,7.

b)

Figure 107 – P12-0.0-7d 164 – After wetting and drying cylcles.

P12-0.0-7d 164 – Back - Mean: 102,0; Std.Dev: 40,6; Min: 27,6; Max: 184,2.

a)

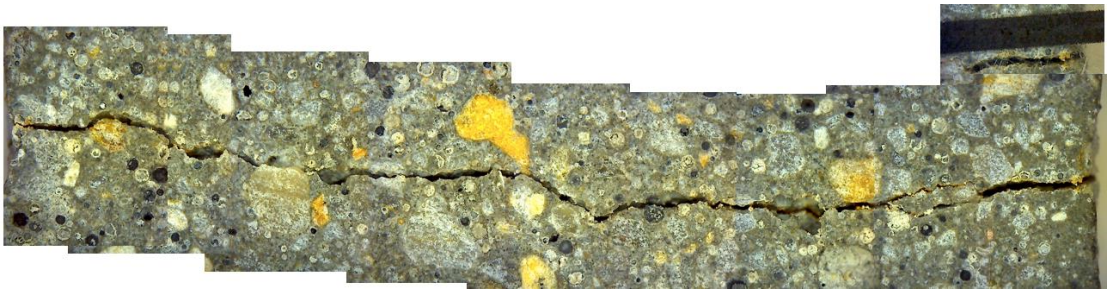

P12-0.0-7d 164 – Front - Mean: 91,5; Std.Dev: 45,7; Min: 17,3; Max: 177,1.
b)
Figure 108 – P12-0.0-7d 164 – After wetting and drying cylcles.

P14-0.0-7d 109 – Back - Mean: 155,2; Std.Dev: 57,4; Min: 75,9; Max: 365,6.
a)

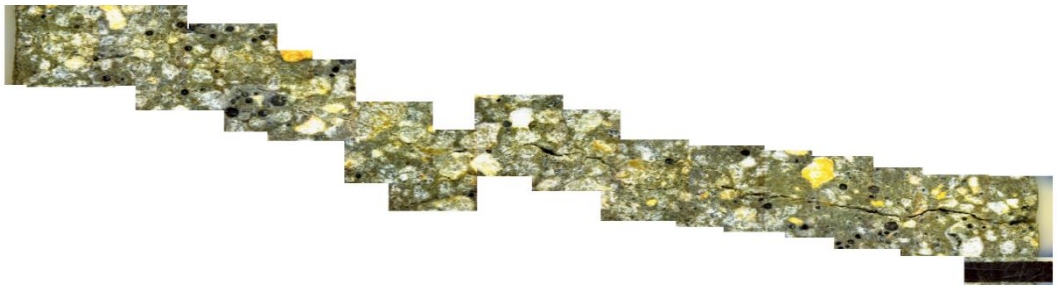

P14-0.0-7d 109 – Front - Mean: 68,5; Std.Dev: 25,6; Min: 22,8; Max: 110,2.
b)
Figure 109 – P14-0.0-7d 109 – After wetting and drying cylcles.

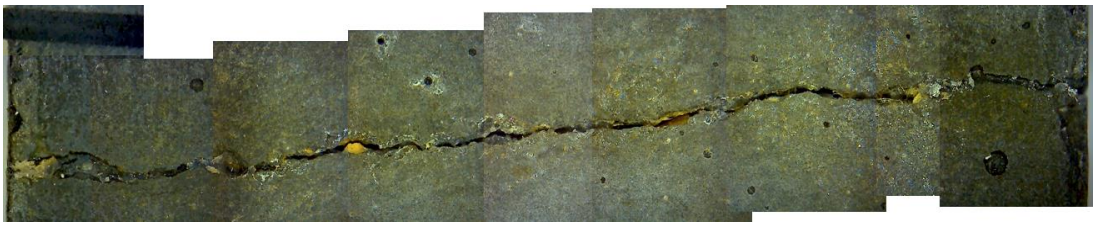

P14-0.0-7d 109 – Back - Mean: 111,7; Std.Dev: 46,2; Min: 49,8; Max: 217,2.

a)

P14-0.0-7d 109 – Front - Mean: 41,4; Std.Dev: 26,6; Min: 12,1; Max: 88,7.
b)
Figure 110 – P14-0.0-7d 109 – After wetting and drying cylcles.

P14-0.0-7d 110 – Back - Mean: 173,5; Std.Dev: 85,0; Min: 83,7; Max: 513,5.
a)

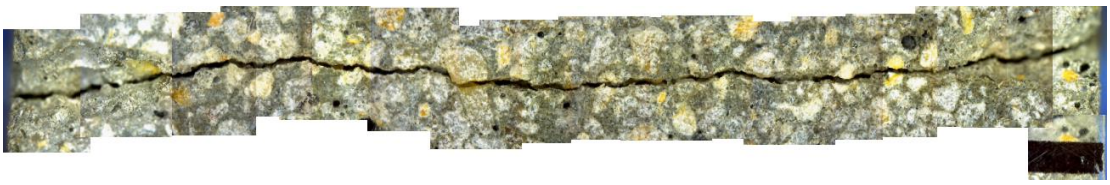

P14-0.0-7d 110 – Front - Mean: 144,0; Std.Dev: 20,6; Min: 110,9; Max: 179,7.
b)
Figure 111 – P14-0.0-7d 110 – After wetting and drying cylcles.

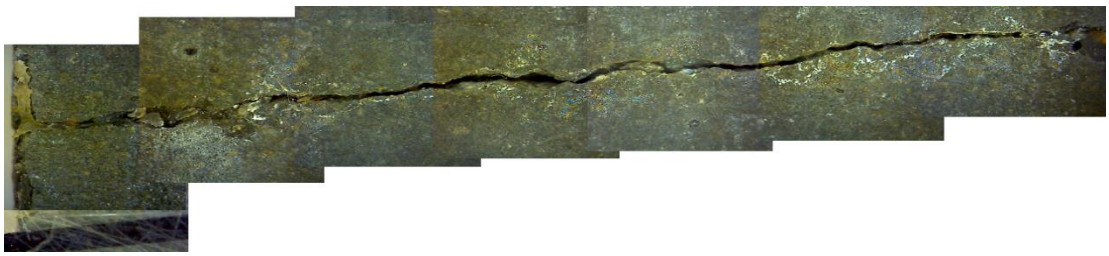

P14-0.0-7d 110 – Back - Mean: 127,8; Std.Dev: 40,5; Min: 58,5; Max: 200,7.

a)

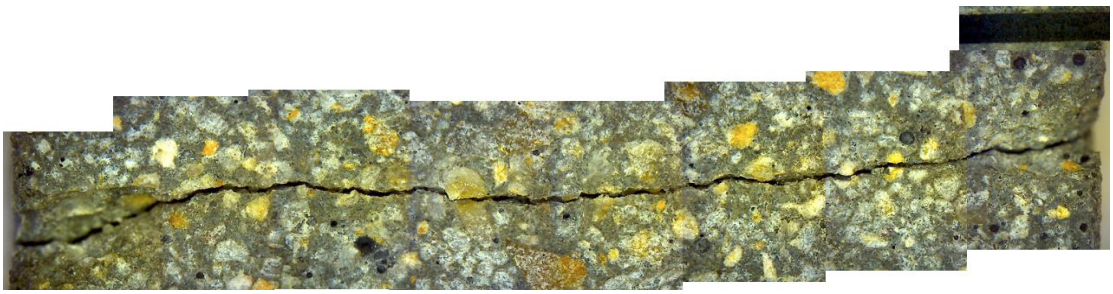

P14-0.0-7d 110 – Front - Mean: 90,2; Std.Dev: 33,6; Min: 15,9; Max: 151,3.

b)

Figure 112 – P14-0.0-7d 110 – After wetting and drying cylcles.

P14-0.0-7d 113 – Back - Mean: 205,0; Std.Dev: 33,1; Min: 140,1; Max: 273,4.

a)

P14-0.0-7d 113 – Front - Mean: 141,6; Std.Dev: 53,8; Min: 67,7; Max: 249,5.

b)

Figure 113 – P14-0.0-7d 113 – After wetting and drying cylcles.

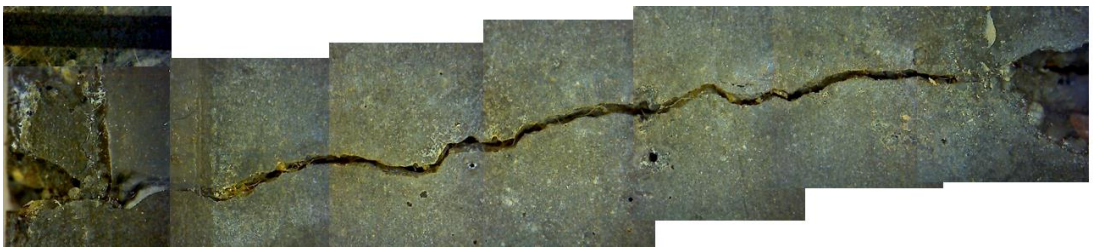

P14-0.0-7d 113 – Back - Mean: 173,9; Std.Dev: 30,8; Min: 117,1; Max: 228,1.

A)

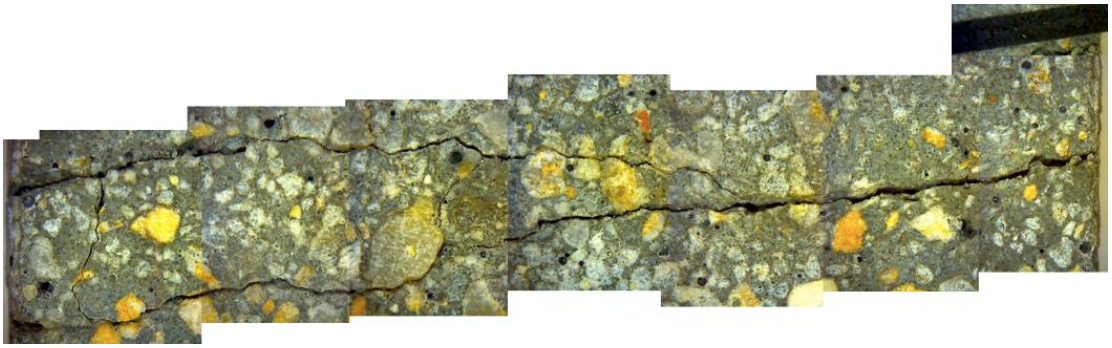

P14-0.0-7d 113 – Front - Mean: 74,7; Std.Dev: 44,9; Min: 11,4; Max: 163,1.

b)

Figure 114 – P14-0.0-7d 113 – After wetting and drying cylcles.

P16-0.0-7d 103 – Back - Mean: 157,5; Std.Dev: 68,1; Min: 55,1; Max: 286,5.

a)

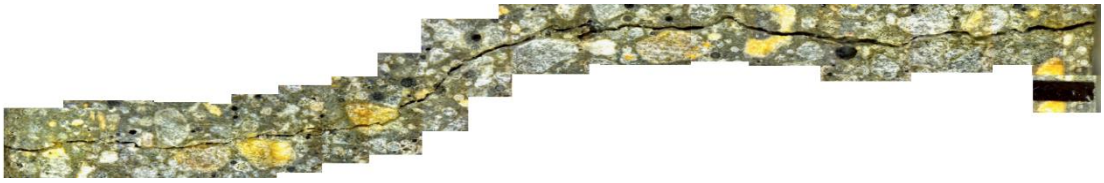

P16-0.0-7d 103 – Front - Mean: 134,4; Std.Dev: 65,9; Min: 52,3; Max: 316,8.

b)

Figure 115 – P16-0.0-7d 103 – After wetting and drying cylcles.

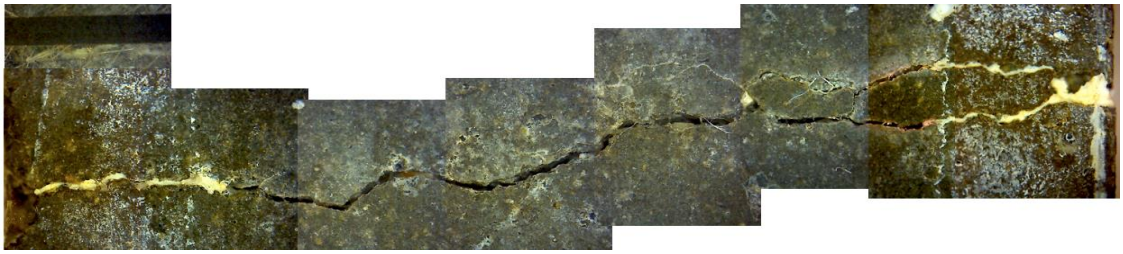

P16-0.0-7d 103 – Back - Mean: 138,0; Std.Dev: 40,3; Min: 65,5; Max: 200,4.

a)

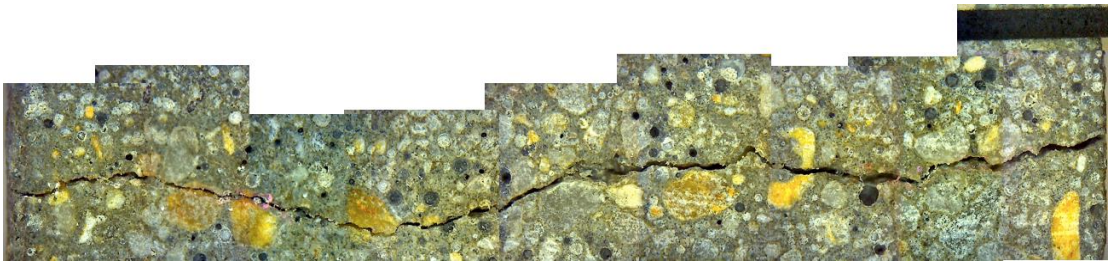

P16-0.0-7d 103 – Front - Mean: 96,2; Std.Dev: 44,5; Min: 20,8; Max: 201,2.

b)

Figure 116 – P16-0.0-7d 103 – After wetting and drying cylcles.

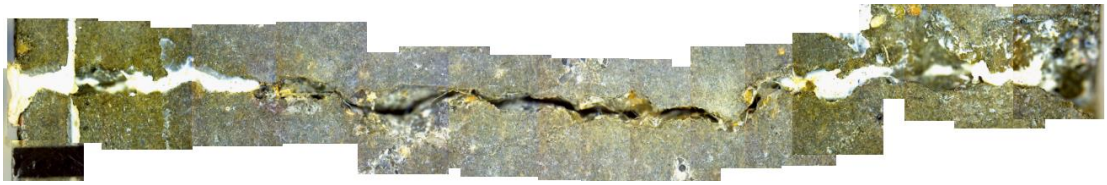

P16-0.0-7d 104 – Back - Mean: 322,3; Std.Dev: 89,5; Min: 192,9; Max: 532,2.

a)

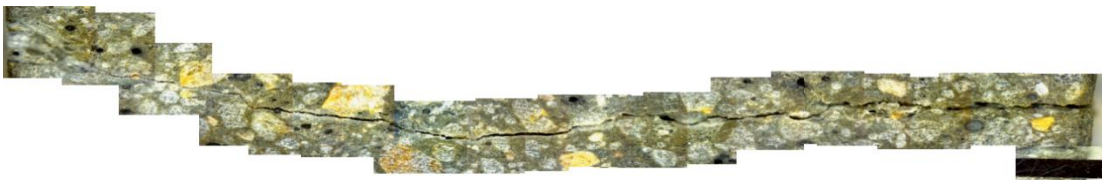

P16-0.0-7d 104 – Front - Mean: 137,5; Std.Dev: 71,7; Min: 46,4; Max: 304,1.

b)

Figure 117 – P16-0.0-7d 104 – After wetting and drying cylcles.

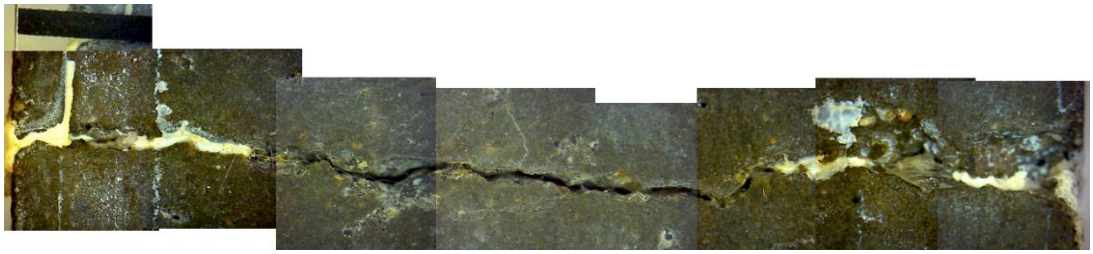

P16-0.0-7d 104 – Back - Mean: 222,5; Std.Dev: 87,6; Min: 44,3; Max: 348,3.

a)

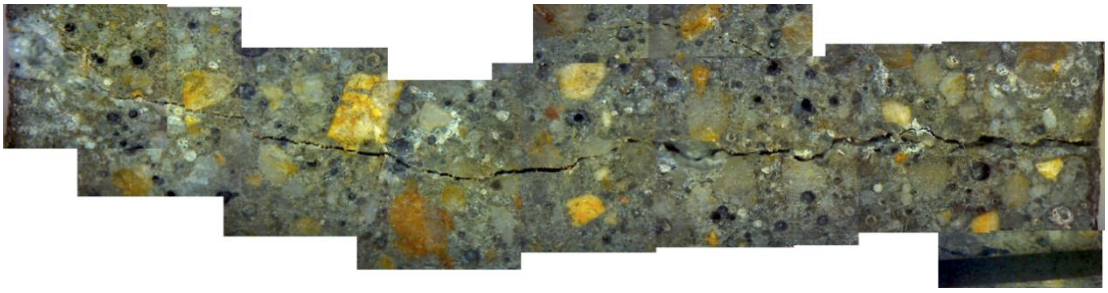

P16-0.0-7d 104 – Front - Mean: 102,3; Std.Dev: 58,5; Min: 43,4; Max: 303,7.

b)

Figure 118 – P16-0.0-7d 104 – After wetting and drying cylcles.

P16-0.0-7d 106 – Back - Mean: 195,2; Std.Dev: 39,0; Min: 108,7; Max: 251,3.

a)

P16-0.0-7d 106 – Front - Mean: 203,6; Std.Dev: 39,3; Min: 127,2; Max: 260,7.

b)

Figure 119 – P16-0.0-7d 106 – After wetting and drying cylcles.

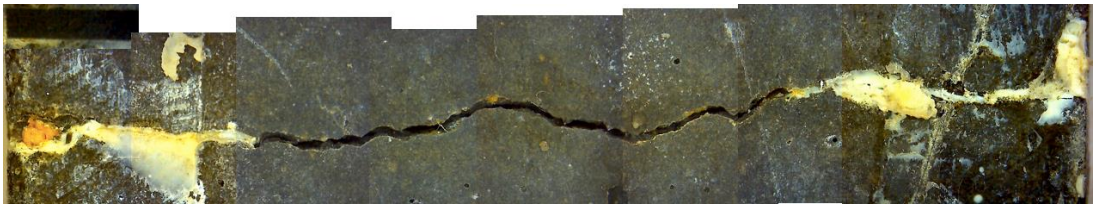

P16-0.0-7d 106 – Back - Mean: 176,2; Std.Dev: 60,5; Min: 55,4; Max: 256,1.

a)

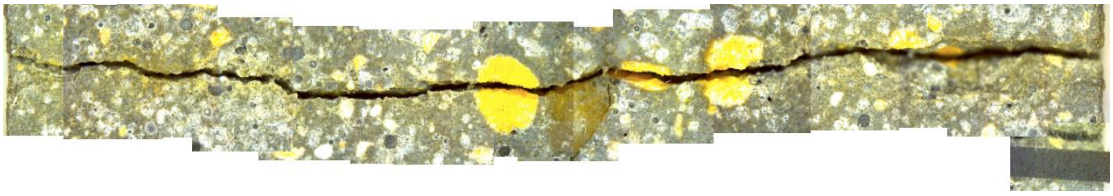

P16-0.0-7d 106 – Front - Mean: 188,6; Std.Dev: 53,3; Min: 55,4; Max: 256,1.

b)

Figure 120 – P16-0.0-7d 106 – After wetting and drying cylcles.

P18-0.0-7d 121 – Back - Mean: 252,2; Std.Dev: 51,8; Min: 151,8; Max: 326,8.

a)

P18-0.0-7d 121 – Front - Mean: 198,1; Std.Dev: 46,5; Min: 96,7; Max: 310,9.

b)

Figure 121 – P18-0.0-7d 121 – After wetting and drying cylcles.

P18-0.0-7d 121 – Back - Mean: 213,9; Std.Dev: 47,2; Min: 153,3; Max: 315,8.

a)

P18-0.0-7d 121 – Front - Mean: 138,5; Std.Dev: 60,4; Min: 34,1; Max: 291,8.

b)

Figure 122 – P18-0.0-7d 121 – After wetting and drying cylcles.

P18-0.0-7d 124 – Back - Mean: 207,5; Std.Dev: 63,2; Min: 126,4; Max: 340,8.

a)

P18-0.0-7d 124 – Front - Mean: 170,3; Std.Dev: 43,3; Min: 54,3; Max: 228,9.

b)

Figure 123 – P18-0.0-7d 124 – After wetting and drying cylcles.

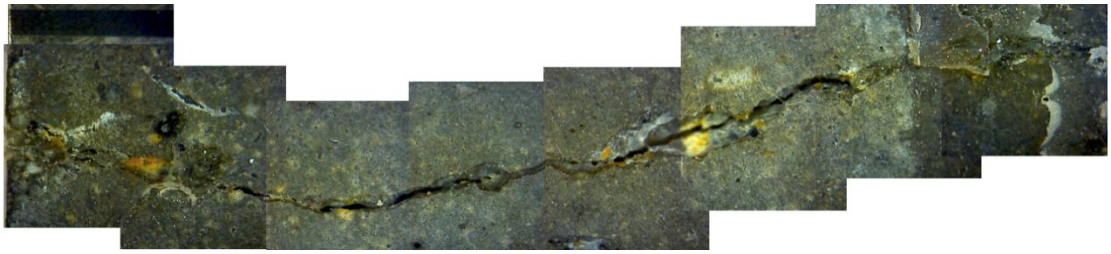

P18-0.0-7d 124 – Back - Mean: 181,6; Std.Dev: 67,6; Min: 71,1; Max: 296,9.

a)

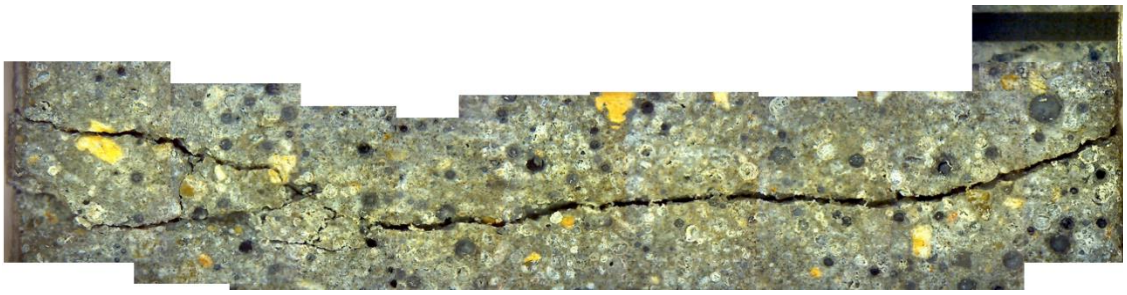

P18-0.0-7d 124 – Front - Mean: 127,9; Std.Dev: 61,0; Min: 17,5; Max: 228,1.

b)

Figure 124 – P18-0.0-7d 124 – After wetting and drying cylcles.

P18-0.0-7d 125 – Back - Mean: 186,1; Std.Dev: 58,2; Min: 41,4; Max: 244,4.

a)

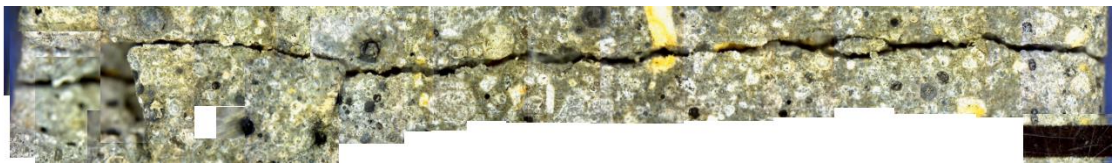

P18-0.0-7d 125 – Front - Mean: 170,9; Std.Dev: 59,0; Min: 84,0; Max: 279,3.

b)

Figure 125 – P18-0.0-7d 125 – After wetting and drying cylcles.

P18-0.0-7d 125 – Back - Mean: 167,3; Std.Dev: 48,6; Min: 62,4; Max: 244,3.

a)

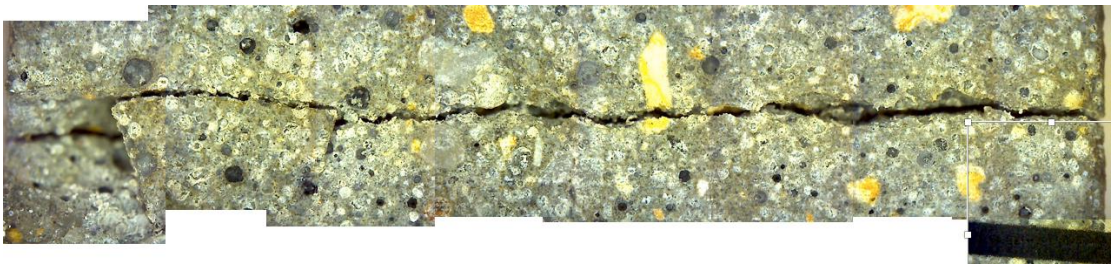

P18-0.0-7d 125 – Front - Mean: 126,9; Std.Dev: 64,2; Min: 47,1; Max: 278,6.

b)

Figure 126 – P18-0.0-7d 125 – After wetting and drying cylcles.